2016

CLEAN COMBUSTION CONTROL IN A COMPRESSION IGNITION ENGINE

Prasad Sajjan Divekar
University of Windsor

CLEAN COMBUSTION CONTROL IN A COMPRESSION IGNITION ENGINE

by

Prasad Sajjan Divekar

A Dissertation

Submitted to the Faculty of Graduate Studies

through the Department of Mechanical, Automotive and Materials Engineering

in Partial Fulfillment of the Requirements for

the Degree of Doctor of Philosophy

at the University of Windsor

Windsor, Ontario, Canada

2016

CLEAN COMBUSTION CONTROL IN A COMPRESSION IGNITION ENGINE

by

Prasad Sajjan Divekar

APPROVED BY:

_____

Dr. C. R. Koch, External Examiner
Department of Mechanical Engineering, University of Alberta

_____

Dr. X. Xu, Outside Reader
Department of Civil and Environmental Engineering

_____

Dr. D. Ting, Programme Reader
Department of Mechanical, Automotive and Materials Engineering

_____

Dr. J. Tjong, Programme Reader
Department of Mechanical, Automotive and Materials Engineering

_____

Dr. M. Zheng, Co-advisor
Department of Mechanical, Automotive and Materials Engineering

_____

Dr. X. Chen, Co-advisor
Department of Electrical and Computer Engineering

August 23, 2016

DECLARATION OF ORIGINALITY

I hereby certify that I am the sole author of this dissertation and that the framework and the details of the technical core of the dissertation have not been published. The proof of the majority of findings has mostly been refereed and produced to original research publications in journals and professional conferences with myself being the first author.

I certify that, to the best of my knowledge, my dissertation does not infringe upon anyone's copyright nor violate any proprietary rights and that any ideas, techniques, quotations, or any other material from the work of other people included in my thesis, published or otherwise, are fully acknowledged in accordance with the standard referencing practices. Furthermore, to the extent that I have included copyrighted material that surpasses the bounds of fair dealing within the meaning of the Canada Copyright Act, I certify that I have obtained a written permission from the copyright owner(s) to include such material(s) in my dissertation and have included copies of such copyright clearances to my appendix.

I declare that this is a true copy of my dissertation, including any final revisions, as approved by my dissertation committee and the Graduate Studies office, and that this dissertation has not been submitted for a higher degree to any other University or Institution.

ABSTRACT

The primary objective of this dissertation is to develop combustion control strategies, that can reduce the thermal efficiency penalty associated with clean combustion in modern compression ignition engines. The clean combustion targets of simultaneously low oxides of nitrogen (NO_X) and smoke emissions are selected as the platforms for demonstrating the dynamic control strategies on a single cylinder research engine.

First, parametric analyses, including exhaust gas recirculation (EGR) calculations, are performed using a zero-dimensional engine cycle simulation model. Thereafter, two combustion strategies are experimentally investigated, namely the single-shot diesel strategy and the dual-fuel strategy. The single-shot diesel combustion strategy employs a single direct injection of diesel with the use of moderate levels of EGR. In the dual-fuel combustion strategy, port injection of ethanol is utilized in addition to the direct injection of diesel and the application of EGR. The results of parametric analyses and engine experiments provide guidelines for the development of a systematic control strategy.

Closed-loop combustion control systems are implemented for regulating the fuel injection commands, by which the combustion phasing is effectively controlled on a cycle-by-cycle basis in both the diesel and dual-fuel combustion strategies. The fuel injection control is integrated into the systematic control strategy for simultaneously controlling the air and fuel systems. The intake boost pressures, EGR rates, and fuelling strategies are dynamically selected, depending on the engine load level. By implementing the systematic control, both the NO_X and smoke targets are achieved over a wide engine load range, while retaining the thermal efficiency of conventional diesel combustion.

DEDICATION

This dissertation is dedicated to my parents,

Sajjan Bhimrao Divekar

and

Usha Sajjan Divekar.

ACKNOWLEDGEMENTS

With great pleasure, I take the opportunity to thank my advisors, Prof. Ming Zheng, and Prof. Xiang Chen for the inspiration, guidance, and encouragement I received from them throughout the Ph.D. program. The regular and excellent feedback on my work has helped me in developing critical thinking and a technical ability that will stay with me throughout my career. I would also like to express my gratitude towards my committee members, Dr. David Ting, Dr. Jimi Tjong, and Dr. Xiaohong (Iris) Xu for their valuable guidance in this research. Special thanks to the external examiner, Professor C.R. Koch from University of Alberta, for his helpful suggestions for improving the quality of my Ph.D. dissertation.

I would like to acknowledge the support I received from my colleagues at the Clean Combustion Engine Laboratory. Dr. Meiping Wang, Dr. Usman Asad, Dr. Xiaoye Han, Qingyuan Tan, Dr. Shui Yu, Dr. Tadanori Yanai, Dr. Xiao Yu, Kelvin Xie, Tongyang Gao, Marko Jeftic, Zhenyi Yang, Shouvik Dev, Geraint Bryden, Chris Aversa, and Mark Ives are thanked for their invaluable assistance in my research. Additionally, I would like to thank the lab members for proof-reading the dissertation and for their constructive criticism. Special thanks to Bruce Durfy, who has helped immensely in the fabrication of the components used in the experimental setup at the laboratory. Many thanks to the staff at the MAME department and at the office of Graduate Studies for handling the paperwork related to my assistantships and for arranging the external examiner.

I am also grateful for the support from the University of Windsor, AUTO21, the Canada Research Chair Program, Canada Foundation for Innovation, Ontario Innovation Trust,

Natural Sciences and Engineering Research Council of Canada for the research support. I would also like to acknowledge the Ford Motor Company, and in particular Dr. Jimi Tjong for allowing me to work at the PERDC, Windsor facility where I gained invaluable industry experience.

Finally, but not the least, I would like to thank my wife, Madalina, for understanding my commitments as a Ph.D. student and for her love and patience.

Prasad Sajjan Divekar

Windsor, Ontario

Canada

August 2016

TABLE OF CONTENTS

LIST OF TABLES

LIST OF FIGURES

NOMENCLATURE

Acronyms

AHRR	Apparent Heat Release Rate	[J/°CA]
AI	Analog Input	[-]
AO	Analog Output	[-]
CA	Crank Angle	[°CA]
CA05	Crank Angle of 5% Heat Release	[°CA]
CA50	Crank Angle of 50% Heat Release	[°CA]
CA95	Crank Angle of 95% Heat Release	[°CA]
CCEL	Clean Combustion Engine Laboratory	[-]
CD	Combustion Duration	[°CA]
CAN	Controller Area Network	[-]
CAI	California Analytical Instruments	[-]
CI	Compression Ignition	[-]
CN	Cetane Number	[-]
CO	Carbon Monoxide	[-]
COV	Coefficient of Variation	[%]
CR	Compression Ratio	[-]
DAQ	Data Acquisition	[-]
DIO	Digital Input Output	[-]
DFC	Dual-fuel Combustion	[-]

DI	Direct-injection	[-]
DIO	Digital Input and Output	[-]
DMA	Direct Memory Access	[-]
DOC	Diesel Oxidation Catalyst	[-]
DPF	Diesel Particulate Filter	[-]
ECU	Engine Control Unit	[-]
EGR	Exhaust Gas Recirculation	[-]
EOC	End of Combustion	[°CA]
EPA	Environmental Protection Agency	[-]
ES	Extremum Seeking	[-]
EVO	Exhaust Valve Opening	[°CA]
FFT	Fast Fourier Transform	[-]
FIFO	First-in First-out	[-]
FPGA	Field Programmable Gate Array	[-]
FSN	Filter Smoke Number	[FSN]
H_2O	Water	[-]
HC	Hydrocarbon	[-]
HCCI	Homogeneous Charge Compression Ignition	[-]
HFID	Heated Flame Ionization Detector	[-]
HPP	High-pressure Pump	[-]
HTC	High Temperature Combustion	[-]
IC	Internal Combustion	[-]

ID	Ignition Delay	[ms]
IMEP	Indicated Mean Effective Pressure	[bar]
IVC	Intake Valve Closing	[°CA]
LHV	Lower Heating Value	[MJ/kg]
LNT	Lean NO_X Trap	[-]
LPP	Low-pressure Pump	[-]
LTC	Low Temperature Combustion	[-]
MAF	Mass Air Flow	[g/s]
MFB	Mass Fraction Burnt	[-]
MK	Modulated Kinetics	[-]
N_2	Nitrogen	[-]
NDIR	Non-dispersive Infra-red	[-]
NI	National Instruments	[-]
NO	Nitric Oxide	[-]
NO_2	Nitrogen Dioxide	[-]
NO_X	Oxides of Nitrogen	[-]
O_2	Oxygen Gas	[-]
OS	Operating System	[-]
PCI	Pre-mixed Compression Ignition	[-]
PCV	Pressure Control Valve	[-]
PFI	Port Fuel Injection	[-]
PID	Proportional Integral Derivative	[-]

PM	Particulate Matter	[-]
ppm	Parts per Million by Volume	[ppm]
PREDIC	PREmixed Lean Diesel Combustion	[-]
RCCI	Reactivity Controlled Compression Ignition	[-]
rpm	Revolutions per Minute	[rpm]
RT	Real-time	[-]
SCR	Selective Catalytic Reduction	[-]
SI	Spark Ignition	[-]
SOC	Start of Combustion	[°CA]
SOI	Start of Injection	[°CA]
SSDC	Single-shot Diesel Combustion	[-]
TDC	Top Dead Centre	[-]
TTL	Transistor-transistor Logic	[-]
TWC	Three-way Catalytic Converter	[-]
UNIBUS	UNIform Bulky Combustion System	[-]
US	United States	[-]
USB	Universal Serial Bus	[-]
VCV	Volume Control Valve	[-]
VGT	Variable Geometry Turbocharger	[-]
VVT	Variable Valve Timing	[-]

Symbols

A_s	Combustion Chamber Surface Area	[m^2]
a	Crank Radius	[m]
C_1	Heat Transfer Model Parameter	[-]
C_2	Heat Transfer Model Parameter	[-]
C_f	Fuel Molecular Composition Parameter	[-]
$C_1H_\beta O_\gamma$	Fuel Molecular Formula	[-]
$C_1H_{\beta_1}O_{\gamma_2}$	Fuel-A for Dual-fuel Consideration	[-]
$C_1H_{\beta_2}O_{\gamma_2}$	Fuel-B for Dual-fuel Consideration	[-]
CD	Combustion Duration	[ºCA]
$\overline{CD}$	Heat Release Duration Ratio	[-]
CD_1	Duration of First Stage of Combustion	[°CA]
$[CO_2]_{int}$	Intake CO_2 Concentration	[%]
$[CO_2]_{exh}$	Exhaust CO_2 Concentration	[%]
$(dp/d\theta)_{max}$	Peak Pressure Rise Rate	[bar/°CA]
$\overline{HR}$	Heat Release Energy Ratio	[-]
HR_1	Fuel Energy in First Stage Heat Release	[J]
l	Connecting Rod Length	[m]
m_{cyl}	Mass of Cylinder Charge	[g/cycle]
m_{egr}	Mass of Recirculated Exhaust Gases	[g/cycle]
m_f	Mass of Fuel	[g/cycle]

n_{int}	Moles of Intake Charge	[mol/cycle]
n_{egr}	Moles of Recirculated Exhaust Gases	[mol/cycle]
n_{exh}	Moles of Exhaust Gases	[mol/cycle]
n_{f}	Moles of Fuel	[mol/cycle]
n_{f_1}	Moles of Fuel-A	[mol/cycle]
n_{f_2}	Moles of Fuel-B	[mol/cycle]
n_{O_2}	Intake Moles of O_2	[mol/cycle]
n_{CO_2}	Intake Moles of CO_2	[mol/cycle]
$n_{\mathrm{H}_2\mathrm{O}}$	Intake Moles of H_2O	[mol/cycle]
n_{N_2}	Intake Moles of N_2	[mol/cycle]
$[\mathrm{O}_2]_{\mathrm{air}}$	Ambient O_2 Concentration	[%]
$[\mathrm{O}_2]_{\mathrm{int}}$	Intake O_2 Concentration	[%]
$[\mathrm{O}_2]_{\mathrm{exh}}$	Exhaust O_2 Concentration	[%]
p	Cylinder Pressure	[bar]
p_{inject}	Common-rail Fuel Injection Pressure	[MPa]
p_{int}	Intake Manifold Pressure	[bar]
p_{max}	Peak Cylinder Pressure	[bar]
Q_{app}	Apparent Heat Release	[J]
Q_{f}	Fuel Energy	[J]
Q_{ht}	Heat Transfer	[J]
$\bar{R}$	Universal Gas Constant	[J/mol.K]

r_{CO_2}	CO_2 EGR Ratio	[-]
r_{O_2}	O_2 EGR Ratio	[-]
r_{mol}	Molar EGR Ratio	[-]
r_{mass}	Mass EGR ratio	[-]
S_p	Mean Piston Speed	[m/s]
T	Bulk Gas Temperature	[K]
T_{max}	Peak Cylinder Bulk Gas Temperature	[K]
T_{int}	Intake Manifold Temperature	[°C]
T_{wall}	Cylinder Wall Temperature	[K]
U	Internal Energy	[J]
V	Cylinder Volume	[m^3]
V_c	Clearance Volume	[m^3]
V_s	Swept Volume	[m^3]
W	Piston Work	[J]
θ_{SOC}	Crank Angle for Start of Combustion	[°CA]
θ	Crank Angle	[°CA]
λ_{air}	Fresh Air Excess Ratio	[-]
λ_{in-cyl}	In-cylinder Air Excess Ratio	[-]
χ	Port-injection Fuel Energy Ratio	[-]
χ'	Port-injection Fuel Molar Ratio	[-]
χ_{eth}	Ethanol Fraction	[-]

CHAPTER I

1. INTRODUCTION

Internal combustion (IC) engines currently remain the preferred choice among the available powertrain options for automobiles [1], [2]. The IC engines typically burn hydrocarbon fuels to produce mechanical work and the products of combustion are exhausted to the atmosphere. The emission of toxic combustion products into the atmosphere poses major health and environmental concerns [3]. Therefore, the exhaust emissions, such as oxides of nitrogen (NO_X), particulate matter (PM), unburnt hydrocarbons (HC), and carbon monoxide (CO) are strictly regulated in North America and other parts of the world [4]. In addition, carbon dioxide (CO_2) regulations are in place to address the climate change and energy security concerns [5].

1.1. The Compression Ignition Engine

The two common IC engine types are the compression ignition (CI) engine and the spark ignition (SI) engine. When compared to the SI engines, the CI engines exhibit several advantages. The higher geometric compression ratio (CR) and the fuel-lean operation of the CI engine contribute to the high thermal efficiency [3]. Furthermore, the unthrottled operation throughout the engine load range yields a better part-load efficiency compared to that of the SI engine [3]. In addition to the higher efficiency, the mechanical reliability and the ability to operate under full-load conditions for an extended period have made the CI engine the preferred option for medium-duty and heavy-duty engine applications. The development of small displacement, high-speed diesel engines has also promoted the use of CI engines in the passenger car sector.

Additional advantages of the CI engine over the SI engine include the typically lower engine-out HC and CO emissions [6], while the engine-out NO_X emissions are at a comparable level between the two engine types [7]. The CI engine, however, emits significantly larger amounts of PM and suffers from the NO_X-PM trade-off [8], wherein the technologies adopted for NO_X reduction often result in an increase in the PM. Furthermore, aftertreatment of the CI engine exhaust is a greater challenge than that of the SI engine. The SI engine operates under stoichiometric conditions and implements the three-way catalytic convertor (TWC) for exhaust aftertreatment. The TWC is effective in reducing the NO_X to nitrogen (N_2) and oxygen (O_2), and oxidizing the HC and CO to CO_2 and water (H_2O). For facilitating the reactions in the TWC, a sufficiently high exhaust temperature is necessary in addition to the periodic absence of O_2 in the exhaust gases.

The exhaust of the CI engine normally contains ample amounts of oxygen. Moreover, the temperature of the exhaust gases is typically lower than that of the SI engine, and varies significantly with the engine load level. Thus, the TWC technology is unsuitable for exhaust aftertreatment in CI engines. More complex aftertreatment devices such as the diesel oxidation catalysts (DOC), diesel particulate filters (DPF), lean NO_X traps (LNT), and selective catalytic reduction (SCR) systems are implemented in combination with in-cylinder emission reduction strategies to reduce the tail-pipe emissions from CI engines [9]. However, some of the emission control strategies, including the use of aftertreatment systems, impose fuel efficiency penalties in CI engines [10].

1.2. Emission and Efficiency Regulations

In North America, the CI engines are primarily used for heavy-duty highway trucks, urban buses, and off-highway equipment [11]. The exhaust emissions of these engines are regulated by the United States (US) Environmental Protection Agency (EPA) and are kept in-line by Environment Canada. The EPA regulations for NO_X and PM emissions [5] that apply to the on-road heavy-duty trucks are summarized in Figure 1.1.

Figure 1.1 US EPA Emission Regulations for Heavy-duty Diesel Engines

The simultaneous reductions of NO_X and PM emissions continue to be a challenge for diesel engines. Modern diesel engines are equipped with complex air and fuel management systems to reduce the in-cylinder NO_X and PM emissions. In addition, multiple aftertreatment systems are in place to treat the diesel exhaust so that the tailpipe emissions are within the regulated limits. For example, Table 1.1 lists a few technologies

implemented on truck engines over the past two decades [12]. Some of the engine technologies used for emission control have resulted in a thermal efficiency reduction. For instance, a nearly 3% (absolute) reduction in the brake thermal efficiency was reported for the 2004 model year truck engines compared to the previous model year engines [12]–[14].

Table 1.1 Technology Integration Example for Cummins Engines

Year	Technology
1991	Electronic Fuel Injection
1997	High-pressure Common-Rail Fuel Injection
2004	Cooled Exhaust Gas Recirculation (EGR), Variable Geometry Turbocharging (VGT)
2007	Wall Flow Diesel Particulate Filtration, NO_X Adsorption
2010	SCR

The recent additions to the EPA regulations are the CO_2 emission limits, that have been in effect since 2014. The current and proposed CO_2 emission regulations [5] applied to heavy-duty trucks are presented in Figure 1.2.

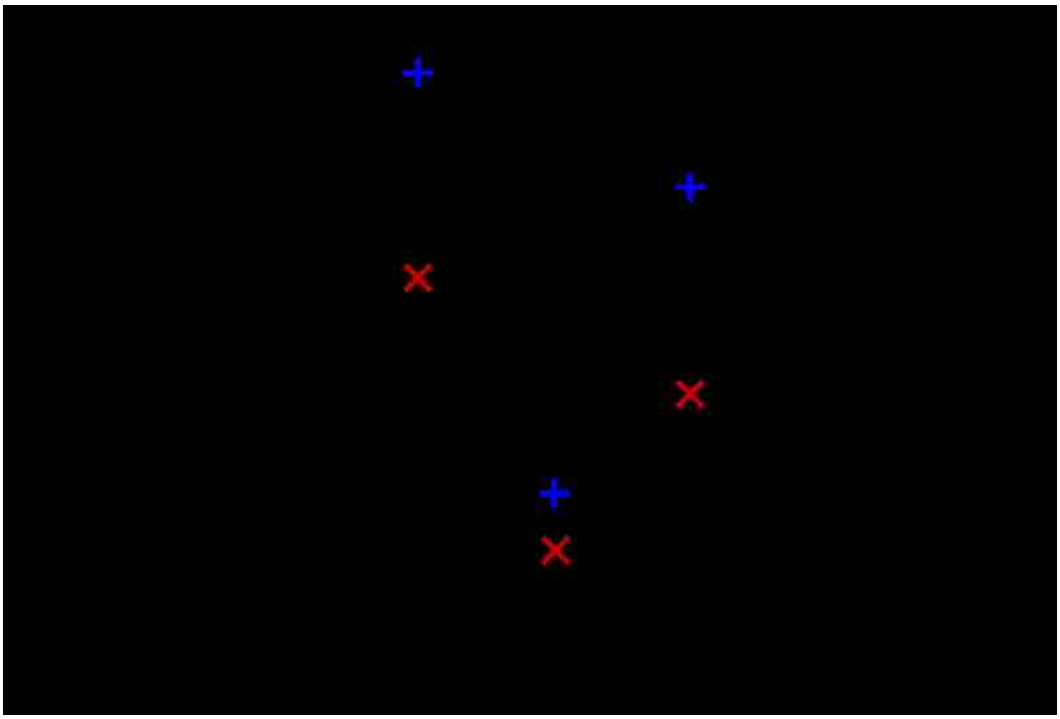

Figure 1.2 US EPA CO_2 Emission Standards for Heavy-duty Diesel Engines

When hydrocarbon fuels are used, the amount of CO_2 in the exhaust directly relates to the fuel consumption, as illustrated in APPENDIX A. Therefore, a reduction of CO_2 emissions requires an improvement in the thermal efficiency of the engine, in addition to other strategies for reducing the overall vehicle fuel consumption. Moreover, the CO_2 regulations are expected to become more stringent for heavy-duty engines in the near future [15]. Similar regulations are in effect for the light-duty vehicles, which are also likely to become increasingly stringent in the future [4]. As a result, thermal efficiency improvements in diesel engines are necessary for their use in the heavy-duty trucks and the light-duty passenger cars. To simultaneously meet the emission and efficiency regulations, a more effective integration of the emission control and efficiency improvement technologies is therefore required.

1.3. CI Engine Control Systems

Before the introduction of electronic engine control, the CI engines implemented a combination of mechanical, pneumatic and hydraulic subsystems for actuator control [16]. A schematic of a typical engine control system for a traditional CI engine equipped with a single-stage turbocharger and a mechanically operated fuel injection system [16] is shown in Figure 1.3. Complex mechanical linkages enable the control of fuel injection timing and quantity based on the engine speed and torque demand. Governor-based idle and maximum engine speed control are also integrated into the fuel injection system. The air supply system is primarily comprised of a turbocharger and an intercooler. The turbocharger utilizes the energy from the engine exhaust to raise the pressure of the intake air. A pneumatically-operated wastegate is used to bypass some of the exhaust gases across the turbocharger turbine to prevent over-boosting of the engine intake [17]. Control systems that limit the fuel quantity at low intake boost pressures are also implemented to reduce the smoke level.

As numerous control actions are performed by the mechanical control systems, the control complexity increases significantly when additional hardware components are integrated into the engine for emission reduction. Moreover, the precision of the control actions based solely on the mechanical, pneumatic, and hydraulic linkages is insufficient to meet the stringent emission regulations [18]. Thus, the use of electronic sensors and actuators in conjunction with an engine control unit (ECU) is a common approach for modern CI engines.

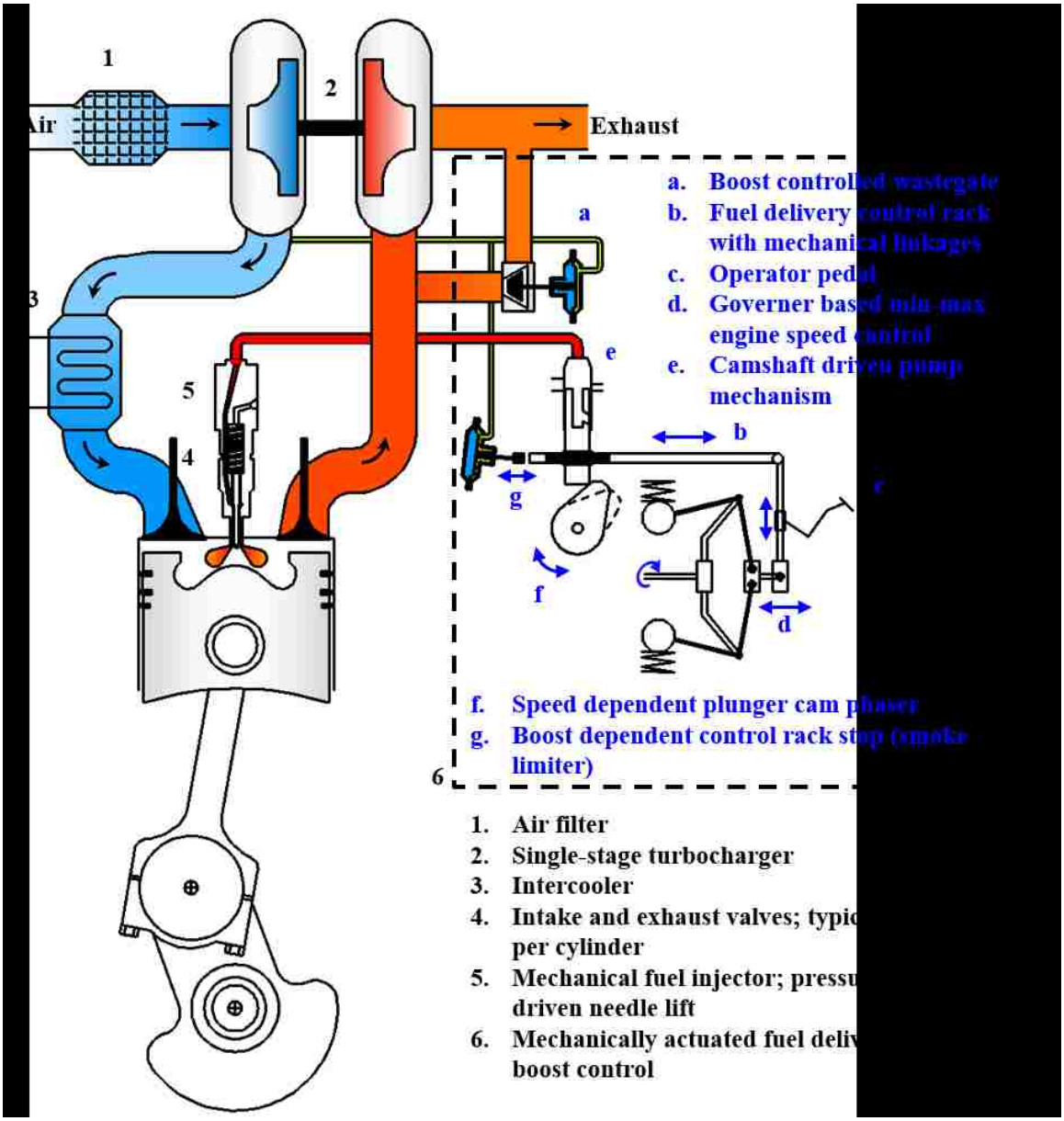

Figure 1.3 Classical Diesel Engine Control Layout

A schematic of a modern CI engine is presented in Figure 1.4. In contrast to the mechanically operated CI engine shown in Figure 1.3, the modern CI engine incorporates emission control technologies. These include the common-rail fuel injection, two-stage turbocharging, variable valve actuation (VVA), dual-loop EGR, and exhaust aftertreatment.

The common-rail injection system and electronically operated fuel injectors facilitate multiple injection events in one engine cycle. The air supply system, for the example shown in Figure 1.4, consists of two turbochargers and a dual-loop EGR system. The turbochargers utilize VGT actuators to electronically regulate the boost pressure and the exhaust backpressure at each stage of the turbocharging system. The dual-loop EGR system comprises the high-pressure and low-pressure EGR paths [19]. The high-pressure EGR path connects the upstream of the VGT to the downstream of the compressor, and the VGT vanes maintain a positive backpressure to drive the exhaust gases through the EGR path. In the low-pressure EGR path, the exhaust gases from downstream of the turbocharger are recirculated into the intake air, before entering the compressor. The EGR valves and the VGT actuators work in coordination to maintain the desired intake boost and EGR levels.

The modern diesel engines also utilize a complex exhaust aftertreatment system. A representative configuration is shown in Figure 1.4. The DOC and the DPF are fitted upstream of the low-pressure EGR loop. The SCR system is mounted downstream of the DOC-DPF assembly for NO_X emission control. An ammonia oxidation catalyst (AOC) is also installed downstream of the SCR for reducing ammonia slip. An array of sensors including mass air flow (MAF), pressure, temperature, oxygen, and NO_X sensors are deployed for the feedback based control of the intake boost, EGR, fuel injection, and aftertreatment systems. A cylinder pressure sensor is also shown in the schematic. However, the measurement of cylinder pressure is currently not a common practice in production CI engines [20].

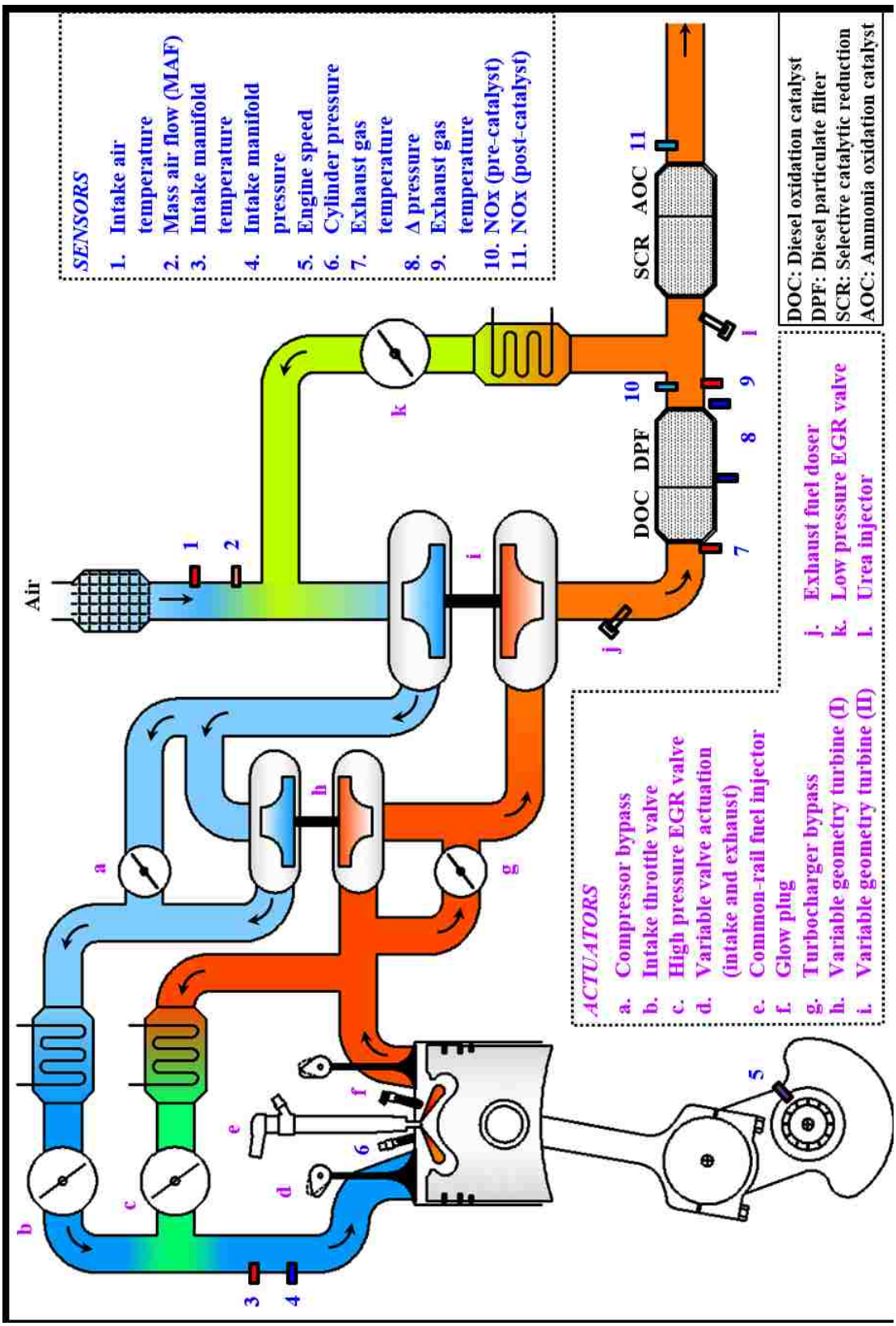

Figure 1.4 Modern Diesel Engine Control Layout

1.4. Engine Calibration and Control Design

The ECU generates the control commands for a large number of electronic actuators employed on the modern CI engine. The actuator setpoints are stored on the ECU memory. The setpoint values are generated during the engine calibration process, which is usually carried out in engine dynamometer test cells. Adjustments are also made to the setpoints depending on the engine operating conditions, the atmospheric conditions, and several other engine and vehicle parameters. A typical engine calibration process [21] is summarized in Figure 1.5. The process is governed by several objective functions and constrains that include engine performance targets and actuator physical limitations.

The experimental engine mapping procedure for developing the actuator setpoint maps is highly complex and requires a significant amount of time. For instance, in engines that use the common-rail system, several variables such as injection pressure, number of fuel injections per cylinder per cycle, and the duty cycle of each injection event require calibration. It is pertinent to mention that several approaches for standardization of the calibrations across engine platforms are in place, at least within the same engine manufacturer. Nevertheless, each new technology implemented in the engine platform causes an increase in the complexity of the operating maps, and hence the calibration effort [22].

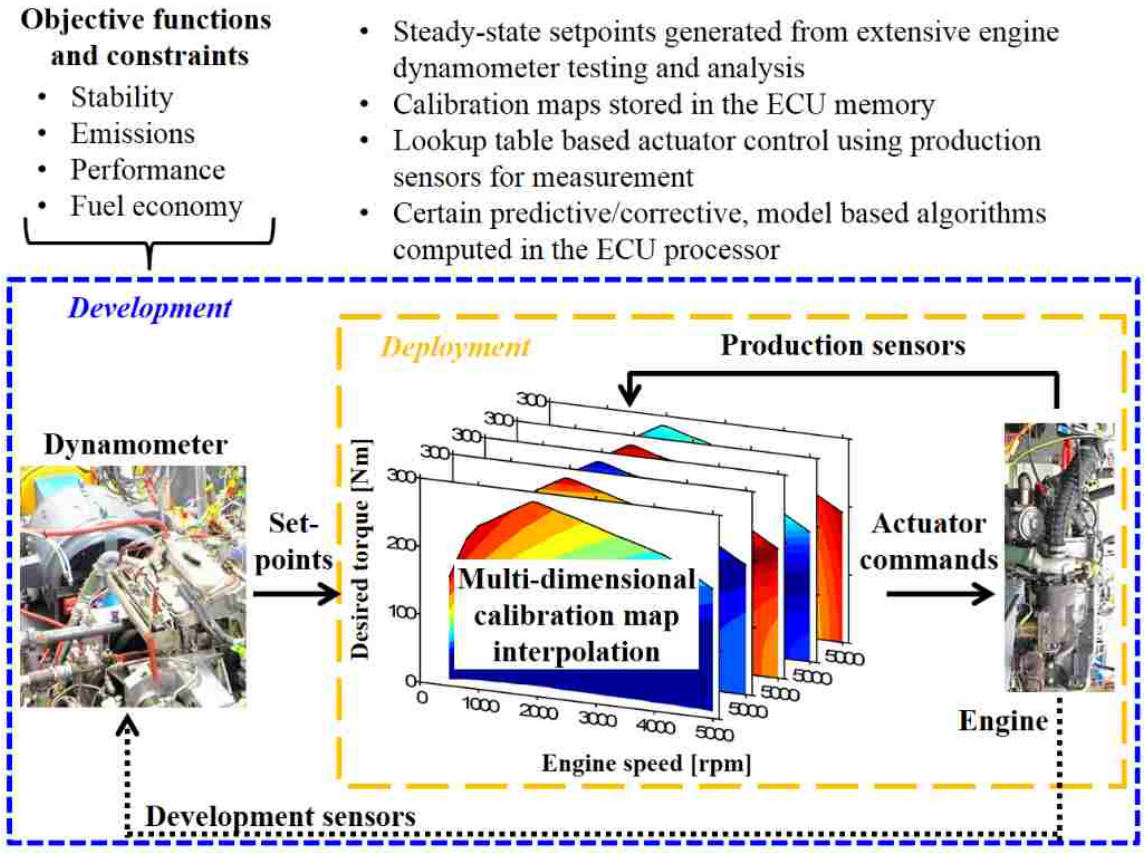

Figure 1.5 Typical Engine Calibration and ECU Operation

In summary, the increased stringency of the regulatory constraints in emissions and efficiency may require the deployment of additional sensors and actuators to facilitate clean and efficient combustion strategies in CI engines. At the same time, the addition of hardware components on the engine increases the calibration effort and control complexity. Control strategies that can reduce the calibration effort and limit the sensor requirements are necessary. The model-based control systems that are developed on the test bench and then deployed in the ECU software are preferred. The model-based control system development is also supported by the increasing on-board computing power on the modern ECU [23].

1.5. Scope of Work

Dynamic control strategies are developed in this dissertation, that can reduce the energy efficiency penalties typically associated with the simultaneous reduction of NO_X and smoke emissions in modern CI engines. A high compression ratio (18.2:1) common-rail diesel engine is adopted as the research platform to benefit from its potentially high thermal efficiency. The test engine is equipped with the following modern diesel engine hardware: common-rail fuel injection, boosted intake, and EGR. In addition to the standard engine hardware, the intake manifold of the test engine is fitted with a port fuel injection system for implementing the dual-fuel combustion (DFC) strategy. The single-shot diesel combustion (SSDC) and the ethanol-diesel DFC strategies are experimentally investigated, supported by parametric calculations with zero-dimensional (zero-D) engine cycle simulations.

The test engine is controlled using a modular control platform that includes real-time (RT) computers and field programmable gate array (FPGA) devices. The test engine and the control setup provide a platform to demonstrate the dynamic control strategies that can regulate the combustion process to reduce exhaust emissions, to improve thermal efficiency, and to maintain stable engine operation over a wide engine load range.

1.6. Dissertation Significance

This dissertation work focuses on the control of in-cylinder reductions of NO_X and smoke emissions by implementing the clean combustion strategies. The thermal efficiency of clean combustion is improved by applying systematic control. The primary contributions of the dissertation include:

1. Identification of boundary conditions for the experimental study by conducting parametric engine cycle simulations with a detailed EGR analysis.

2. Experimental investigation of low emission and high efficiency pathways with the SSDC and DFC strategies. The adjustment of EGR rate, the modulation of combustion phasing, and the regulation of ethanol-to-diesel ratio are used as the primary control variables during the experimental study, the results of which are used to develop the dynamic combustion control strategies.

3. Cycle-by-cycle control of combustion phasing and engine load using the RT-FPGA enabled cylinder pressure analysis. Improvements in combustion stability are achieved by implementing cycle-by-cycle control in the clean combustion region.

4. Development of dynamic control strategies to demonstrate the systematic regulation of EGR rate, combustion phasing, and combustion strategy switching.

1.7. Dissertation Outline

The dissertation consists of eight chapters and seven appendices. The dissertation outline is shown in Figure 1.6. Chapter 1 provides a concise overview of the CI engine hardware and control technologies. The regulatory and consumer requirements that drive the continuous improvements in IC engine technologies are highlighted. The motivation for improving engine control is explained in this chapter. A brief literature review of clean combustion strategies and control methods for CI engines is presented in Chapter 2. The emission benefits of diesel LTC are introduced, and the challenges associated with the implementation and control of LTC are described. The impacts of fuel property

modifications on the emissions from CI engines are discussed. The studies of DFC are reviewed, and the associated control challenges are summarized.

An overview of the research methodologies implemented in this dissertation is provided in Chapter 3. The engine performance and emission targets adopted in the experimental work are introduced. The laboratory equipment and the experimental methods are described in this chapter. Details of the hardware and software architectures implemented for engine control are also provided.

A zero-D engine cycle simulation code is developed, that includes a simple characterization of EGR. Calculations are carried out to study the effects of engine operating parameters on the engine performance, and to identify limiting conditions for engine testing. Chapter 4 describes the calculation steps and the results of the parametric simulation study. The results of steady-state engine tests are presented in Chapter 5. The experimental investigation includes the systematic testing of the SSDC strategy and the diesel-ethanol DFC strategy.

The dynamic cycle-by-cycle regulation of the fuel injection using the cylinder pressure feedback is explained in Chapter 6. The cylinder pressure analysis technique, the controller design, and the test results are presented. In Chapter 7, the fuel injection control algorithm and a simplified mathematical model of the test engine are integrated into a systematic control architecture to simultaneously regulate the air and fuel systems of the test engine. The proposed systematic control architecture is discussed in detail, along with representative test results. A summary of the contributions of this dissertation is presented in Chapter 8. Finally, the recommendations for future work are provided.

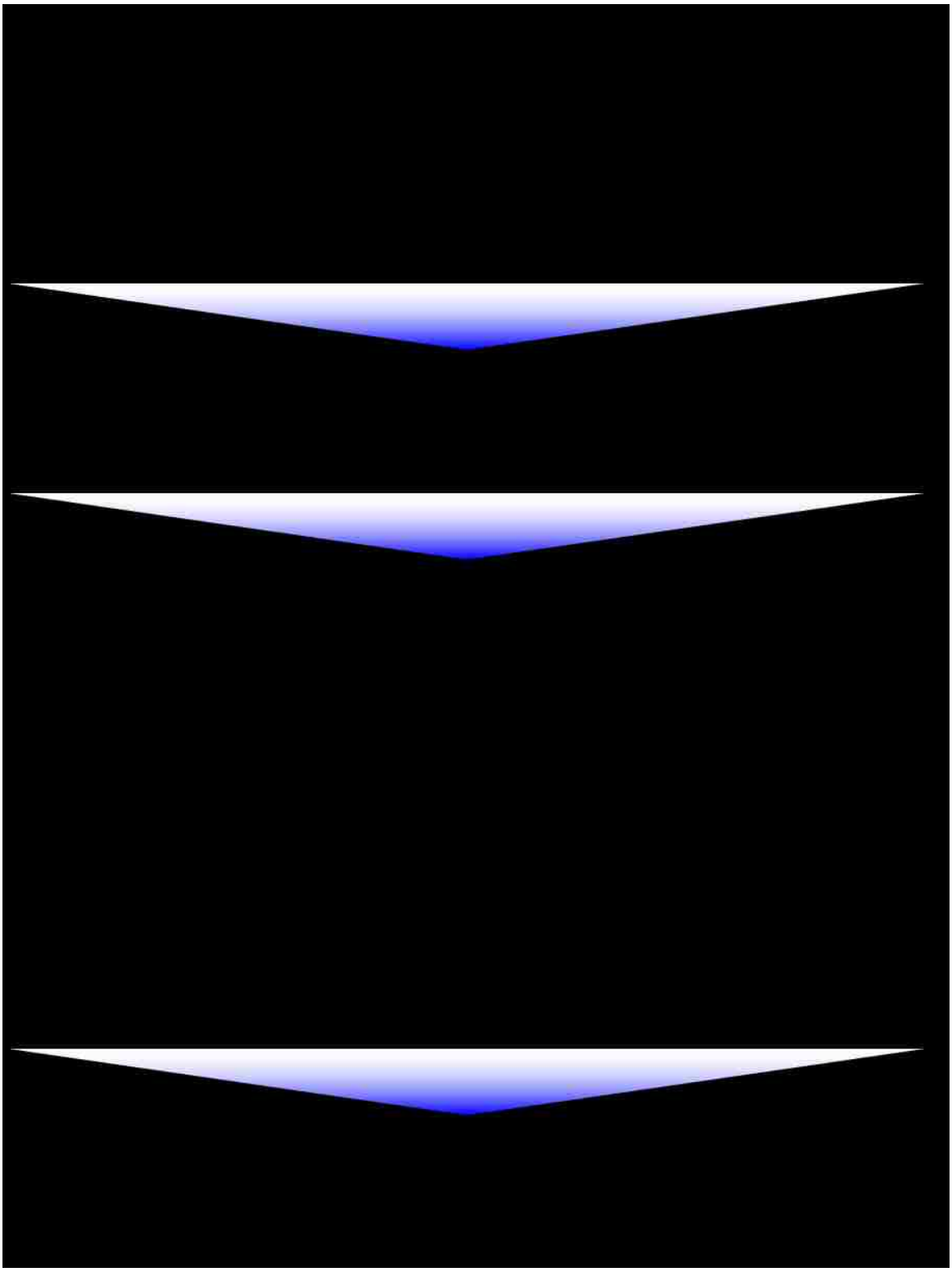

Figure 1.6 Dissertation Outline

CHAPTER II

2. LITERATURE REVIEW

A brief summary of previous and ongoing researches in CI engine combustion is presented in this chapter. The literature review is divided into three sections. The low temperature combustion (LTC) strategies that can achieve ultra-low NO_X and smoke emissions using diesel fuel are reviewed in the first section. The second section presents a brief review on the combustion of alternative fuels and fueling strategies in CI engines. The final section summarizes the challenges and progresses of clean combustion control in modern CI engines.

2.1. Diesel Low Temperature Combustion

The ignition and combustion characteristics of diesel engines can be explained with a heat release rate diagram. The heat release rate (HRR) is an indication of the rate of fuel combustion, which is calculated from the measured cylinder pressure. A representative example of conventional diesel combustion is shown in the upper plot of Figure 2.1. The cylinder pressure, the HRR, and the rate of injection (ROI) are plotted against the crank angle. The short ignition delay followed by the overlap between the injection and combustion events, suggests that a part of the air and fuel mixing occurs during the combustion event. The temporal overlap between the fuel injection and combustion events generally leads to diffusion burning in a diesel engine [24].

The lower plot of Figure 2.1 shows an example of the diesel low temperature combustion (LTC). Both the test cases presented in Figure 2.1 have matching diesel

injection pressures and commands. However, in contrast to the conventional diesel combustion, when LTC is enabled, the combustion event is largely separated from the fuel injection event, as seen from the ROI and HRR traces. In this case, LTC is enabled by applying heavy amounts of EGR, which effectively prolongs the ignition delay [25].

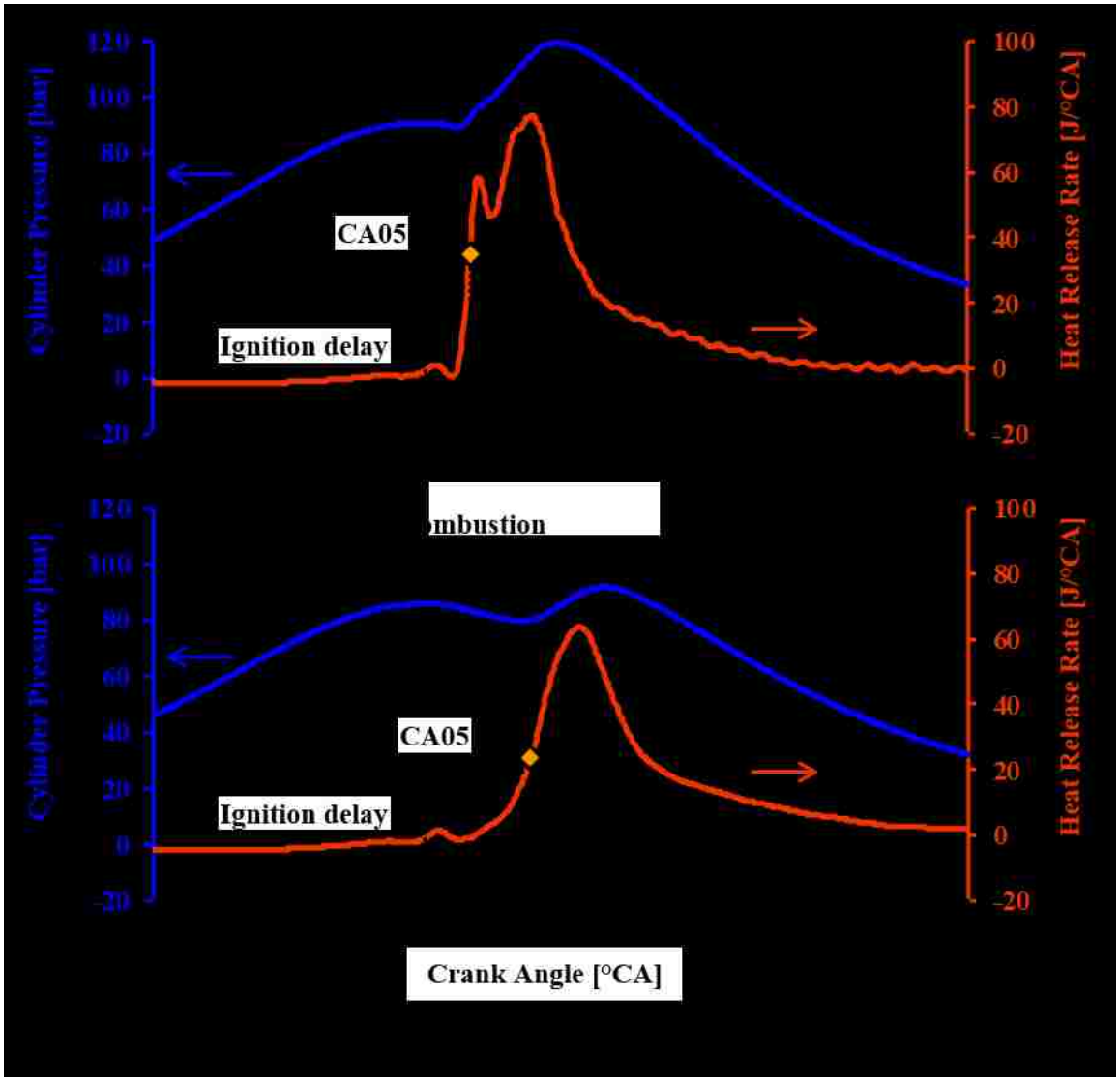

Figure 2.1 Diesel HTC versus LTC: Pressure and Heat Release

By enabling LTC, the NO_X and smoke emissions are simultaneously reduced to ultra-low levels. To understand the emission characteristics of the two test cases, a conceptual chart

of smoke and NO_X formation regions [26], [27] is shown in Figure 2.2. During diffusion combustion, the locally fuel-rich and high temperature conditions prevail as the air-fuel mixing takes place simultaneously with the combustion process, thereby promoting the formation of smoke [24]. At the same time, the diffusion flame tends to localize near stoichiometric regions, where the high flame temperature produces high NO_X emissions [8]. Thus, during diffusion burning, the flame temperatures and the air-fuel ratios pass through both the smoke and NO_X formation regions [24], [26], [27].

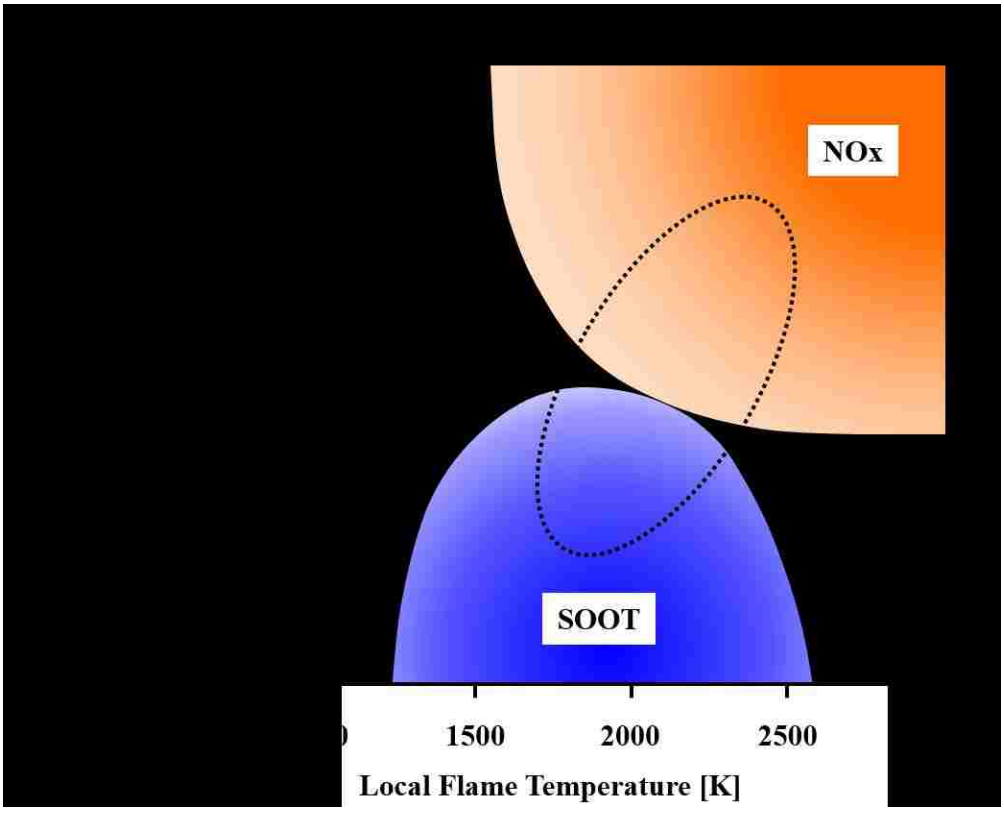

Figure 2.2 Conceptual Representation of NO_X and Smoke Formation

Therefore, the goal of LTC is to enhance the mixing process between the fuel and air [28], [29]. By preparing a lean (or diluted) and pre-mixed cylinder charge before the onset of combustion, the smoke and NO_X formation regions are avoided [24], [27]. The

diesel LTC strategies either advance or postpone the injection events away from the injection window of conventional diesel combustion [24], [30], as shown in Figure 2.3. In addition to the off-phasing of injection, inert dilution of the intake is applied by the use of heavy amounts of EGR [31]. These strategies create a separation between injection and combustion, thereby prolonging the mixing time. Even though ultra-low NO_X and smoke emissions are achieved, the thermal efficiency of diesel LTC cycles is often lower than that of conventional HTC [29]. Besides, the LTC strategies are typically limited to low engine load levels [28], [32]–[36].

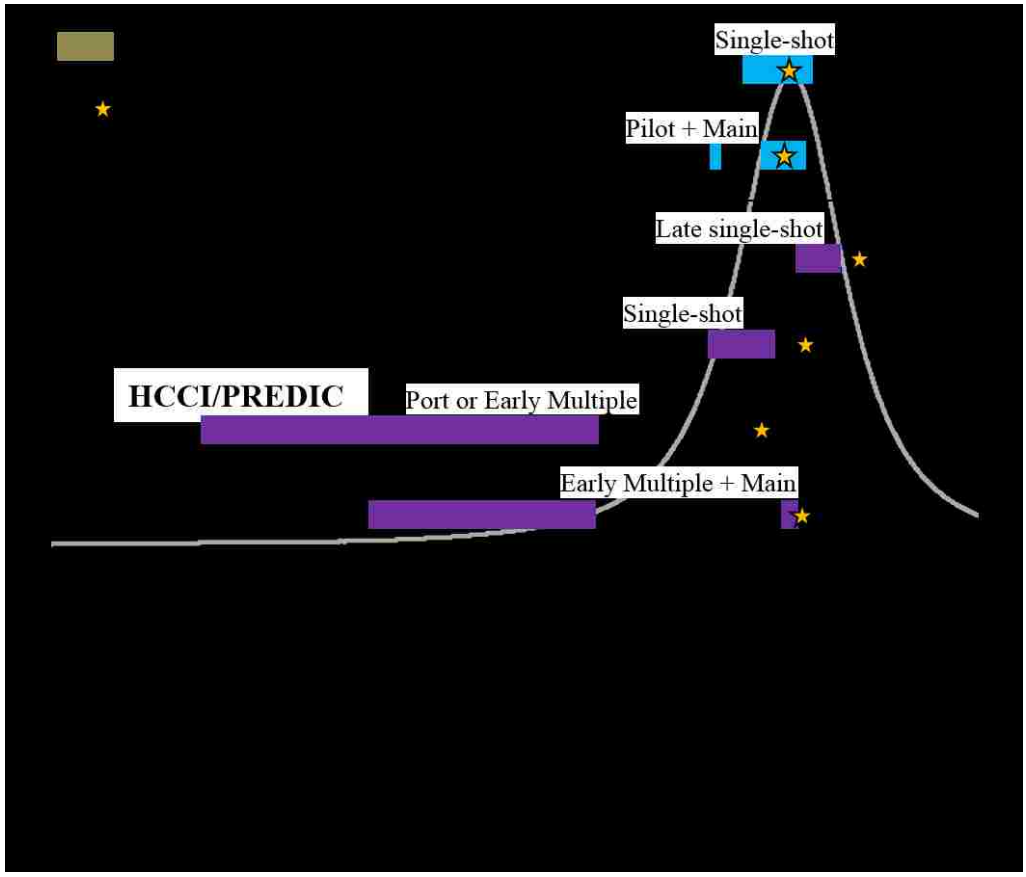

Figure 2.3 Common Low Temperature Combustion Strategies with Diesel

2.2. Combustion of Alternative Fuels in Compression Ignition Engines

Fundamentally, engine operation under the LTC regime prefers a lean (or diluted) and homogeneous air-fuel mixture that auto-ignites towards the end of the compression stroke. However, diesel fuels have relatively high viscosities and boiling temperatures, hence they require a longer mixing times to prepare homogeneous mixtures. Diesel fuels also have high tendencies to auto-ignite, which limit the mixing time prior to ignition, especially when the engine load level is increased. Therefore, conventional diesel fuels may not be suitable for facilitating LTC over a wide engine load range [37], [38].

Among the commercially available fuels, diesel and gasoline have high volumetric and mass-based energy densities, which make them suitable for mobile applications. The energy densities of some commercially available fuels are summarized in Figure 2.4. The gaseous fuels such as H_2 and natural gas have high mass-based energy densities, and are suitable for LTC [5], [39]–[41]. But for vehicle use, these fuels have to be compressed to high pressures for onboard storage.

Other liquid fuels such as alcohols and biodiesels that carry oxygen within the fuel molecules have a lower energy density. Nevertheless, combustion of such fuels in CI engines has demonstrated a reduction in the smoke emissions due to the fuel borne oxygen [42]–[45]. Moreover, these fuels can be produced from biomass feedstock and are considered to be renewable [46], [47].

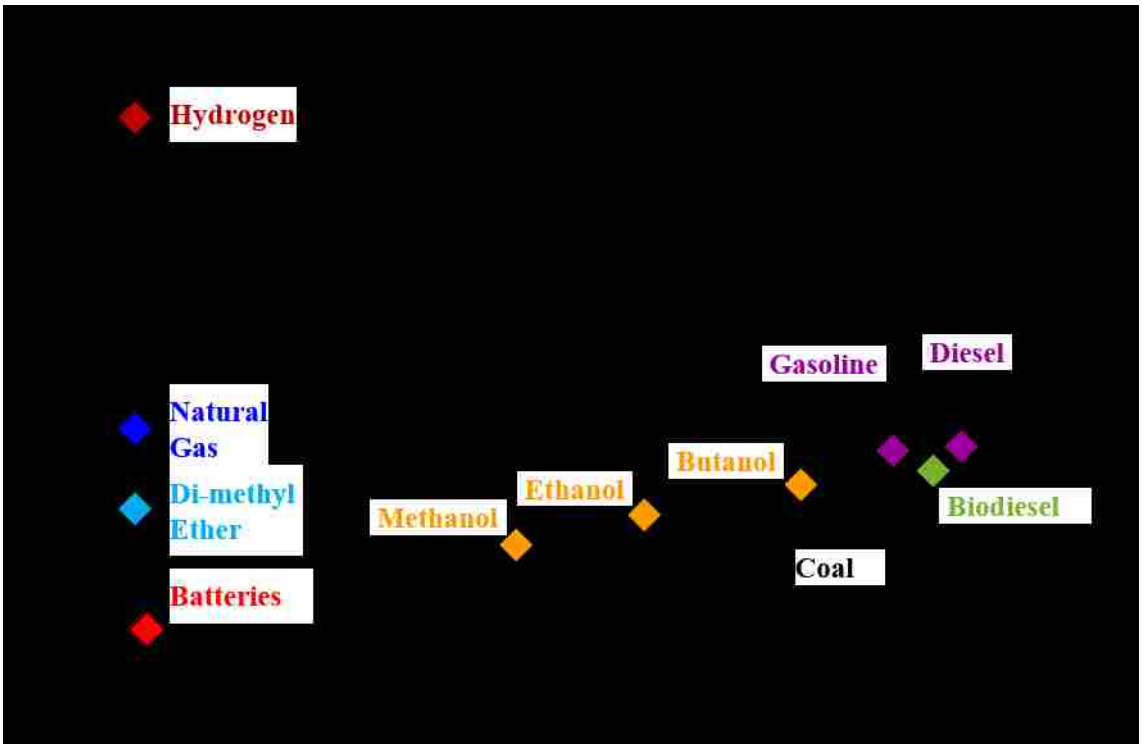

Figure 2.4 Energy Densities of Common Fuels and Energy Storage Devices

Apart from the energy content, the suitability of a fuel for LTC depends upon its physical and chemical properties that influence the fuel-air mixing and combustion processes. The major fuel properties that affect the mixing of fuel and air include the boiling point, volatility, viscosity, and latent heat of evaporation; whereas the ignition characteristics are typically evaluated from the fuel Cetane or Octane number. The properties of some common fuels are presented in Figure 2.5. A detailed summary of the fuel properties is included in APPENDIX B.

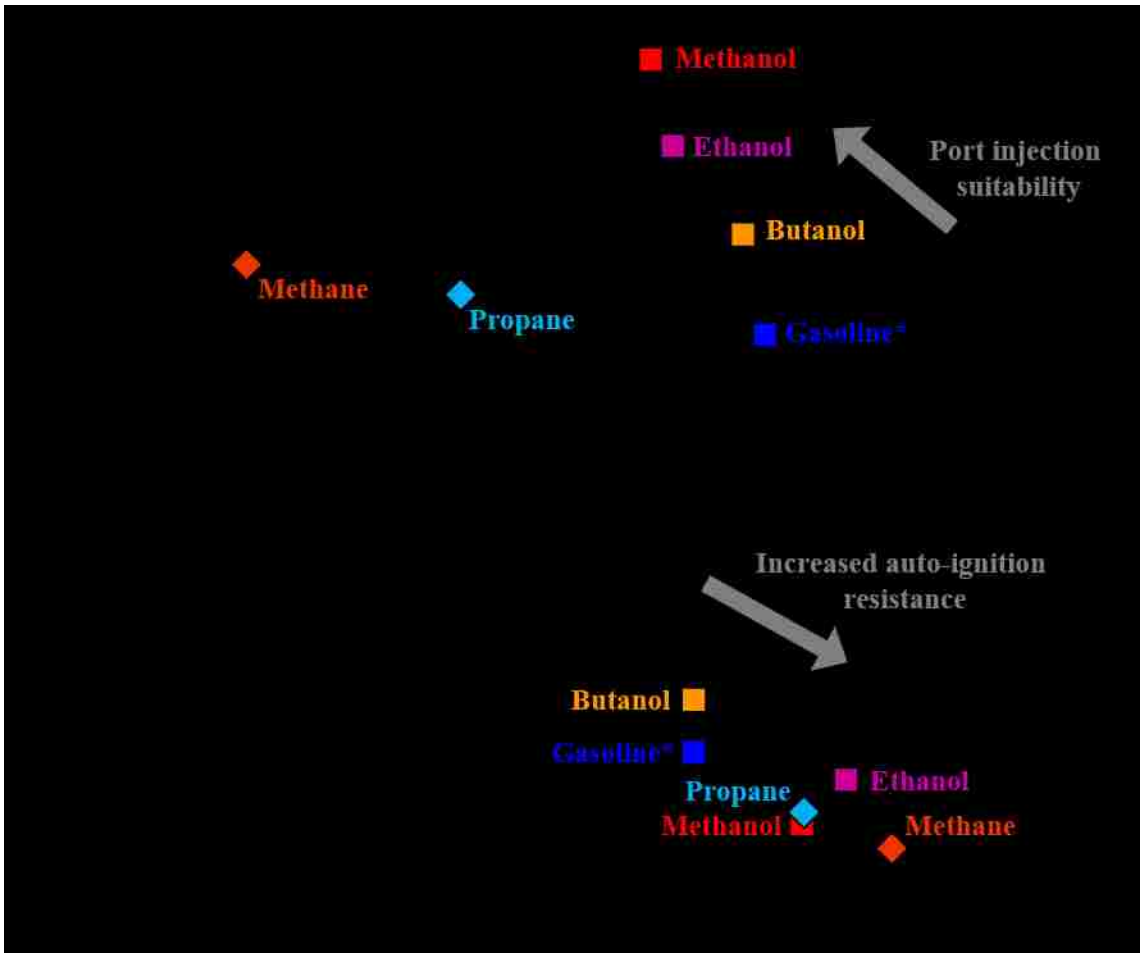

Figure 2.5 Port Injection Suitability and Ignition Properties of Selected Fuels

The fuel with a lower boiling point can readily evaporate and form a homogeneous mixture with the surrounding air inside the combustion chamber. The combustion of this pre-mixed fuel-air mixture generally leads to ultra-low smoke emissions [48]. The NOx emissions can also be low if the mixture is sufficiently lean or diluted [45]. In addition to the low boiling point, if the fuel has a high latent heat of vaporization, the evaporation of this fuel results in the cooling of the cylinder charge [43]. The lower compression-end temperature following the cylinder charge cooling can potentially yield lower combustion temperatures and NO_X emissions [43]. The Cetane number (CN) and the Octane Number

(ON) are often used as standard measures for the ignition quality of fuels in CI and SI engines, respectively. While a high CN typically denotes better auto-ignition characteristics of a fuel, a high ON implies more resistance to auto-ignition [49].

To investigate the suitability of fuel properties for LTC enabling, researchers have tested fuels with a broad range of ignition characteristics, fuel chemistry, and volatility in CI engines [10], [37], [38], [50]–[54]. In general, highly reactive fuels, such as diesel, are better suited for LTC under low load conditions [35]. If fuels with high auto-ignition resistance are employed, the low load LTC operation is challenged by the combustion stability and thermal efficiency penalties [37]. On the contrary, the fuels with a lower reactivity are suitable for high load operation under premixed LTC conditions, while the highly reactive fuels can undergo premature ignition [38], [54]. The overall conclusion from the studies of fuel property effect on CI LTC is that a dynamic modification of fuel reactivity may be necessary for a stable operation over a wide engine operating range [10], [37], [53].

Accordingly, the on-board fuel blending strategies, that incorporate two fuels and two fuel supply systems are studied extensively. These on-board fuel blending strategies are commonly identified as the dual-fuel combustion (DFC) strategies. The DFC strategy typically employs a low pressure port injection system and a high pressure direct injection system [10], [54], [55]. The port injection system prepares a lean and homogeneous air-fuel mixture using a fuel that has a high auto-ignition resistance and high volatility [56]. The direct injection system uses a high reactivity fuel, which acts as a reliable ignition source for the lean and premixed mixture, that is prepared by the port

ignition system [43], [48], [55], [57]–[59]. The ignition and the combustion processes are primarily governed by the ratio between the quantities of the two fuels [10] or by the injection timing of the direct injection fuel [60]–[63].

2.3. Opportunities for Control of Clean Combustion in CI Engines

When low engine-out NO_X and smoke emissions are desired, the control of combustion is more critical, compared to the control of conventional HTC. For enabling clean combustion, precise control over the ignition process is necessary, while also ensuring an adequate time for mixture preparation. If the fuel-air mixture is not sufficiently premixed and lean (or diluted), the HTC regions are difficult to avoid [27]. Moreover, the timing of ignition, relative to the TDC, is critical, because very early ignition can result in high peak cylinder pressures and pressure rise rates [64]. On the contrary, very late ignition can cause combustion instabilities [65].

In general, the mixture preparation and ignition processes are largely controlled by the scheduling of the fuel injection, along with the regulation of intake charge quantity and composition. The electronic engine control systems on modern CI engines provide an effective platform to enable the highly premixed clean combustion [34]. Specifically, the high-pressure common-rail fuel injection system facilitates the precise control over the timing and duration of multiple injection events [66]. The enabling of the LTC strategies, summarized in Figure 2.3, is primarily attributed to the fuel injection flexibility of the high pressure fuel injection system [30]. Moreover, the addition of port injection to the fuel system offers more freedom for the control of fuel delivery, while also permitting the use of two fuels [10], [55]. Thus, the fuel injection system comprises of numerous control

variables, such as number of direct injections, injection timing, injection duration, injection pressure, and port-injection quantity. However, the regulation of these fuel injection variables is generally based on lookup tables [67], which require significant calibration effort [68]. A recent development includes the integration of a cylinder pressure sensor in a glow-plug [69], thereby providing opportunities to develop fuel injection control algorithms based on cylinder pressure feedback [20], [70]–[72].

The air-path control hardware on a modern CI engine is equally complex. With the use of multi-stage turbocharging, high-pressure EGR, and low-pressure EGR, a wide range of intake boost pressures and EGR rates can be employed [73]. The application of simultaneously high intake boost pressures and EGR ratios is possible [74], which is often necessary for the enabling of clean combustion [25]. Furthermore, numerical models, electronic sensors, and actuators are deployed in the air-path, which facilitate the use of model-based air-path control algorithms, such as the regulation of the intake oxygen concentration and air-fuel ratio [67], [75]–[80].

In summary, the literature review highlights that diesel LTC strategies are applicable at low load levels. The engine load range can be extended by dynamically modifying the fuel properties, for instance by employing the DFC strategy. For LTC, a tight control over the engine operating parameters is necessary, including the fuel delivery and air-path parameters. The integration of the cylinder pressure measurement into the engine control system presents a potential for the improvements in the design of the engine control system.

CHAPTER III

3. RESEARCH METHODOLOGY

3.1. Research Targets

The literature review presented in Chapter 2 suggested that the current NO_X and smoke emission regulations could be met with the diesel low temperature combustion (LTC) strategies without exhaust aftertreatment. However, the practical implementation of diesel LTC is restricted by the load limits, thermal efficiency penalties, control challenges, and hardware constraints. The current approach adopted in production diesel engines includes the operation in the HTC regime coupled with the use of selective catalytic reduction (SCR) and diesel particulate filter (DPF) in the exhaust aftertreatment. Low-to-moderate EGR rates are applied to reduce the NO_X emissions, to maintain the low smoke emissions, and to attain the high thermal efficiency.

The CI engines may continue to use complex aftertreatment systems to meet the stringent tailpipe emission regulations in the near future [81]. The proposed NO_X emission regulations of 0.027 g/kW-hr (0.02 g/hp-hr) would require a NO_X aftertreatment efficiency of up to 99.5% [15], which could be cost prohibitive. A combination of in-cylinder emission reduction and exhaust aftertreatment strategies may be required to satisfy the future emission regulations. This dissertation work focuses on the control of in-cylinder reductions of NO_X and smoke, while lowering the associated thermal efficiency penalty. A target value of 0.5 g/kW-hr is selected for the engine-out NO_X emissions across the entire engine load range as a platform to develop dynamic control strategies. In addition, a smoke emission target of 0.05 g/kW-hr is selected to attain

simultaneously low engine-out smoke and NO_X emissions, and thereby to potentially reach the future ultralow emission targets with the combined use of practical aftertreatment techniques. Besides the emission targets, the following operability and stability limits are set:

1. The peak cylinder pressure is limited to 170 bar.
2. The peak pressure rise rate is constrained to 15 bar/°CA.
3. The standard deviation of CA50 (STD_{CA50}) is lower than ±1°CA.
4. The coefficient of variation of IMEP (COV_{IMEP}) is under 5%.

The peak cylinder pressure, in part, is constrained by the noise, vibration, and harshness (NVH) concerns. The peak pressure rise rate is normally limited to 6~8 bar/°CA in light-duty diesel engines, but in heavy-duty diesel engines this upper limit can be increased to 15 bar/°CA [58] with better noise attenuation design. The combustion control and stability targets are adopted to ensure that the cyclic variations are within the normally accepted limits [3].

3.2. Research Methodology

The literature review, on the fuel impacts in CI engines, has highlighted the advantages of the dual-fuel configuration in terms of emission reduction, combustion controllability, and load applicability. Therefore, the single-shot diesel combustion (SSDC) and the dual-fuel combustion (DFC) strategies are investigated in this research, which are then used to develop the dynamic combustion control strategies.

The research methodology is summarized in Figure 3.1; therein the approach adopted to meet the research targets is highlighted. First, parametric analysis is conducted using numerical simulations to help identifying the boundary conditions for the engine experiments, and to develop a better understanding of the experimental results. An EGR calculation routine is developed as a part of the numerical simulations. Expressions are derived for estimating the correlation between EGR application and the change in intake gas composition for both the SSDC and DFC strategies.

The impact of the above combustion strategies on engine thermal efficiency is evaluated at various engine load levels under steady-state testing conditions. In order to maintain the thermal efficiency levels similar to that of the conventional diesel combustion, the SSDC strategy is adopted to achieve the research targets at low-load operating conditions, whereas the DFC strategy is implemented at high load levels.

The results of steady-state tests with both the SSDC and DFC strategies highlight the effectiveness of the diesel injection command for the control of the combustion phasing. Therefore, a controller is developed to regulate the combustion phasing on a cycle-by-cycle basis. The measured cylinder pressure is used as the primary feedback for the design of the control algorithm. A systematic control architecture is subsequently developed to integrate the regulations of the boost, EGR rate, and fuel injection commands, to attain the research targets. The control setpoints are selected referring the parametric analyses and basing on the experimental results. These setpoints are adjusted depending upon the engine load levels. Experiments are conducted to demonstrate the dynamic control with the two combustion strategies at varying IMEP levels.

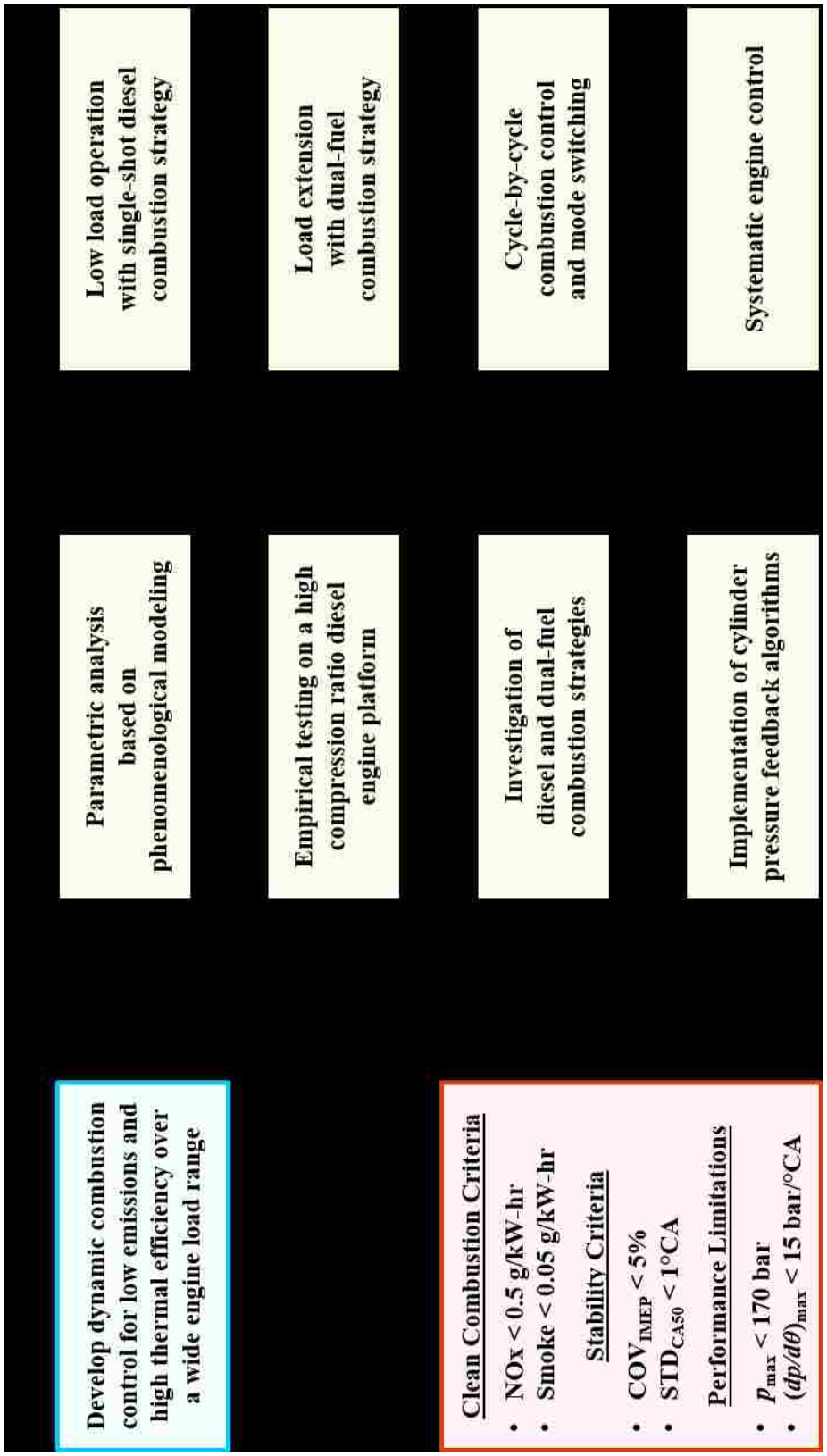

Figure 3.1 Schematic of Research Methodology

3.3. Experimental Setup

The current section presents the detailed descriptions of the test engine setup, the test control system, and the measurement equipment. The procedures for data acquisition and synchronization between the measurement devices are explained, followed by a discussion of the post-processing techniques.

3.3.1. Test Engine

The experiments are mostly performed on a production 2.0 L Ford Puma common-rail diesel engine. The detailed specifications of the test engine are summarized in Table 3.1. The engine is coupled to a non-motoring eddy-current dynamometer. The base engine is modified to separate the intake and exhaust systems of the first cylinder from the other three cylinders. The research and measurements are conducted on the first cylinder like a single cylinder engine, while the remaining three cylinders are operated in the conventional high temperature combustion (HTC) mode. Unlike a motoring dynamometer, a non-motoring dynamometer cannot maintain the engine speed at the desired setpoint if the engine operates below a certain load level. By operating these three cylinders in the stable combustion regime, potentially unstable combustion strategies can be investigated on the research cylinder using this non-motoring dynamometer.

A piezo-electric, un-cooled, and glow-plug mounted pressure transducer (AVL GU-13P) is installed in the research cylinder for in-cylinder pressure measurements. The membrane of the pressure transducer is nearly flush-mounted to minimize the resonance effects in the pressure data.

An external conditioning unit regulates the coolant temperature to a setpoint of 80°C during the tests. The temperature is chosen to represent a fully warmed up engine. The original oil circulation system is used for the lubrication of the engine components. External measurement systems are added for monitoring the oil pressure and temperature. Alarms are in place to warn the operator if the coolant or oil conditions are outside the safe limits.

Table 3.1 Test Engine Specifications

Engine Type	4-cylinder; 4-stroke Ford DuraTorq® Puma
Displacement	1998 cm^3 (499.5 cm^3 / cylinder)
Bore x Stroke	86 mm x 86 mm
Connecting Rod	155 mm
Compression ratio	18.2:1
Peak Cylinder Pressure	170 bar
Injector	Solenoid type 6 holes; Φ: 0.13 mm; Umbrella angle: 155°
Injection System	Delphi common-rail
Rail Pressure	Up to 160 MPa

3.3.2. Intake Boost and EGR System

Figure 3.2 shows a schematic of the test setup outlining the intake boost and EGR components. The intake air is supplied to the research cylinder from an oil-free dry air compressor. An electro-pneumatic pressure regulator is installed in the intake system to control the intake air pressure. An air flow meter is mounted in the intake path that measures the volumetric flow rate of air. An intake surge tank is installed between the flow meter and the intake manifold to isolate the cyclic pulsations generated by the intake valve opening, that may otherwise introduce substantial cyclic variations, in addition to errors in flow rate measurements. The pressure and temperature of the fresh intake air are measured. Using these measurements, the volumetric flow rate is converted to the mass air flow (MAF) rate following the ideal gas law.

An exhaust surge tank is installed in the exhaust path. The surge tank helps to retain a steady backpressure that facilitates a stable EGR flow, in part, by dampening the exhaust pressure waves. The mean exhaust backpressure is regulated using a backpressure valve mounted downstream of the exhaust surge tank. An electro-pneumatic pressure regulator is used to control the opening of the backpressure valve. A diesel oxidation catalyst (DOC) is mounted in the exhaust line upstream of the surge tank to oxidize the CO and HC emissions and, thus, to avoid the potential accumulation of these combustible gases in the surge tank. The research cylinder is also fitted with a high-pressure, cooled EGR system. The EGR path is connected downstream of the exhaust surge tank, but upstream of the backpressure valve. An EGR valve is installed downstream of the EGR cooler. The EGR rate is controlled by simultaneously adjusting the EGR valve opening and the pressure difference between the exhaust tank backpressure and the intake boost pressure.

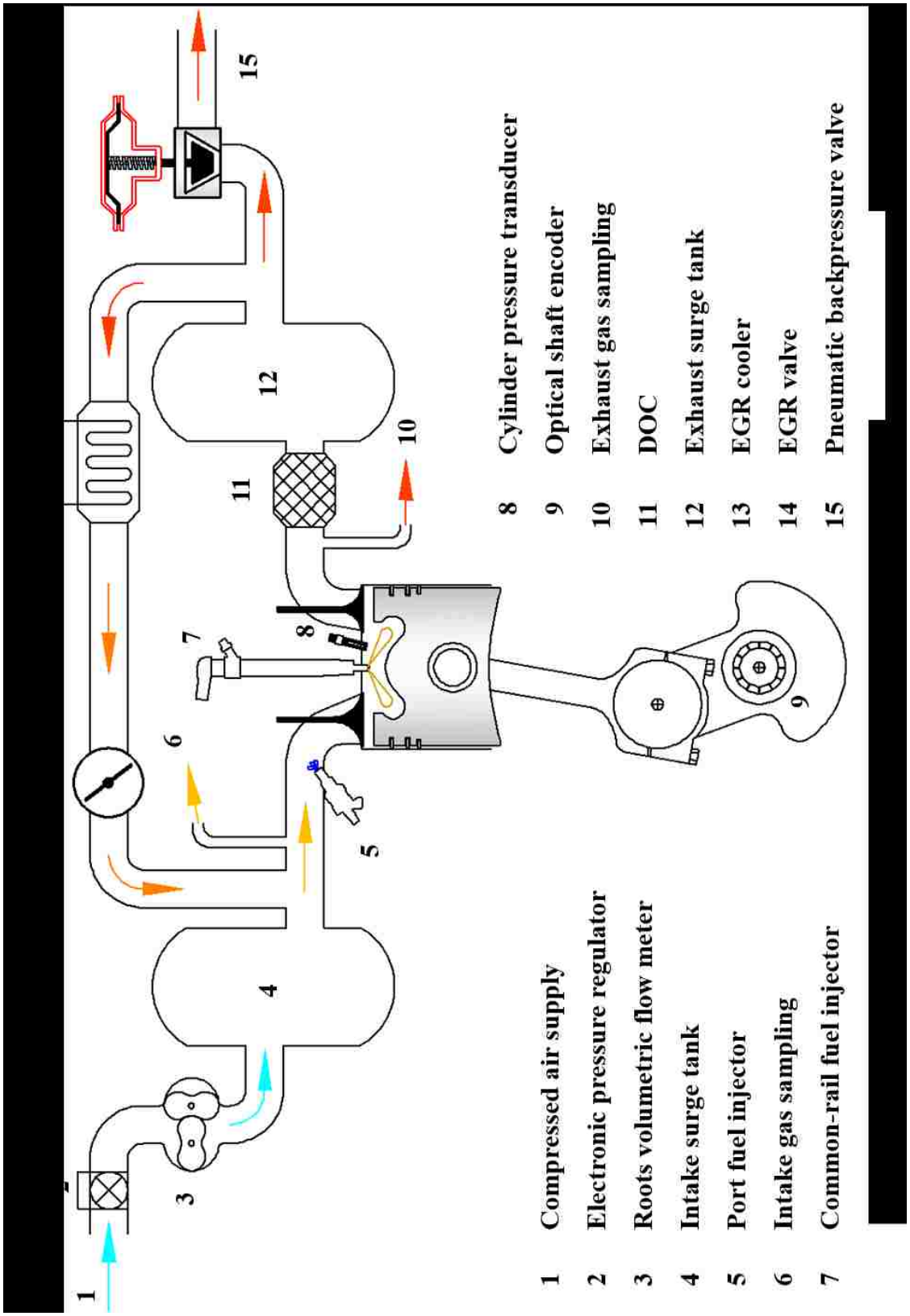

Figure 3.2 Test Engine Setup

3.3.3. Fuel Systems

The fuel systems comprise of a high pressure common-rail diesel direct injection system and a low pressure ethanol port fuel injection system. Figure 3.3 shows a schematic of the fuel systems.

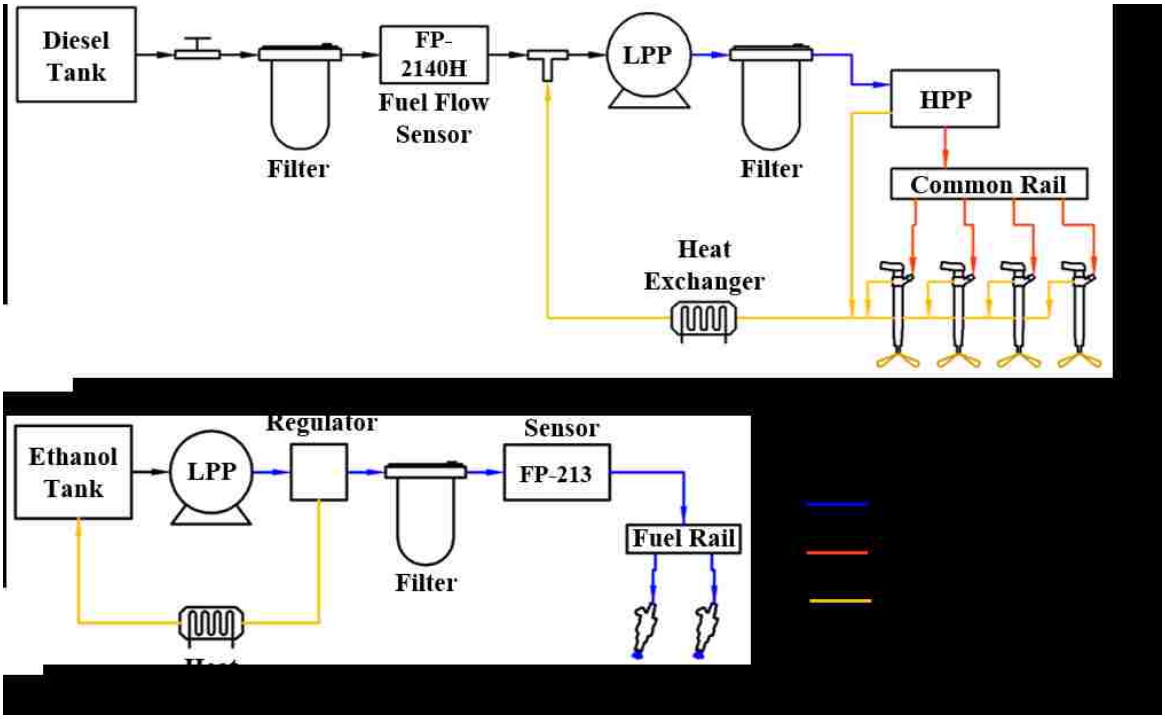

Figure 3.3 Fuel System Schematic

The diesel fuel supply consists of a low pressure line that feeds fuel to the high-pressure pump. The main components of the low pressure circuit are a fuel storage tank, a set of fuel filters, a fuel flow metering sensor, and a low pressure feed pump. The high-pressure pump supplies the diesel fuel to all the four cylinders through the common-rail. The fuel returned from the high-pressure pump and the injectors is cooled using a heat exchanger, prior to being sent back to the upstream of the feed pump, yet downstream of the fuel metering sensor. The common-rail pressure is controlled to a setpoint using a potential

controller. The fuel injection commands for each of the four injectors are independently controlled.

In addition to the common-rail fuel injection, a port fuel injection system is integrated into the test setup to deliver ethanol fuel into the intake runners of the research cylinder. An in-house built low-pressure fuel supply system provides the moderately pressurized ethanol to a fuel rail. An alcohol tolerant fuel metering sensor is installed in the fuel supply line to measure the ethanol flow rate. When the DFC strategy is implemented, both of the diesel and ethanol injections are used in coordination. To facilitate the investigation, an ethanol fraction (χ_{eth}) is defined in Equation (3.1) to indicate the energy contribution from the ethanol fuel, in relevance to the total fuel.

$$\chi_{eth} = \frac{m_{eth} LHV_{eth}}{m_{diesel} LHV_{diesel} + m_{eth} LHV_{eth}} \tag{3.1}$$

where, m_{eth} and m_{diesel} are the measured fuel flow rates of ethanol and diesel, respectively. LHV_{eth} and LHV_{diesel} are the lower heating values (LHV) of the ethanol and diesel. The steady-state volumetric flow measurements are averaged over 60 seconds, which are then converted to a fuel mass flow rate by applying a fixed fuel density conversion using the density of the test fuel. The test fuel specifications, including the LHV and fuel density values, are listed in Table 3.2 [82]–[85]. A more detailed list of fuel properties is included in APPENDIX B.

Table 3.2 Test Fuel Specifications

Fuel	Diesel	Ethanol
Density at 15°C [kg/m³]	846	788
Viscosity at 40°C [cSt]	2.5	1.52
Cetane Number [-]	46.5	8~11
Octane Number [-]	~25	110~115
Lower Heating Value [MJ/kg]	42.1	26.9
Oxygen Content by Mass [%]	0	34.78
Boiling Temperature at Atmospheric Pressure [°C]	246~388	78.3
$C_1H_\beta O_\gamma$ [-]	$C_1H_{1.87}$	$C_1H_3O_{0.5}$

3.3.4. Emission Analyzers

The intake and exhaust gas compositions are measured by a dual-bank gas analyzer system. The sampled exhaust and intake gases are passed through the sample conditioning units consisting of a chiller unit, a heated pump and a series of filters, to provide clear and dry samples to the analyzer benches. The exhaust gas analyzer bench measures the volumetric concentrations of NO_X, HC, CO, CO_2, and O_2 in the exhaust. The intake gas analyzer bench measures the volumetric concentrations of CO_2 and O_2 in the intake flow. The measurements of CO_2 concentration in the intake and exhaust streams are used to

evaluate the EGR ratio. The CO_2 based EGR ratio (r_{CO_2}) is the ratio of the intake CO_2 concentration, $[CO_2]_{int}$, to the exhaust CO_2 concentration, $[CO_2]_{exh}$.

$$r_{CO_2} = \frac{[CO_2]_{int}}{[CO_2]_{exh}} \tag{3.2}$$

The main specifications the emission measurement units are presented in Table 3.3.

Table 3.3 Intake and Exhaust Gas Analyzers

Analyzers Type	Emission type	Range	Model No.
Heated chemiluminescence detector (HCLD)	NO (ppm) NO_2 (ppm)	0-0.3%	CAI Model 600-HCLD
Heated flame ionization detector (HFID)	HC (ppm C_1)	0-0.3%	CAI Model 300M-HFID
Non-dispersive infrared (NDIR) detector	Exh. CO (ppm) and CO_2 (%), Int. CO_2 (%)	0-0.2% and 0-0.5% 0-8% and 0-40% 0-2% and 0-10%	CAI Model 300 CAI Model 200 CAI Model 602P
Paramagnetic detector	Int. O_2 (%), Exh. O_2 (%)	0-25% 0-25%	
Smoke meter	Smoke (FSN)	0-10 FSN	AVL Model 415S

Note: CAI: California Analytical Instruments, Inc.
AVL: Anstalt für Verbrennungskraftmaschinen List

The smoke emissions in the exhaust gases are measured using an AVL smoke meter. The intake gas is sampled from the downstream of the EGR mixing location, and the upstream of the port fuel injection location. The exhaust sampling point is located in the exhaust manifold, upstream of the location of the safeguarding DOC.

In addition to the emission analyzer benches, a production level Bosch NO_X sensor is also installed in the exhaust path. The sensor is mounted on the exhaust pipe downstream of the exhaust backpressure valve, which measures the concentrations of O_2 and NO_X in the exhaust gases. In practical use, the production sensor can give second by second reading [86] that is much faster than the reporting of the laboratory NO_X analyzers.

3.4. Test Management

3.4.1. Air System Management and Data Acquisition

A set of seven desktop computers is used for enabling the control actions, facilitating the data acquisition tasks, and providing an intuitive user interface for the management of the engine tests. The control platform is shown in Figure 3.4.

The desktop computers running Windows® operating systems are equipped with data acquisition (DAQ) devices, each dedicated for certain aspects of the test control and measurement. Each desktop computer executes a control program written in the LabVIEW® programming language. A high speed local Ethernet network forms the communication link between each computer for synchronous data logging. Table 3.4 provides further details of the DAQ devices installed on the desktop computers.

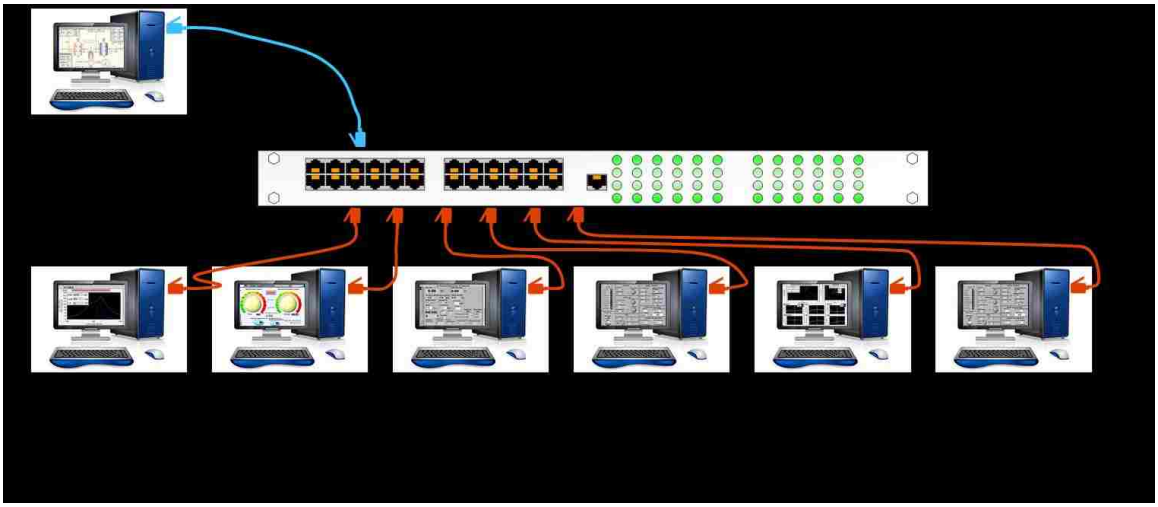

Figure 3.4 Test Control and Data Synchronization

Table 3.4 Summary of Data Acquisition Devices

Computer Tasks	DAQ Devices	Technical Specifications
Cylinder pressure recording	NI PCI-6122	4 AI (Simultaneous), 8 DIO
Boost and EGR control	NI PCI-6229 NI USB-8473 (Two units)	32 AI, 4 AO, 48 DIO High Speed CAN
Air and fuel management	NI PCI-6220	16 AI, 24 DIO
Temperature monitoring	NI SCXI 1102 NI PCI-6220	96 Thermocouple 16 AI, 24 DIO
Emissions monitoring	NI PCI-6229	32 AI, 4 AO, 48 DIO
Real-time heat release analysis	NI PCI 6229	32 AI, 4 AO, 48 DIO

Note: DAQ: Data Acquisition
AI: Analog Input
AO: Analog Output
DIO: Digital Input Output
NI: National Instruments
PCI: Peripheral Component Interconnect
CAN: Controller Area Network
USB: Universal Serial Bus

3.4.2. Cylinder Pressure Measurement and Analysis

The cylinder pressure indicating system consists of a pressure transducer, a charge amplifier (Kistler 5010B) [87], and a crank shaft mounted optical encoder (Gurley 9125S) [88]. The cylinder pressure data acquisition is crank angle resolved with a sampling interval of 0.1°CA, and the data is recorded for 200 consecutive cycles under

stable engine operating conditions. Continuous recording of cylinder pressure data is also conducted for the entire duration of the engine test at a resolution of 1°CA. The data recorded at the higher resolution is used for the analysis of steady-state engine tests, while the continuous recording is primarily used for troubleshooting purposes.

The pressure trace for each engine cycle is analyzed individually for the evaluation of combustion characteristics. First, a second-order low-pass Butterworth filter [89] is applied to the pressure trace. The cut-off frequency of the filter is set to 4000 Hz for the data collected from the test engine. The filtered pressure trace is pegged against the intake manifold pressure at the crank angle of intake valve closing. The filtered and pegged pressure trace is used to calculate the combustion characteristics for each engine cycle. The peak cylinder pressure, the peak pressure rise rate, and the apparent heat release rate (AHRR) are calculated from the filtered cylinder pressure traces. For the online calculation of the AHRR, the heat-transfer, crevice volume effects, and gas composition effects are ignored. The expression for AHRR is presented in Equation (3.3).

$$\frac{dQ_{app}}{d\theta} = \frac{1}{\gamma - 1}\left[\gamma p \frac{dV}{d\theta} + V \frac{dp}{d\theta}\right] \tag{3.3}$$

where, p is the cylinder pressure and V is the cylinder volume at crank angle θ. The ratio of specific heats, γ, is selected as 1.37 for the heat release analysis. The cumulative apparent heat release is calculated by integrating the AHRR between the start of combustion (SOC) and the end of combustion (EOC). The crank angle of 5% apparent heat release (CA05), the crank angle of 50% apparent heat release (CA50), and the crank angle of 95% apparent heat release (CA95) are then identified. The CA50 represents the

crank angle location of the central midway of the combustion event, while the crank angle duration between CA05 and CA95 represents the primary combustion duration (CD). The crank angle duration between the start of the diesel injection and the CA05 is considered as the ignition delay (ID). The net IMEP is calculated for each combustion cycle, and the standard deviation of IMEP (STD_{IMEP}) is computed for the steady-state 200 cycle operation using Equation (3.4).

$$STD_{IMEP} = \sqrt{\frac{1}{n}\sum_{i=1}^{n}(IMEP_i - \mu_{IMEP})^2} \tag{3.4}$$

where, $IMEP_i$ is the IMEP calculated for each engine cycle, and μ_{IMEP} is the average IMEP for 200 consecutive engine cycles. The coefficient of variation of IMEP (COV_{IMEP}) is then calculated, as follows:

$$COV_{IMEP} = \frac{STD_{IMEP}}{\mu_{IMEP}} \tag{3.5}$$

3.4.3. Fuel System Control

Compared to the intake boost and EGR control systems, the fuel system control is required to operate at a much faster rate (in microsecond to millisecond resolution). Furthermore, the fuel control hardware on a research engine must provide the flexibility to regulate the fuel injection pressure and the injection scheduling, and thereby facilitate the investigation of advanced combustion strategies. The fuel injection process has a large impact on the engine operation, whereas a malfunction in the fuel system may result in catastrophic damage. Due to the lack of prompt control over code execution priorities

on a Windows® operating system, the architecture implemented for the air system management is not suitable for fuelling control. Therefore, embedded controllers that run the LabVIEW Real-Time (RT) operating system are employed for the fuel system control. The RT is designed to run applications with very precise timing and a high degree of reliability. The program executed on the RT follows the timing and execution priorities that are set during the programming stage [90]. For the fuel system control, the program that executes on the RT has an update rate equal to the engine cycling frequency, and thus varies deterministically with the engine speed.

The fuelling control architecture is presented in Figure 3.5. The embedded controllers house field-programmable gate array (FPGA) devices that have reconfigurable hardware logic blocks and interconnects. Unlike the RT processor, when the code written for execution on the FPGA is compiled, the logic blocks and interconnections within the FPGA hardware are used. The control program designed for implementing on an FPGA device is transformed into a hardware circuit that performs the logic directly in the hardware. As a result, the FPGA code is truly parallel in nature and the operations including the DAQ tasks are executed on dedicated hardware resources [91]. The FPGA is used for fuelling control. The time resolved regulation of the duration of injection is achieved at a microsecond resolution, while the crank angle resolved control of the start of injection is obtained at a 0.1°CA resolution.

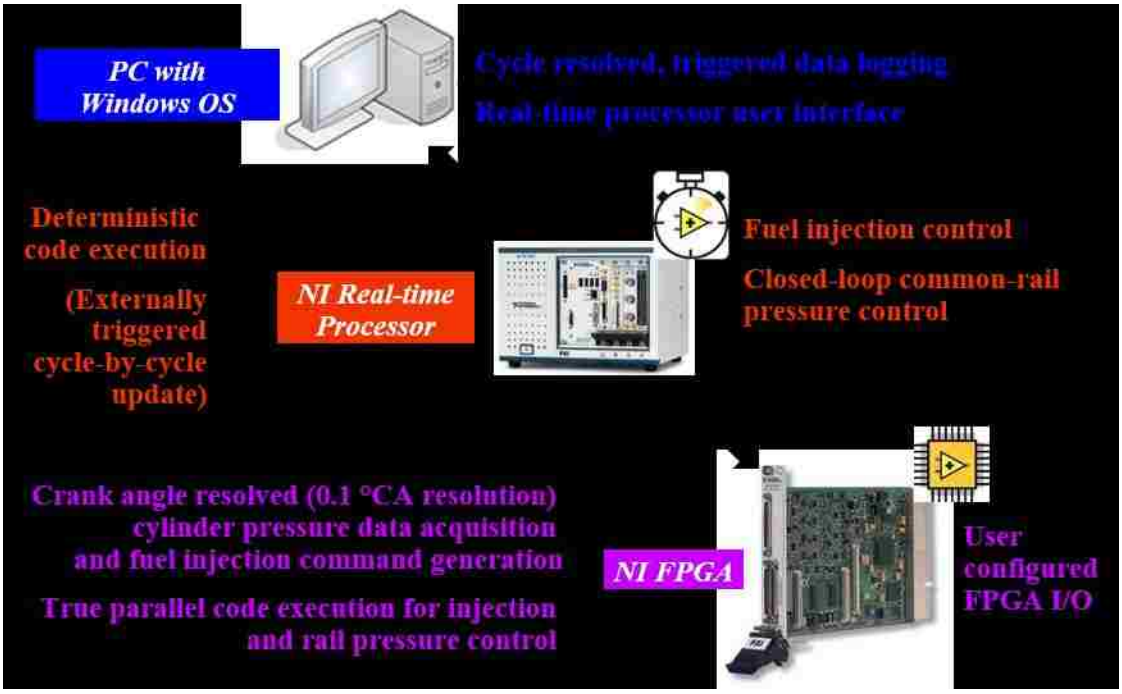

Figure 3.5 Injection Control and Cylinder Pressure Feedback

A schematic of the hardware connections is shown in Figure 3.6. The transistor-transistor logic (TTL) commands are generated on the FPGA using dedicated digital channels. The TTL commands are used to provide control signals for driving the fuel injectors and for controlling the common-rail high-pressure pump. Dedicated digital channels are used for commanding the high-pressure common-rail diesel injection and the low-pressure ethanol injection. The injector power driver modules receive the control TTL signals and energize the injectors accordingly. An independent FPGA code generates the commands necessary for regulating the pressure control valve (PCV) and the volume control valve (VCV) on the high-pressure pump. The control commands are written on digital channels and interface with the power drive units that translate the control commands into the PCV and VCV duty cycles. Apart from generating control commands for the fuel injection system, the FPGA is also used to acquire cylinder pressure data at a 0.1°CA resolution.

The cylinder pressure information acquired by the FPGA is transmitted to the embedded controller via the PCI extensions for instrumentation (PXI) [92] interface.

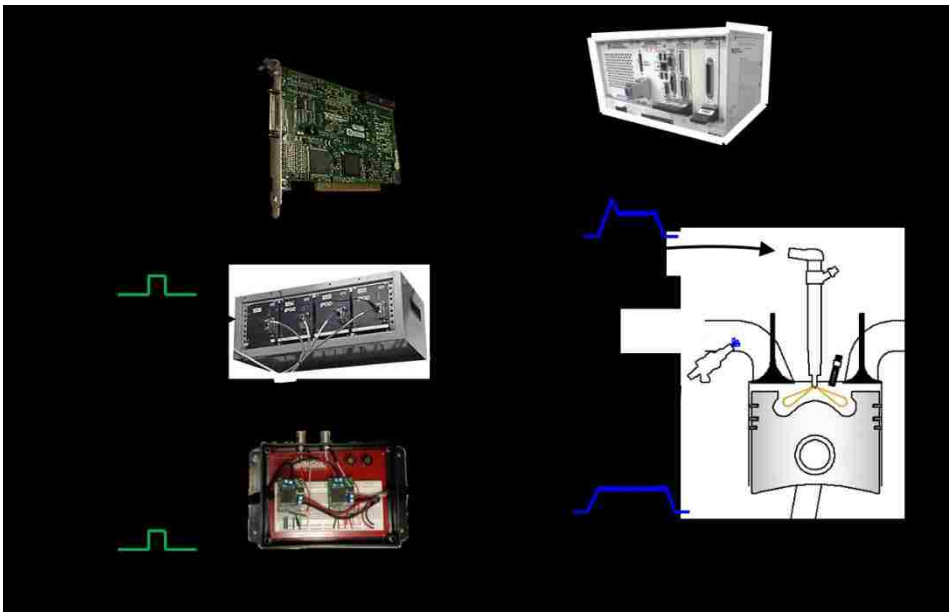

Figure 3.6 Hardware Connections for Injection Control

CHAPTER IV

4. PARAMETRIC ANALYSIS

Parametric calculations are carried out using a zero-dimensional (zero-D) engine cycle simulation program. In the simulation program, thermodynamic principles and empirical correlations are used to track the in-cylinder processes. A simple EGR calculation routine is integrated into the zero-D engine cycle simulations. In the current chapter, first the EGR calculations are discussed. The zero-D engine cycle calculations are then described. Finally, the results of the parametric analysis are presented.

4.1. EGR Analysis

For the EGR calculations, the five primary components of the cylinder charge are considered, namely, N_2, O_2, CO_2, H_2O, and a hydrocarbon fuel, noted as $C_1H_\beta O_\gamma$ [3]. The concentrations of these primary components in the intake and exhaust vary depending on the intake boost, EGR rate, fuel type, and fuel quantity. Although the by-products of combustion, such as CO, HC, NO_X and smoke are crucial from the emission control perspective, the concentrations of these combustion products are usually at negligible levels for EGR ratio calculations, and are not included in this analysis.

4.1.1. Analytical Approach

In the absence of EGR and under the assumption of complete combustion, the combustion reaction can be written as follows. The fuel is expressed as $C_1H_\beta O_\gamma$ to indicate the atom ratios of the fuel.

$$n_f\left(C_1H_\beta O_\gamma\right) + n_{O_2}O_2 + n_{N_2}N_2 \longrightarrow$$
$$n_f CO_2 + \frac{\beta}{2}n_f H_2O + n_{N_2}N_2 + \left(n_{O_2} + \frac{\gamma}{2}n_f - n_f - \frac{\beta}{4}n_f\right)O_2 \tag{4.1}$$

However, when EGR is applied, the combustion reaction is written by considering the presence of CO_2 and H_2O in the intake.

$$n_f\left(C_1H_\beta O_\gamma\right) + n_{O_2}O_2 + n_{N_2}N_2 + n_{H_2O}H_2O + n_{CO_2}CO_2 \longrightarrow$$
$$\left(n_{CO_2} + n_f\right)CO_2 + \left(n_{H_2O} + \frac{\beta}{2}n_f\right)H_2O + n_{N_2}N_2 + \left(n_{O_2} + \frac{\gamma}{2}n_f - n_f - \frac{\beta}{4}n_f\right)O_2 \tag{4.2}$$

The intake charge comprises of a mixture of N_2, O_2, CO_2, and H_2O. The fuel is added to the mixture, which after combustion yields the products that consist of the same gaseous components but in varying concentrations. In Equation (4.2), n_f is the mole number of the fuel, n_{O_2} is the mole number of O_2, n_{N_2} is the mole number of N_2, n_{CO_2} is the mole number of CO_2, and n_{H_2O} is the mole number of H_2O in the intake. The intake molar gas quantities (n_{int}) and the exhaust molar gas quantities (n_{exh}) are calculated as follows,

$$n_{int} = n_{O_2} + n_{N_2} + n_{CO_2} + n_{H_2O} + n_f \tag{4.3}$$

$$n_{exh} = n_{int} + \left(\frac{\gamma}{2} + \frac{\beta}{4}\right) n_f \tag{4.4}$$

A molar analysis is performed at the control system, which comprises of the mixing location of recirculated exhaust gases and fresh air, as shown by the schematic in Figure 4.1. A molar EGR ratio (r_{mol}) is used to express the EGR amount as a mole fraction of the total cylinder charge. r_{mol} can be written as,

$$r_{mol} = \frac{n_{int} - n_{air}}{n_{int}} \tag{4.5}$$

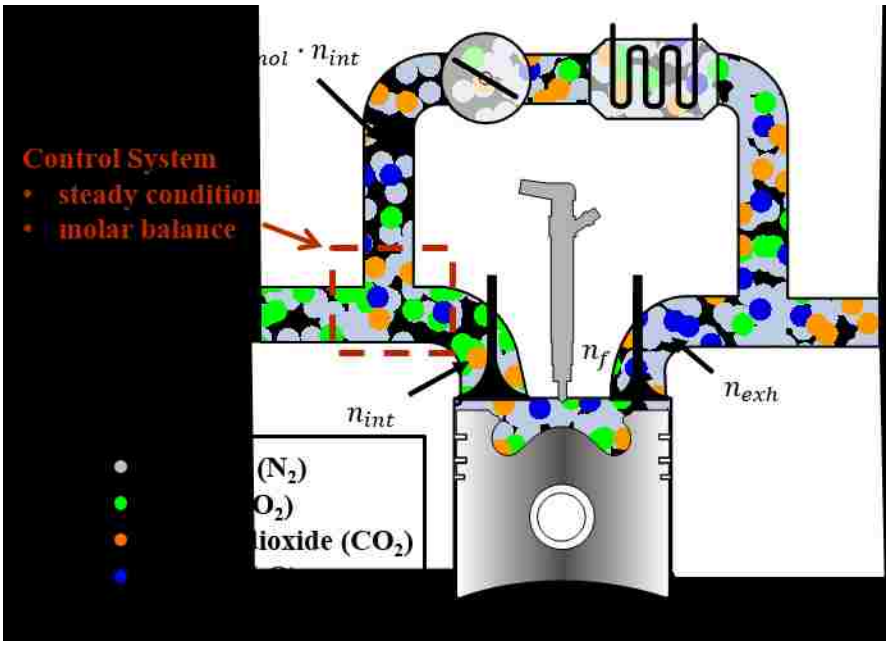

Figure 4.1 Schematic Representation of EGR Molar Balance

By applying the molar balance to the intake manifold as a mixer, expressions for the volumetric concentrations of the individual gases in the intake and exhaust manifolds can be derived by assuming steady flow conditions. The final expressions for the intake O_2 concentration, $[O_2]_{int}$, and the exhaust O_2 concentration, $[O_2]_{exh}$, are listed in

Equations (4.6) and (4.7). The detailed derivations and the expressions for other gas species are included in APPENDIX D.

$$[O_2]_{int} = \frac{[O_2]_{air} \cdot n_{air}\left[1 + \left(\frac{\gamma}{2} + \frac{\beta}{4}\right)\frac{n_f}{n_{int}}\right] + r_{mol}\left(\frac{\gamma}{2} - \frac{\beta}{4} - 1\right)n_f}{n_{air} + \left(\frac{\gamma}{2} + \frac{\beta}{4}\right)n_f} \tag{4.6}$$

$$[O_2]_{exh} = \frac{[O_2]_{air} \cdot n_{air} + \left(\frac{\gamma}{2} - \frac{\beta}{4} - 1\right)n_f}{n_{air} + \left(\frac{\gamma}{2} + \frac{\beta}{4}\right)n_f} \tag{4.7}$$

where, $[O_2]_{air}$ is the volumetric concentration of O_2 in ambient air.

By assuming the primary composition of the intake gases behaving like thermodynamic ideal gas, the n_{int} is correlated to the intake manifold temperature (T_{int}), pressure (p_{int}), and cylinder volumetric efficiency (η_V) [3], as shown in Equation (4.8).

$$n_{int} = \eta_V \frac{p_{int} \cdot V_s}{\bar{R} \cdot T_{int}} \tag{4.8}$$

where, V_s is the swept volume and $\bar{R}$ is the ideal gas constant.

The EGR analysis is developed using a fuel formula $C_1H_\beta O_\gamma$. However, for fuels such as diesel, the fuel formula is solely a representation of the atom ratios of C, H, and O of the fuel.

4.1.2. Air-fuel Ratio Considerations

The air excess ratio (λ) is commonly used to represent the strength of the air-fuel mixture. However, this concept needs to be revisited when the intake air is diluted with the recirculated exhaust gases. Two air excess ratio terms are adopted from [93] to address the effect of EGR application on the air-fuel ratio. The air excess ratio based on fresh air is called the *fresh air excess ratio* (λ_{air}). The air excess ratio that accounts for the EGR is called the *in-cylinder air excess ratio* ($\lambda_{in\text{-}cyl}$). Using the EGR analysis adopted in this work, an expression for the fresh air excess ratio is presented in Equation (4.9). The derivation of the expression is presented in APPENDIX D.

$$\lambda_{air} = \frac{1 + C_f[O_2]_{exh}}{\left(\frac{[O_2]_{air} - [O_2]_{exh}}{[O_2]_{air}}\right)} \tag{4.9}$$

where C_f is a constant for a given fuel depending on the fuel formula.

$$C_f = \frac{\left(\frac{\gamma}{2} + \frac{\beta}{4}\right)}{\left(1 + \frac{\beta}{4} - \frac{\gamma}{2}\right)} \tag{4.10}$$

Similarly, the in-cylinder air excess ratio is,

$$\lambda_{in-cyl} = \frac{1 + C_f[O_2]_{exh}}{\left(\frac{[O_2]_{int} - [O_2]_{exh}}{[O_2]_{int}}\right)} \tag{4.11}$$

It should be noted that the in-cylinder residual gas effect is still not considered in Equation (4.11).

4.1.3. Extension to Dual-fuel Combustion

When the dual-fuel combustion (DFC) strategy is considered, the EGR analysis can be complicated due to the different fuel compositions and the varying fuel quantities. The EGR analysis for the DFC scenario can be greatly simplified by defining an equivalently blended fuel, $C_1H_\beta O_\gamma$. The fuel produces the same ratios of moles of the primary exhaust gas components when it replaces the two test fuels.

The two fuels used for the current DFC analysis are represented as follows:

1. $C_1H_{\beta_1}O_{\gamma_1}$
2. $C_1H_{\beta_2}O_{\gamma_2}$

The combustion reactions for the dual-fuel scenario can be written as,

$$\begin{aligned} &n_{f_1}\left(C_1H_{\beta_1}O_{\gamma_1}\right) + n_{f_2}\left(C_1H_{\beta_2}O_{\gamma_2}\right) + n_{O_2}O_2 + n_{N_2}N_2 + n_{H_2O}H_2O + n_{CO_2}CO_2 \\ &\longrightarrow \left(n_{O_2} + \frac{\gamma_1}{2}n_{f_1} + \frac{\gamma_2}{2}n_{f_2} - n_{f_1} - n_{f_2} - \frac{\beta_1}{4}n_{f_1} - \frac{\beta_2}{4}n_{f_2}\right)O_2 + \\ &\left(n_{CO_2} + n_{f_1} + n_{f_2}\right)CO_2 + \left(n_{H_2O} + \frac{\beta_1}{2}n_{f_1} + \frac{\beta_2}{2}n_{f_2}\right)H_2O + n_{N_2}N_2 \end{aligned} \tag{4.12}$$

In Equation (4.12), n_{f_1} and n_{f_2} are the mole numbers of the two fuels. A molar fuel ratio, $\bar{\chi}$, is defined as the ratio of the mole number of one fuel to the total moles of the two fuels.

$$\bar{\chi} = \frac{n_{f_2}}{n_{f_1} + n_{f_2}} \tag{4.13}$$

$\bar{\chi}$ can be derived from the fuel energy fraction, χ, defined in Equation (3.1). By comparing Equation (4.12) to Equation (4.2), the following expressions can be derived for the equivalently blended fuel.

$$n_f = n_{f_1} + n_{f_2} \tag{4.14}$$

$$\beta = \beta_2 \cdot \bar{\chi} + \beta_1(1 - \bar{\chi}) \tag{4.15}$$

$$\gamma = \gamma_2 \cdot \bar{\chi} + \gamma_1(1 - \bar{\chi}) \tag{4.16}$$

Using the equivalent fuel formulation, if the fuel energy fraction is known, the EGR analysis from the previous subsections can be directly applied to the dual-fuel strategy.

4.2. In-cylinder Processes

The EGR analysis is integrated into a zero-D thermodynamic calculation. The in-cylinder process, from intake valve closing (IVC) to exhaust valve opening (EVO), is analyzed by considering the combustion chamber as a closed system that exchanges heat and work with the surrounding [3], [94]. The first law of thermodynamics is applied to the closed system. The test engine specifications are used to set up the simulation. The mass and composition of the trapped gas are fixed at IVC. An energy balance is carried out at discrete time-steps of 1°CA between the IVC and EVO. The details of the model calculations are presented in this subsection, while a description of the calculation routine is included in APPENDIX D.

The first law of thermodynamics is applied to the control volume as follows:

$$dU = dW + dQ_{ht} + dQ_f \tag{4.17}$$

where, dU is the change in the internal energy of the control volume during the calculation interval, dW is the boundary work associated with the piston displacement, dQ_{ht} is the cylinder wall heat transfer, and dQ_f is the energy released during combustion.

The changes in the volume and the instantaneous pressure are used to quantify the piston work.

$$dW = pdV \tag{4.18}$$

The piston cranking mechanism yields the relation between the cylinder volume, V, and the crank angle, θ [94].

$$V = V_c + \frac{V_s}{2}\left[1 + \frac{l}{a} - cos(\theta) - \left(\left(\frac{l}{a}\right)^2 - sin^2(\theta)\right)^{1/2}\right] \tag{4.19}$$

where, V_c is the combustion chamber volume, V_s is the displacement volume, l is the connecting rod length, and a is the crank radius. V_c is also the clearance volume during the gas exchange process for a 4-stroke engine.

The Woschni's wall heat transfer model [94] is used to calculate the heat loss. The model is summarized as follows,

$$dQ_{ht} = h_w A_s [T - T_{wall}] \tag{4.20}$$

where,

$$h_w = C_1 B^{-0.2} p^{0.8} T^{-0.55} w^{0.8} \tag{4.21}$$

while,

$$w = C_2 S_p + \frac{V_d T_{ref}}{p_{ref} V_{ref}} [p - p_{mot}] \tag{4.22}$$

A_s is the combustion chamber surface area, B is the cylinder bore diameter, S_p is the mean piston speed, and p_{mot} is the instantaneous motored cylinder pressure in the absence of combustion. T_{ref}, p_{ref}, and V_{ref} are the reference states used for calculating the heat transfer following the combustion event. The wall heat transfer coefficients, C_1 and C_2, and the combustion chamber wall temperature, T_{wall}, are selected to match the simulated cylinder pressure traces with the measured cylinder pressure traces for the test engine. These heat transfer coefficients are fixed during the simulation study.

In Equation (4.17), dQ_f is a representation of the energy released during combustion. The Wiebe function [94] is used to impose a fuel burn profile for the calculation of the combustion energy release. The function is presented as follows,

$$x_i = 1 - exp\left[-\sigma_1 \left(\frac{\theta - \theta_{SOC}}{CD}\right)^{\sigma_2}\right] \tag{4.23}$$

where, x_i is the normalized cumulative heat release. The shape of the heat release may be changed by varying the coefficients σ_1 and σ_2. The location of the heat release and the combustion duration can be varied by adjusting the parameters for the crank angle of start of combustion (θ_{SOC}) and the combustion duration (CD). The rate of heat release is,

$$dQ_f = \frac{dx_i}{d\theta} n_f LHV_f \tag{4.24}$$

where, LHV_f is the lower heating value of the fuel on a molar basis. For representing a multi-stage combustion event, multiple Wiebe type functions are combined.

4.3. Results of Parametric Analysis

4.3.1. Interactions Among Intake Boost, EGR, and Fuelling Amount

Simulations are carried out to understand the interactions among the intake boost pressure, the EGR rate and the fuelling amount. First the intake boost pressure and the fuel quantity are varied, while maintaining a fixed EGR level. A contour map is shown in Figure 4.2, in which the intake O_2 concentration and the in-cylinder air excess ratio are plotted against the intake boost pressure and the IMEP levels. Calculation points 'A' and 'B' are marked to explain the results. At point 'A' an IMEP of 6.5 bar is attained at an intake boost level of 2 bar absolute and an EGR level of 40%. The intake O_2 concentration and the in-cylinder air excess ratio at this point are 18% and 4.1, respectively. When the fuel quantity is increased while maintaining a fixed intake boost level, an IMEP of 15.5 bar is obtained at calculation point 'B'. At this point, the intake O_2 concentration is reduced to 14% and the in-cylinder air excess ratio is 1.4.

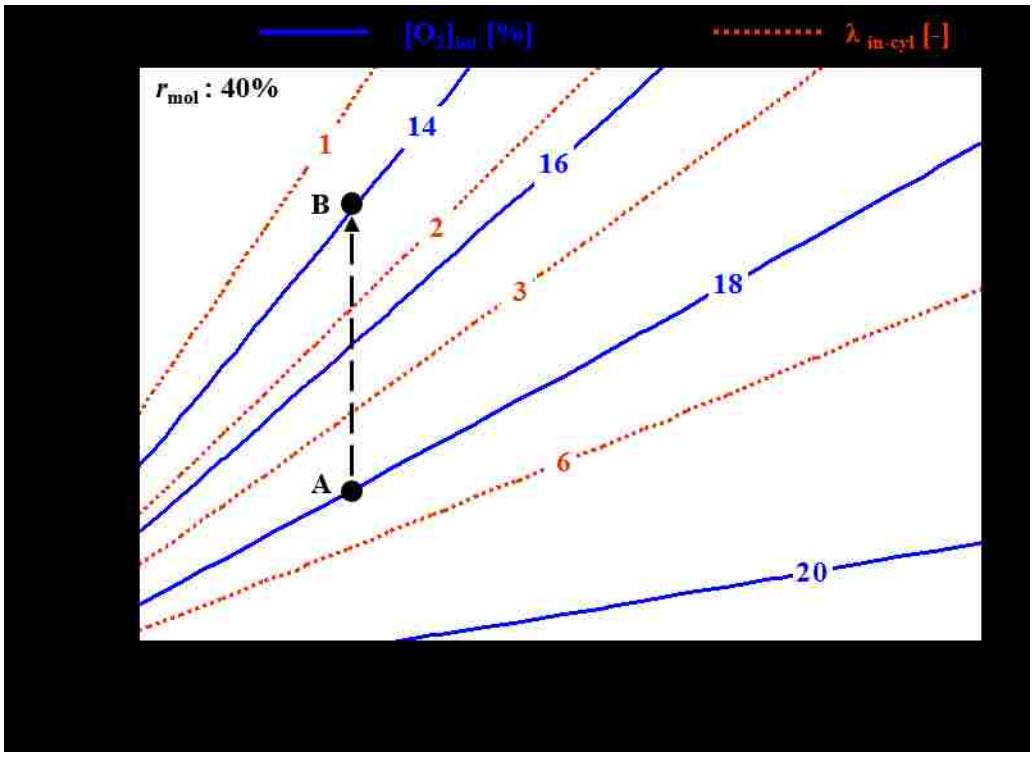

Figure 4.2 Effect of p_{int} and IMEP on p_{max} and $\lambda_{in\text{-}cyl}$ at 40% EGR

The EGR ratio and the fuel quantity are then varied, while the intake boost pressure is held constant. A contour map of intake O_2 concentration and in-cylinder air excess ratio is shown in Figure 4.3, in which the EGR ratio and the IMEP are the variables. The calculation points 'A' and 'B' are marked on the contour map, which represent the same calculation points as those marked in Figure 4.2. When the engine load level is increased to 16 bar IMEP by simultaneously reducing the EGR level to attain point 'C', the same intake O_2 concentration of 18% can be maintained. However, the in-cylinder air excess ratio reduces to nearly 2 at point 'C'. A higher in-cylinder air excess ratio may be attained at this condition by simultaneously increasing the intake boost pressure.

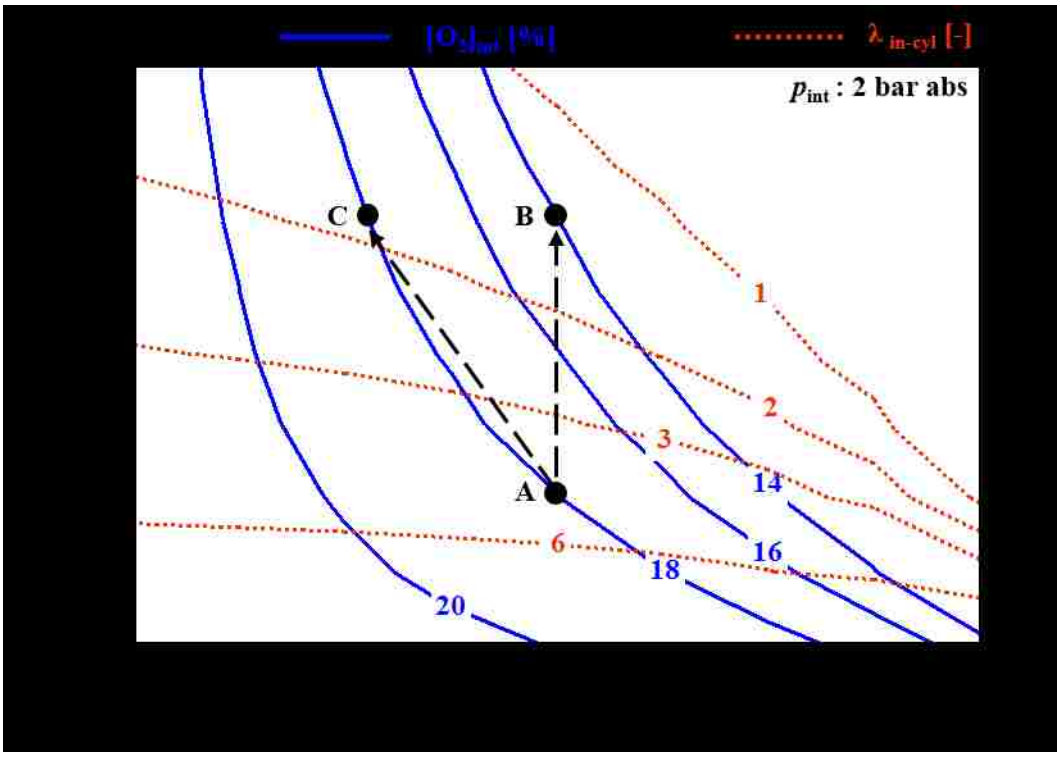

Figure 4.3 Effect of EGR and IMEP on $[O_2]_{int}$ and $\lambda_{in\text{-}cyl}$

Based on the simulation results presented in this subsection, some major considerations for the application of EGR can be summarized. First, when the fuel amount is increased without changing the intake boost level at a fixed EGR ratio, the in-cylinder O_2 concentration and the in-cylinder air excess ratio simultaneously reduce. Second, if a fixed in-cylinder O_2 concentration is to be maintained at a certain intake boost level, the EGR ratio should be reduced when the fuel amount is increased. Finally, when the EGR level is increased at a fixed intake boost pressure, the maximum attainable IMEP is reduced due to a lower in-cylinder air excess ratio.

4.3.2. Impact of Heat Release Patterns

Closed-cycle simulations are conducted to evaluate the influence of heat release profiles on the engine performance. The impacts of phasing and shaping of heat release on the

thermal efficiency and the peak pressure rise rate are evaluated using the simulations. The effects of heat release phasing and combustion duration on the indicated thermal efficiency and peak pressure rise rate are shown in Figure 4.4 by the simulation. The contours of thermal efficiency suggest that the combustion phasing has a much stronger impact on the efficiency than the combustion duration. An excessively long combustion duration can result in the deterioration of thermal efficiency. The thermal efficiency is the highest when the combustion phasing is within 366°CA to 372°CA for the simulated engine geometry and input conditions.

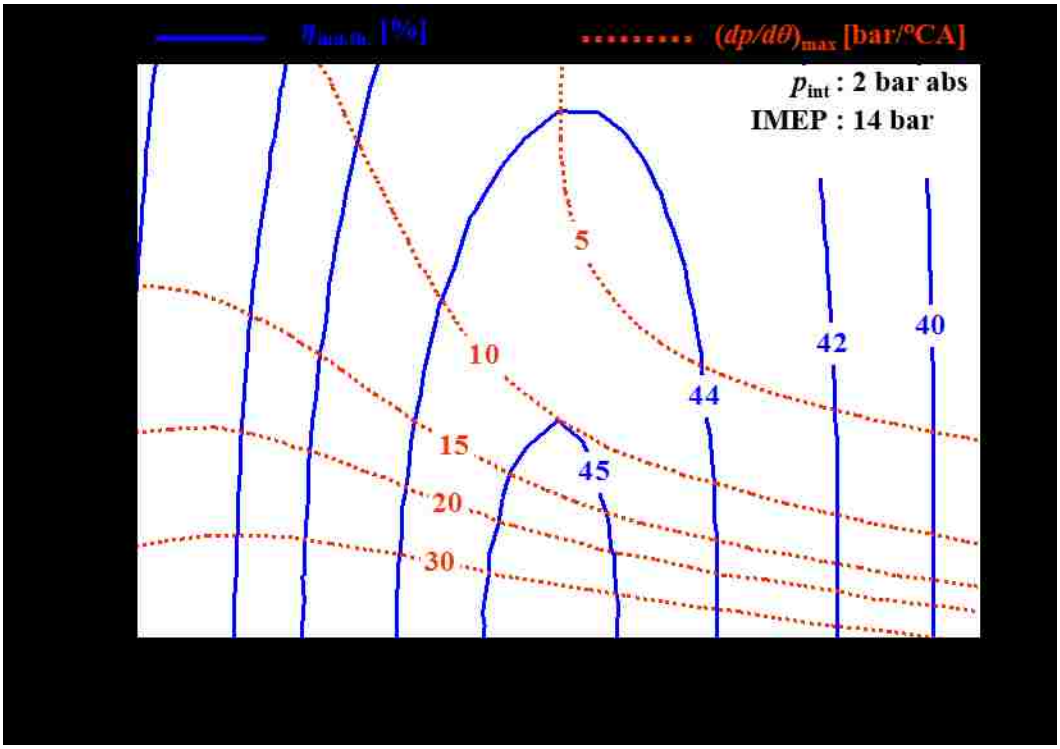

Figure 4.4 Effect of CA50 and CD on Thermal Efficiency and $(dp/d\theta)_{max}$

The combustion phasing and duration also influence the peak pressure rise rate. The peak pressure rise rate increases as the combustion duration becomes short, regardless of the

combustion phasing. Moreover, as the combustion phasing is advanced, the peak pressure rise rate increases substantially.

Besides the combustion phasing and duration, the shape of the heat release rate can also influence the thermal efficiency and the peak pressure rise rate. Two combustion shape metrics are defined to parameterize the heat release shape. For a two stage heat release, a heat release duration ratio ($\overline{CD}$) is defined as the duration of the first stage of heat release normalized against the total heat release duration, as shown in Equation (4.25).

$$\overline{CD} = \frac{CD_1}{CD} \tag{4.25}$$

where, CD_1 is the crank angle duration of the first stage of heat release and CD is the total combustion duration. Further, the heat release energy ratio ($\overline{HR}$) is defined as the ratio of the heat release during the first stage (HR_1) to the total heat release (HR) as shown by Equation (4.26). Based on Equation (4.25) and Equation (4.26), a value of zero or 100% for the shape parameters of heat release represents a single stage heat release profile.

$$\overline{HR} = \frac{HR_1}{HR} \tag{4.26}$$

The heat release duration ratio and the heat release energy ratio are varied with the shaping parameters in Figure 4.5 and Figure 4.6. Two Wiebe functions are employed to generate the two stages of heat release.

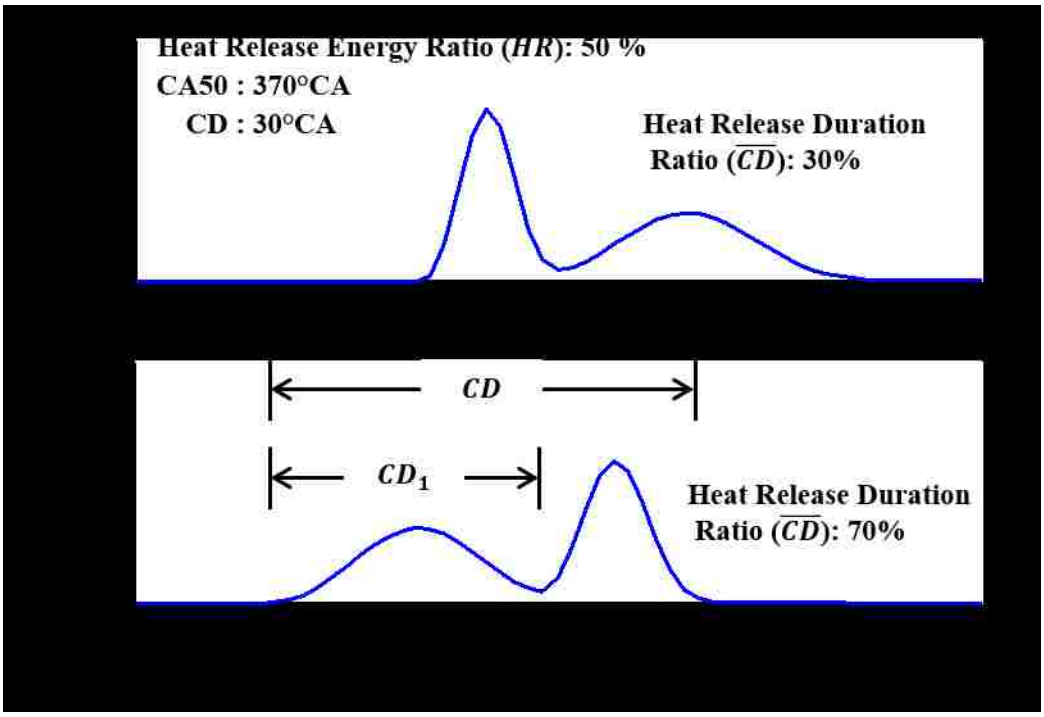

Figure 4.5 Illustration of Heat Release Duration Ratio

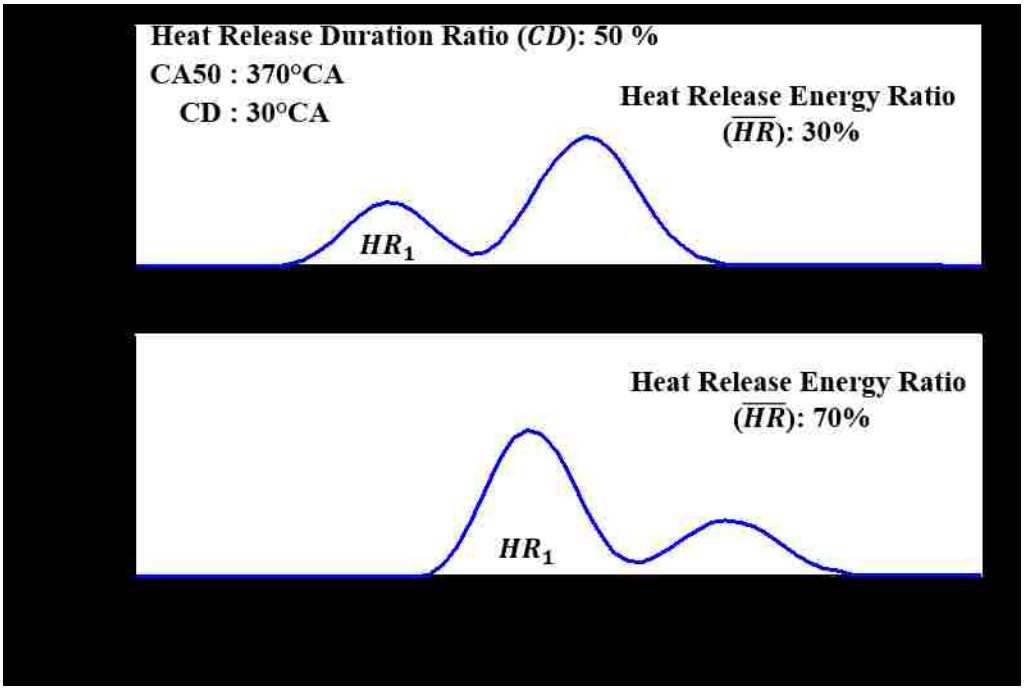

Figure 4.6 Illustration of Heat Release Energy Ratio

Figure 4.7 shows the simulated peak pressure rise rate when the energy ratio of the two stage heat release varies. If the durations of the two stages of heat release are equal, the lowest peak pressure rise rate is attained when the second stage contains nearly 70% of the total fuel energy. The combustion phasing and duration, along with the IMEP, can influence the pressure rise rate. Even so, the results suggest that a larger heat release in the second stage can obtain a lower pressure rise rate at an overall optimum combustion phasing.

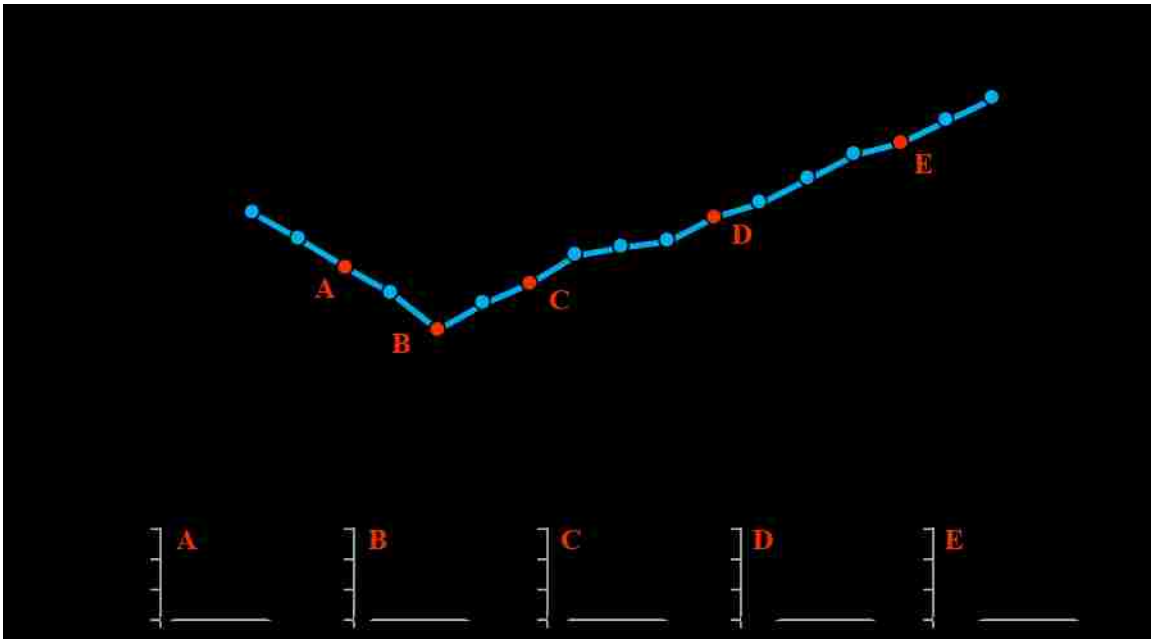

Figure 4.7 Heat Release Energy Ratio Effect on $(dp/d\theta)_{max}$

Figure 4.8 shows contour plots of peak pressure rise rate when both the heat release energy ratio and the heat release duration ratio are varied at a fixed combustion phasing and duration. If the first stage of heat release carries a smaller fraction of the total fuel energy, a relatively shorter duration of the first stage of heat release is desirable to attain

low pressure rise rates. Similarly, if a larger fraction of the total fuel energy is released during the first stage of heat release, the duration should be substantially longer.

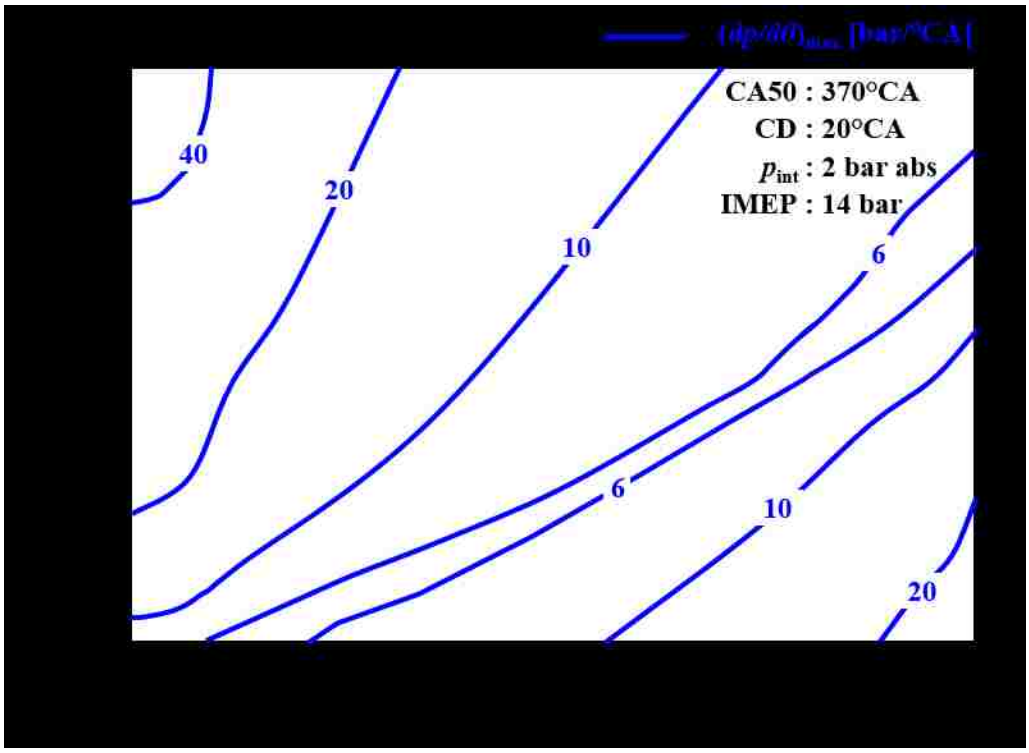

Figure 4.8 Effect of Heat Release Shape on $(dp/d\theta)_{max}$

4.3.3. Combustion Efficiency Effect

The calculations conducted in the previous sections assumed complete combustion. The assumption of complete combustion may be acceptable for diesel HTC where the combustion efficiency can exceed 99.5% [95]. However, the consideration of incomplete combustion is important for the clean combustion strategies, in which the combustion inefficiency can contribute significantly to the thermal efficiency penalty. The combustion efficiency is calculated by accounting for the energy associated with the increase in the HC and CO emissions in the exhaust. Thereby, only the evaporative HC is counted, whereas the heavy HC, soot, and hydrogen emissions are not considered.

Moreover, the HC that escape to the oil sump are also not counted. The expression used for the calculation of combustion efficiency is presented as follows:

$$\eta_{comb} = 1 - \left(\frac{m_{HC} \cdot LHV_{HC} + m_{CO} \cdot LHV_{CO}}{m_f \cdot LHV_f} \right) \tag{4.27}$$

where, m_{HC} and m_{CO} are the mass quantities of HC and CO in the exhaust, while m_f is the mass of fuel. The LHV of diesel fuel (LHV_f) is used as the LHV of HC emissions (LHV_{HC}). The LHV of CO (LHV_{CO}) is assigned to the CO emissions. The calculation results are plotted in Figure 4.9.

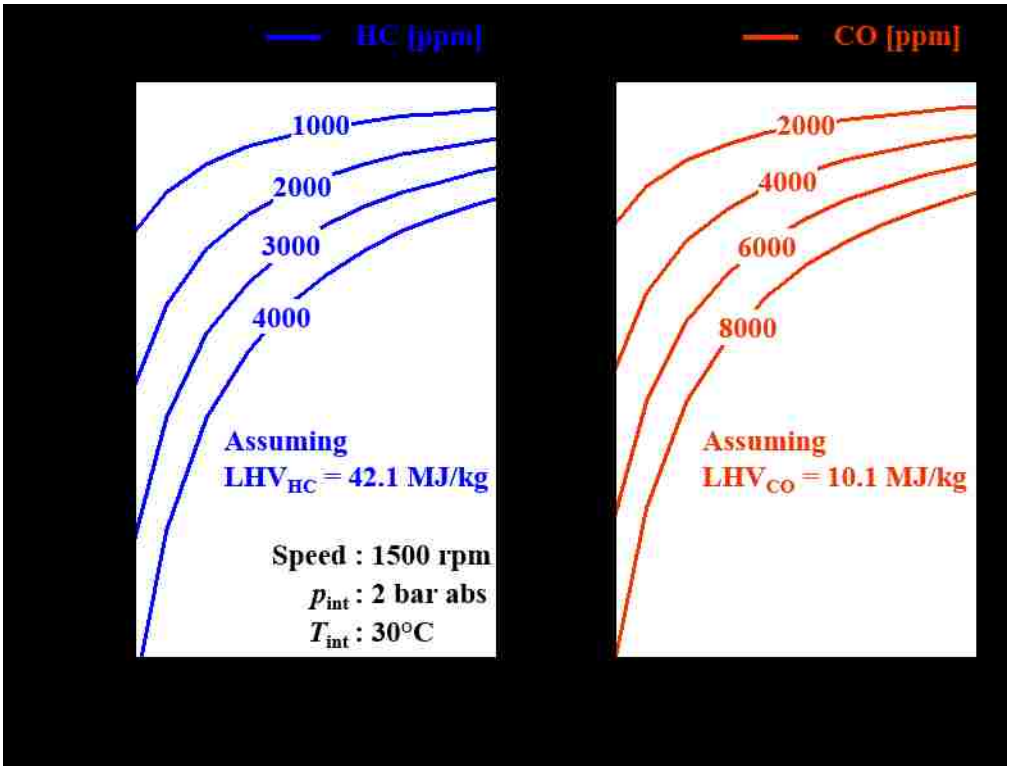

Figure 4.9 Combustion Efficiency Penalty from Exhaust HC and CO

The results show that the HC emissions cause a larger combustion efficiency penalty at a lower IMEP, than at a higher IMEP. For instance, 1000 ppm of HC in the exhaust

translates to nearly 98% combustion efficiency at 10 bar IMEP, whereas the same HC concentration at 4 bar IMEP results in 94% combustion efficiency. Comparable results are obtained by calculating the combustion efficiency associated with the CO emissions in the exhaust.

4.4. Summary of Parametric Analysis

A detailed EGR analysis is conducted to evaluate the effectiveness of EGR on the reduction of intake O_2 concentration. Thereafter, the EGR correlations are extended to account for the DFC. The EGR analysis is integrated into a zero-D simulation routine for the calculation of the in-cylinder parameters. Parametric analyses are conducted via simulation, for the influence of EGR, intake boost pressure, and fuel quantity on the intake O_2 concentration and in-cylinder air excess ratio. The impacts of heat release parameters on the thermal efficiency and peak pressure rise rate are studied by varying the heat release phasing, duration, and shape. The fuel penalties associated with HC and CO emissions are studied to evaluate the effect of their concentrations on the combustion efficiency at different engine load levels.

The parametric simulation results provide certain guidelines for the experimental testing, e.g. for setting up the safe operating limits. The parametric calculations are referenced in later chapters for developing a better understanding of the engine test results and for designing model-based control strategies.

CHAPTER V

5. TESTING OF DIESEL AND DUAL-FUEL COMBUSTION

Engine tests are conducted by employing single-shot diesel combustion (SSDC) and dual-fuel combustion (DFC) strategies. For the SSDC strategy, the common-rail fuel injection system is employed to deliver diesel fuel near the TDC. For the DFC strategy, the direct injection of diesel is accompanied by the intake port injection of ethanol. The application of EGR and the modulation of diesel injection timing are selected as the primary emission control techniques for the SSDC strategy. For the DFC strategy, in addition to the application of EGR and the adjustment of diesel injection timing, the regulation of the ethanol-to-diesel ratio is selected as an emission control technique.

The impact of the emission control techniques on the thermal efficiency and the performance constraints, such as the peak cylinder pressure, the peak pressure rise rate, and the combustion stability, are evaluated at varying engine load levels. Suitable engine operating ranges for the two combustion strategies are identified to reduce the thermal efficiency penalty associated with the attainment of ultra-low NO_X and smoke emissions. The use of high fuel injection pressure and high intake boost pressure can suppress the smoke emissions. However, high fuel injection pressures can lead to increased power consumption for the high-pressure pump [81]. The intake boost pressure is typically constrained by the turbocharging system and the cylinder pressure limits of the engine hardware [31]. Therefore, an attempt is made to employ the minimum yet sufficient injection pressure and boost pressure for the realization of low NO_X and smoke emissions.

5.1. Single-shot Diesel Combustion at Low Engine Load

5.1.1. Impact of EGR at Fixed Fuel Injection Timing

Engine tests are conducted to study the effect of EGR on emissions and efficiency at an intake boost pressure of 1.5 bar absolute and a fuel injection pressure of 90 MPa. During the engine test, the EGR ratio is varied while the injection timing and duration are fixed. Previous research on the use of EGR has suggested that a lower intake O_2 concentration significantly reduces the NO_X emissions [8], [96]. As the EGR ratio is increased at a fixed intake boost pressure and a fixed fuelling quantity, the intake O_2 concentration subsequently reduces. Therefore, in Figure 5.1, the indicated smoke and NO_X emissions are plotted against the measured intake O_2 concentration for the EGR sweeping test.

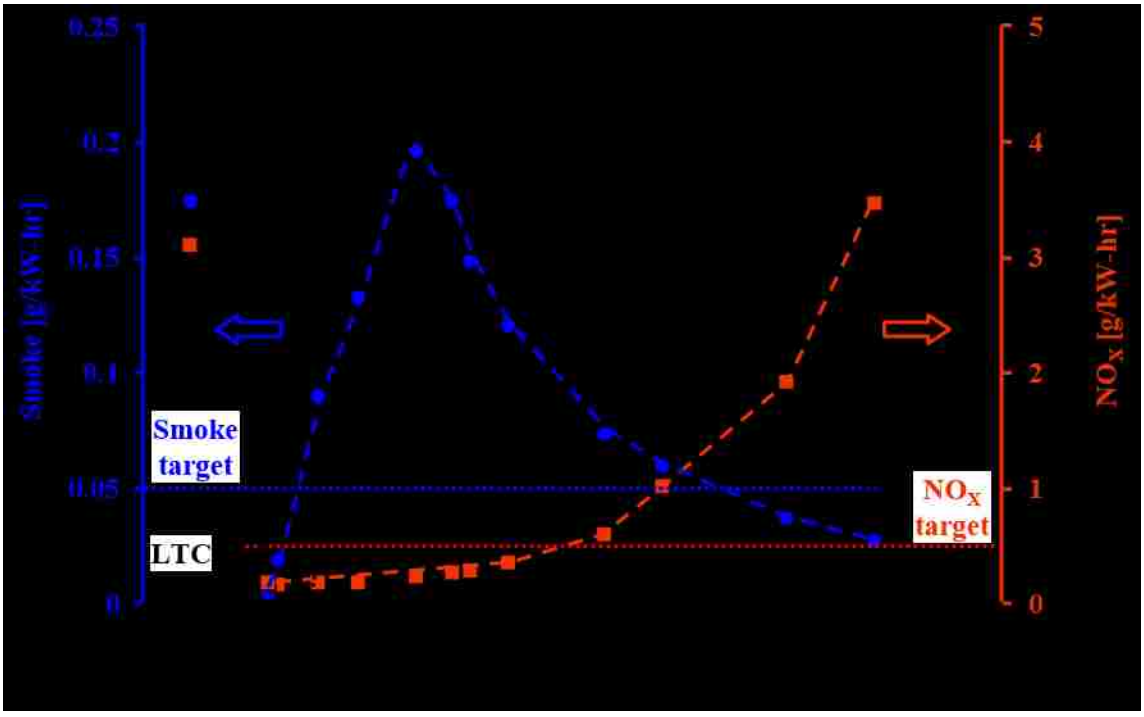

Figure 5.1 SSDC – EGR Sweep: NO_X and Smoke

The NO_X-smoke trade-off is observed, in which the reduction of NO_X is accompanied by an increase of smoke, until the intake O_2 concentration is lower than 13%. When the intake O_2 concentration is reduced below 13%, the smoke begins to drop while NO_X continues to reduce, and ultimately ultra-low NO_X and smoke emissions are achieved at 11.5% intake O_2 concentration. The region, where simultaneously low NO_X and smoke emissions are attained, is typically identified as the LTC region [25].

The in-cylinder pressure and the heat release rate traces for selected data points of the EGR sweeping test are plotted in Figure 5.2. For a high intake O_2 concentration, the heat release profile resembles conventional diesel combustion with pre-mixed and diffusion combustion stages, as previously shown in Figure 2.1.

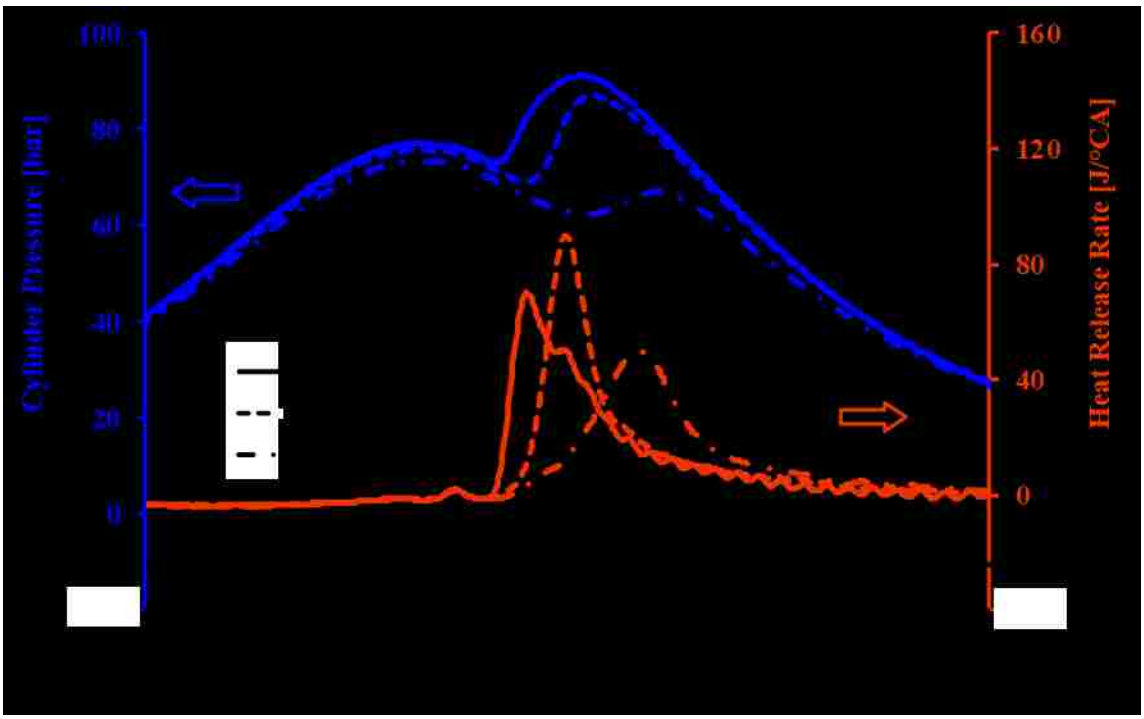

Figure 5.2 SSDC – EGR Sweep: Cylinder Pressure and AHRR

When the EGR ratio is increased and the intake O_2 concentration is reduced to 14.3%, the longer ignition delay shifts the combustion further into the expansion stroke. The increased inert dilution and the delayed combustion phasing result in a lower flame temperature, thereby causing a significant reduction in the NO_X emissions. However, the lower flame temperature and the lower oxygen availability also promote the formation, and inhibit the oxidation, of the smoke, resulting in higher smoke emissions. When the intake O_2 concentration is reduced to 11.5%, the heat release trace indicates that the combustion phasing is further delayed, and the combustion duration is longer. At this condition, a larger ignition delay enhances the air-fuel mixing process, which inhibits the smoke formation.

The indicated thermal efficiency and the combustion efficiency are presented in Figure 5.3. When the intake O_2 concentration reduces from 19% to 14%, there is no apparent change in the thermal efficiency and the combustion efficiency. However, at intake O_2 concentrations lower than 14%, the thermal efficiency and combustion efficiency reduce significantly. The increase in the HC and CO emissions, as shown in Figure 5.4, explains the reduction in combustion efficiency. The CO emissions initially increase modestly with the application of EGR, whereas at high EGR rates, the rise in CO emissions is more pronounced. With the reduced O_2 availability, the CO formed during early stages of combustion is not completely oxidized [97]. The HC emissions remain insignificant until high EGR rates are applied. At high EGR rates, the reduced flame temperature and the lack of oxygen inhibit the complete oxidation of the hydrocarbons. The results of exhaust hydrocarbon speciation have suggested that the HC emissions contain extensive light hydrocarbon species [98].

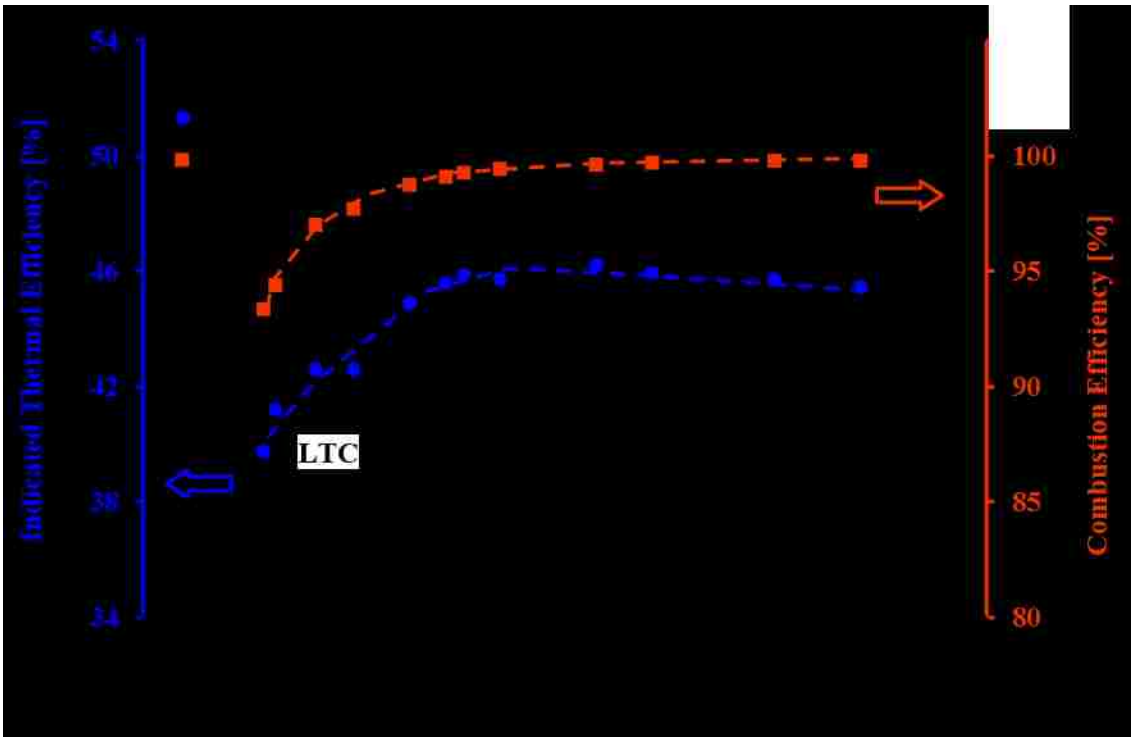

Figure 5.3 SSDC – EGR Sweep: η_{th} and η_{comb}

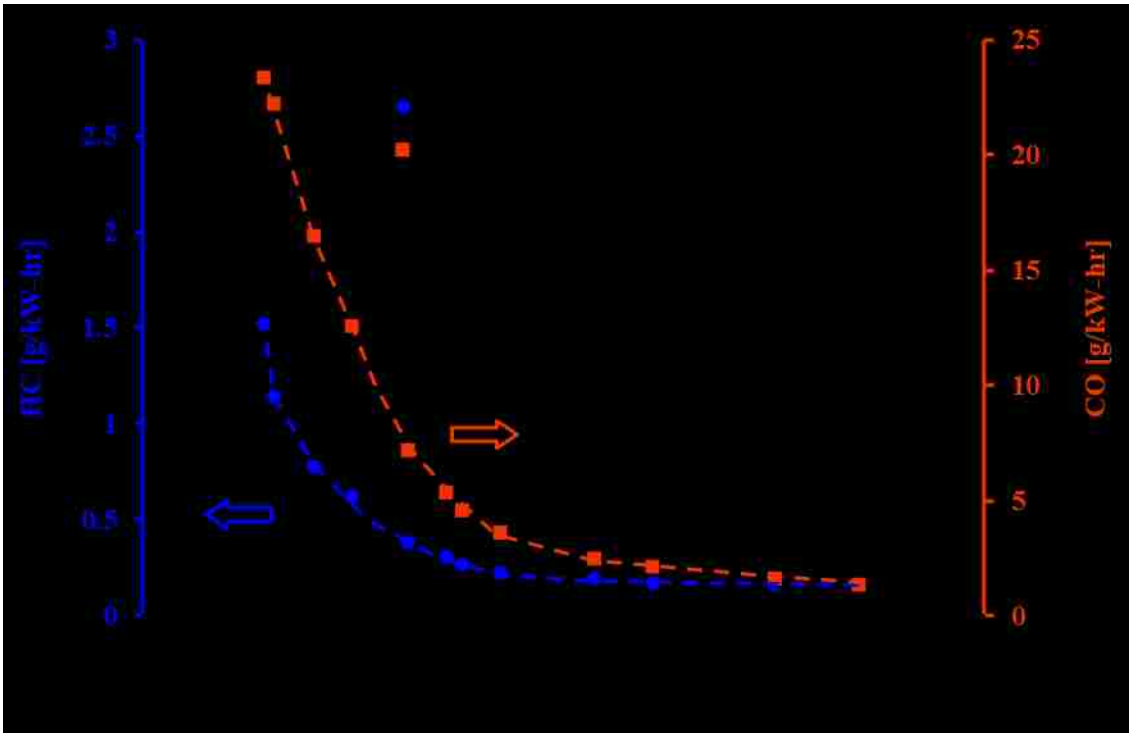

Figure 5.4 SSDC – EGR Sweep: HC and CO

As discussed in Section 4.3.2, the thermal efficiency is also affected by the combustion phasing and duration. Therefore, the impacts of EGR on the CA50 and the combustion duration are demonstrated in Figure 5.5. With the increase in EGR, the combustion phasing is gradually shifted later in the expansion stroke; the combustion duration is also steadily extended. The CA50 change is more sensitive when the intake O_2 concentration is lower than 14%. In addition to the lower combustion efficiency, the late combustion phasing and the long combustion duration at higher EGR rates may contribute to the large reduction in thermal efficiency.

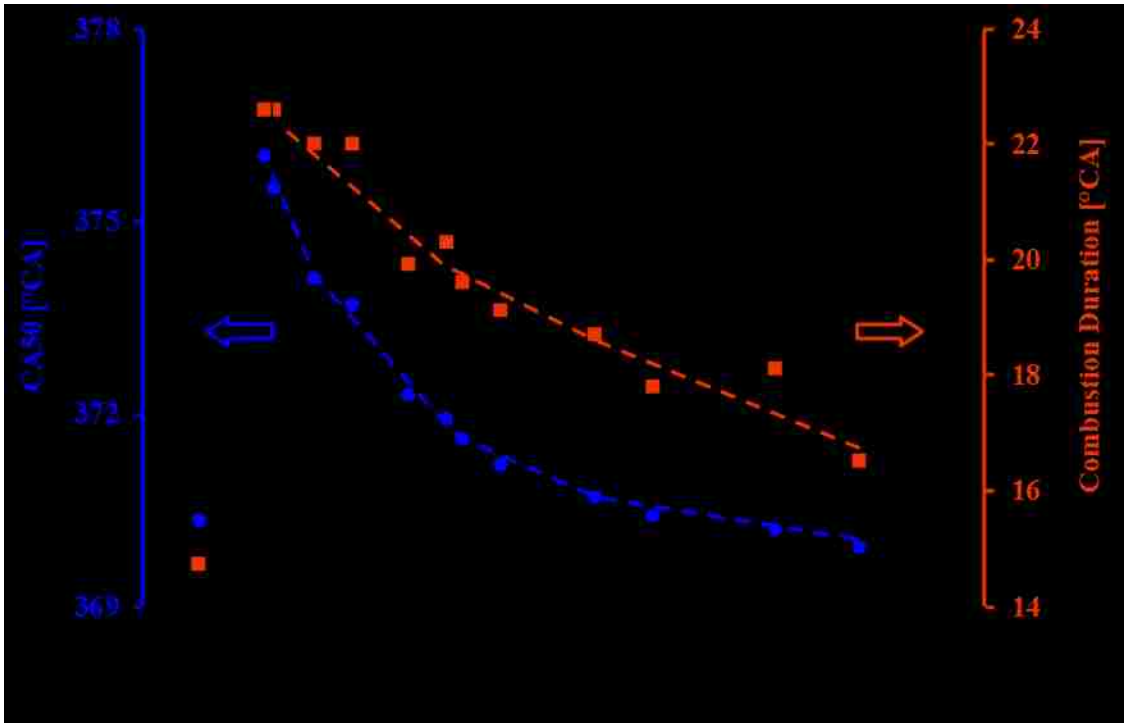

Figure 5.5 SSDC – EGR Sweep: CA50 and CD

The NO_X and smoke emission results from the EGR sweep test suggest that the target NO_X emissions of 0.5 g/kW-hr can be achieved around 15% intake O_2 concentration, but the smoke emissions exceed the target value of 0.05 g/kW-hr at this EGR level. The

target NO_X and smoke emissions are attained under LTC conditions, however with a thermal efficiency penalty of more than 5% (absolute), compared to the engine operation without EGR.

5.1.2. Application of EGR with Fuel Injection Timing Adjustments

The results presented in the previous subsection demonstrate the effectiveness of EGR application towards in-cylinder NO_X reduction, but with a smoke emission penalty. The heavy use of EGR can simultaneously reduce the NOx and smoke emissions by enabling LTC. However, the extensive use of EGR may cause a substantial reduction in thermal efficiency. To evaluate the possibility of achieving the target NO_X and smoke emissions without incurring a large thermal efficiency penalty, an EGR sweeping test is conducted at a lower engine load level of 4 bar IMEP, but with a higher injection pressure of 120 MPa and an elevated intake boost pressure of 2 bar absolute. Adjustments are also made to the diesel injection timing during the test to maintain a fixed CA50 setpoint of 368°CA. The diesel injection duration is fixed during the EGR sweeping test.

The ignition delay and the injection timing are plotted against the intake O_2 concentration in Figure 5.6. As the intake O_2 concentration is reduced, the ignition delay gradually increases. As a result, at low intake O_2 concentrations, the injection timing is subsequently advanced to maintain the CA50 at the setpoint value.

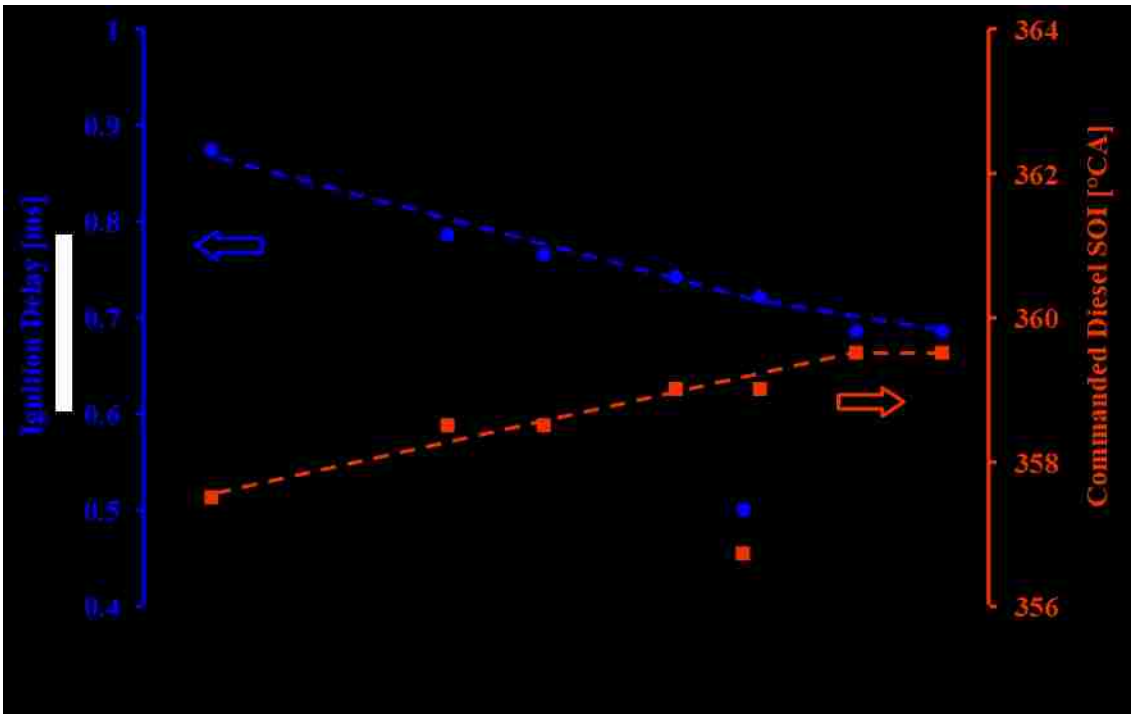

Figure 5.6 SSDC – EGR Sweep at Fixed CA50: ID and SOI

The smoke and NO_X emission results of the EGR sweeping test with fixed CA50 are shown in Figure 5.7. Similar to the test results presented in Section 5.1.1, the NO_X emissions reduce consistently with the increase in EGR. When the EGR is increased to the intake O_2 concentration lower than 15% by volume, the NO_X emissions are reduced to comply with the target value of 0.5 g/kW-hr. However, an increase in the smoke emissions is observed, which highlights the NO_X smoke trade-off. Nevertheless, the smoke emissions are significantly lower compared to the previous test conditions and are within the target value of 0.05 g/kW-hr. The lower engine load level along with the elevated fuel injection and intake boost pressures suppress the smoke emissions at high EGR levels.

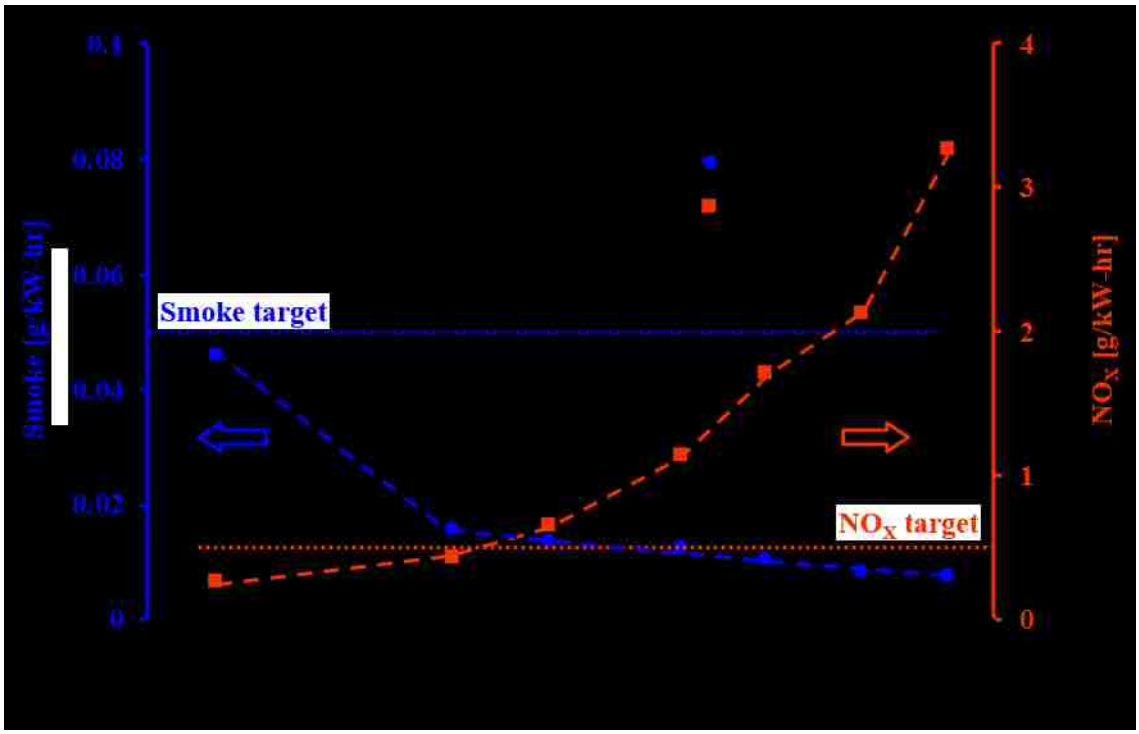

Figure 5.7 SSDC – EGR Sweep at Fixed CA50: NO_X and Smoke

The thermal efficiency and the combustion efficiency are shown in Figure 5.8. By fixing the CA50 at the setpoint value throughout the EGR sweep, noticeable improvements in both the combustion efficiency and the thermal efficiency are observed when compared with the EGR sweeping test presented in Section 5.1.1. Moreover, the NO_X and smoke emission targets are achieved at a higher intake O_2 concentration of around 14.5% compared to the previous test. Therefore, a further increase in the EGR rate is not necessary. By limiting the intake O_2 concentration to 14.5%, the reduction in the combustion efficiency, associated with the high intake dilution, is avoided.

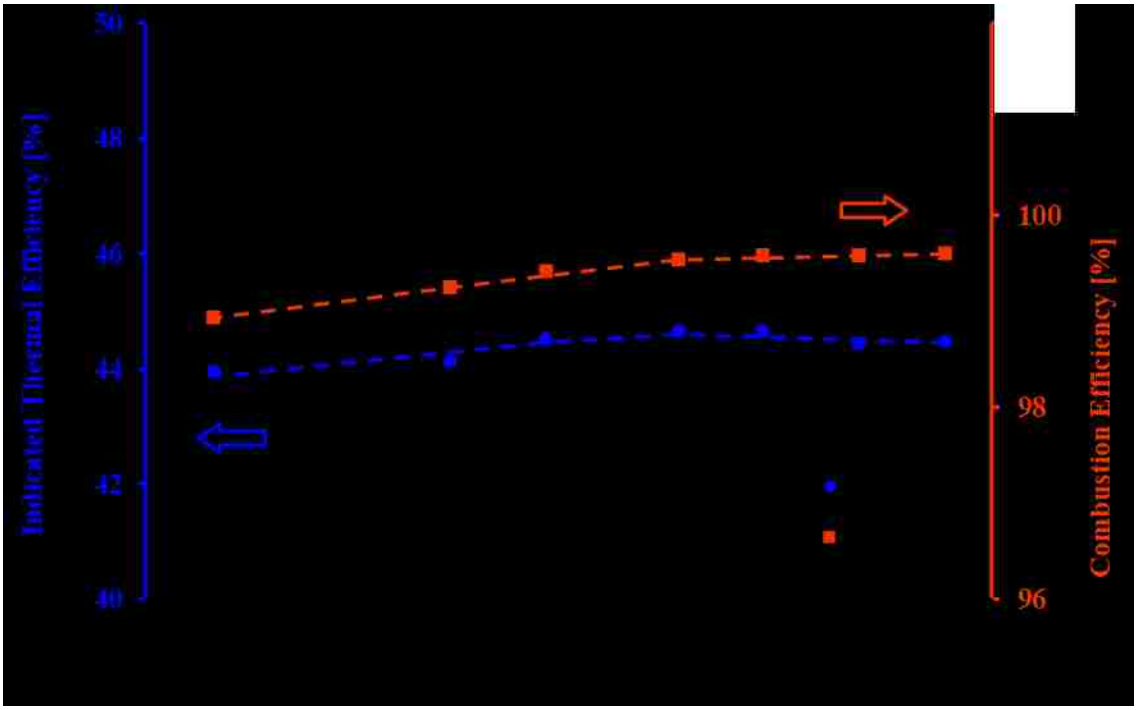

Figure 5.8 SSDC – EGR Sweep at Fixed CA50: η_{th} and η_{comb}

5.2. Clean Combustion with Single Diesel Injection at Increased Load

5.2.1. Impact of EGR and Combustion Phasing at 10 bar IMEP

As the engine load is increased, simultaneous reductions of NO_X and smoke emissions become more challenging. Engine tests are conducted at 10 bar IMEP to evaluate the effects EGR and fuel injection timing on the emissions and efficiency. The SSDC strategy is utilized at a fuel injection pressure of 150 MPa. An intake boost pressure of 2 bar absolute is applied. EGR sweeping tests are conducted at two CA50 setpoints, 369ºCA and 380ºCA. The injection duration is fixed for each set of tests to attain the nominal IMEP of 10 bar at 0% EGR. The diesel injection timing is advanced as the EGR rate is increased to maintain the CA50 at the setpoint value for each set of tests.

The NO_X and smoke emissions measured during the EGR sweeping tests are shown in Figure 5.9. The hollow markers represent the results of the EGR sweeping tests at a CA50 setpoint of 369ºCA, whereas the solid markers represent the results at a CA50 setpoint of 380ºCA. In both the test cases, EGR effectively reduces the NO_X emissions. A delayed combustion phasing also results in a further reduction of NO_X emissions at a given EGR level.

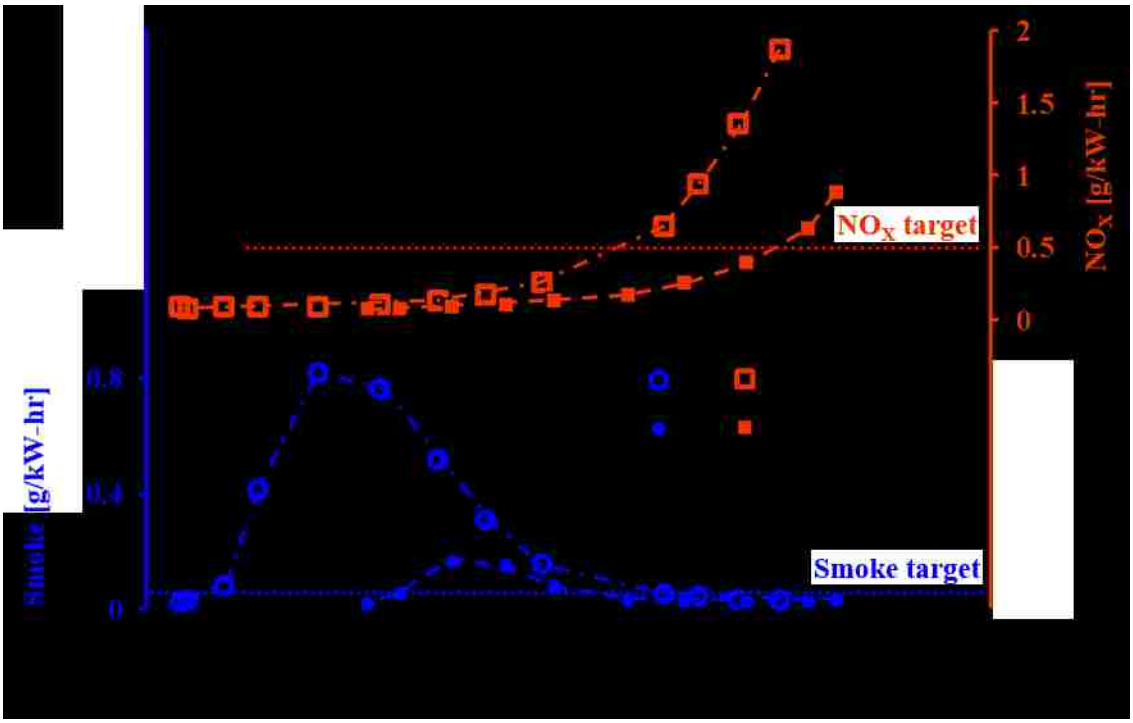

Figure 5.9 SSDC – EGR Sweeps at 10 bar IMEP: NO_X and Smoke

The smoke emissions tend to increase with the application of EGR, thereby displaying the NO_X-smoke trade-off. However, at high EGR levels, a simultaneous reduction of NO_X and smoke emissions is observed. This trend is consistent for both the test sets. Nevertheless, a late combustion phasing significantly decreases the smoke peak.

Consequently, less EGR is necessary to achieve a simultaneous NO_X and smoke reduction when the combustion phasing is deferred to the early expansion stroke.

The indicated thermal efficiency and combustion efficiency results are presented in Figure 5.10. The combustion efficiency remains high as the EGR rate is initially increased, but a sharp drop is observed at high EGR levels when LTC is enabled. Previous studies have reported that a significant reduction of the combustion temperature and the lower O_2 availability at high EGR levels result in a partial oxidation of the fuel, thereby increasing the CO and HC emissions in the exhaust [25], [36], [99]. The rises in both the CO and HC emissions contribute to a reduction in the combustion efficiency.

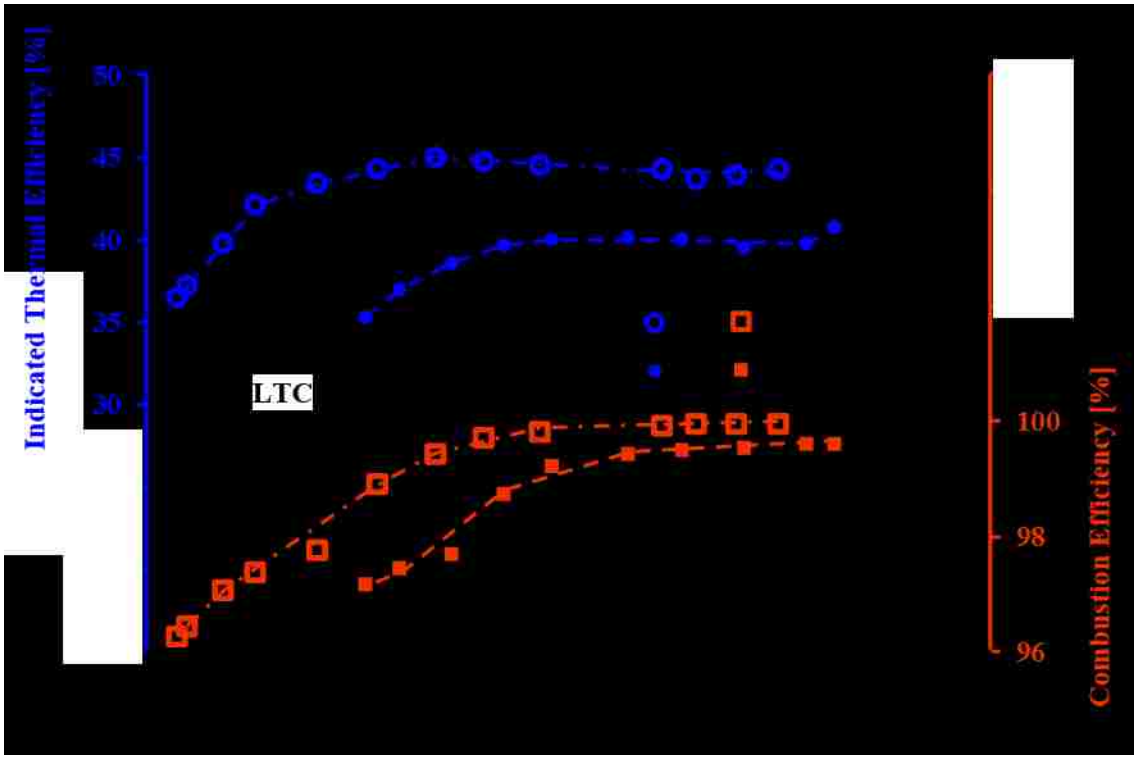

Figure 5.10 SSDC – EGR Sweeps at 10 bar IMEP: η_{th} and η_{comb}

A consistently lower indicated thermal efficiency is observed at high intake O_2 concentrations, when the CA50 setpoint is later in the expansion stroke. However, at low intake O_2 concentrations where LTC is enabled, a sharp drop in the indicated thermal efficiency is observed for both the combustion phasing tests. The large reduction of the combustion efficiency contributes to the corresponding reduction in the indicated thermal efficiency under the LTC regime.

In summary, when the engine load is increased to 10 bar IMEP, the NO_X and smoke targets become increasingly difficult to reach without compromising the indicated thermal efficiency. Even though ultra-low NO_X and smoke emissions can be achieved at 10 bar IMEP by applying heavy EGR, or by delaying the combustion phasing, a substantial deterioration in the thermal efficiency is observed.

5.2.2. Engine Load Limit for Single-shot Diesel Combustion

The results presented in the previous subsections show that the EGR application is effective for attaining the selected emission targets at low loads. However, at increased engine load levels, the use of EGR results in high smoke emissions. The heavy use of EGR can enable LTC, but this strategy exhibits a considerable thermal efficiency penalty. To further illustrate the effect of engine load on the SSDC strategy, EGR sweeping tests are conducted at different load levels, as shown in Table 5.1. The NO_X and smoke emissions are presented in Figure 5.11. Note that the emission data is plotted on a log scale. The smoke emissions exhibit an increasing trend as the engine load increases, even though the intake boost and fuel injection pressures are raised. In the 3 bar and 4 bar IMEP test cases, the target emissions can be attained by increasing the EGR rate. At

10 bar IMEP, however, heavy EGR application is necessary to achieve simultaneously low NO_X and smoke emissions. At higher loads, the EGR application becomes increasingly difficult because of excessive smoke emissions.

Table 5.1 Summary of SSDC Engine Load Extension Tests

IMEP [bar]	3.0	4.0	10.0	16.0
Intake Boost Pressure [bar]	1.30	2.00	2.00	2.25
Injection Pressure [MPa]	90	120	150	150
CA50 [°CA]	365.0	368.0	369.0	372.0

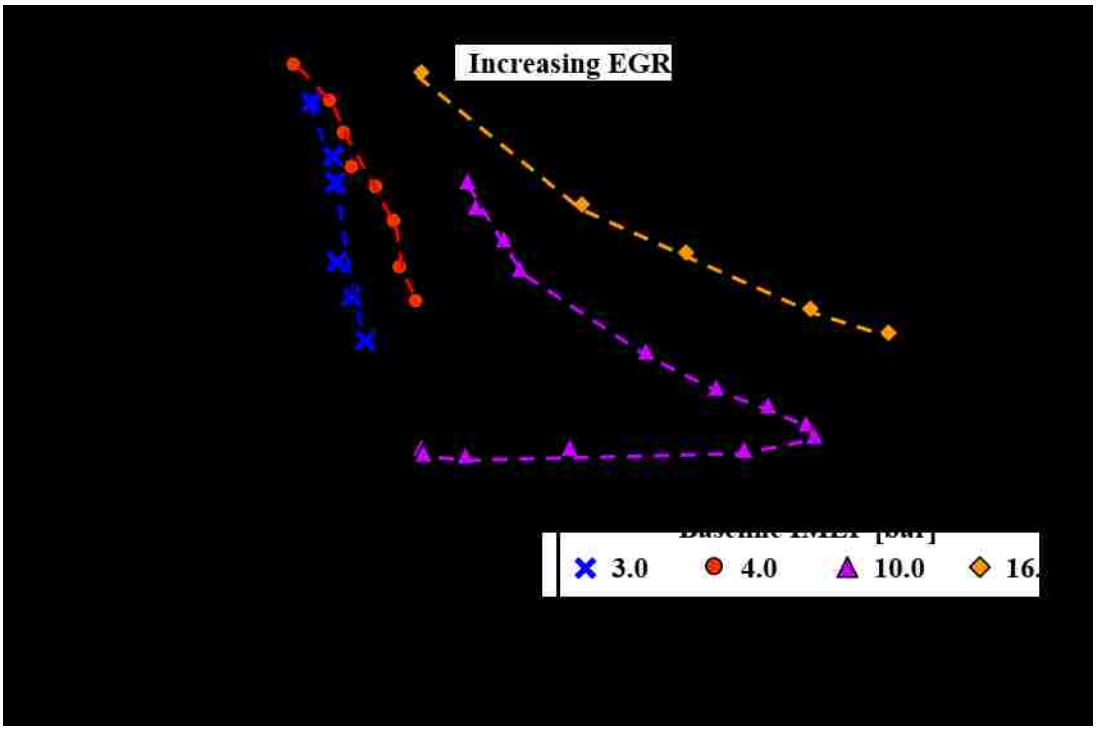

Figure 5.11 SSDC: Impact of Load on NO_X-smoke Trade-off

5.3. Diesel-ethanol Dual-fuel Combustion

The DFC strategy has been identified as a promising solution to extend the engine load level in the low NO_X and smoke regime [10], [48], [55], [58], [59], [61], [63]. This strategy combines the port injection of a fuel of high volatility and low cetane number with the in-cylinder injection of diesel fuel. Ethanol is selected as the port injection fuel for this study. Ethanol has relatively high volatility that enhances its evaporation process during premixing with air. Ethanol also has a relatively high auto-ignition temperature that helps to avoid premature ignition during a compression stroke. In addition, ethanol benefits from its currently large production and distribution infrastructure as it is a commercial gasoline fuel blend [100]. More details of the physical and chemical properties of ethanol are given in Figure 2.5 and APPENDIX B.

5.3.1. Effect of Ethanol-to-diesel Ratio on DFC

The primary target of the DFC tests is to overcome the smoke emission penalty that is observed during the SSDC tests when EGR is applied. With the DFC strategy, the use of EGR is expected to lower the NO_X emissions while the addition of port fuel injection may reduce the smoke emissions. An engine test is conducted at 10 bar IMEP and 14.5% intake O_2 concentration, whereas with varied ethanol fraction (χ_{eth}). As noted in Equation (3.1), χ_{eth} is determined on the basis of the relative energy contribution from the ethanol compared to the total fuel energy. During the test, the diesel injection duration and timing are adjusted to maintain the nominal IMEP and CA50. Small adjustments are also made to the EGR rate to keep the intake O_2 concentration around 14.5%.

The smoke and NO_X emission results are plotted in Figure 5.12. A noticeable reduction in smoke emissions is observed as the ethanol fraction is increased in the DFC mode. When the ethanol fraction is greater than 0.5, smoke emissions are ultra-low (lower than 0.01 g/kW-hr). The NO_X emissions remain below 0.5 g/kW-hr throughout the test. The low NO_X emissions are attributed to the high EGR rate and the use of ethanol. The tests show that NO_X consistently reduces when the ethanol quantity is increased. The port delivered ethanol makes a premixed charge that is lean and diluted, which contributes to the lower NO_X emission. Additionally, the ethanol evaporation during the compression stroke results in a lower compression temperature, that may also contribute to the lower NO_X emissions [43].

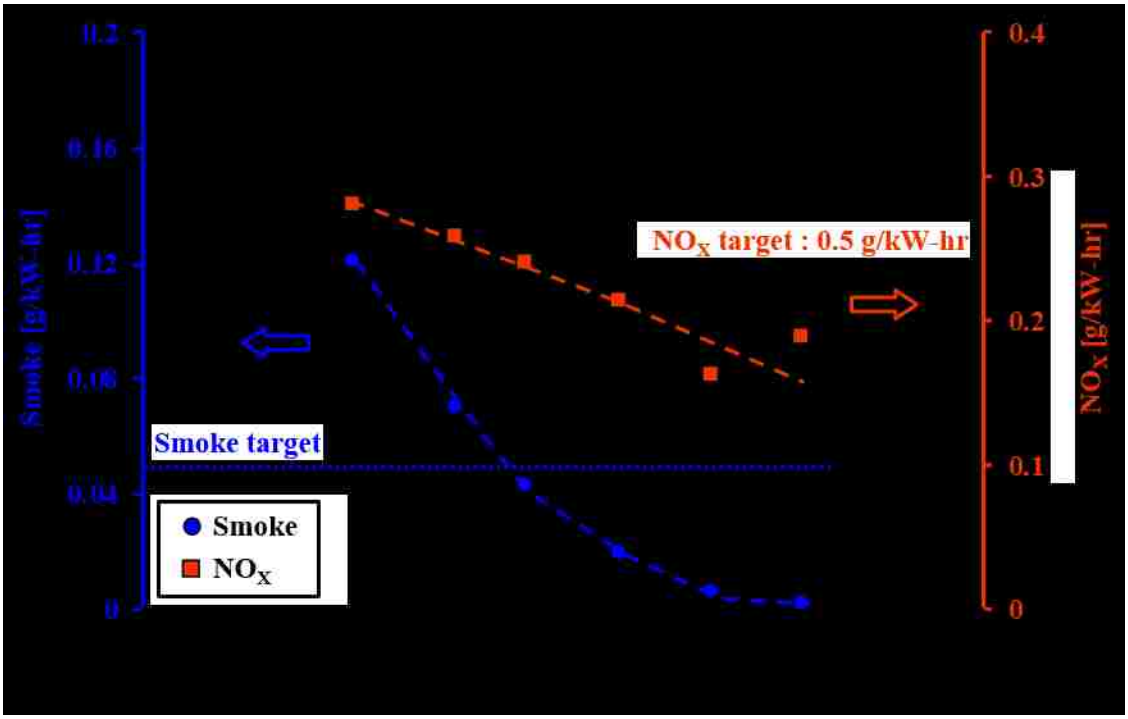

Figure 5.12 DFC – Ethanol Fraction Effect: NO_X and Smoke

The cylinder pressure and heat release rate are plotted at two ethanol fractions in Figure 5.13. The ignition delay is shorter for the test case with an ethanol fraction of 0.2, compared to the test case with an ethanol fraction of 0.63. The heat release rate profiles indicate that the use of a lower ethanol fraction tends to produce a greater degree of diffusion combustion, which may contribute to the high smoke emissions. As the ethanol fraction is increased, the premixing of air and fuel is enhanced and the smoke emissions are consistently reduced. Moreover, the presence of oxygen within the ethanol fuel molecule also helps to suppress the formation of smoke.

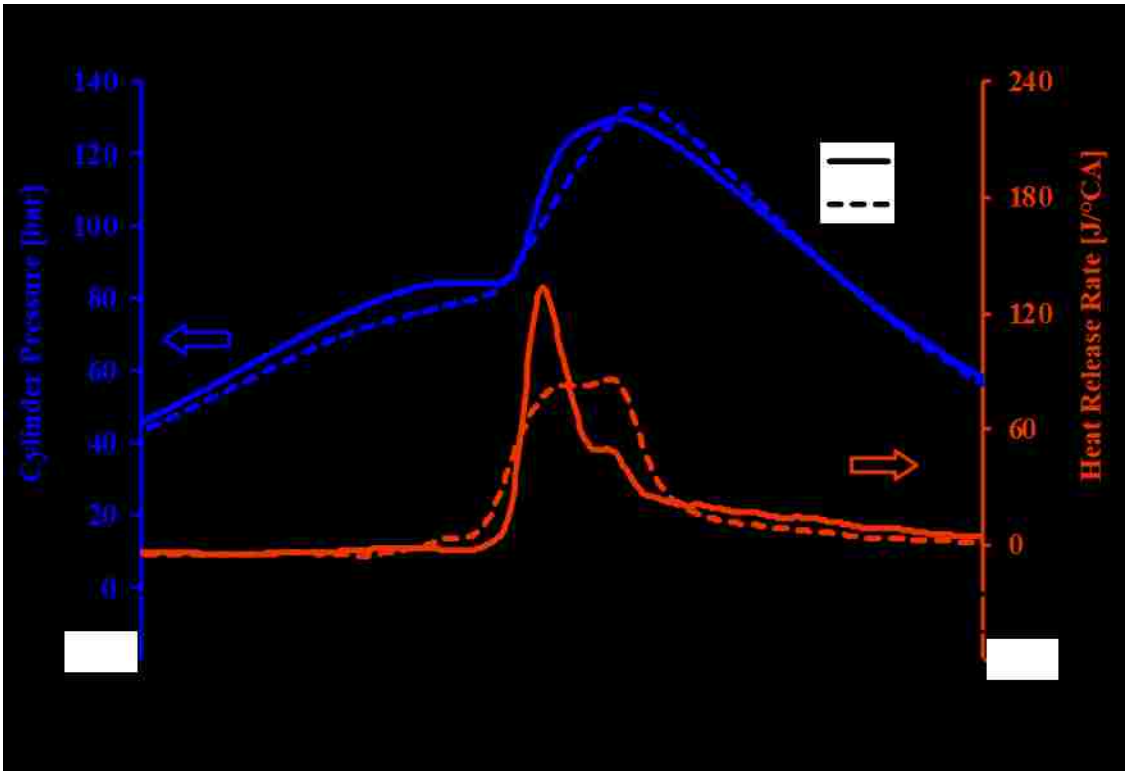

Figure 5.13 DFC – Ethanol Fraction Effect: Cylinder Pressure and AHRR

The indicated thermal efficiency and the combustion efficiency results are presented in Figure 5.14. When the ethanol fraction is increased, an overall reduction in the thermal

efficiency, of nearly 1% absolute, is observed. The combustion efficiency also reduces when the ethanol fraction is initially increased. The HC and CO emissions are plotted in Figure 5.15 to explain the combustion efficiency trends. The HC emissions initially rise when the ethanol fraction is increased to 0.45. The HC emissions may result from a portion of the pre-mixed fuel that is trapped in the crevice volumes [43], [101], [102]. Similar to the trends in HC emissions, the CO emissions increase when the ethanol fraction is initially raised. However, at higher ethanol fractions, such as above 0.45, the CO emissions tend to reduce. At high ethanol fractions, the increased strength of the ethanol-air mixture may improve the CO oxidation tendency [43].

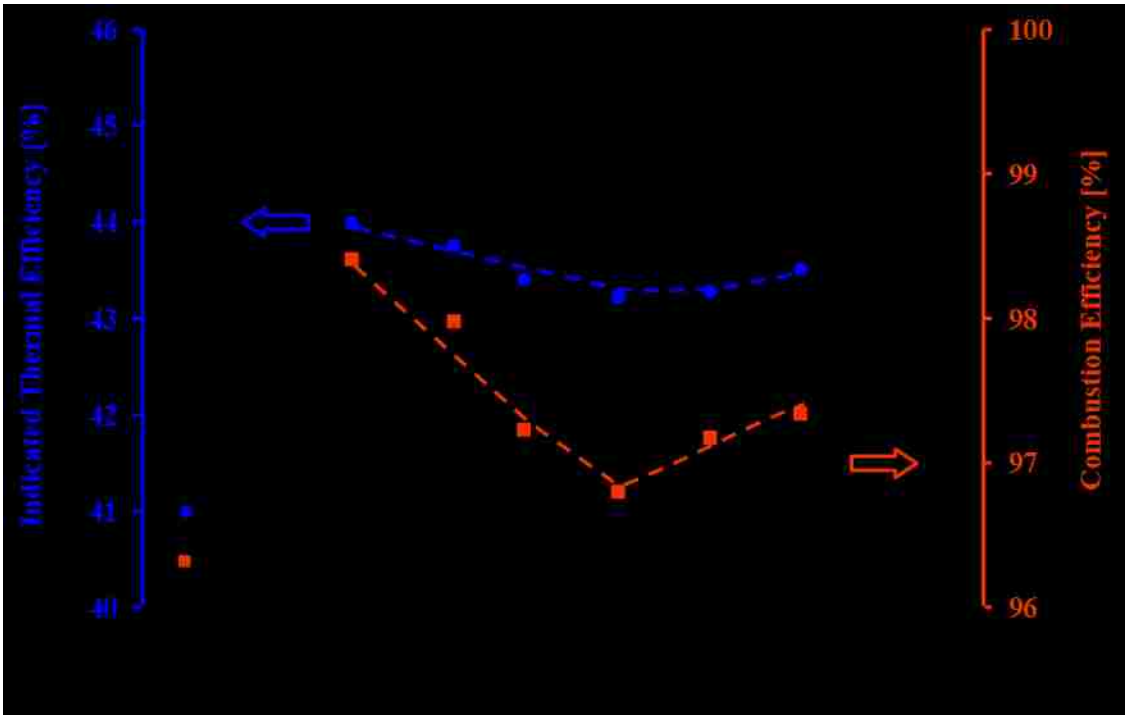

Figure 5.14 DFC – Ethanol Fraction Effect: η_{th} and η_{comb}

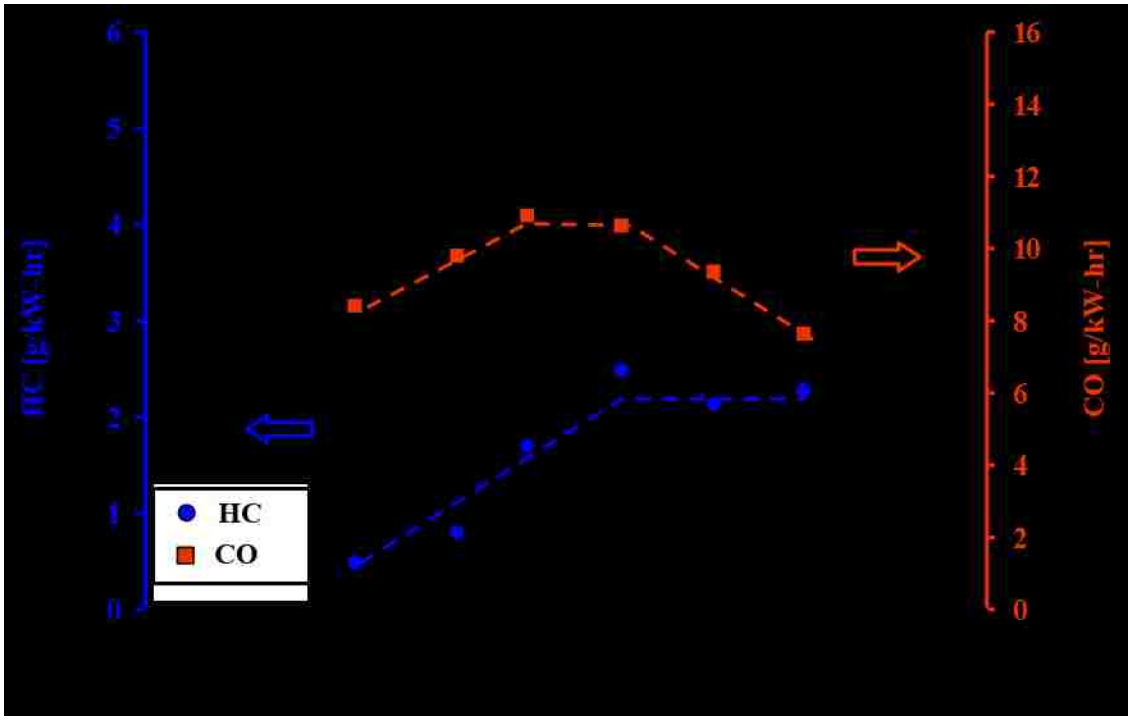

Figure 5.15 DFC – Ethanol Fraction Effect: CO and HC

The peak pressure rise rate and the peak cylinder pressure are shown in Figure 5.16. Under the testing conditions, although the peak cylinder pressure is consistently lower than the target value of 170 bar, the peak pressure rise rate exceeds the target value at ethanol fractions lower than 0.45. When the ethanol fraction is increased beyond 0.45, the peak pressure rise rate promptly reduces. As seen in Figure 5.13, the premixed portion of the heat release rate is sharp for the DFC strategy when a relatively small ethanol fraction is employed. However, when the ethanol fraction is increased, a majority of the indicated work is produced by flame propagation across the combustion chamber. Under such conditions, the heat release rate profile suggests that the premixed combustion is more gradual. Therefore, higher ethanol fractions result in a lower peak pressure rise rate.

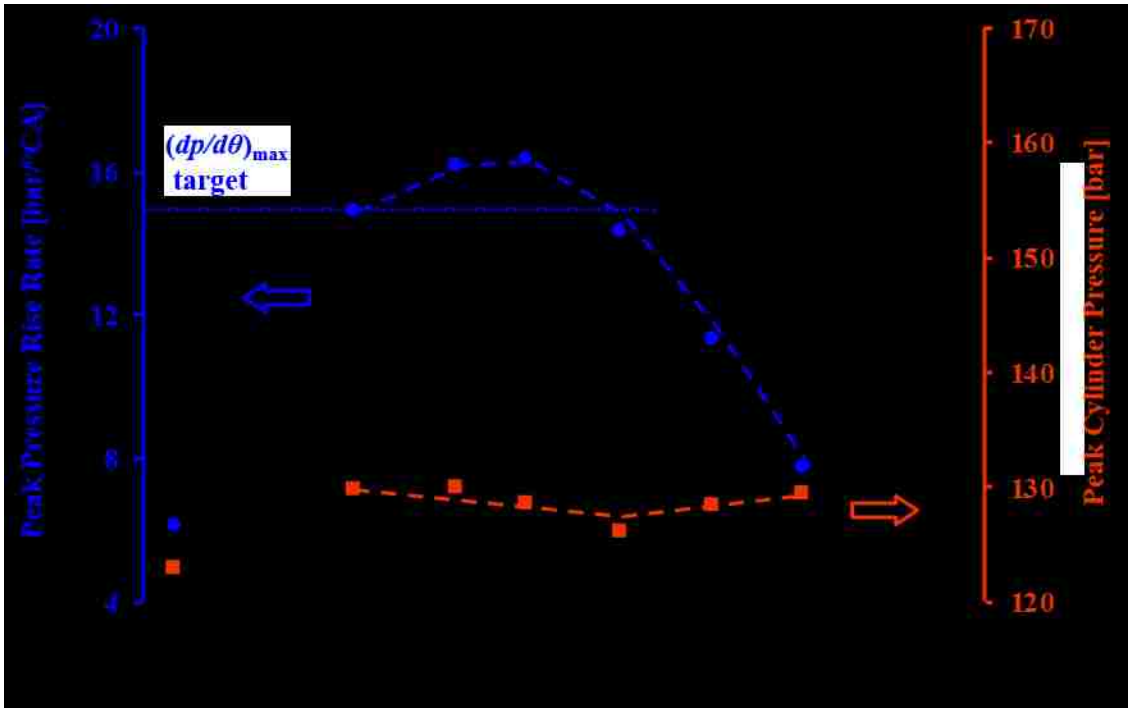

Figure 5.16 DFC – Ethanol Fraction Effect: $(dp/d\theta)_{max}$ and p_{max}

The combustion of a homogeneous and lean fuel-air mixture is generally associated with increased cycle-to-cycle variations and reduced combustion controllability. To evaluate these aspects, the commanded diesel injection timing and the standard deviation of CA50 (STD_{CA50}) are shown in Figure 5.17. Note that the COV_{IMEP} is consistently lower than 3% during the test, and therefore the trends in the COV_{IMEP} are not reported here. The diesel injection timing is progressively advanced at higher ethanol fractions to maintain the CA50 at 367.5°CA. The standard deviation of the CA50 remains low, even when the diesel SOI is significantly advanced at high ethanol fractions. The results suggest that the diesel injection timing has effective control over the CA50 for the tested conditions.

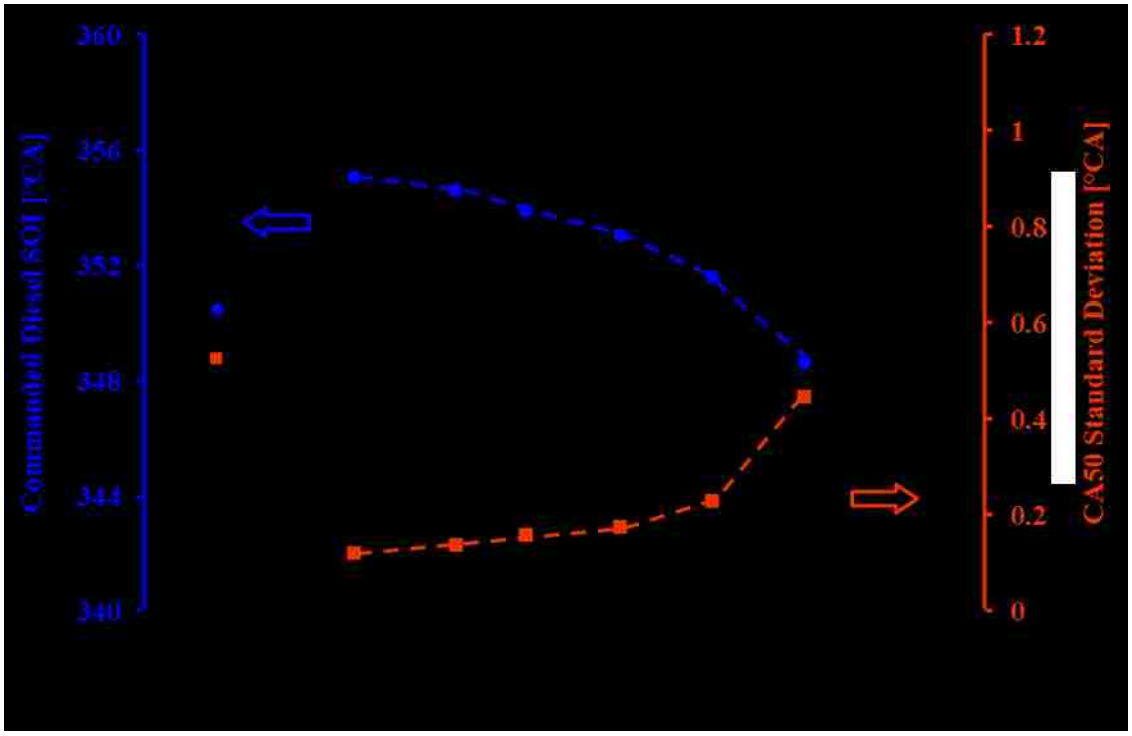

Figure 5.17 DFC – Ethanol Fraction Effect: Diesel SOI and STD_{CA50}

In summary, at 10 bar IMEP, the DFC strategy can attain the NO_X and smoke targets when moderate EGR rates are applied. With this strategy, the thermal efficiency is significantly higher compared to the SSDC strategy. Moreover, the combustion phasing is effectively controlled by the diesel injection timing during DFC.

5.3.2. Dual-fuel Combustion at Low Engine Load

Tests are performed at 4 bar IMEP to study the impacts of the DFC strategy on the emissions and efficiency. EGR sweeping tests are conducted at two ethanol fractions of zero and 0.5. The EGR sweeping test at zero ethanol fraction represents the SSDC strategy, for direct comparison with the DFC strategy. The smoke and NO_X emissions are shown in Figure 5.18. While the NO_X-smoke trade-off is observed for the zero ethanol fraction test case, the smoke emissions remain lower than 0.01 g/kW-hr for the test case

with 0.5 ethanol fraction. The NO_X emissions are reduced when the ethanol fraction is increased, but the use of EGR is still the effective technique to attain the NO_X target.

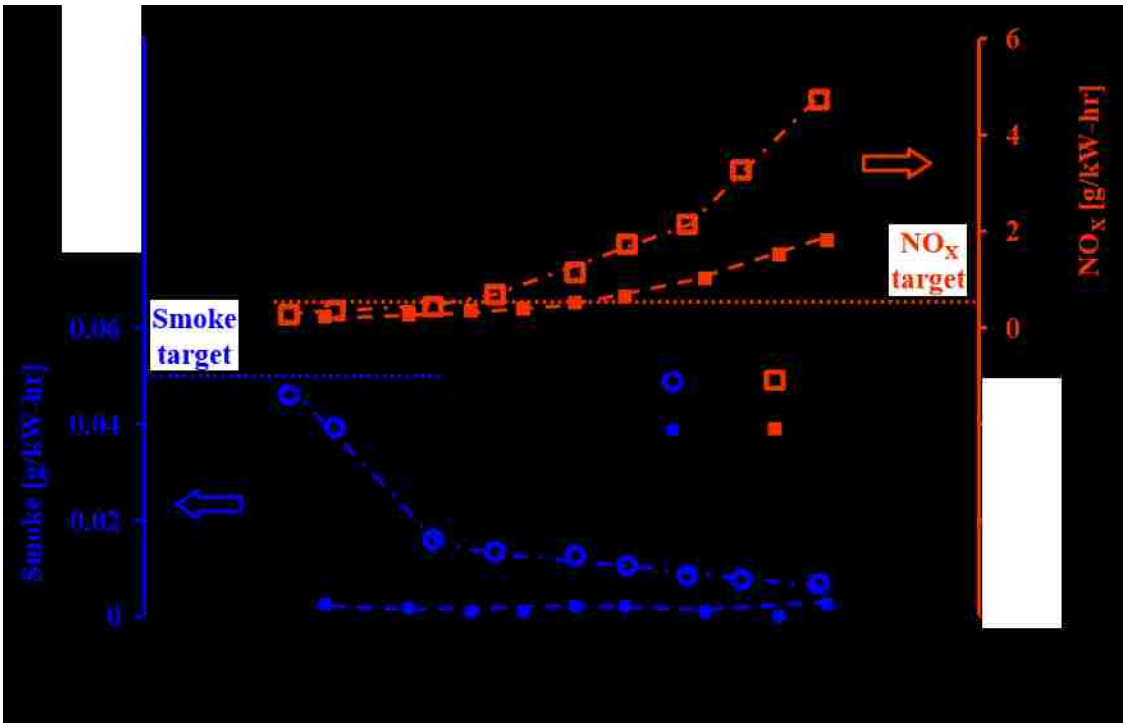

Figure 5.18 DFC – EGR Effect at 4 bar IMEP: Smoke and NO_X

The thermal efficiency and the combustion efficiency for the EGR sweeping tests are plotted in Figure 5.19. The thermal efficiency is consistently lower for the DFC strategy when compared to the SSDC strategy. The lower combustion efficiency for the DFC case (approximately 4% absolute) may contribute to the thermal efficiency reduction. The HC and CO emissions for the two EGR sweeping tests are shown in Figure 5.20. Both of the HC and CO emissions are significantly higher for the DFC test case, than those for the SSDC test case. At the low engine load, the HC and CO emissions result in a significant combustion inefficiency (Section 4.3.3). Therefore, these emissions contribute to a much larger reduction in thermal efficiency at 4 bar IMEP than at 10 bar IMEP.

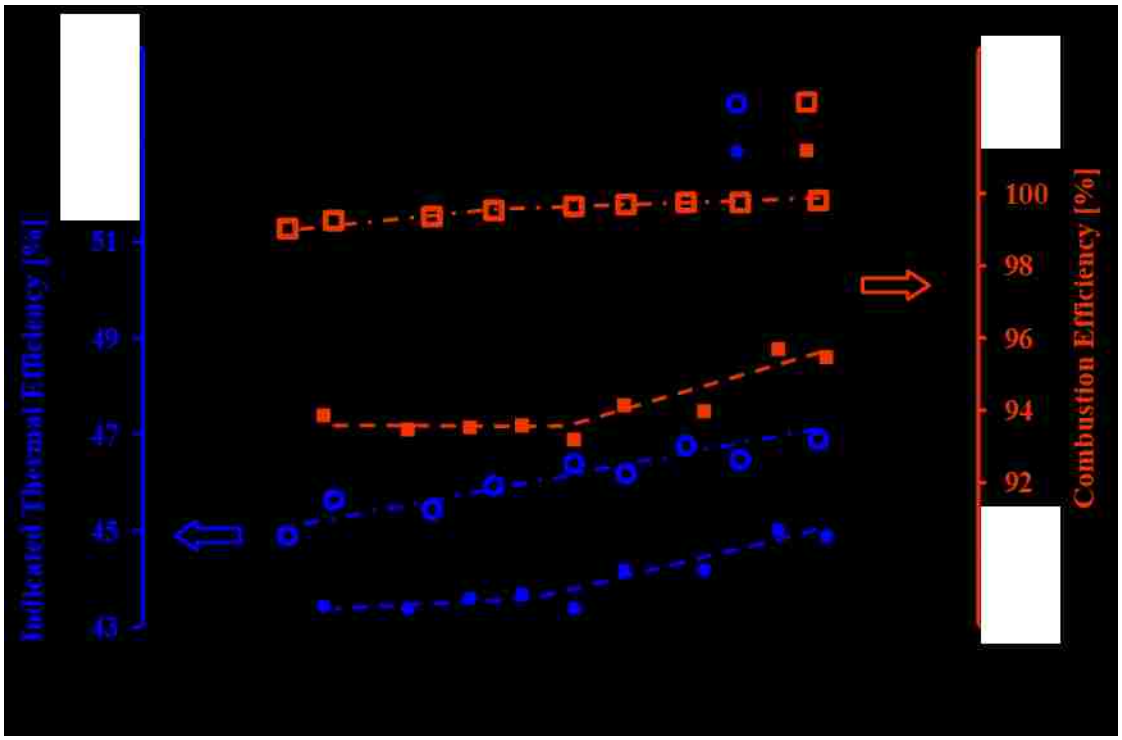

Figure 5.19 DFC – EGR Effect at 4 bar IMEP: Thermal Efficiency

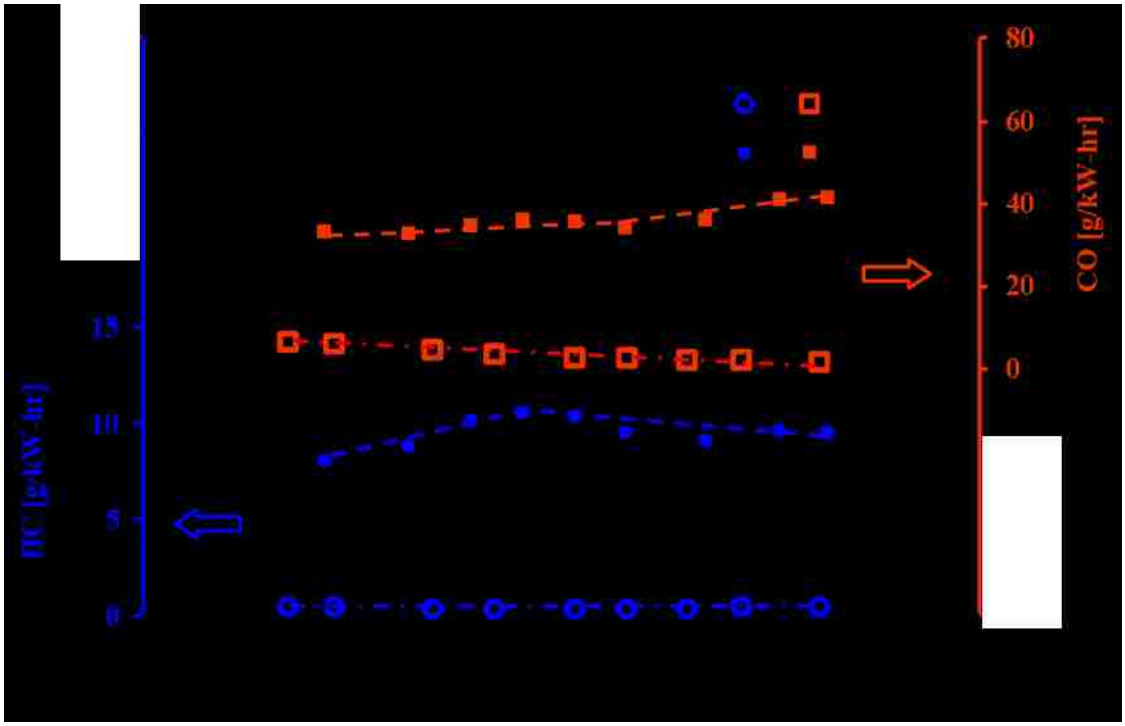

Figure 5.20 DFC – EGR Effect at 4 bar IMEP: CO and HC

5.3.3. Load Extension with Dual-fuel Combustion

The impact of the DFC strategy on the NO_X and smoke emissions at increased load levels is investigated by conducting an EGR sweeping test at 13 bar IMEP. For comparison, the test results from an EGR sweeping test conducted at 10 bar IMEP are also presented. The increase in IMEP from 10 bar to 13 bar is achieved by raising the ethanol fraction from 0.60 to 0.68 in addition to increasing the total fuel supply. The intake boost pressure, the fuel injection pressure, and the combustion phasing are fixed for both the tests.

The smoke and NO_X emissions are presented in Figure 5.21. The smoke emissions are generally higher at increased load conditions, especially when the intake O_2 concentration is below 15%. The lower air-fuel ratio may increase the smoke formation even though the increase in the load level is primarily achieved by raising the premixed fuel fraction. The NO_X emissions also tend to be higher for the high load test when the intake O_2 concentration is above 15%. Due to the fixed intake pressure, the 13 bar IMEP test case has a lower air-fuel ratio that may lead to higher flame temperatures and increased NO_X emissions.

The indicated thermal efficiency and the combustion efficiency are presented in Figure 5.22. The combustion efficiency is higher at 13 bar IMEP than at 10 bar IMEP. A larger difference in the combustion efficiency is observed when the intake O_2 concentration is higher than 15%. Nonetheless, the indicated thermal efficiency is similar for both the engine tests, even though the combustion efficiency is higher at 13 bar IMEP.

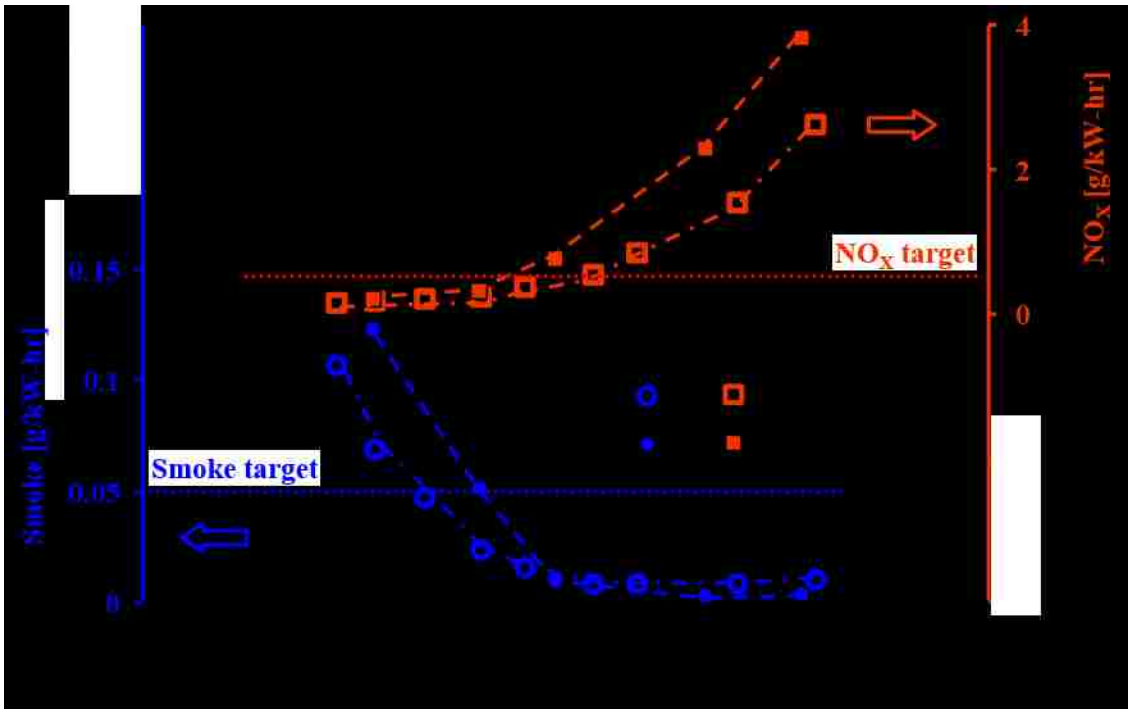

Figure 5.21 DFC – EGR Effect at Increased Load: Smoke and NO_X

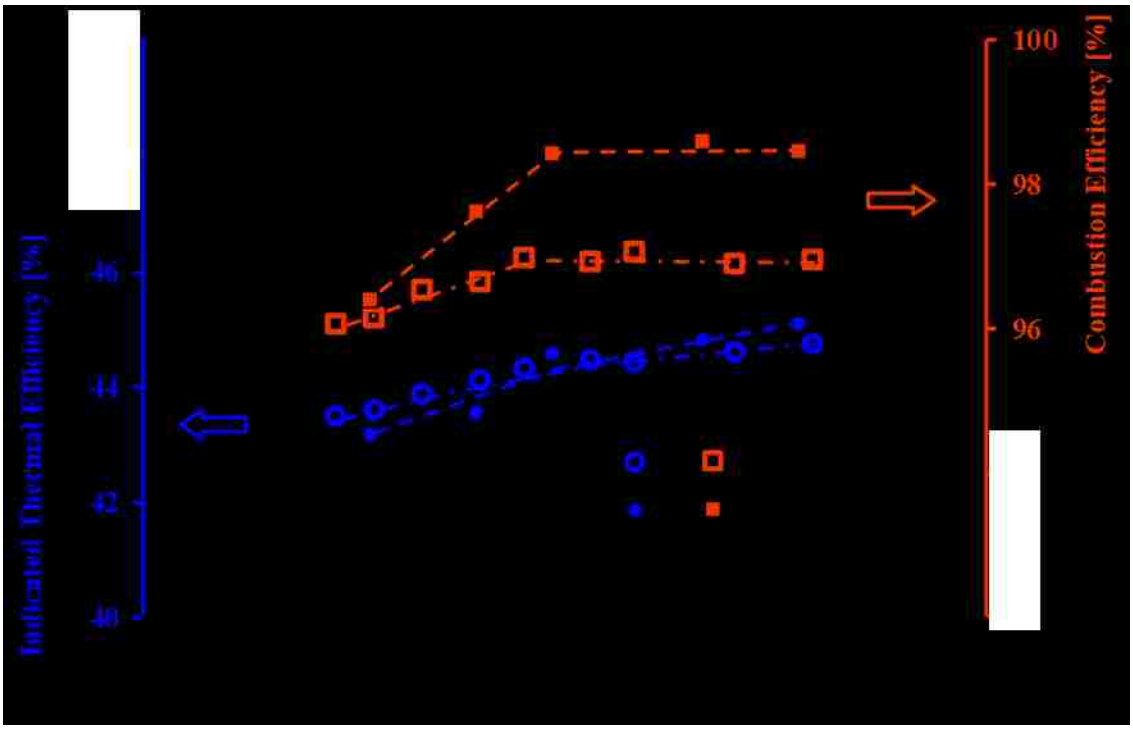

Figure 5.22 DFC – EGR Effect at Increased Load: Thermal Efficiency

Figure 5.23 presents the peak cylinder pressure and the peak pressure rise rate. The peak cylinder pressure monotonously reduces when EGR is applied for both testing cases. The peak cylinder pressure is consistently higher for the 13 bar IMEP test case when compared to the 10 bar IMEP test case. Moreover, for the 13 bar IMEP test case, the peak cylinder pressure is at the peak pressure limit of 170 bar when the intake O_2 concentration is higher than 16%, but reduces at lower intake O_2 concentrations. The peak pressure rise rate is beyond the selected limit of 15 bar/°CA at both of the IMEP levels when the intake O_2 concentration is above 14%. However, the peak pressure rise rate also reduces with higher EGR rates.

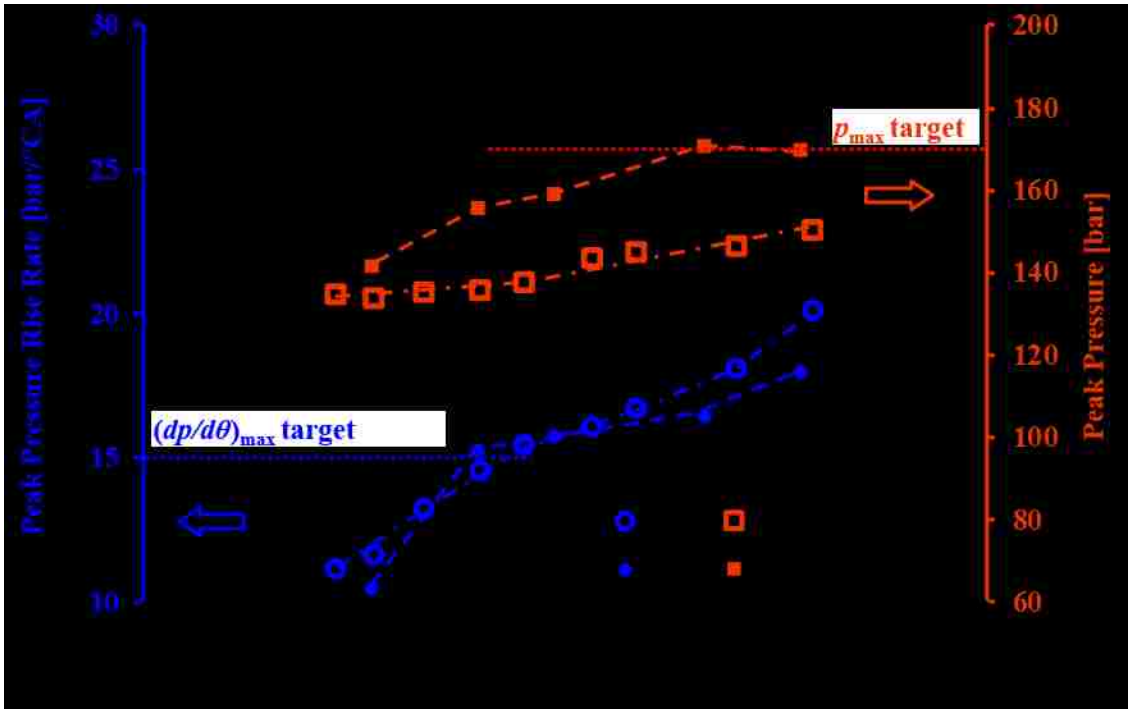

Figure 5.23 DFC – EGR Effect at Increased Load: p_{max} and $(dp/d\theta)_{max}$

In order to achieve further increases in engine load, several strategies need to be implemented. An increase in intake boost pressure is necessary to maintain an overall

lean air-fuel mixture. The combustion phasing should be delayed to contain the peak cylinder pressure and the peak pressure rise rate within the engine operating limits. Furthermore, the load increase should be achieved by increasing the ethanol fraction to maintain relatively low smoke emissions. Using these strategies, the engine load can be gradually increased up to 19.2 bar IMEP, which represents the full load condition for the test engine. The smoke and NO_X emissions for the test cases at different IMEP levels are presented in Figure 5.24. The test conditions and the thermal efficiency for the test points are summarized in Table 5.2.

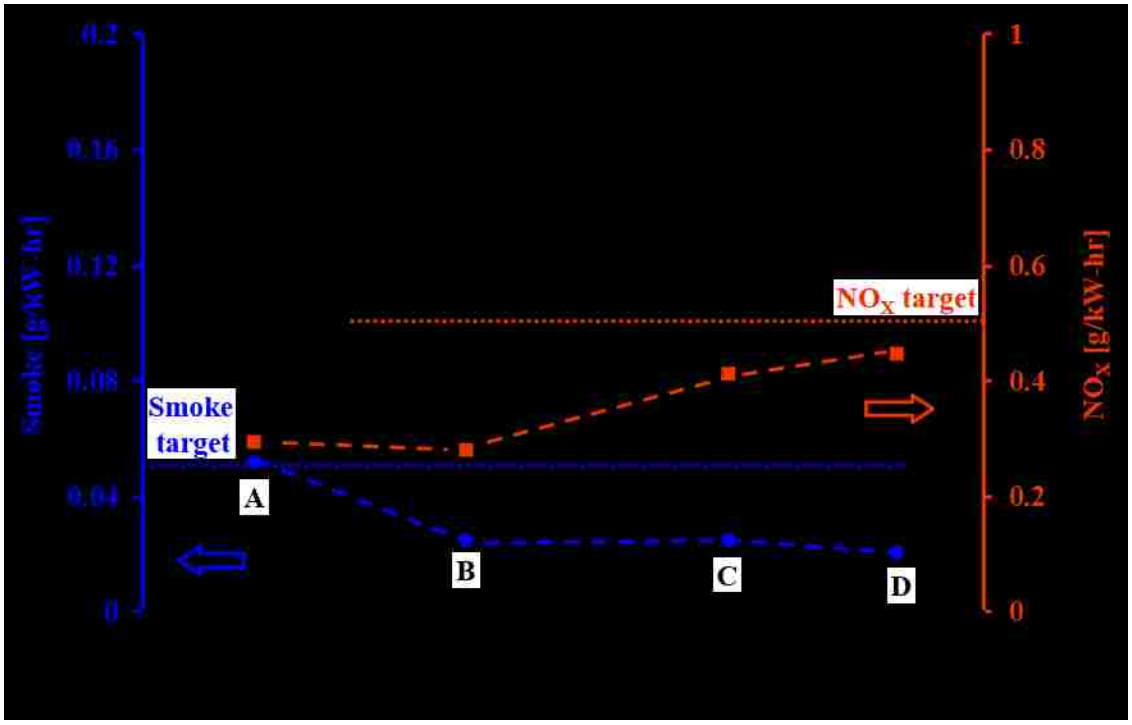

Figure 5.24 Sample Pathway Towards Full-load Operation Under DFC

Table 5.2 Summary of Dual-fuel Engine Load Extension Tests

Data point	A	B	C	D
IMEP [bar]	13.1	15.1	17.6	19.2
Intake Boost Pressure [bar abs]	2.0	2.3	2.5	2.5
Injection Pressure [MPa]	120	120	150	150
Intake O_2 Concentration [%]	14.0	14.6	14.3	14.2
Ethanol Fraction [-]	0.68	0.72	0.84	0.86
CA50 [°CA]	368.3	372.3	373.9	374.0
Ind. Thermal Efficiency [%]	43.3	43.5	44.0	43.7

The results of the load extension test show that the target values of NO_X and smoke emissions are achieved by increasing the intake boost pressure and the ethanol fraction, while maintaining the intake O_2 concentration around 14%. Moreover, the thermal efficiency is maintained at a similar level for mid-to-high IMEP test points. The cylinder pressure curves and the heat release traces for the test cases are shown in APPENDIX E.

5.4. Summary of Diesel and Dual-fuel Combustion Tests

The SSDC and DFC engine tests are conducted to determine the effects of EGR application and diesel injection timing on the exhaust emissions and the efficiency. The major findings from the two strategies are summarized in this section.

When the SSDC strategy is implemented, the dilution of the intake charge by the application of EGR is effective for the reduction of NO_X emissions. However, the use of EGR results in a smoke emission penalty, particularly at high load levels. LTC can be enabled by applying extensive EGR, wherein simultaneously low NO_X and smoke emissions are attainable. The enabling of LTC, however, is often associated with a large thermal efficiency penalty. Nevertheless, the target NO_X levels of 0.5 g/kW-hr and smoke levels of 0.05 g/kW-hr can be achieved at low-load conditions by applying a moderate intake charge dilution without incurring a significant thermal efficiency penalty.

DFC is enabled by the port-injection of ethanol and the direct injection of diesel. Although the use of EGR is necessary to facilitate the NO_X emission reduction, the smoke emissions can be significantly reduced by increasing the ethanol fraction. Increases in the exhaust HC and CO emissions are observed in the DFC strategy, which contribute to the combustion inefficiency. The combustion efficiency penalty is more prominent at low loads than at high loads. As the smoke emissions are suppressed by the increase in ethanol fraction even at high EGR ratios, the engine load level can be raised in the DFC strategy, while at the same time satisfying the target NO_X and smoke emission levels. Engine load levels of up to 19.2 bar IMEP are attained with the DFC strategy by carefully modulating the intake boost pressure, injection pressure, and combustion phasing. Moderate EGR levels are consistently applied to maintain the intake O_2 concentration at nearly 14% to achieve the target NO_X levels.

CHAPTER VI

6. CLOSED-LOOP COMBUSTION CONTROL

Diesel HTC typically exhibits a strong coupling between the injection timing and the combustion phasing due to the short ignition delay (as short as a fraction of one millisecond). The abundance of oxygen, the high-pressure fuel injection, and the very low auto-ignition resistance of the diesel fuel contribute to the short ignition delay. However, when low NO_X and smoke emissions are achieved (e.g. by the application of heavy EGR, late combustion phasing, and port fuel injection), the coupling between the injection timing and the combustion event is weakened. Although these combustion strategies can produce low NO_X and smoke emissions, steady-state test results have suggested that a precise control over ignition by fuel injection is necessary. Therefore, improvements on combustion control are made under closed-loop control, for regulating the diesel injection timing and duration by using the cylinder pressure measurement as feedback.

The current chapter first introduces the cylinder pressure analysis that is implemented for the design of the closed-loop combustion control. Thereafter, the controller developed to regulate the diesel injection command and track the IMEP and CA50 setpoints is described. The response of the controller to a step-change in the setpoint values is evaluated. Finally, EGR sweeps are conducted using both the single-shot diesel combustion (SSDC) and dual-fuel combustion (DFC) strategies to demonstrate the improvements in engine performance using the closed-loop combustion control.

6.1. Cycle-by-cycle Cylinder Pressure Analysis

The research engine is fitted with a cylinder pressure transducer and an optical encoder for acquiring the crank angle resolved cylinder pressure. For the cycle-by-cycle combustion control with cylinder pressure feedback, the pressure data is acquired on a field-programmable gate array (FPGA) device. A real-time (RT) controller is used to conduct the filtering and analysis of the cylinder pressure.

6.1.1. Cylinder Pressure Acquisition

Figure 6.1 shows a schematic describing the data acquisition with the FPGA device and the cylinder pressure analysis using the RT controller. A 16-bit analog input channel on the FPGA device is allocated for acquiring the cylinder pressure signal after it is processed by the charge amplifier. The data acquisition (DAQ) is triggered at the gas exchange TDC by using the encoder index signal in combination with the CAM position sensor signal. Once the DAQ is triggered, the encoder tick signal (0.1°CA resolution) is used as the sampling clock for acquiring the cylinder pressure. Direct memory access (DMA) registers on the LabVIEW FPGA are used to promptly store the cylinder pressure data onto the FPGA memory prior to transferring it to the RT system without incurring data loss. The DMA first-in first-out (FIFO) provide access to the elements in the same order as they are received [103].

The time available during the exhaust process is used to transfer the acquired pressure data to the RT. Only the cylinder pressure data corresponding to the compression and expansion strokes is used for this analysis. A second order forward-reverse Butterworth filter [89] is applied to the raw pressure signal. The cylinder pressure is then pegged to

the value of the intake manifold pressure at the crank angle of intake valve closing. The intake manifold pressure is acquired through the local network interface, as described in Section 3.4.

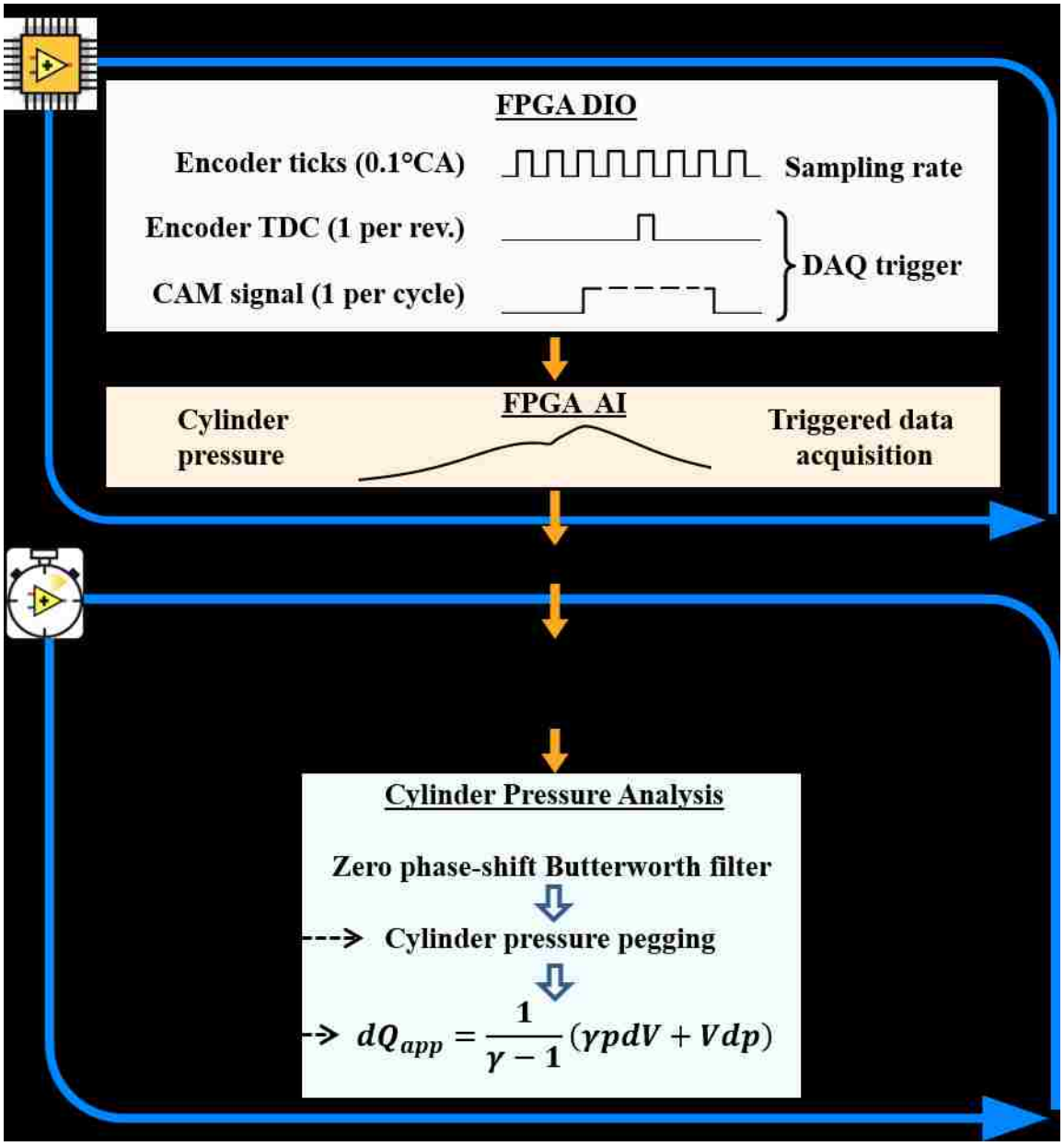

Figure 6.1 Schematic of Cycle-by-cycle Cylinder Pressure Analysis

6.1.2. Real-time Heat Release Analysis

The apparent heat release rate (AHRR) is calculated on the RT controller using the acquired cylinder pressure data and the stored cylinder volume data. The expression for the AHRR is previously presented in Equation (3.3). The intermediate calculations necessary for computing the AHRR are useful for analyzing the combustion characteristics. For instance, the pressure rise rate, $dp/d\theta$, is calculated as an intermediate step during the AHRR calculation, and its peak value can be easily identified to compute the peak pressure rise rate. Similarly, the gross IMEP can be computed by conducting a numerical integration of the $p \cdot dV/d\theta$ term in Equation (3.3) and then dividing the value by the swept volume. The gross IMEP is used for the closed-loop control of the engine load.

After calculating the AHRR, it is necessary to estimate the start of combustion (SOC) and the end of combustion (EOC), to evaluate the combustion phasing. In this research, the CA50 is selected as the indicator of combustion phasing. A fairly accurate estimation of the CA50 on a cycle-by-cycle basis is necessary for developing the combustion phasing control strategy. To limit the computation complexity, a simple yet robust algorithm for the estimation of SOC and EOC is developed in this work as shown in a schematic of the calculation routine in Figure 6.2. Specifically, first the crank angle corresponding to the peak of the AHRR is identified. The SOC is then identified as the crank angle at which the first zero value of AHRR occurs prior to the peak value. Similarly, the EOC is identified as the first zero crossing later than the location of the peak AHRR. After the SOC and the EOC have been identified, the cumulative heat release within the SOC-to-EOC window is computed. The CA50 is defined as the crank angle location at which

50% of the cumulative heat release has occurred. Similarly, the CA05 and the CA95 are identified for estimating the ignition delay and the combustion duration conforming to the definitions introduced in Section 3.4.2. It is noted that the method for detecting the SOC and the EOC may produce erroneous results if the AHRR has multiple zero-crossings, such as in the case of split combustion [104].

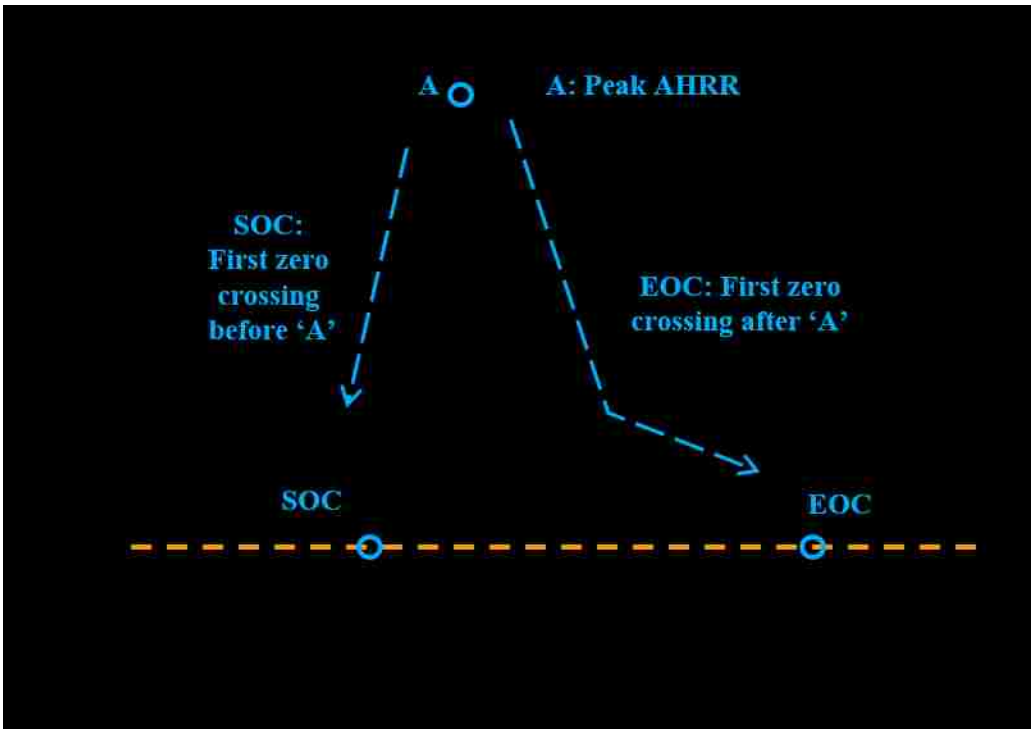

Figure 6.2 Illustration of Real-time Heat Release Analysis

Other methods have been developed in the past for CA50 estimation that avoid the calculation of AHRR, thereby making them less computational demanding. The Rasseweiler and Withrow's method [105], the pressure ratio management method [106], and the pressure departure ratio method [107] are a few of the CA50 estimation techniques. Note that by computing the AHRR in real-time, the peak cylinder pressure, peak pressure rise rate, IMEP, CA05, and CA95 are simultaneously obtained.

6.2. Closed-loop Control of Diesel Injection

6.2.1. CA50 Control

The diesel SOI timing has a strong influence on the CA50 in both of the SSDC and DFC strategies when the target CA50 is within a narrow crank angle window. Representative steady-state engine test results are compiled in Figure 6.3 to identify the region where the CA50 is responsive to variations in the diesel SOI timing. The same test results are presented in Figure 6.4 after normalizing the diesel SOI against a reference SOI. For each curve, the diesel SOI value at a CA50 of 368ºCA is set as the reference value of zero. The other SOI values are presented as a difference between the actual SOI and the reference SOI.

The ignition delay is affected by the engine load, the EGR amount, the intake boost, the diesel injection pressure, and the ethanol fraction, which, in turn, influences the correlation between SOI and CA50. By normalizing the SOI, the impact of the SOI on the CA50 is highlighted. Based on the results presented in Figure 6.4, when the normalized SOI is later than nearly −15°CA and earlier than nearly +10°CA, the CA50 varies linearly with the SOI. The linear region is selected for designing the CA50 control, and therefore the variation in the normalized SOI is restricted within the range of −15°CA to +10°CA. Furthermore, the earliest CA50 is limited to 360°CA to avoid pre-TDC combustion. Therefore, a range of CA50 between 360°CA to 378°CA is selected for the CA50 control, as marked in Figure 6.4.

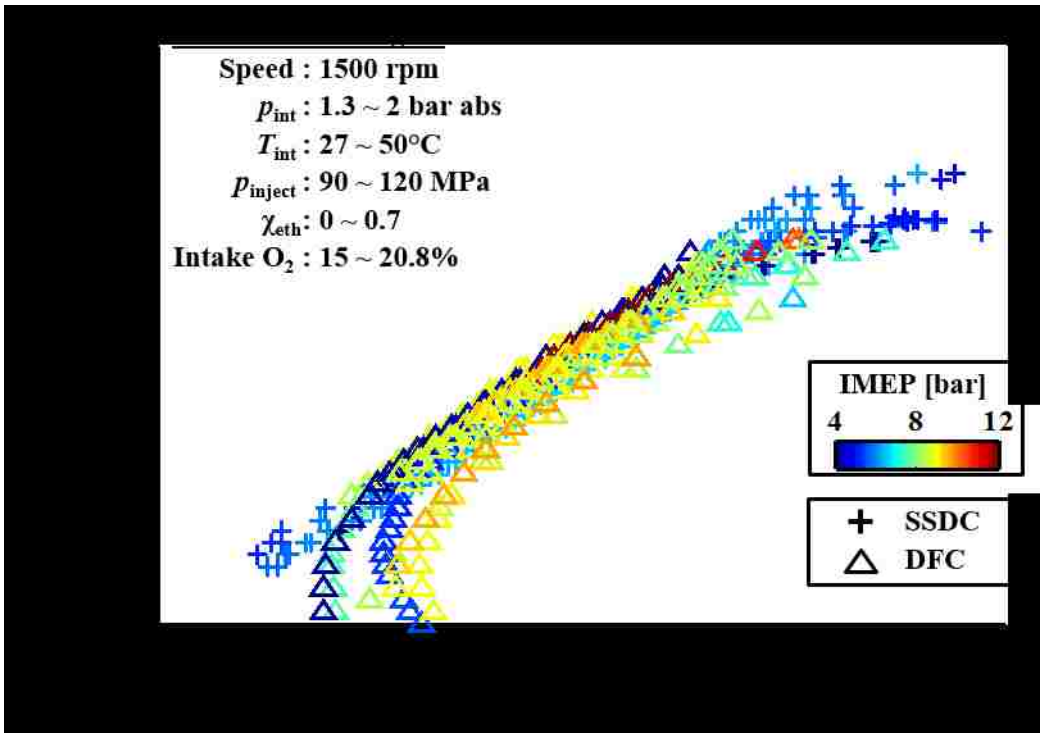

Figure 6.3 SOI versus CA50 for SSDC and DFC

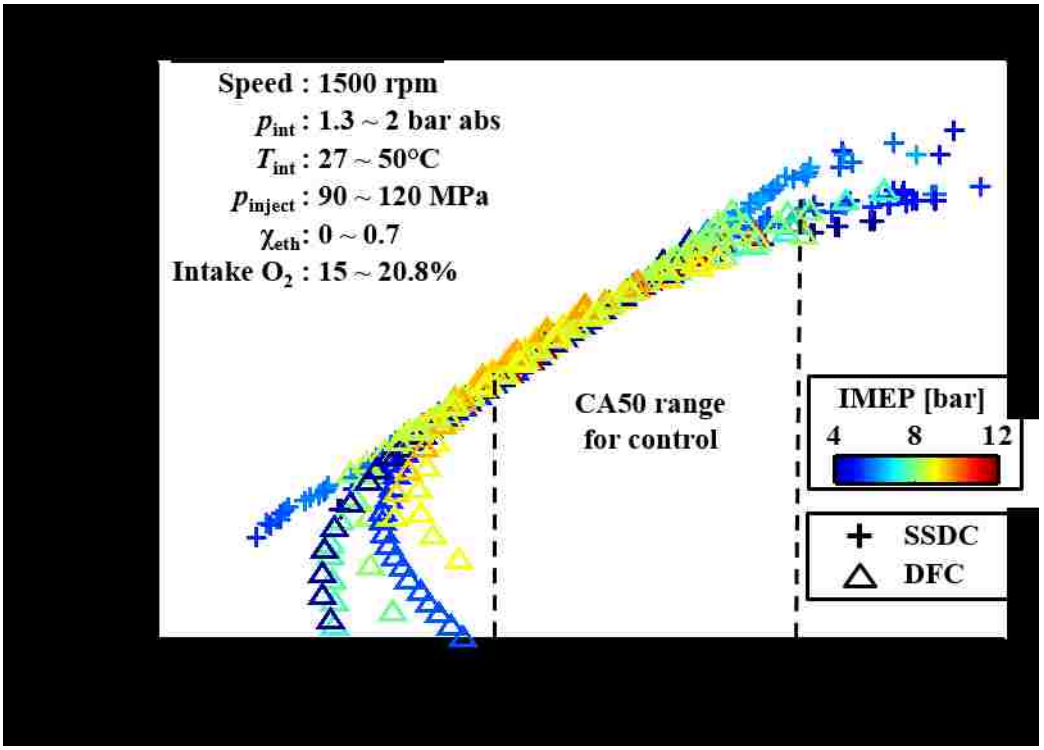

Figure 6.4 Closed-loop CA50 Control Region for SSDC and DFC

A proportional controller is implemented for the control of diesel SOI; the structure of the controller is shown in Figure 6.5. The difference between the CA50 setpoint and the CA50 feedback is multiplied with a proportional gain, k_p. The product is added to the previous diesel SOI. The SOI is advanced if the CA50 is later than the CA50 setpoint, and the SOI is retarded if the CA50 is earlier than the CA50 setpoint. The allowable change in the SOI between two engine cycles is constrained by a saturation block to avoid large variations in the SOI. The proportional gain and the upper and lower limits of the saturation block are tuned during the controller development stage and are fixed thereafter. The final controller settings are listed in Table 6.1. An additional safety limit is applied to the controller that shuts-off the fuel injection if the CA50 feedback is outside the pre-defined range of 360°CA to 378°CA.

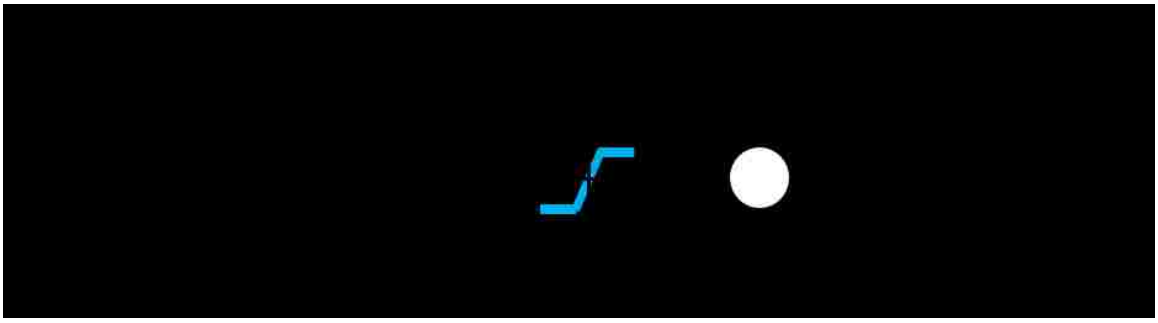

Figure 6.5 Proportional Controller for Closed-loop Control of CA50

6.2.2. IMEP Control

The control system for the diesel injection duration is similar to that of the diesel injection timing. The commanded diesel injection duration is used as the control variable for the closed-loop IMEP control. Injector characterization tests are conducted on a stand-alone injector bench, and the results are plotted in Figure 6.6. Additional details of

the injector characterization are presented in APPENDIX F. A nearly linear relationship is observed between the commanded injection duration and the amount of fuel delivered during the injection event. A proportional controller is implemented to regulate the commanded diesel injection duration, and therefore to adjust the injected fuel quantity.

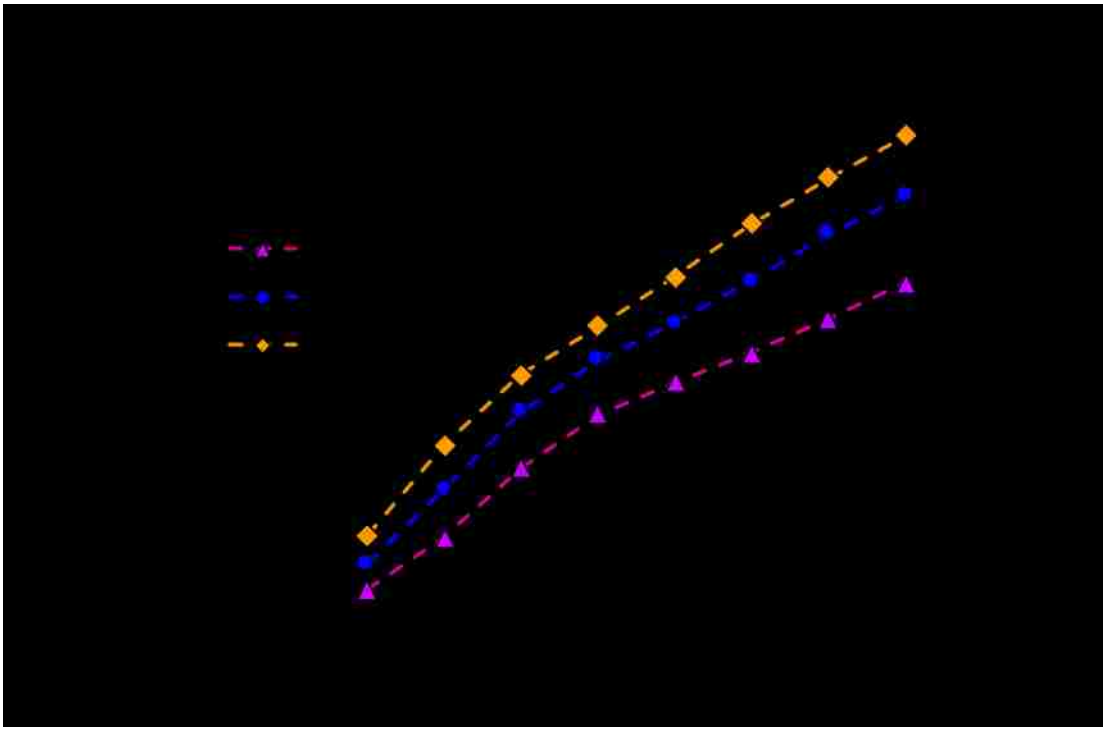

Figure 6.6 Injected Fuel Amount versus Commanded Injection Duration

The gross IMEP is used as the feedback for the diesel injection duration control. The feedback is compared to the IMEP setpoint. Based on the feedback, an adjustment is made to the previously commanded diesel injection duration on a cycle-by-cycle basis. The saturation block limits the maximum change in the injection command that is allowed every engine cycle. The controller gains and the saturation limits for the IMEP controller are fixed throughout the engine tests. An upper limit is also set over the total injection duration.

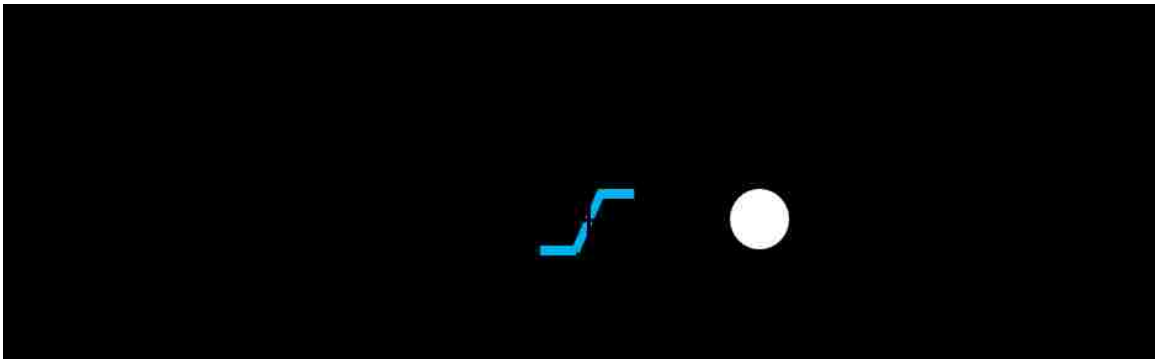

Figure 6.7 Proportional Controller for Closed-loop Control of IMEP

When the closed-loop CA50 and IMEP controllers are active, safety checks are performed on a cycle-by-cycle basis to ensure that the performance metrics are within safe limits. The CA50, IMEP, peak pressure, and peak pressure rise rate values for each cycle are compared with the safe limits. If any of the safety limits are exceeded, both the diesel and ethanol injection commands are immediately turned off to ensure that no damage is incurred to the test engine.

Table 6.1 Controller Settings for CA50 and IMEP Control

	CA50 Control	IMEP Control
Proportional gain	1	10
Maximum change per cycle	±0.2°CA	±5 μs
Minimum error value for control action	0.2°CA	0.2 bar

6.3. Test Results with Closed-loop Combustion Control

The closed-loop combustion control system is verified on the test engine by conducting two sets of engine tests. First, the response of the CA50 and IMEP controllers is evaluated by introducing step-changes in the CA50 and IMEP setpoints. EGR sweeping tests are then conducted with the closed-loop control, and the results are compared with those without closed-loop control.

6.3.1. Step Response of IMEP and CA50 Control

With closed-loop control over the IMEP and CA50, the IMEP setpoint is changed from 5.5 bar to 4.5 bar while the CA50 setpoint is fixed at 369.7°CA. The IMEP setpoint and the measured IMEP feedback during the IMEP step-change test are presented in Figure 6.8. The results suggest that the change of 1 bar IMEP is executed in nearly eight engine cycles. The commanded diesel injection duration and timing are shown in Figure 6.9. A maximum injection duration change of 5 μs per engine cycle is allowed which can be seen from the results of the step-change test. When the IMEP is changed, small adjustments are made to the diesel injection timing to maintain the CA50 near the setpoint. During the IMEP step-change, the CA50 is maintained within ± 1°CA of the setpoint, while the standard deviation of CA50 is 0.3ºCA.

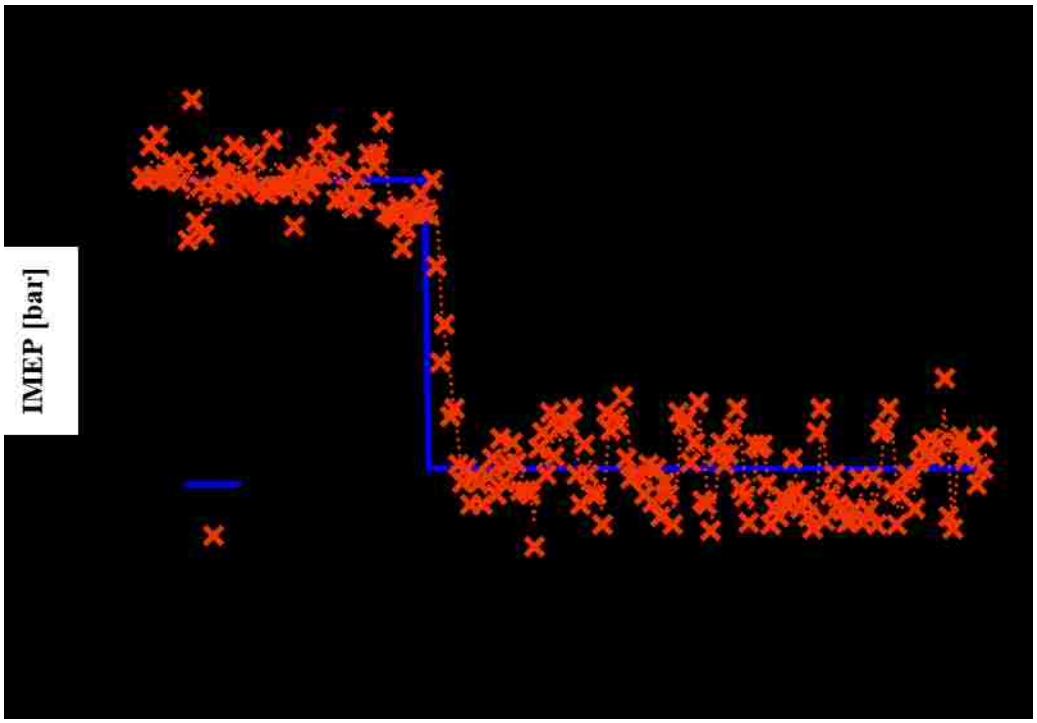

Figure 6.8 IMEP Setpoint Step-change: Closed-loop IMEP Control

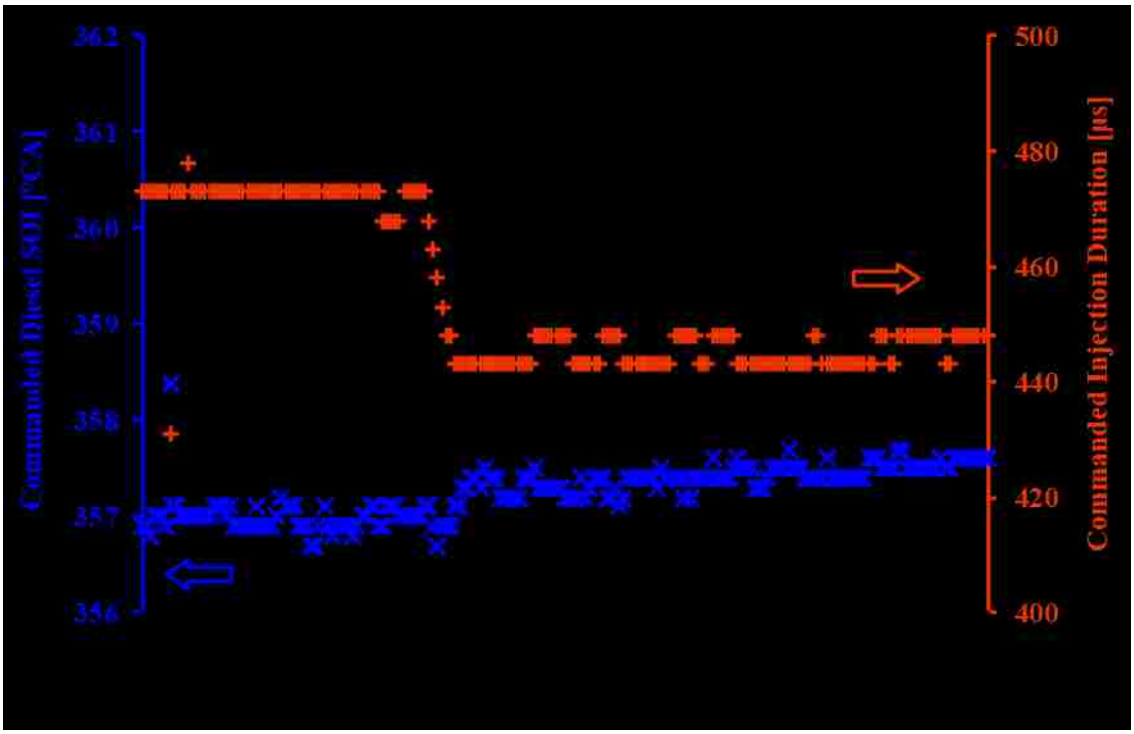

Figure 6.9 IMEP Setpoint Step-change: Diesel Injection Commands

A similar engine test is conducted to evaluate the performance of the closed-loop CA50 control. The CA50 setpoint is changed from 368°CA to 376°CA, while the IMEP setpoint is held constant at 5.5 bar. The CA50 setpoint and the cycle-by-cycle CA50 feedback are shown in Figure 6.10. The results show that nearly 20 engine cycles are required to delay the CA50 by 8°CA.

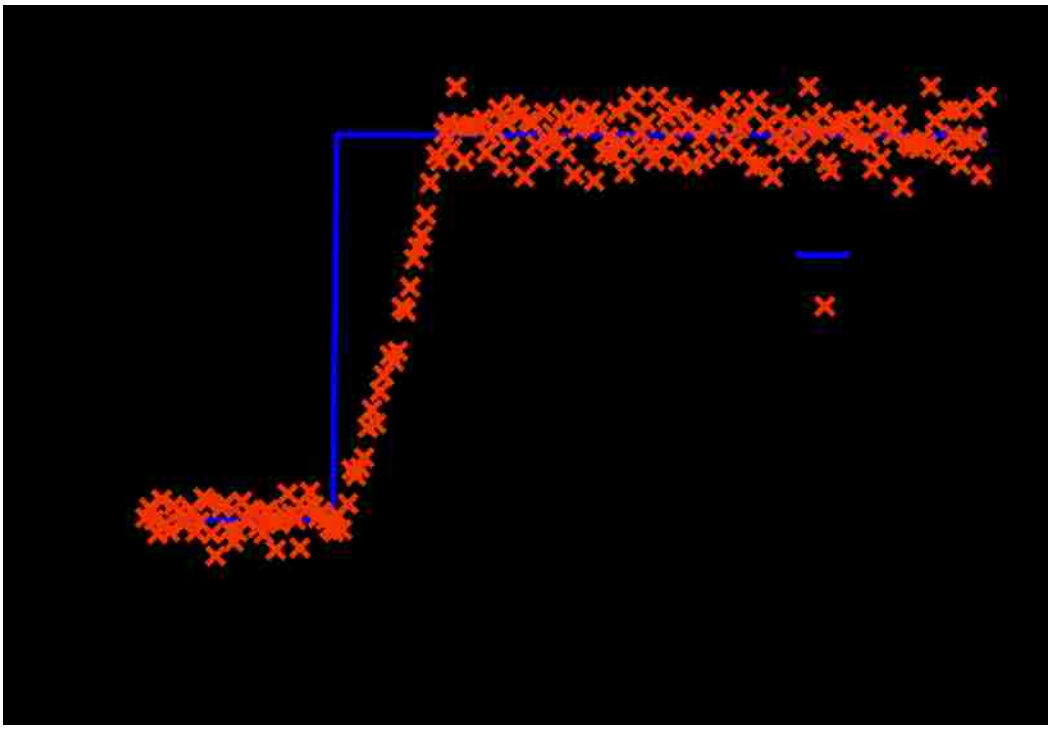

Figure 6.10 CA50 Setpoint Step-change: Closed-loop CA50 Control

The commanded diesel injection timing and duration are presented in Figure 6.11. When the CA50 setpoint is changed from 368°CA to 376°CA, the commanded injection timing is gradually delayed. The maximum adjustment in the commanded SOI is limited to 0.2°CA per engine cycle, which causes the gradual change in the CA50. The commanded injection duration is also plotted in Figure 6.11 for the 200 engine cycles during the CA50 step-change test. When the CA50 is delayed, the thermal efficiency reduces, which

may result in a lower IMEP if the commanded injection duration is fixed. Therefore, in order to maintain the IMEP around the setpoint, the IMEP controller increases the injection duration from 480 µs to 495 µs under closed-loop control. By adjusting the commanded diesel injection duration, the closed-loop IMEP controller is capable of maintaining the IMEP around the setpoint value. The COV_{IMEP} during the CA50 step-change test is 1.9%.

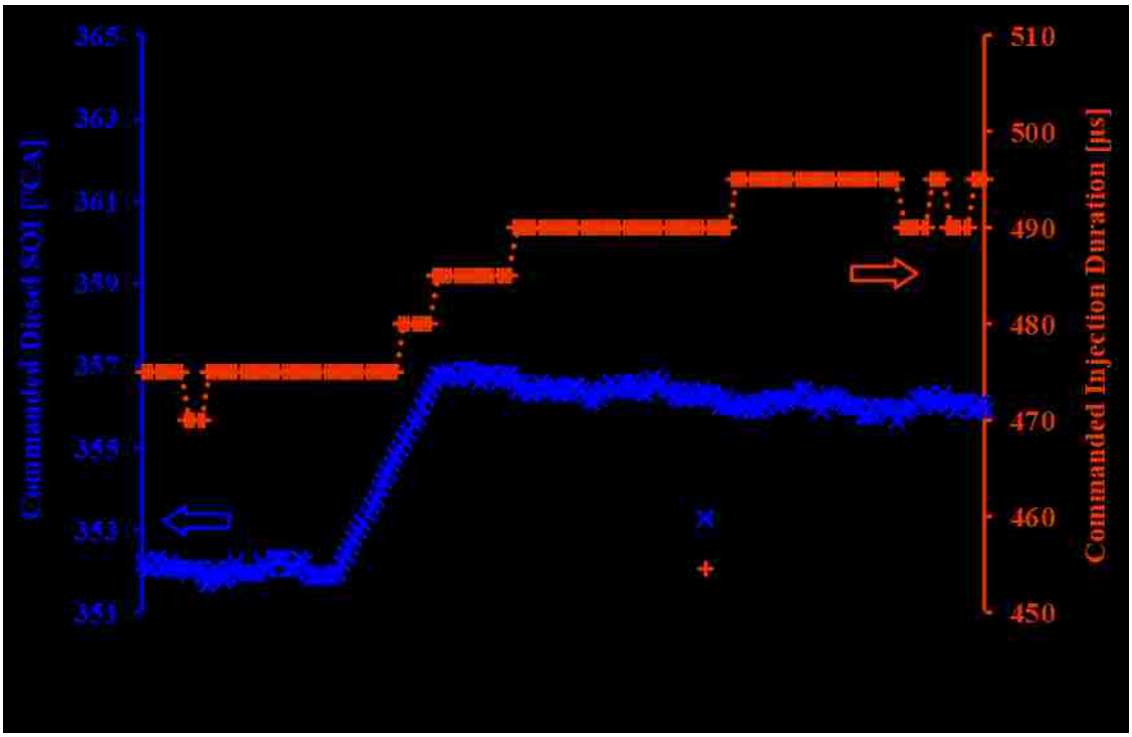

Figure 6.11 CA50 Setpoint Step-change: Diesel Injection Commands

6.3.2. Control Comparisons with SSDC EGR Sweeps

The results presented in Chapter 5 indicate that the ignition delay typically prolongs with an increase in EGR. If the injection timing is fixed, the combustion phasing delays as EGR increases. Furthermore, an extended increase in EGR may deteriorate the indicated thermal efficiency, which may lower the IMEP substantially if the fuelling amount is

fixed. Therefore, by implementing the closed-loop IMEP and CA50 control, the effect of EGR application on the combustion phasing and the IMEP can be compensated. To demonstrate the effectiveness of closed-loop control, EGR sweeping tests are conducted with closed-loop IMEP and CA50 control using the SSDC strategy at an IMEP of 5.5 bar. The results are compared with those of fixed fuel injection. The CA50 and the IMEP results are plotted against the intake O_2 concentration in Figure 6.12. The hollow markers represent the results of fixed control tests, in which the diesel injection timing is held constant, while the solid markers represent the results of the closed-loop control tests.

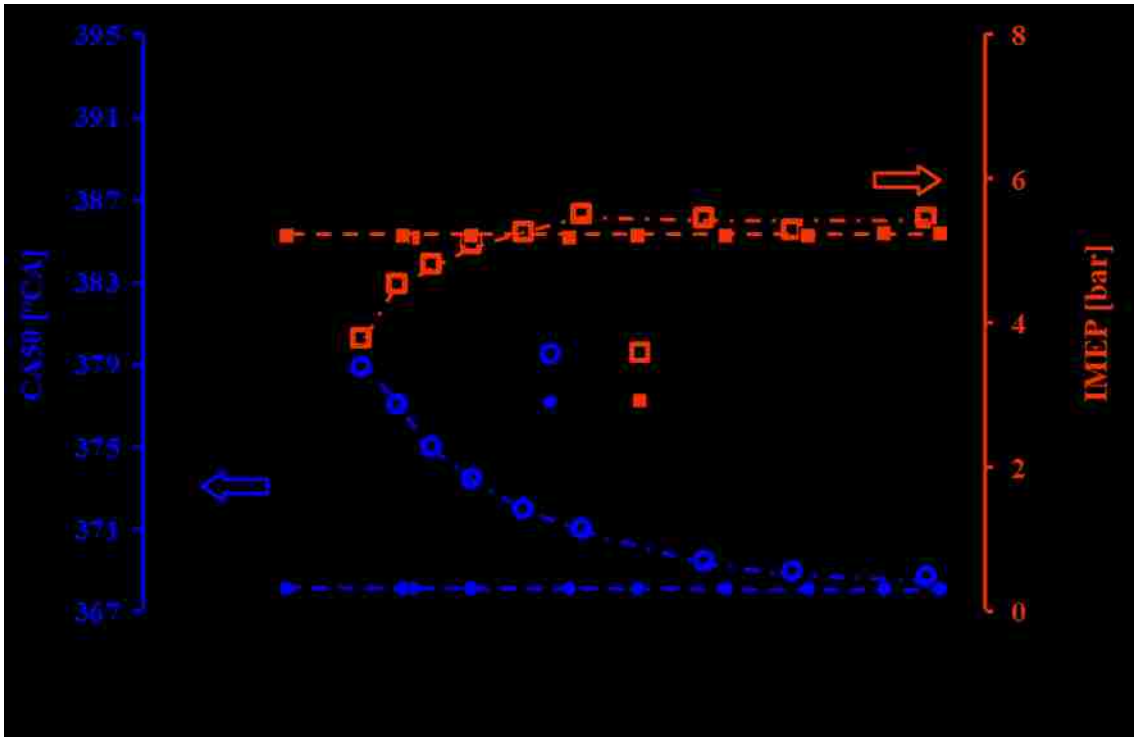

Figure 6.12 Control Comparison with SSDC EGR Sweeps: CA50 and IMEP

When the diesel injection command is fixed, the reduction in the intake O_2 concentration is accompanied by a delay in CA50 and a deduction in IMEP. In contrast, when the

dynamic fuel injection control is enacted, both the CA50 and the IMEP remain near the setpoint, largely independent of the EGR level.

The commanded diesel injection timing and duration are shown in Figure 6.13. When the control is active, the diesel injection timing is progressively advanced by the closed-loop CA50 controller.

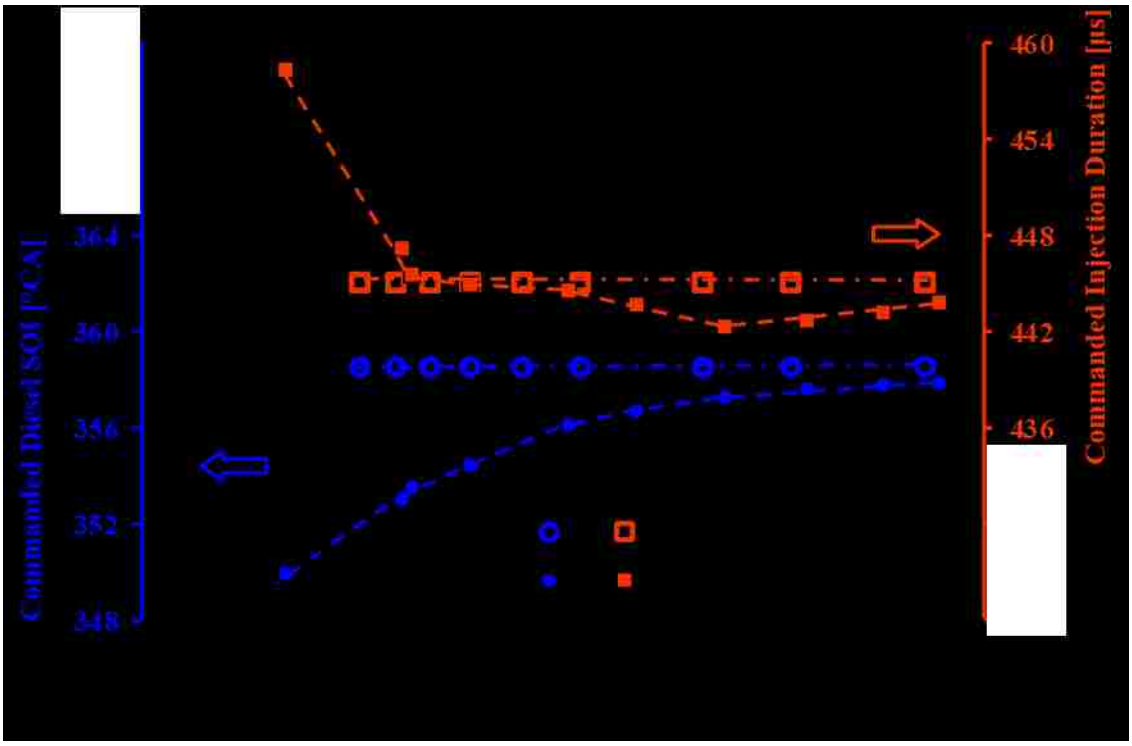

Figure 6.13 Control Comparison with SSDC EGR Sweeps: Injection

The commanded injection duration is also adjusted by the closed-loop IMEP controller as the EGR level changes. At low EGR levels, a small reduction in the injection duration is necessary to maintain the IMEP around the setpoint, suggesting a small improvement in the thermal efficiency at low EGR levels. When the intake O_2 concentration is lower than

14%, the controller substantially increases the injection duration, signifying that a lower thermal efficiency is incurred.

The smoke and NO_X emissions for the two EGR sweeping tests are plotted in Figure 6.14. An insignificant variation is observed in the NO_X emissions with and without the closed-loop diesel injection control. In contrast, a large rise in the smoke emissions is observed at high EGR levels when the closed-loop control is active. The larger diesel injection quantity and the earlier CA50 may contribute to the sharp increase in the smoke emissions when closed-loop diesel injection control is active.

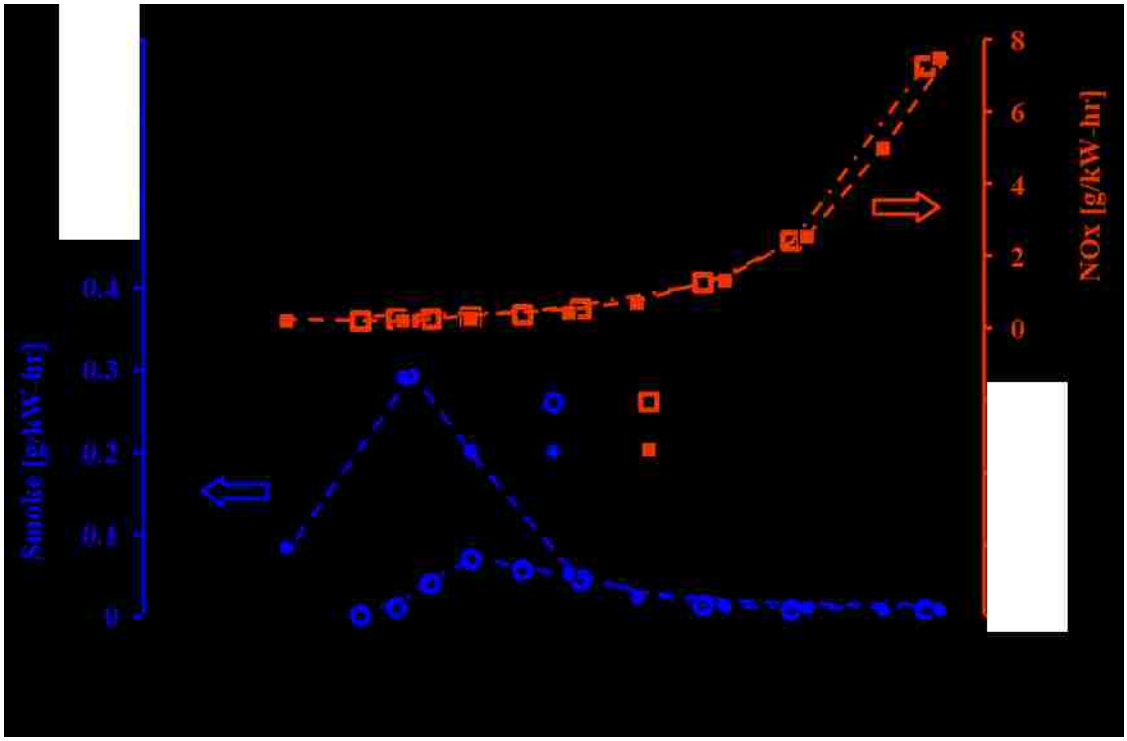

Figure 6.14 Control Comparison with SSDC EGR Sweeps: Smoke and NO_X

The COV_{IMEP} and the STD_{CA50} are presented in Figure 6.15. At high EGR levels, a large improvement in combustion stability is achieved with the active injection control.

However, at low EGR levels, the combustion stability deteriorates with the closed-loop combustion control, when compared to the fixed injection.

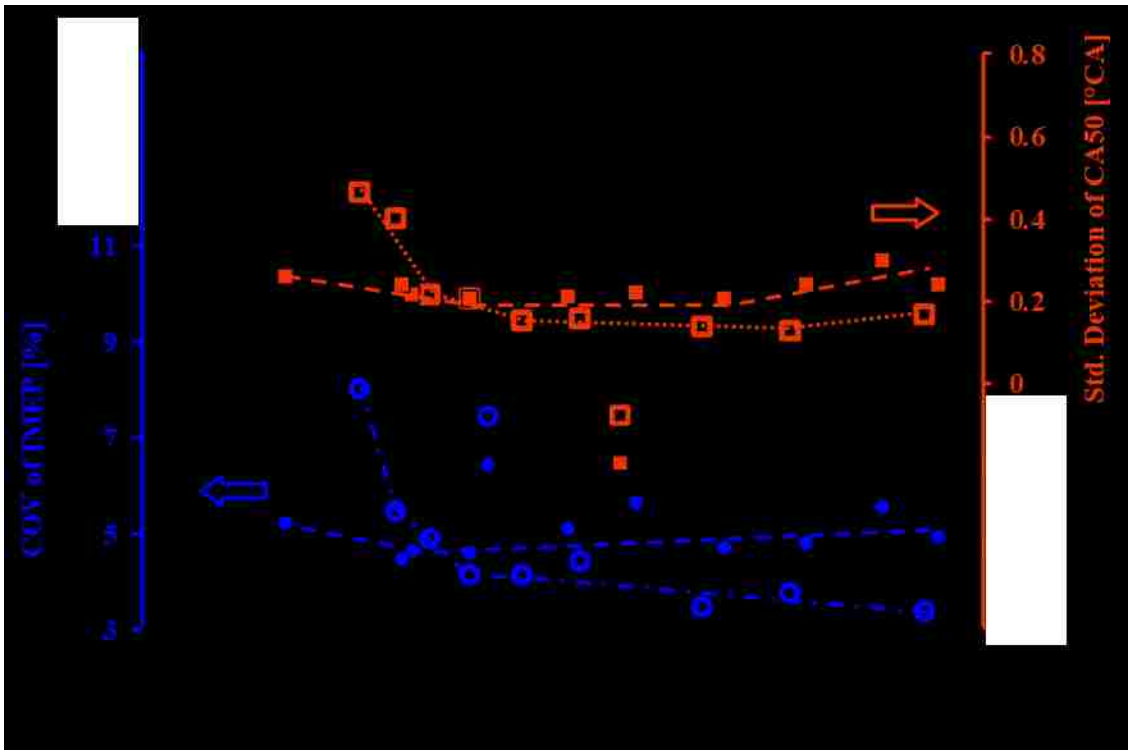

Figure 6.15 Control Comparison with SSDC EGR Sweeps: Stability

6.3.3. Control Comparisons with DFC EGR Sweeps

The DFC strategy is effective in achieving ultra-low NO_X and smoke emissions at increased engine loads when moderate levels of EGR are applied. To investigate the efficacy of implementing closed-loop control in the DFC strategy, EGR sweeping tests are conducted at 10 bar IMEP. Initially, the diesel injection duration and the ethanol injection duration are fixed to obtain an ethanol fraction of 0.6. The diesel injection timing is adjusted such that the CA50 is at 368°CA. First, the EGR sweep is conducted while the injection parameters are not varied. Second, the EGR sweep is repeated with the closed-loop control, where the diesel injection timing and duration are controlled to

maintain the target CA50 and IMEP. During this EGR sweeping test, the ethanol injection is not adjusted. Therefore, the ethanol fraction may vary when the diesel injection duration is changed.

The CA50 and the IMEP are plotted in Figure 6.16. Under fixed control, as the intake O_2 concentration is reduced, the CA50 is delayed and the IMEP is reduced. However, when the combustion control is enacted, both the CA50 and the IMEP are held around the setpoint values by adjusting the diesel injection command, except at 10% intake O_2 concentration, where the IMEP is slightly reduced.

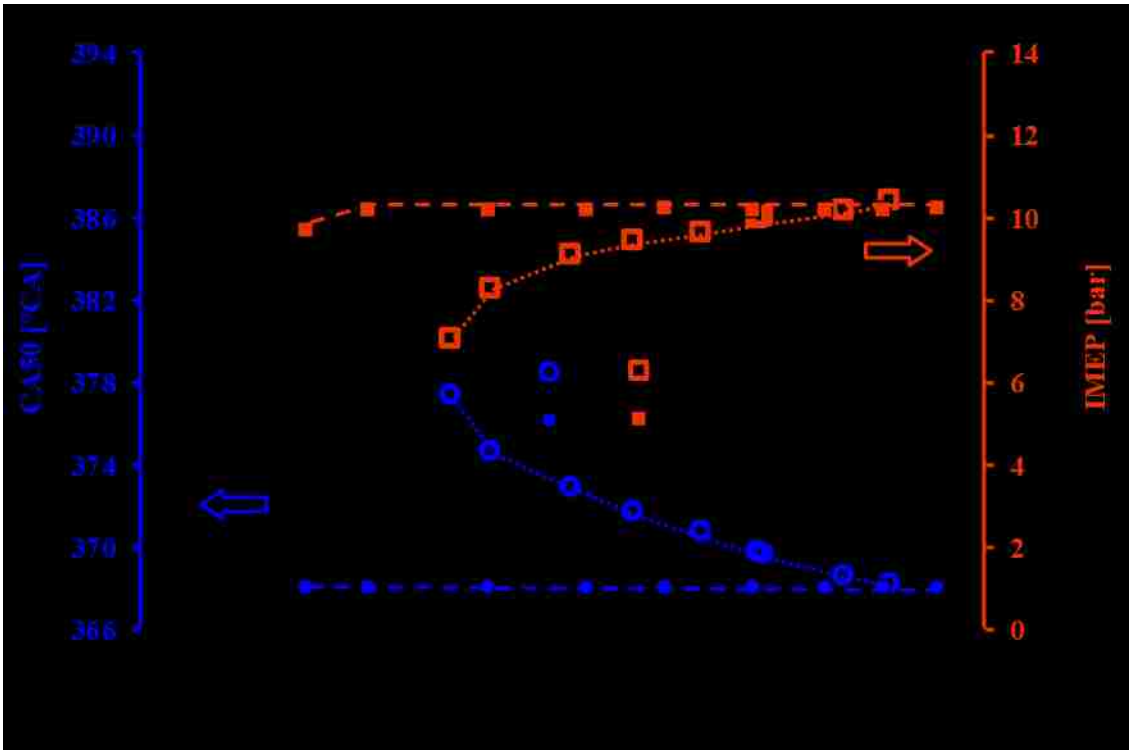

Figure 6.16 Control Comparison with DFC EGR Sweeps: CA50 and IMEP

The diesel injection timing and duration are presented in Figure 6.17. Under closed-loop control, the diesel injection duration increases at high EGR levels to maintain the IMEP

near the setpoint as the intake O_2 concentration reduces. In this case, the diesel injection duration is limited to a maximum value of 480 µs. Therefore, at 10% intake O_2 concentration, further increase in the diesel injection duration is not permitted by the controller. The CA50 is maintained around the setpoint value by advancing the diesel injection timing as the EGR level is increased.

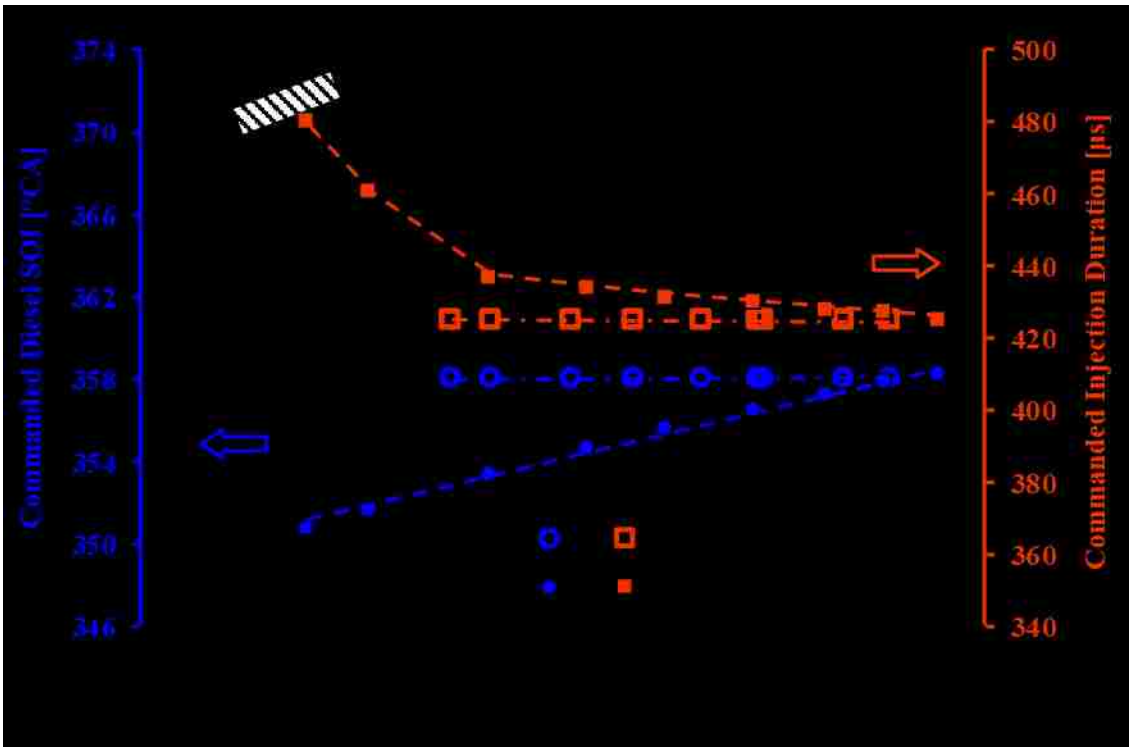

Figure 6.17 Control Comparison with DFC EGR Sweeps: Injection

The control comparisons of the smoke and NO_X emissions during the DFC tests are presented in Figure 6.18. The results show that the NO_X emissions are similar during the two EGR sweeping tests. The smoke emissions, on the contrary, rise sharply when the intake O_2 concentration is lower than 14% for the test with active injection control. The rise in the smoke is partially caused by the substantial increase in the diesel injection duration at the low intake O_2 concentration levels.

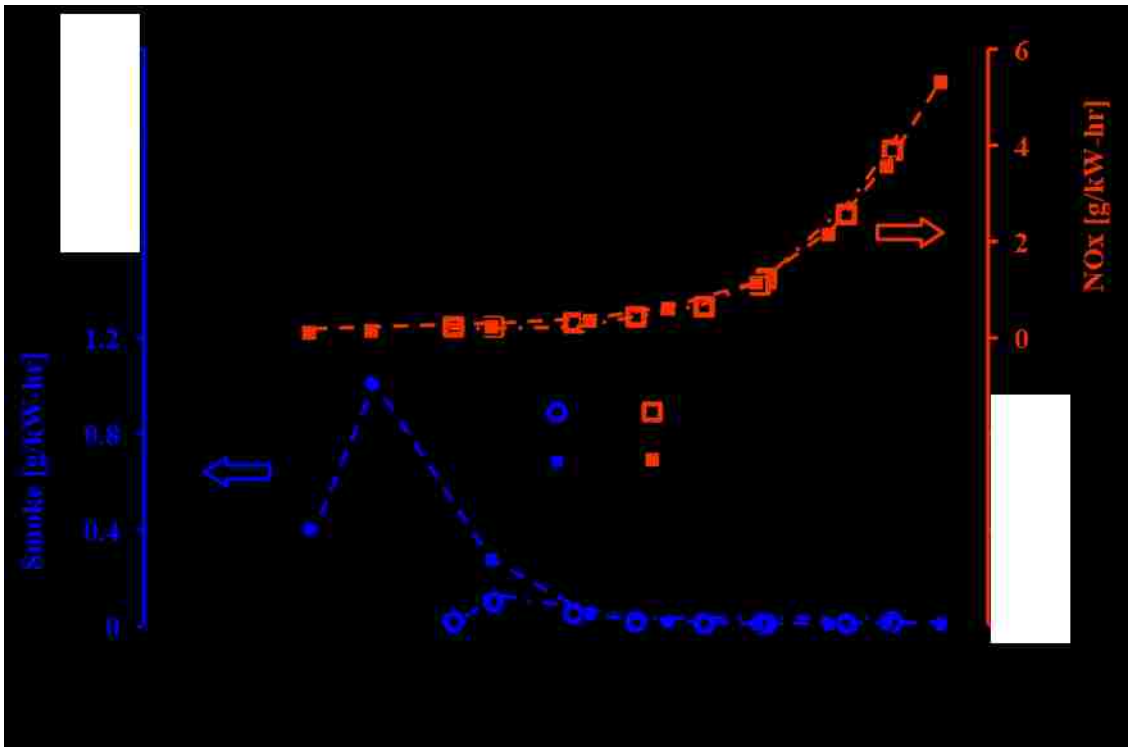

Figure 6.18 Control Comparison with DFC EGR Sweeps: Smoke and NO_X

The COV_{IMEP} and STD_{CA50} are shown in Figure 6.19. The COV_{IMEP} increases abruptly for the EGR sweeping test without the active injection control as the EGR level is raised. The cyclic variations in the CA50 also increase consistently with the increase in the EGR level. When the diesel injection control is active, an improvement in the combustion stability is observed at the low intake O_2 concentrations.

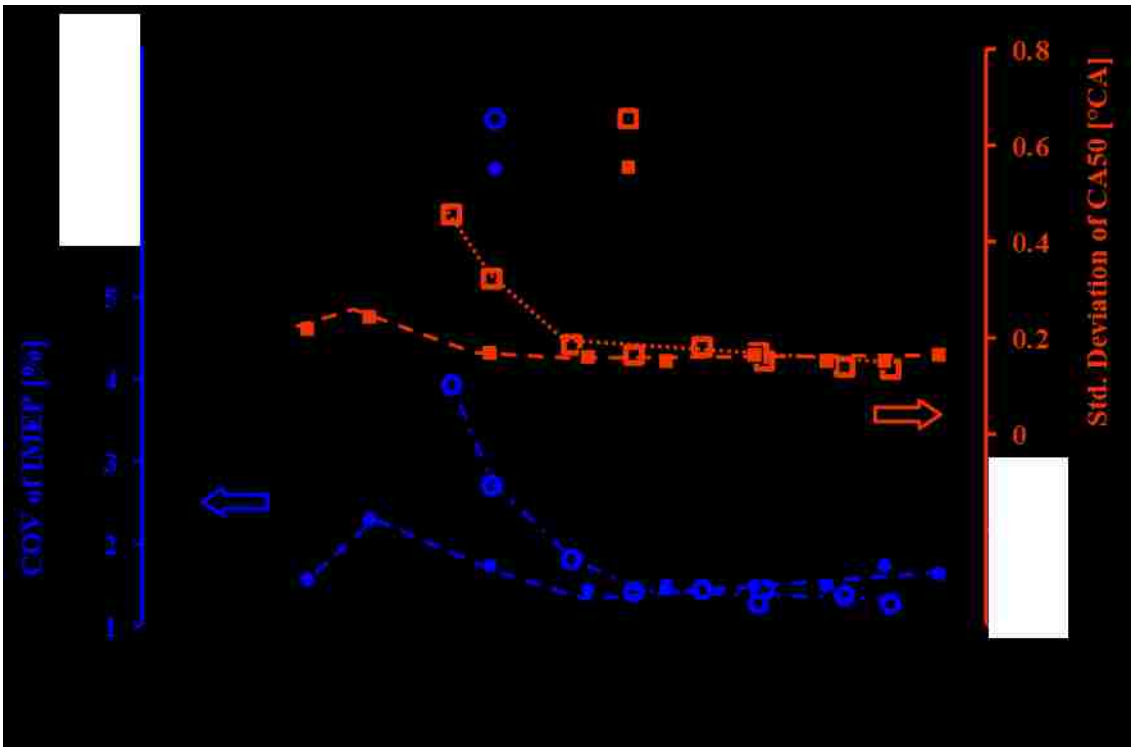

Figure 6.19 Control Comparison with DFC EGR Sweeps: Stability

6.4. Summary of Closed-loop Combustion Control

A closed-loop control system is developed for regulating the diesel injection command dynamically by using the cylinder pressure measurement as the feedback. Based on the results of steady-state testing with the SSDC and DFC strategies, the control over the diesel injection command is effective for maintaining a desired combustion phasing in both the strategies. Therefore, a proportional controller is developed for modulating the diesel injection timing to achieve a desired CA50 setpoint. Similarly, the diesel injection duration is controlled using a proportional controller to regulate the IMEP level. The RT-FPGA system ensures the cycle-by-cycle fuel injection control for the engine cycle resolved analysis of cylinder pressure and the execution of the control algorithm.

The performance of the dynamic control system is demonstrated with the help of two sets of engine tests. First, the step-response of the controller is demonstrated for both of the IMEP and CA50 control with the diesel strategy. Second, EGR sweeping tests are conducted using the SSDC and DFC strategies, and the results are compared with EGR sweep tests conducted without closed-loop diesel injection control. By regulating the IMEP and the CA50 dynamically to the setpoint regardless of the intake O_2 concentration, an improvement in the combustion stability is attained under both the combustion strategies.

CHAPTER VII

7. DESIGN AND DEMONSTRATION OF SYSTEMATIC CONTROL

The results presented in Chapter 5 highlighted the advantages of adapting two combustion strategies, the single-shot diesel combustion (SSDC) and the dual-fuel combustion (DFC), at different engine load levels for achieving clean combustion over a wide engine load range. However, the use of two combustion strategies, and the associated control requirements, would further complicate the design and calibration of engine controllers. In the current chapter, a systematic controller is developed to reduce the calibration effort associated with the enabling of the clean combustion strategies.

7.1. Systematic Control Architecture

The architecture of systematic control is proposed in a block diagram, as shown in Figure 7.1. The closed-loop control block represents the diesel injection controller, based on the fast feedback of cylinder pressure, as discussed in Chapter 6. The dynamic target block provides the setpoints for the closed-loop controller. In the conventional engine control scenario, the dynamic target represents the values stored in the calibrated lookup tables [108]. In the current research, the dynamic target is designed based on the results of the engine tests with the SSDC and DFC strategies.

A simplified engine model is integrated into the systematic control. The structure of the systematic control is similar to the model-based feed-forward control architecture [67]. The results of the model calculations are used as inputs to the dynamic target block. The

numerical expressions for the EGR and in-cylinder calculations, as presented in Chapter 4, are simplified for implementing on the real-time (RT) controller.

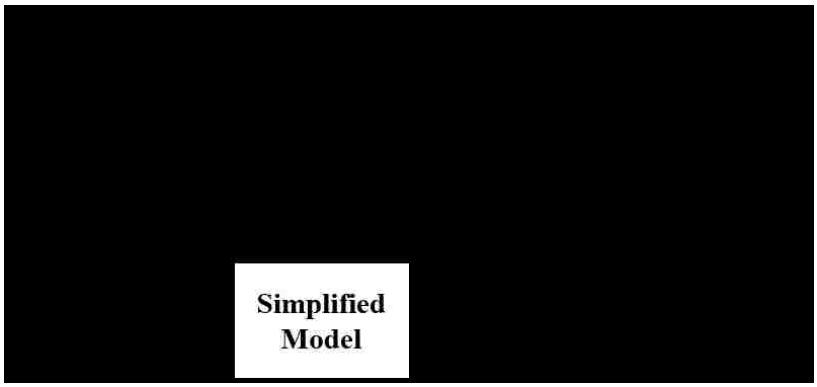

Figure 7.1 Systematic Control Architecture

In the subsequent sections, a more detailed discussion is provided for each block of the systematic control architecture followed by the engine test results. The detailed description of the simplified model is provided in APPENDIX G.

7.2. Dynamic Target for Air-path Control

The dynamic target block provides the setpoint values to the closed-loop controller, which forms a critical part of the control architecture presented in Figure 7.1. In this section, the dynamic targets for the air-path system are discussed in detail. The engine test data presented in this section highlights the overall trends observed during the engine testing phase.

7.2.1. Intake O_2 and NO_X correlation

The suitable intake O_2 concentration for NO_X reduction depends on the engine load and the intake boost pressure at any given EGR ratio. The intake O_2 concentration is used for

measuring the effectiveness of EGR, instead of the EGR ratio [93]. Thus, the intake O_2 concentration is selected as the preferred parameter from the NO_X control perspective. In Figure 7.2, the NO_X emissions are plotted against the intake O_2 concentration for EGR sweeping tests conducted over a range of testing conditions. Different marker types are used to distinguish between the SSDC and DFC strategies, and the marker colors indicate the load levels.

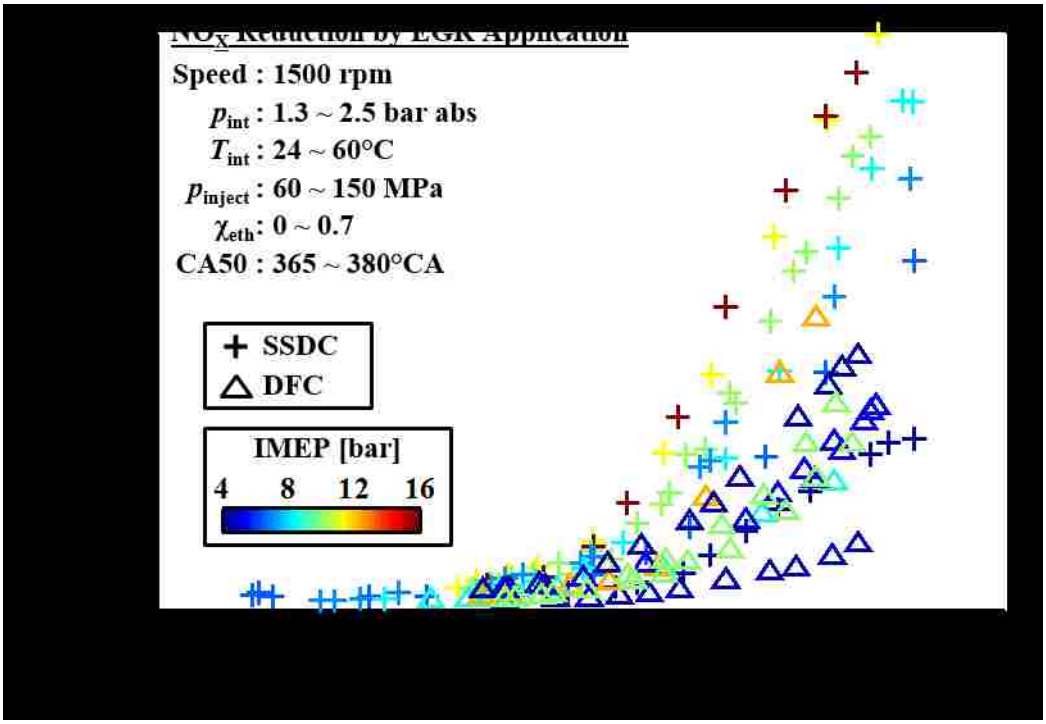

Figure 7.2 NO_X versus Intake O_2 Concentration for SSDC and DFC Strategies

In Figure 7.3, the same test data is normalized to the NO_X level at zero EGR condition for each test set, and is presented as the NO_X reduction based on Equation (7.1**)**.

$$NOx\ Reduction = \frac{NOx_{\text{zero } EGR} - NOx}{NOx_{\text{zero } EGR}} \tag{7.1}$$

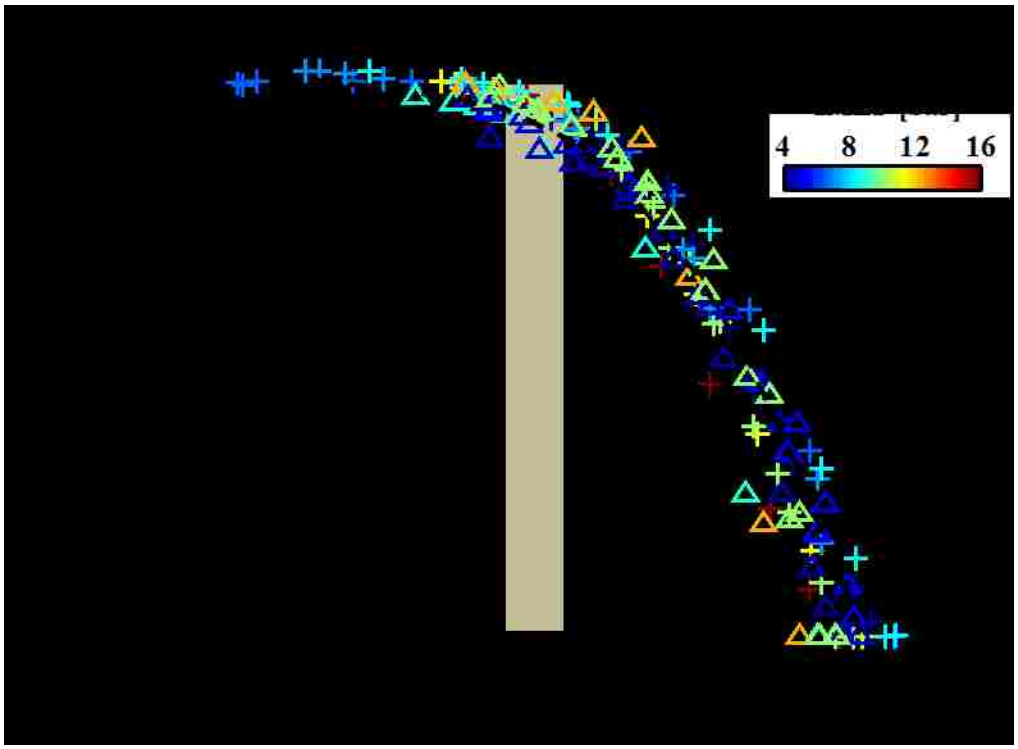

Figure 7.3 NO_X Reduction for SSDC and DFC Strategies

The NO_X emission results in Figure 7.3 represent the following trends:

- When the data is presented as the reduction in NO_X emissions with respect to the intake O_2 concentration, all the test data sets tend to overlay. These trends highlight the sensitivity of the NO_X emissions reduction to the intake O_2 concentration.
- The NO_X emission reduction is significant until the intake O_2 concentration is lowered to nearly 14~15%. When the intake O_2 concentration is decreased further, the reduction of the NO_X emissions becomes less prominent. This trend demonstrates a challenge of achieving ultra-low NO_X emissions. Intake O_2 concentrations of 14~15% are selected as the target for EGR control during the systematic control.

7.2.2. In-cylinder Air Excess Ratio and Smoke Correlation

While the NO_X emissions depict a straightforward trend with the inert dilution at the intake, the smoke is affected by several engine operating variables, such as intake boost pressure, EGR rate, fuel amount, injection pressure, and ignition delay. The in-cylinder air excess ratio is selected as a smoke control parameter in this work. As shown in Equation (4.11), the in-cylinder air excess ratio is a function of the intake boost, the EGR ratio, and the fuelling quantity.

The smoke emissions from representative EGR sweeping tests are shown in Figure 7.4. The results are plotted against the in-cylinder air excess ratio and the intake O_2 concentration, while the color of the marker denotes the indicated smoke emissions for each test point. The two sets of test results represent the SSDC and the DFC strategies. The SSDC tests are conducted at 5 bar IMEP and 90 MPa injection pressure, while the intake boost pressure varies from 1.5 bar to 2 bar absolute. The DFC tests are conducted at 10 bar IMEP and 120 MPa injection pressure with two intake boost pressure levels of 2 bar and 2.5 bar absolute.

During the EGR sweep, the in-cylinder air excess ratio decreases consistently with the reduction in the intake O_2 concentration. An increase in the smoke emissions is observed as the intake O_2 concentration reduces. For the test cases with the higher boost pressure, the in-cylinder air excess ratio is consistently higher, and the smoke emissions at the same intake O_2 concentration level are lower. The test results presented in Figure 7.4 highlight the effectiveness of higher air excess for smoke reduction.

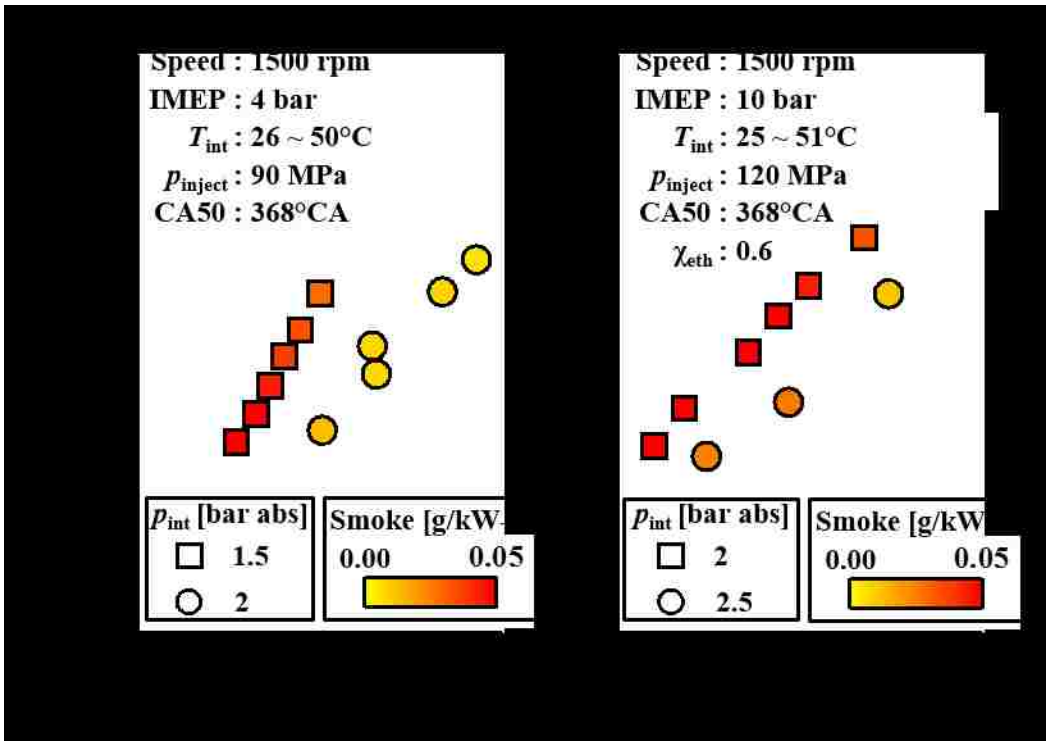

Figure 7.4 Effect of $[O_2]_{int}$ and $\lambda_{in\text{-}cyl}$ on Smoke Trends

7.2.3. Air-path Control Considerations

The results presented in the previous subsection suggest that the use of EGR is effective for reducing the NO_X emissions, whereas a larger in-cylinder air excess ratio is beneficial for lower smoke emissions. However, the application of EGR results in a reduction of the intake O_2 concentration, which at a fixed intake boost pressure causes a subsequent reduction in the in-cylinder air excess ratio. Therefore, an adequate control strategy for regulating the intake boost pressure and the EGR flow rate is necessary so that a lean in-cylinder charge is maintained while achieving the 14~15% intake O_2 concentration (necessary for NO_X reduction). As the EGR flow rate is typically not measured, the intake boost and the fresh mass air flow (MAF) rate are controlled to attain these air-path targets. A contour map of intake boost pressure and MAF is presented in Figure 7.5. The

map is generated using the zero-D engine cycle simulation routine discussed in APPENDIX D. Simulations are conducted by varying the intake boost pressure, MAF and fuel amounts while the intake O_2 concentration and the heat release characteristics are kept constant. The color contours represent the IMEP levels corresponding to the increased fuelling amounts. Iso-lines of in-cylinder air excess ratio and peak cylinder pressure are overlaid on the same contour plot.

The trends presented in Figure 7.5 can be explained as follows; while maintaining a fixed intake O_2 concentration of 14%, a relatively high in-cylinder air excess ratio can be attained by increasing the intake boost pressure while maintaining a similar MAF level. In addition to the intake O_2 concentration, if the in-cylinder air excess ratio is fixed, the model calculations suggest that a unique combination of intake boost pressure and MAF values is necessary at a particular IMEP level. Therefore, the dynamic targets are designed for the air-path control at each engine load level, in which the intake boost pressure and the MAF setpoints are selected. These setpoints correspond to the target values of intake O_2 concentration and in-cylinder air excess ratio.

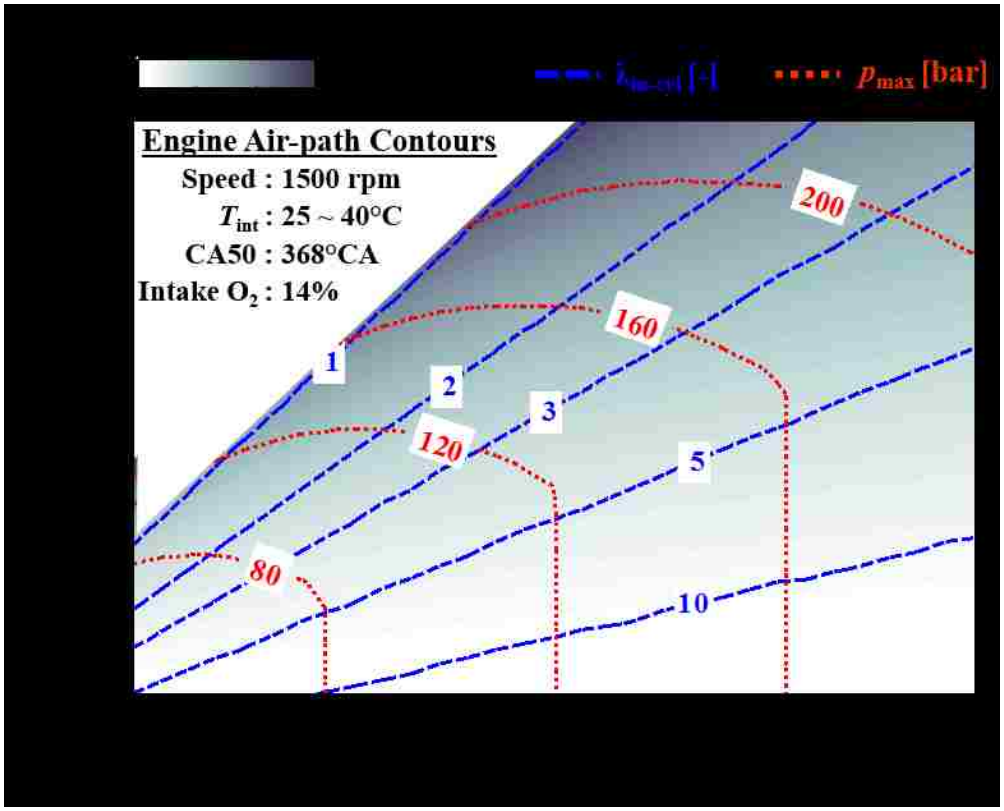

Figure 7.5 Contour Map of p_{int} and MAF at Varying Loads and a Fixed $[O_2]_{int}$

The selection of a target value for the in-cylinder air excess ratio is constrained by the hardware limitations, as partially shown in Figure 7.5 by the contours of peak cylinder pressure. At a fixed intake O_2 concentration, the range of air excess ratio shrinks as the engine load increases due to the peak cylinder pressure limits. Furthermore, the increase in the intake boost pressure, simultaneously at high EGR rates, is limited by the operating characteristics of the turbocharging hardware on production engines [17].

7.3. Dynamic Target for Combustion Control

7.3.1. Preferred CA50

The parametric analysis, of the combustion phasing on the thermal efficiency, suggests that a high thermal efficiency is achieved when the CA50 is maintained in a narrow crank angle window between 366°CA to 372°CA (Figure 4.4). In practice, a later CA50 can reduce the NO_X emissions and lower the peak pressure rise rate [95]. Representative test results with varying CA50 from the two combustion strategies, SSDC and DFC, are presented in Figure 7.6.

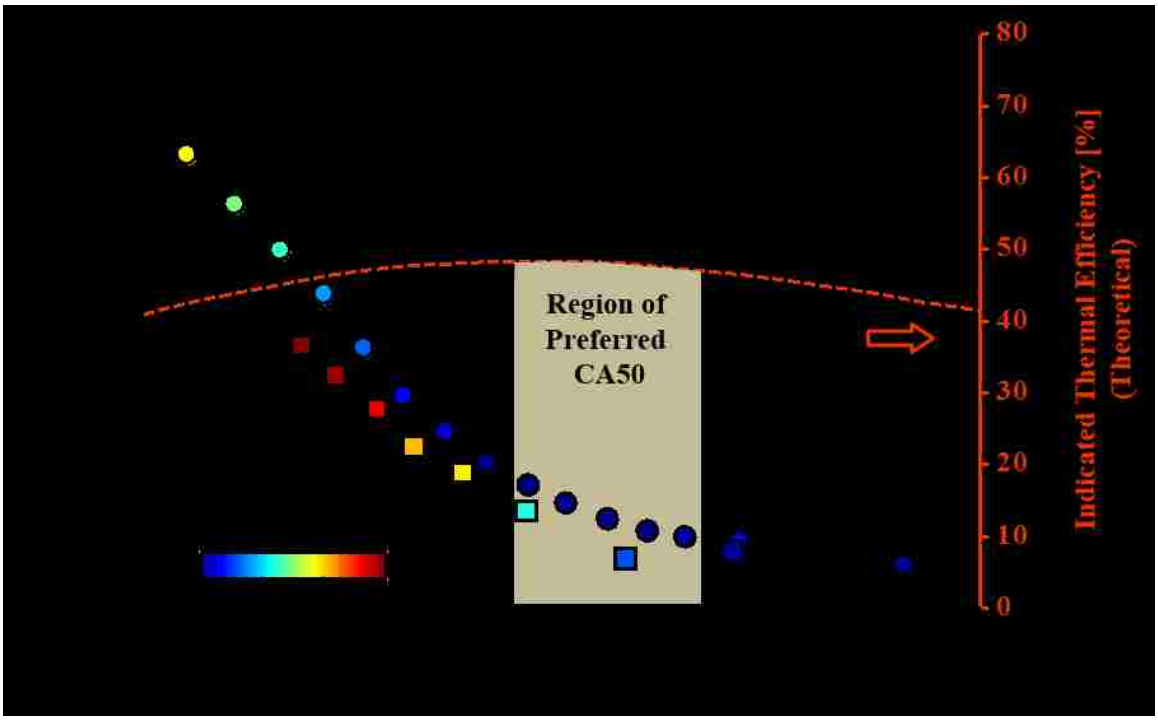

Figure 7.6 Region of CA50 for Thermal Efficiency and NO_X Improvements

The results of parametric simulations of the thermal efficiency are overlaid on the same plot. For obtaining a CA50 target with systematic control, a region of CA50 between 368°CA to 376°CA is selected as the preferred window. Within this window, an earlier

CA50 can improve the thermal efficiency, while a later CA50 is beneficial for the NO_X reduction, and for attaining lower peak pressure rise rates.

7.3.2. Diesel and Dual-fuel Combustion Switching

The investigation of the SSDC and the DFC strategies suggests that switching between the two strategies is necessary for minimizing the NO_X, smoke, and thermal efficiency trade-offs across the engine load range. Representative test results are presented in Figure 7.7 and Figure 7.8 for selecting an IMEP, at which switching between the two strategies is carried out. The thermal efficiency is plotted against the IMEP for selected test points where the NO_X emissions are lower than 0.5 g/kW-hr, and the smoke emissions are lower than 0.05 g/kW-hr. The low NO_X emissions are primarily achieved by EGR application for all the test cases.

In the relevantly high IMEP levels under the SSDC strategy, the simultaneously low NO_X and smoke emissions are achieved at intake O_2 concentrations lower than 11%. However, at these high inert dilution levels, the combustion efficiency is significantly reduced. In the DFC strategy, the reduction in smoke emissions is achieved by increasing the ethanol fraction as the IMEP is raised, whereas an intake O_2 concentration of around 14% is sufficient to reduce the NO_X emissions below 0.5 g/kW-hr. Therefore, at the high IMEP levels, the thermal efficiency is significantly lower in the SSDC strategy, compared to the DFC strategy. On the contrary, at low engine load levels, the thermal efficiency of the DFC strategy is lower than that of the SSDC strategy. The combustion efficiency reduces considerably for the DFC strategy at low load levels, thereby resulting in a lower thermal efficiency.

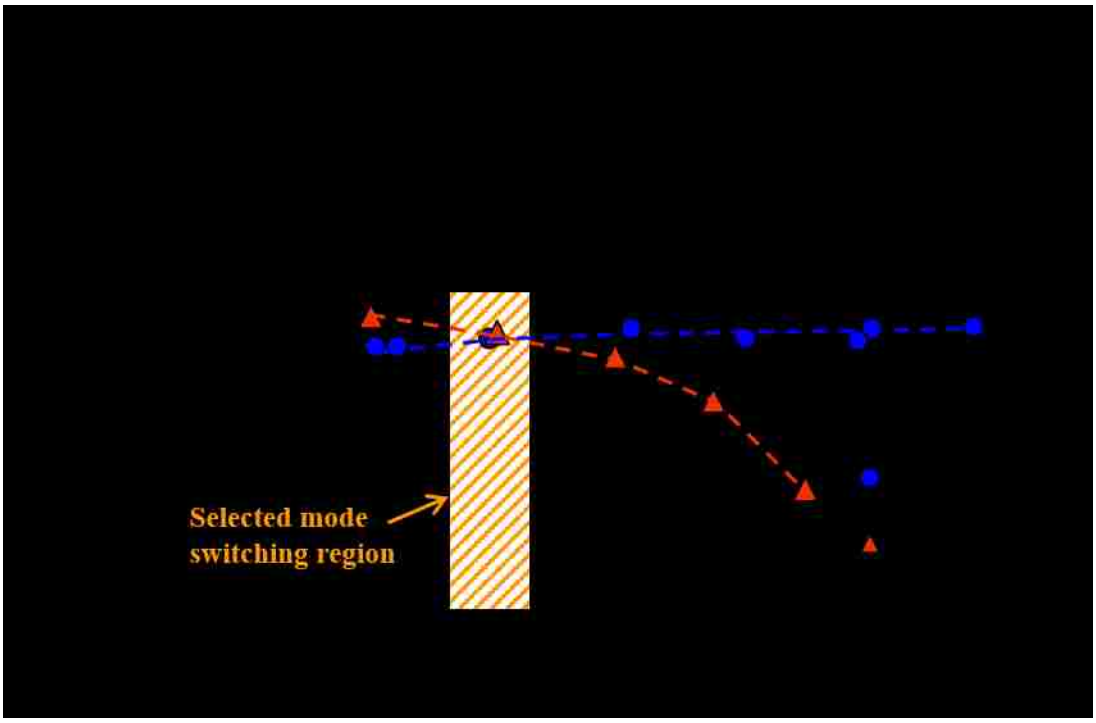

Figure 7.7 Thermal Efficiency versus IMEP for SSDC and DFC

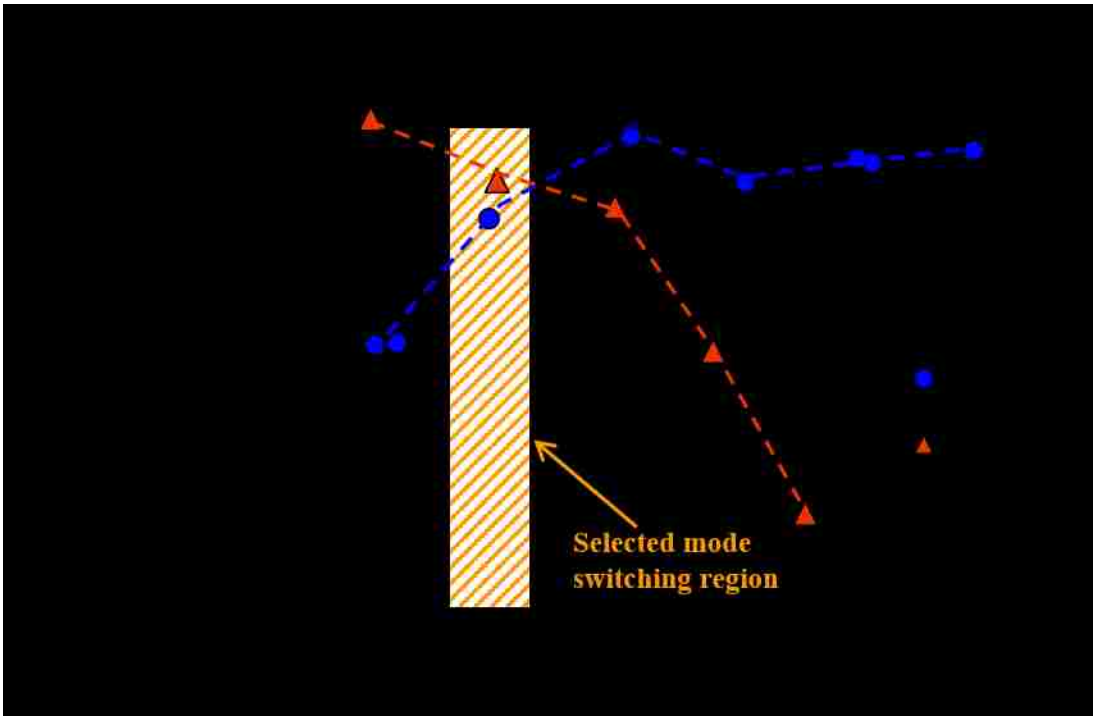

Figure 7.8 Combustion Efficiency versus IMEP for SSDC and DFC

An IMEP of 5~6 bar is selected as the target load level where the switching between the SSDC and the DFC strategies is carried out. At IMEP levels lower than 5 bar, the SSDC strategy is selected, while at IMEP levels above this load level, the DFC strategy is used. A further increase in the engine load level in the DFC strategy is primarily achieved by increasing the ethanol fraction.

7.4. Systematic Control Demonstration

Engine tests are conducted to demonstrate the major aspects of the systematic control. First, the switching between the diesel and the dual-fuel strategies is shown. Thereafter, the load increase from 3 bar IMEP to 10 bar IMEP is demonstrated with simultaneous regulation of the air-path and the fuel systems.

7.4.1. Switching between Diesel and Dual-fuel Combustion

The SSDC and DFC switching is carried out at 5.5 bar IMEP. The test results for the switching from the SSDC to the DFC strategy are shown in Figure 7.9 and Figure 7.10. For demonstration purposes, the engine is operated in the SSDC strategy at steady-state conditions of intake boost and EGR with closed-loop control over CA50 and IMEP. Ethanol is then injected in the intake port with a fixed injection duration of 2.5 ms. The ethanol injection is enabled at cycle number 19 as shown by the ethanol injection command in Figure 7.9. When ethanol is injected, the closed-loop IMEP control gradually reduces the diesel injection duration to maintain the IMEP setpoint. The CA50 feedback and the dynamically commanded diesel SOI are shown in Figure 7.10. The diesel injection timing is advanced by the closed-loop CA50 control algorithm, when the DFC strategy is enabled, to maintain the CA50 at the target value of 368ºCA.

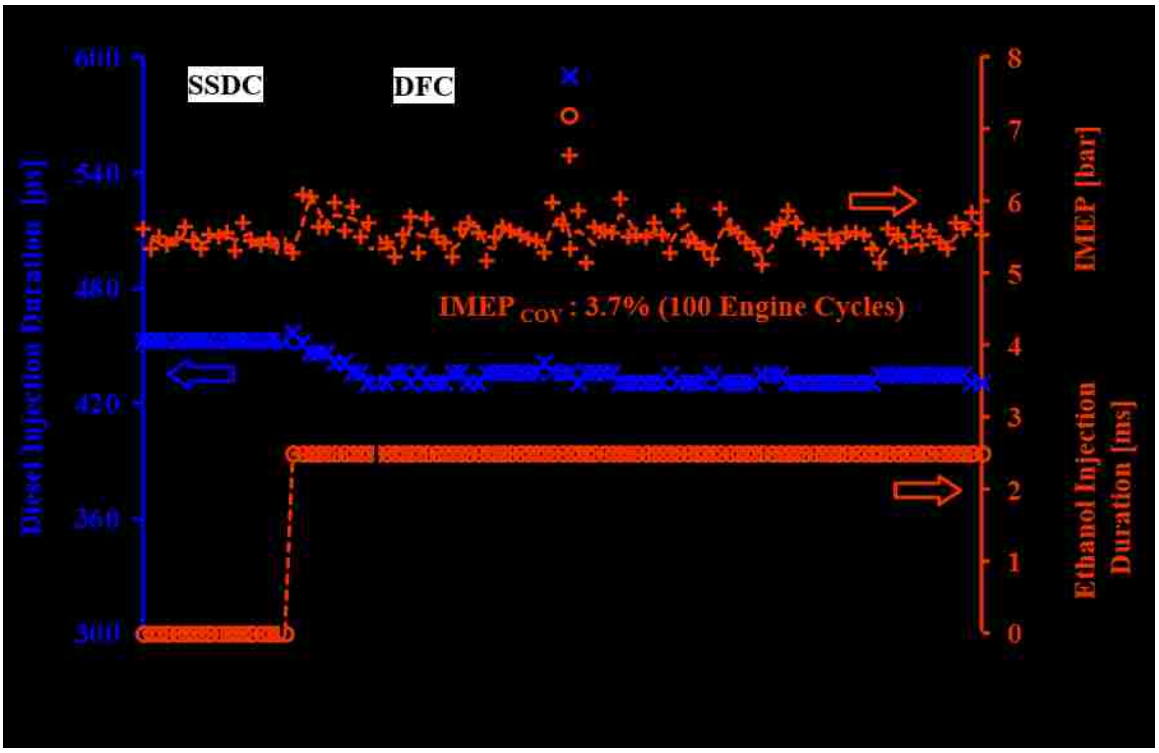

Figure 7.9 SSDC to DFC Switching: Injection Duration and IMEP

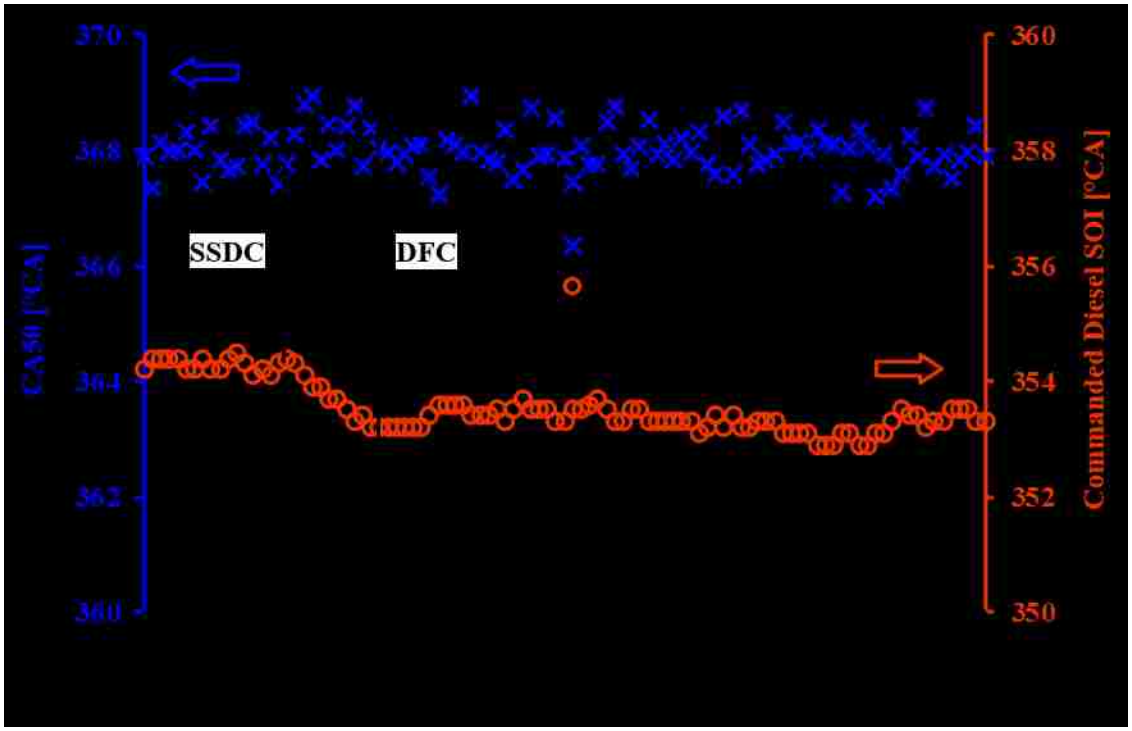

Figure 7.10 SSDC to DFC Switching: CA50 and Diesel SOI

The demonstration tests for the switching from DFC to the SSDC strategy are presented in Figure 7.11. At the beginning of the mode switching test, the engine is operated at steady-state using the DFC strategy. At engine cycle number 67, the ethanol injection is deactivated. The closed-loop IMEP controller increases the diesel injection duration to compensate for the total fuel amount. The diesel SOI and the CA50 are shown in Figure 7.12. The closed-loop CA50 controller effectively delays the diesel injection timing to maintain the target CA50.

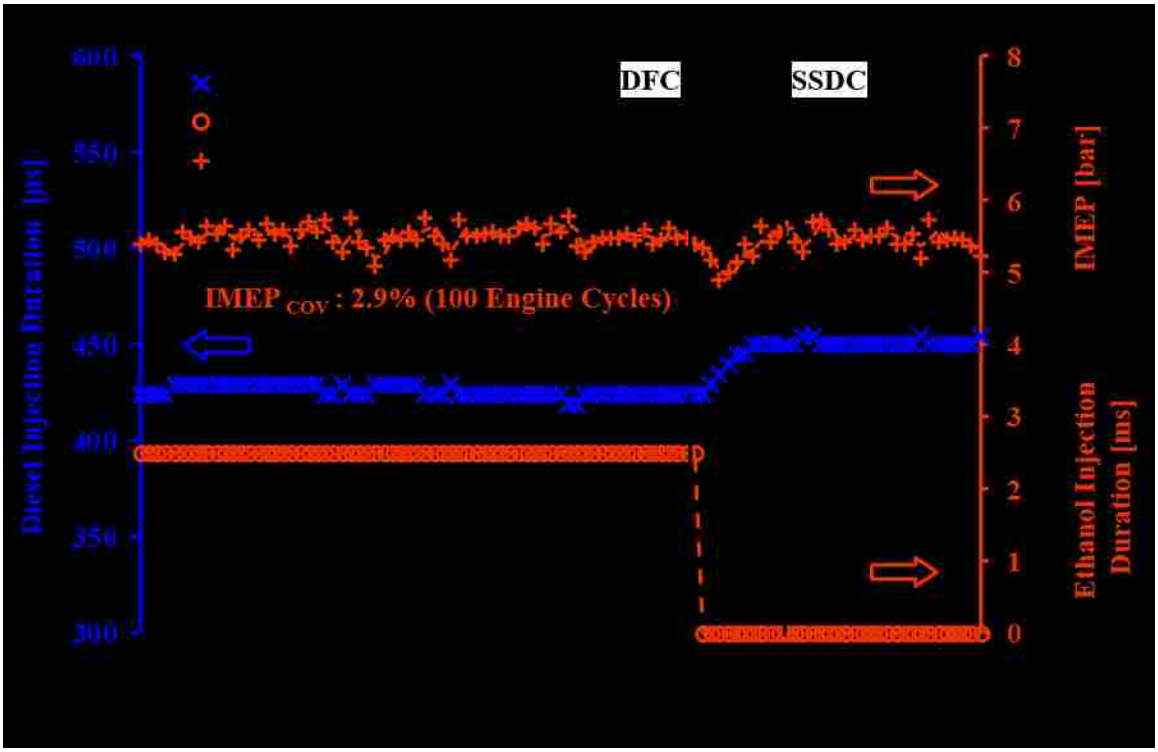

Figure 7.11 DFC to SSDC Switching: Injection Duration and IMEP

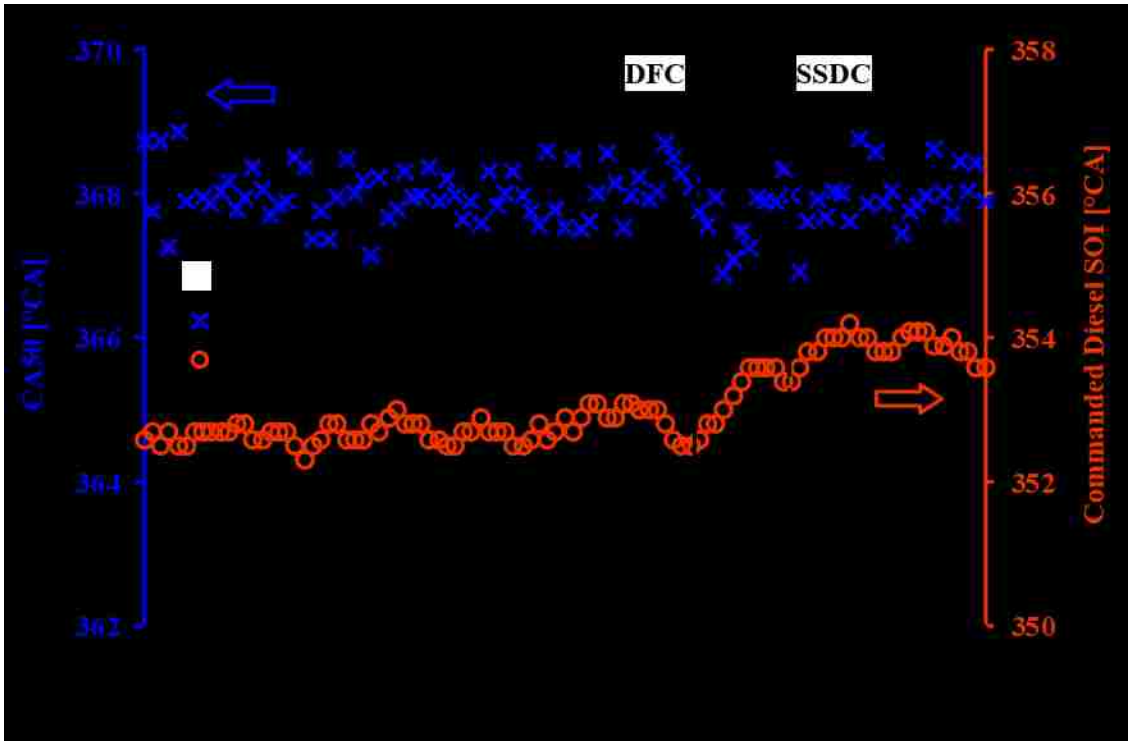

Figure 7.12 DFC to SSDC Switching: CA50 and Diesel SOI

The emission results under steady-state operation of the SSDC and the DFC strategy are presented in Table 7.1. A significant reduction in the smoke emissions is achieved when the combustion strategy is changed from SSDC to DFC. However, switching of combustion modes is accompanied by a noticeable increase in the HC and CO emissions.

Table 7.1 Steady-state Emissions: SSDC and DFC Mode Switching

	Smoke [g/kW-hr]	NO_X [g/kW-hr]	HC [g/kW-hr]	CO [g/kW-hr]
SSDC	0.170	0.30	0.53	8.45
DFC	0.055	0.29	0.95	13.38

7.4.2. Load Sweep with Systematic Control

The control results presented in earlier sections have set the background for the testing of the complete systematic control. The closed-loop injection control, the mode switching scheme, and the numerical engine model are integrated into the systematic control. An IMEP sweeping test is conducted using this control algorithm. Based on the discussions in Section 7.2, guidelines are developed for the intake O_2 concentration and the in-cylinder air excess ratio. A target intake O_2 concentration of 14% is set across the IMEP sweeping test. The in-cylinder air excess ratio is set at a target value of 2 for the 6 bar and 7 bar IMEP levels. At lower loads, a higher in-cylinder air excess ratio is selected to improve the smoke emissions; whereas at higher loads, the target in-cylinder air excess ratio is lowered, primarily to avoid conditions of high peak cylinder pressure.

As presented earlier in Figure 7.5, the engine model provides the boost pressure and the MAF corresponding to the target intake O_2 concentration and the desired in-cylinder air excess ratio at each IMEP level. The target boost pressure and MAF values are achieved by controlling the intake boost pressure regulator, the EGR valve, and the exhaust backpressure valve during the test. The results are shown in Figure 7.13. The targets and the measured values for the intake O_2 concentration and the in-cylinder air excess ratio are shown in Figure 7.14. From the steady-state measurements of intake O_2 concentration, it is observed that by operating the engine at the desired intake boost and MAF levels, the target intake O_2 concentration can be attained at different engine load levels. Furthermore, the in-cylinder air excess ratio calculated from the measurements of intake and exhaust O_2 concentrations closely follows the desired value.

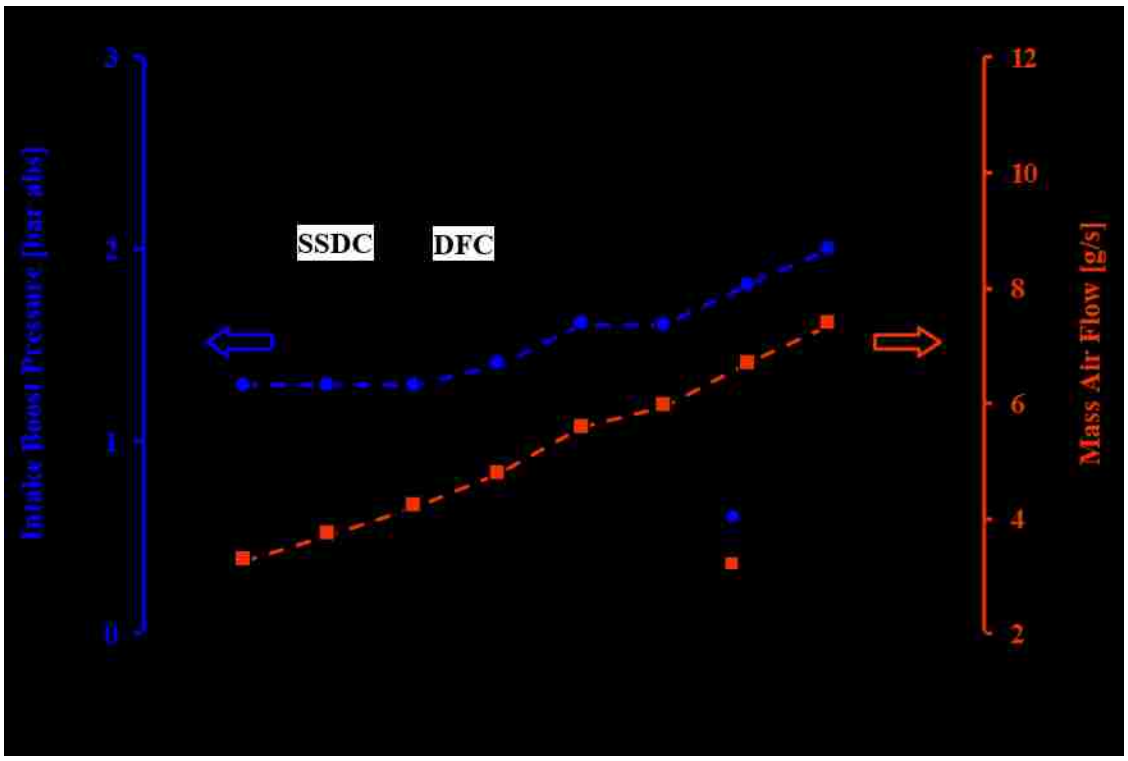

Figure 7.13 IMEP Sweep with Control: p_{int} and MAF

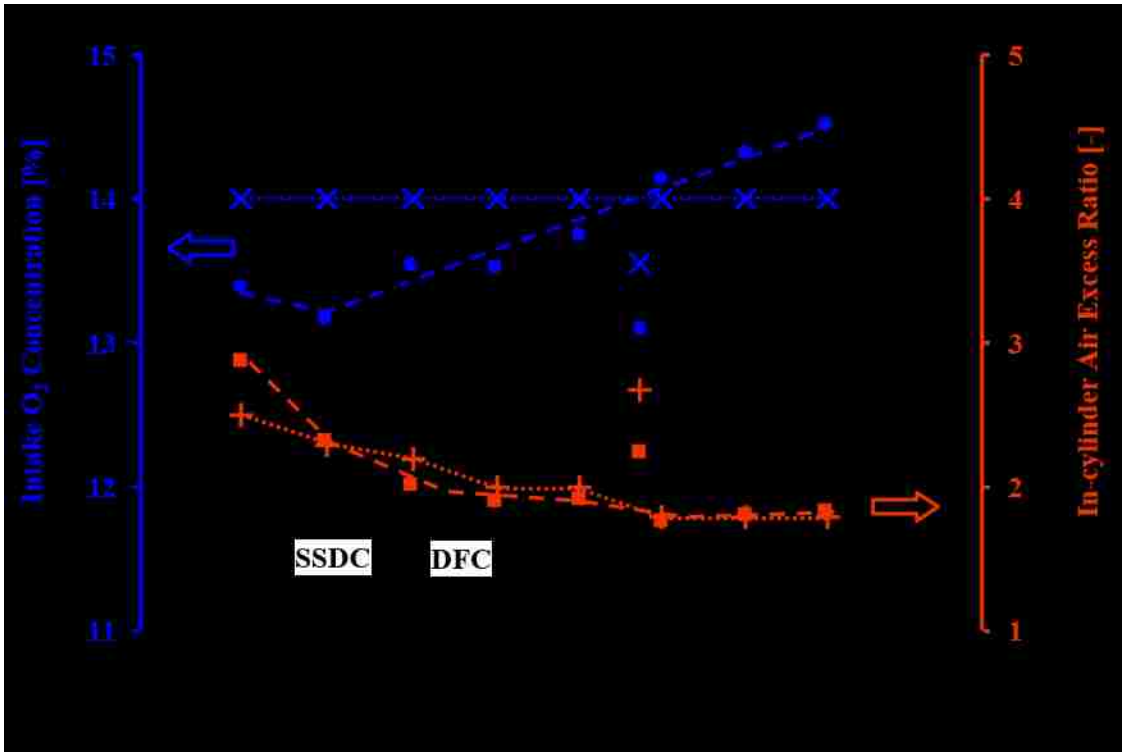

Figure 7.14 IMEP Sweep with Control: $[O_2]_{int}$ and $\lambda_{in\text{-}cyl}$

The NO_X and smoke emissions are presented in Figure 7.15 for the IMEP sweeping test; the mode switching location is marked therein. The NO_X emissions are consistently low during the IMEP sweep, but the smoke emissions exceed the target of 0.05 g/kW-hr in the SSDC strategy at 4 bar IMEP. With further increase in the IMEP and the strategy transition from SSDC to DFC, the smoke emissions reduce drastically.

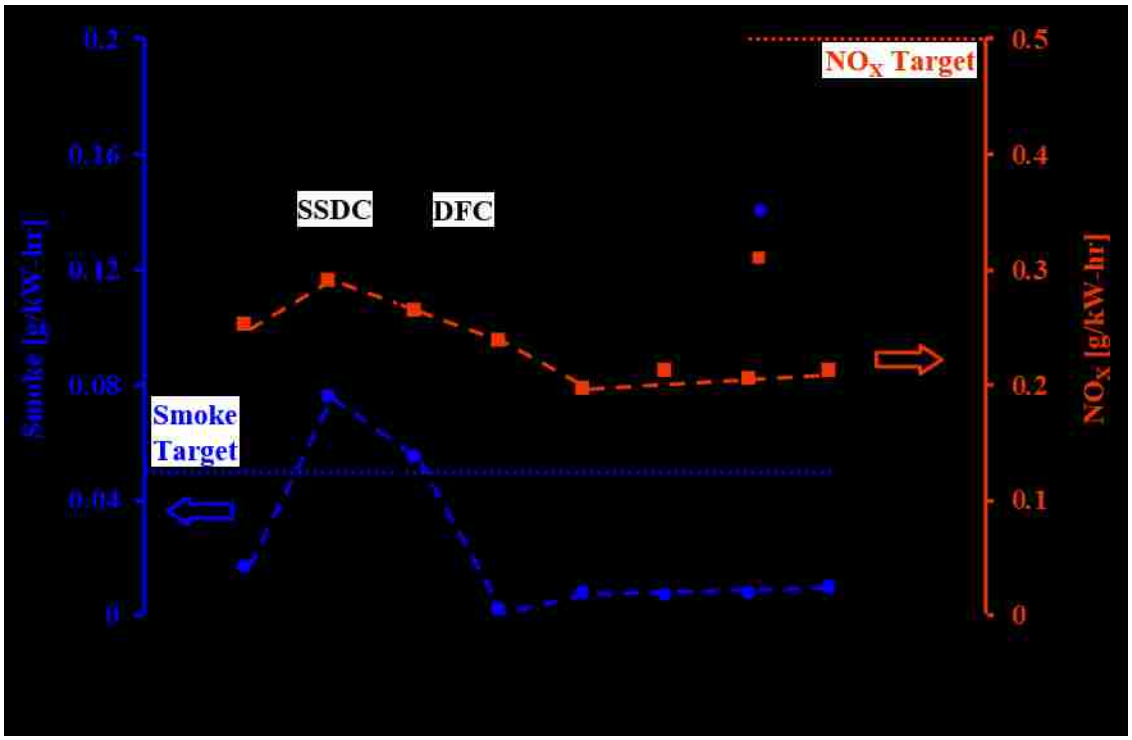

Figure 7.15 IMEP Sweep with Control: Smoke and NO_X

The fuel injection parameters during the IMEP sweeping test are presented in Figure 7.16 and Figure 7.17. The closed-loop control over the diesel injection timing is effective in maintaining the CA50 at the target value of 368°CA across the IMEP sweep. The diesel injection duration is raised initially to achieve the increase in IMEP from 3 bar to 4 bar. Thereafter, the diesel injection duration remains constant for loads higher than 5 bar IMEP, while the ethanol injection duration is increased for achieving higher load levels.

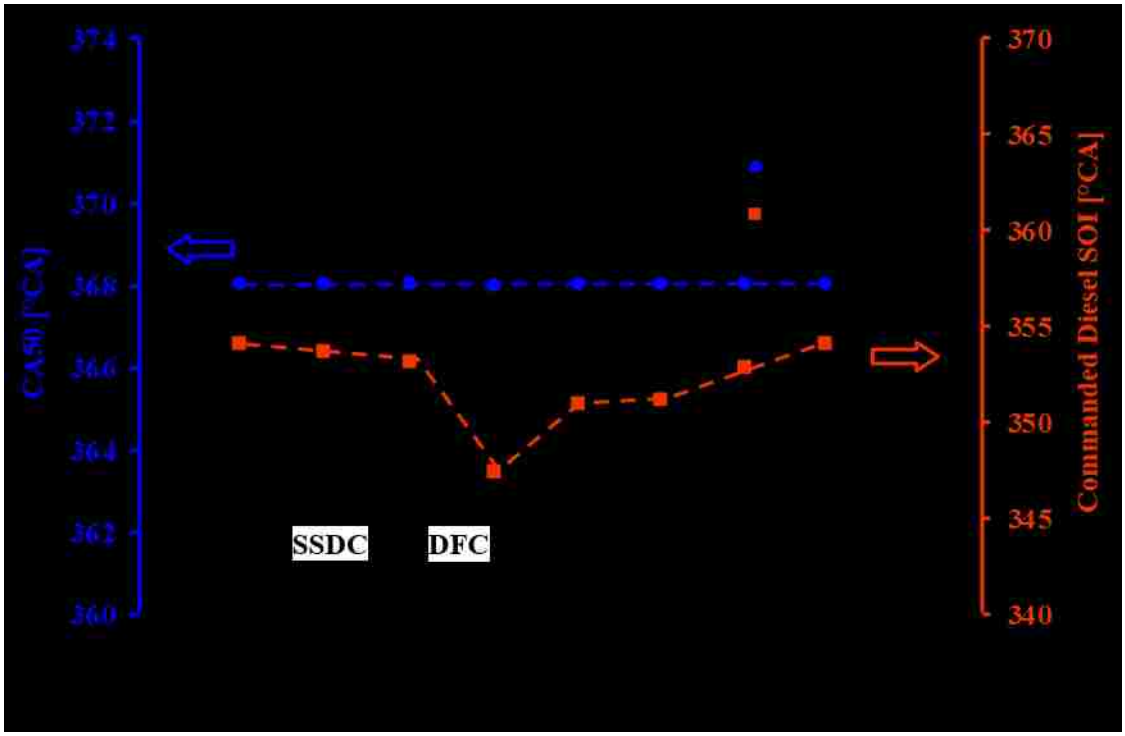

Figure 7.16 IMEP Sweep with Control: CA50 and Diesel SOI

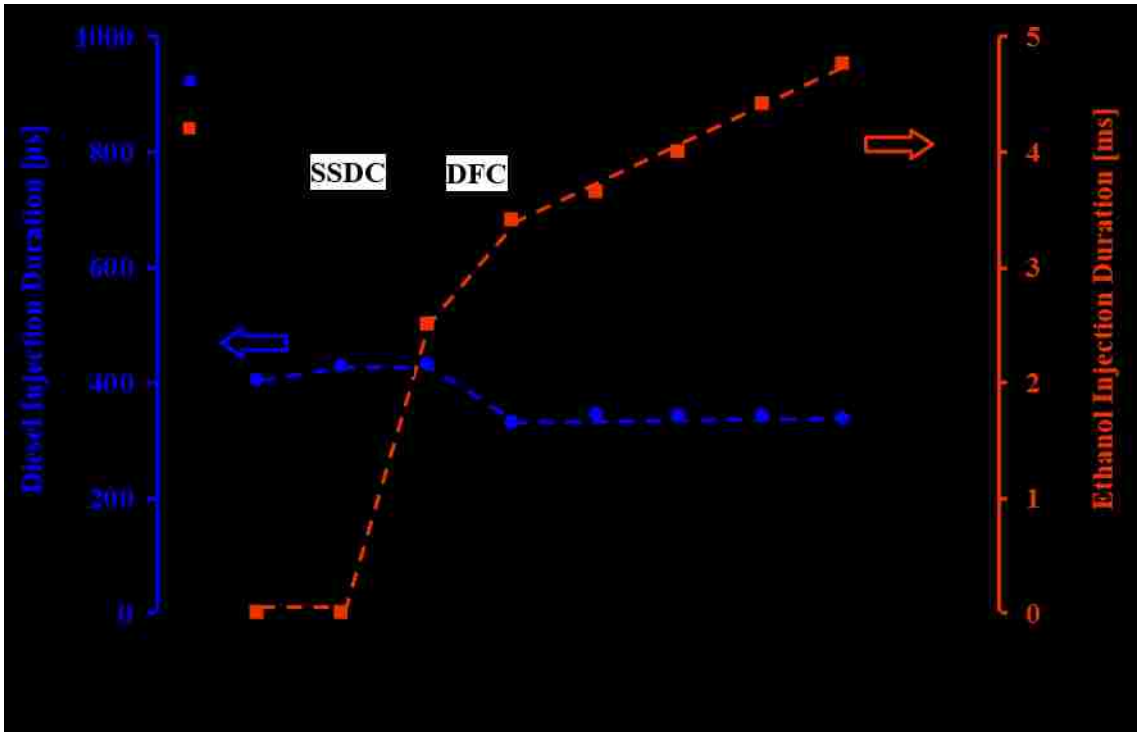

Figure 7.17 IMEP Sweep with Control: Diesel and Ethanol Injection Duration

7.5. Summary of Systematic Control

The closed-loop combustion control for the diesel injection command is integrated into a systematic control architecture for regulating the air and fuel systems simultaneously. The proposed systematic control architecture introduces the dynamic targets for controlling the air-path and the fuel systems. Under the selected testing conditions, these dynamic control targets are summarized as follows.

1. The intake O_2 concentration should be regulated to nearly 14~15%, to attain an effective reduction of NO_X emissions by the application of EGR.
2. A high value of $\lambda_{\text{in-cyl}}$ should be targeted, simultaneously with the intake O_2 concentration target, to reduce the smoke emission penalty associated with the use of EGR.
3. A CA50 window of 368°CA to 376°CA is identified as a desired range for the CA50 setpoint to obtain a high thermal efficiency.
4. The switching between the SSDC and the DFC strategies is conducted at an IMEP of nearly 5 bar to obtain low NO_X and smoke emissions and to reduce the thermal efficiency penalty.

Engine tests are conducted by integrating the dynamic control targets into the systematic control architecture. Representative test results demonstrate that the switching between the SSDC and DFC strategies is achieved without exceeding the IMEP and CA50 stability targets. The simultaneous regulations of the boost, EGR and fuel injection systems are demonstrated by conducting an IMEP sweeping test.

CHAPTER VIII

8. CONCLUSIONS AND FUTURE WORK

The primary goal of this dissertation is to develop dynamic control strategies that can reduce the energy efficiency penalties typically associated with the simultaneous reduction of NO_X and smoke emissions in modern CI engines. Experiments, supported by parametric numerical simulations, are conducted on the test engine to develop and verify the dynamic control. The emission targets for clean combustion (0.5 g/kW-hr for NO_X and 0.05 g/kW-hr for smoke) are met over an IMEP range of 3 bar to 19.2 bar. In addition, the practical engine operating limits of peak cylinder pressure, peak pressure rise rate, and combustion stability are satisfied. The conclusions and the recommendations from the research are presented in the current chapter.

8.1. Numerical Analysis

Zero-dimensional engine cycle simulations, including EGR calculations, are conducted to provide guidelines for the subsequent experimental and control studies. The results are summarized as follows:

- The coordinated adjustments of intake boost pressure and EGR ratio are necessary to achieve a desired inert dilution of the intake charge across the engine load range.
- Based on the simulated engine conditions and modeling assumptions, the highest thermal efficiency is achieved in a narrow combustion phasing window of 366°CA to 372°CA.

- Within the preferred combustion phasing window, if combustion occurs in two stages, a lower pressure rise rate is achieved when a larger portion of the fuel energy is released during the second stage.

- The products of incomplete combustion, HC and CO emissions, represent a larger reduction in the combustion efficiency at low load levels, than at high load levels.

8.2. Steady-state Engine Tests

The single-shot diesel combustion (SSDC) and dual-fuel combustion (DFC) strategies are empirically studied under steady-state testing conditions. The major operating characteristics of the SSDC and DFC strategies, that are suitable for developing the dynamic combustion control, are identified as follows:

- In the SSDC strategy, the target NO_X and smoke levels can be achieved at low-load conditions (4 bar IMEP) by the lowering of the intake O_2 concentration to 14~15% without incurring a significant thermal efficiency penalty.

- At high load levels, simultaneously low NO_X and smoke emissions can be attained by applying high EGR amounts (intake O_2 concentration lower than 11%) to enable LTC. The enabling of LTC, however, is often associated with a large thermal efficiency penalty.

- Similar to the SSDC strategy, EGR is effective for NO_X emission reduction in the DFC strategy. However, in the DFC strategy, the aggravated impact of EGR on the smoke emissions is significantly reduced by the increasing ethanol fraction.

Moreover, the combustion phasing is effectively regulated by adjusting the diesel injection timing even at high ethanol fractions.

- An increase in the exhaust HC and CO emissions is observed in the DFC strategy, which accounts for a lower combustion efficiency. The combustion efficiency is significantly lower at the low load conditions compared to the high load conditions.
- The DFC strategy produces simultaneously low NO_X and smoke emissions even at high engine load levels with suitable modulation of the intake boost pressure, the injection pressure, the combustion phasing, the ethanol fraction, and the EGR rate.

8.3. Closed-loop Combustion Control

A closed-loop control system is developed for the regulation of the diesel injection timing and duration in the SSDC and DFC strategies. The major conclusions are summarized below.

- The regulation of the diesel injection command is effective for the cycle-by-cycle control of combustion phasing and load level in both the SSDC and DFC strategies.
- The RT-FPGA enabled cylinder pressure analysis ensures the cycle-by-cycle feedback of the combustion parameters, and therefore facilitates the closed-loop fuel injection control.
- In both the SSDC and DFC strategies, the improvements in the combustion stability are achieved at high EGR rates by dynamically regulating the IMEP and CA50.

8.4. Systematic Control

The results of the parametric calculations and the experimental work are used to develop the dynamic combustion control targets. The dynamic targets and the closed-loop fuel injection control systems are integrated into a systematic control structure for the regulation of the air-path and the fuel systems. These dynamic control targets and the results of the systematic control are summarized as follows:

- Results compiled from several engine tests suggest that when the intake O_2 concentration is regulated to around 14~15%, a significant reduction in the NO_X emissions is obtained. When a large in-cylinder air excess ratio is used in conjunction with the target intake O_2 concentration, the smoke emission penalty associated with the use of EGR can be reduced. Therefore, the intake boost pressure and the fresh air mass flow rate are simultaneously adjusted to achieve the target values of intake O_2 concentration and the in-cylinder air excess ratio at different engine load levels.

- In both the SSDC and DFC strategies, a preferred combustion phasing window of 368ºCA to 376ºCA is achieved by the implementing closed-loop control over the diesel injection timing.

- The engine is operated in the SSDC strategy at low loads, while at high loads, the DFC strategy is used. By implementing the switching between combustion strategies, the thermal efficiency of clean combustion is improved over a wide engine load range. In this work, the switching between the SSDC and the DFC strategies is conducted at an IMEP of nearly 5.5 bar.

8.5. Recommendations for Future Work

The research presented in this dissertation has focused on developing dynamic control strategies to achieve the emission, stability, and thermal efficiency targets at varied engine load levels, however at a fixed engine speed. By investigating the impact of engine speed on the experimentally developed control guidelines, the dynamic combustion control can be extended to a wider engine operating range. Moreover, the control experiments are conducted on a single-cylinder research engine platform. Thus, the cylinder-to-cylinder interactions in a typical multi-cylinder production engine are not accounted for, during the development of the systematic control. By repeating the experiments on a multi-cylinder engine, the efficacy of the systematic control for production engines can be evaluated.

During this research, extensive controller tuning has not been carried out for designing the closed-loop fuel injection controller. The test results suggest that an improvement in the performance may be achievable by lowering the proportional gain and adding integral control to the current control structure. Furthermore, the injector characterization (presented in APPENDIX F) can be integrated into the fuel injection control to improve the combustion stability under transient conditions, e.g. during mode-switching.

REFERENCES

[1] R. D. Reitz, "Grand Challenges in Engine and Automotive Engineering," *Frontiers in Mechanical Engineering*, vol. 1, p. 1, 2015.

[2] M. N. Taptich, A. Horvath, and M. V. Chester, "Worldwide Greenhouse Gas Reduction Potentials in Transportation by 2050," *Journal of Industrial Ecology*, vol. 20, no. 2, pp. 329–340, 2016.

[3] J. B. Heywood, *Internal Combustion Engine Fundamentals*. New York, USA: McGraw-Hill, 1988.

[4] T. V. Johnson, "Review of Vehicular Emissions Trends," *SAE International Journal of Engines*, vol. 8, no. 3, 2015.

[5] G. McTaggart-Cowan, "Natural Gas for Vehicles: Challenges and Opportunities," NSERC CREATE Combustion Summer School, University of Windsor, Windsor, Canada, 2015.

[6] K. Schindler, "Why Do We Need the Diesel," SAE Technical Paper 972684, 1997.

[7] M. Zheng, "Fundamentals of Clean Engine Technology," Lecture Notes, University of Windsor, Windsor, Canada, 2010.

[8] M. Zheng, G. T. Reader, and J. G. Hawley, "Diesel Engine Exhaust Gas Recirculation—A Review on Advanced and Novel Concepts," *Energy Conversion and Management*, vol. 45, no. 6, pp. 883–900, 2004.

[9] T. V. Johnson, "Diesel Emissions in Review," *SAE International Journal of Engines*, vol. 4, no. 1, pp. 143–157, 2011.

[10] R. D. Reitz and G. Duraisamy, “Review of High Efficiency and Clean Reactivity Controlled Compression Ignition (RCCI) Combustion in Internal Combustion Engines,” *Progress in Energy and Combustion Science*, vol. 46, pp. 12–71, 2015.

[11] ICCT, “The U.S. SuperTruck Program: Expediting the Development of Advanced Heavy-duty Vehicle Efficiency Technologies - ICCT_SuperTruck-program,” 2014. [Online]. Available: http://www.theicct.org/sites/default/files/publications/ICCT_SuperTruck-program_20140610.pdf. [Accessed: 02-Oct-2015].

[12] M. Andreae, “Advanced Engine Technology,” ICCT Workshop on Heavy-duty Vehicle Efficiency: Aligning Standards Internationally, Integration of Engines and Powertrains, San Francisco, USA, 2013.

[13] W. De Ojeda and M. Rajkumar, “Engine Technologies for Clean and High Efficiency Heavy Duty Engines,” *SAE International Journal of Engines*, vol. 5, no. 4, pp. 1759–1767, 2012.

[14] T. Greszler, “The Role of the Internal Combustion Engine in Our Energy Future,” presented at the Directions in Engine-Efficiency and Emissions Research (DEER), Dearborn, USA, 2011.

[15] C. Roberts, “Has the Playing Field Changed Again for Future Diesels,” presented at the ASME Internal Combustion Engine Division Fall Technical Conference, Houston, USA, 2015.

[16] K. Mollenhauer and H. Tschöke, Eds., *Handbook of Diesel Engines*. Berlin Heidelberg, Germany: Springer, 2010.

[17] N. Watson and M. S. Janota, *Turbocharging The Internal Combustion Engine*. Basingstoke, UK: Palgrave Macmillan, 1982.

[18] W. B. Ribbens and N. P. Mansour, *Understanding Automotive Electronics*. Boston, USA: Newnes, 2002.

[19] Y. Huang, J. Colvin, A. Wijesinghe, M. Wang, D. Hou, and Z. Fang, "Dual Loop EGR in Retrofitted Heavy-Duty Diesel Application," SAE Technical Paper 2014-01-1244, 2014.

[20] K. Shahroudi, "Robust Design Evolution and Impact of In-cylinder Pressure Sensors to Combustion Control and Optimization: A Systems and Strategy Perspective," Masters Thesis, Massachusetts Institute of Technology, 2008.

[21] D. Alberer, H. Hjalmarsson, and L. del Re, *Identification for Automotive Systems*, vol. 418. London, UK: Springer, 2012.

[22] C. M. Atkinson, M. Allain, Y. Kalish, and H. Zhang, "Model-Based Control of Diesel Engines for Fuel Efficiency Optimization," SAE Technical Paper 2009-01-0727, 2009.

[23] ETAS, "Measurement, ECU Calibration, and Diagnostics – Development Solutions for Automotive Embedded Systems," Brochure, 2010.

[24] J. E. Dec, "Advanced Compression-ignition Engines—Understanding the In-cylinder Processes," *Proceedings of the Combustion Institute*, vol. 32, no. 2, pp. 2727–2742, 2009.

[25] U. Asad and M. Zheng, "Efficacy of EGR and Boost in Single-injection Enabled Low Temperature Combustion," SAE Technical Paper 2009-01-1126, 2009.

[26] T. Kamimoto and M. Bae, "High Combustion Temperature for the Reduction of Particulate in Diesel Engines," SAE Technical Paper 880423, 1988.

[27] M. Zheng, U. Asad, G. T. Reader, Y. Tan, and M. Wang, "Energy efficiency improvement strategies for a diesel engine in low-temperature combustion," *International Journal of Energy Research*, vol. 33, no. 1, pp. 8–28, Jan. 2009.

[28] S. Kook, C. Bae, P. C. Miles, D. Choi, and L. M. Pickett, "The Influence of Charge Dilution and Injection Timing on Low-Temperature Diesel Combustion and Emissions," SAE Technical Paper 2005-01-3837, 2005.

[29] M. Zheng, Y. Tan, M. C. Mulenga, and M. Wang, "Thermal Efficiency Analyses of Diesel Low Temperature Combustion Cycles," SAE Technical Paper 2007-01-4019, 2007.

[30] N. Shimazaki, H. Akagawa, and K. Tsujimura, "An Experimental Study of Premixed Lean Diesel Combustion," SAE Technical Paper 1999-01-0181, 1999.

[31] U. Asad and M. Zheng, "Tightened Intake Oxygen Control for Improving Diesel Low-temperature Combustion," *Proceedings of the Institution of Mechanical Engineers, Part D: Journal of Automobile Engineering*, vol. 225, no. 4, pp. 513–530, 2011.

[32] S. Kimura, O. Aoki, Y. Kitahara, and E. Aiyoshizawa, "Ultra-clean Combustion Technology Combining a Low-temperature and Premixed Combustion Concept for Meeting Future Emission Standards," SAE Technical Paper 2001-01-0200, 2001.

[33] Y. Kodama, I. Nishizawa, T. Sugihara, N. Sato, T. Iijima, and T. Yoshida, "Full-load HCCI Operation with Variable Valve Actuation System in a Heavy-duty Diesel Engine," SAE Technical Paper 2007-01-0215, 2007.

[34] U. Asad, P. Divekar, M. Zheng, and J. Tjong, “Low Temperature Combustion Strategies for Compression Ignition Engines: Operability Limits and Challenges,” SAE Technical Paper 2013-01-0283, 2013.

[35] U. Asad, X. Han, and M. Zheng, “An Empirical Study to Extend Engine Load in Diesel Low Temperature Combustion,” SAE Technical Paper 2011-01-1814, 2011.

[36] C. Noehre, M. Andersson, B. Johansson, and A. Hultqvist, “Characterization of Partially Premixed Combustion,” SAE Technical Paper 2006-01-3412, 2006.

[37] P. W. Bessonette, C. H. Schleyer, K. P. Duffy, W. L. Hardy, and M. P. Liechty, “Effects of Fuel Property Changes on Heavy-duty HCCI Combustion,” SAE Technical Paper 2007-01-0191, 2007.

[38] G. T. Kalghatgi, “Auto-ignition quality of practical fuels and implications for fuel requirements of future SI and HCCI engines,” SAE Technical Paper, 2005.

[39] N. Saravanan and G. Nagarajan, “An Experimental Investigation on a Diesel Engine with Hydrogen Fuel Injection in Intake Manifold,” SAE Technical Paper 2008-01-1784, 2008.

[40] T. Shudo and Y. Ono, “HCCI Combustion of Hydrogen, Carbon Monoxide and Dimethyl Ether,” SAE Technical Paper 2002-01-0112, 2002.

[41] M. Sjöberg, J. E. Dec, A. Babajimopoulos, and D. Assanis, “Comparing Enhanced Natural Thermal Stratification Against Retarded Combustion Phasing for Smoothing of HCCI Heat-release Rates,” SAE Technical Paper 2004-01-2994, 2004.

[42] M. Zheng, M. C. Mulenga, G. T. Reader, M. Wang, and D. S. Ting, "Influence of Biodiesel Fuel on Diesel Engine Performance and Emissions in Low Temperature Combustion," SAE Technical Paper 2006-01-3281, 2006.

[43] U. Asad, R. Kumar, M. Zheng, and J. Tjong, "Ethanol-fueled Low Temperature Combustion: A Pathway to Clean and Efficient Diesel Engine Cycles," *Applied Energy*, vol. 157, pp. 838–850, 2015.

[44] K. Kohse-Höinghaus, P. Oßwald, T. A. Cool, T. Kasper, N. Hansen, F. Qi, C. K. Westbrook, and P. R. Westmoreland, "Biofuel Combustion Chemistry: From Ethanol to Biodiesel," *Angewandte Chemie International Edition*, vol. 49, no. 21, pp. 3572–3597, 2010.

[45] Z. Chen, J. Liu, Z. Wu, and C. Lee, "Effects of Port Fuel Injection (PFI) of n-Butanol and EGR on Combustion and Emissions of a Direct Injection Diesel Engine," *Energy Conversion and Management*, vol. 76, pp. 725–731, 2013.

[46] T. W. Patzek, "Thermodynamics of the Corn-Ethanol Biofuel Cycle," *Critical Reviews in Plant Sciences*, vol. 23, no. 6, pp. 519–567, 2004.

[47] L. C. de Freitas and S. Kaneko, "Ethanol Demand Under the Flex-fuel Technology Regime in Brazil," *Energy Economics*, vol. 33, no. 6, pp. 1146–1154, 2011.

[48] C. Yu, J. Wang, Z. Wang, and S. Shuai, "Comparative Study on Gasoline Homogeneous Charge Induced Ignition (HCII) by Diesel and Gasoline/Diesel Blend Fuels (GDBF) Combustion," *Fuel*, vol. 106, pp. 470–477, 2013.

[49] R. L. Bechtold, *Alternative Fuels Guidebook: Properties, Storage, Dispensing, and Vehicle Facility Modifications*. Warrendale, USA: Society of Automotive Engineers, 1997.

[50] O. Doğan, "The Influence of n-Butanol/Diesel Fuel Blends Utilization on a Small Diesel Engine Performance and Emissions," *Fuel*, vol. 90, no. 7, pp. 2467–2472, 2011.

[51] M. Mofijur, M. G. Rasul, and J. Hyde, "Recent Developments on Internal Combustion Engine Performance and Emissions Fuelled with Biodiesel-Diesel-Ethanol Blends," *Procedia Engineering*, vol. 105, pp. 658–664, 2015.

[52] Z. Zheng, L. Yue, H. Liu, Y. Zhu, X. Zhong, and M. Yao, "Effect of Two-stage Injection on Combustion and Emissions Under High EGR Rate on a Diesel Engine by Fueling Blends of Diesel/Gasoline, Diesel/n-Butanol, Diesel/Gasoline/n-Butanol and Pure Diesel," *Energy Conversion and Management*, vol. 90, pp. 1–11, 2015.

[53] K. Inagaki, T. Fuyuto, K. Nishikawa, K. Nakakita, and I. Sakata, "Dual-fuel PCI Combustion Controlled by In-cylinder Stratification of Ignitability," SAE Technical Paper 2006-01-0028, 2006.

[54] X. Han, M. Zheng, and J. Wang, "Fuel Suitability for Low Temperature Combustion in Compression Ignition Engines," *Fuel*, vol. 109, pp. 336–349, 2013.

[55] T. Gao, P. Divekar, U. Asad, X. Han, G. T. Reader, M. Wang, M. Zheng, and J. Tjong, "An Enabling Study of Low Temperature Combustion with Ethanol in a Diesel Engine," *Journal of Energy Resources Technology*, vol. 135, no. 4, p. 42203, 2013.

[56] C. S. Weaver and S. H. Turner, "Dual Fuel Natural Gas/Diesel Engines: Technology, Performance, and Emissions," SAE Technical Paper 940548, 1994.

[57] G. A. Karim, *Dual-Fuel Diesel Engines*. Boca Raton, USA: CRC Press, 2015.

[58] Y. Zhang, I. Sagalovich, W. De Ojeda, A. Ickes, T. Wallner, and D. D. Wickman, "Development of Dual-fuel Low Temperature Combustion Strategy in a Multi-cylinder Heavy-duty Compression Ignition Engine Using Conventional and Alternative Fuels," SAE Technical Paper 2013-01-2422, 2013.

[59] N. R. Walker, F. D. F. Chuahy, and R. D. Reitz, "Comparison of Diesel Pilot Ignition (DPI) and Reactivity Controlled Compression Ignition (RCCI) in a Heavy-Duty Engine," presented at the ASME Internal Combustion Engine Division Fall Technical Conference, Houston, USA, 2015.

[60] Y. Wu, R. Hanson, and R. D. Reitz, "Investigation of Combustion Phasing Control Strategy During Reactivity Controlled Compression Ignition (RCCI) Multi-cylinder Engine Load Transitions," *Journal of Engineering for Gas Turbines and Power*, vol. 136, no. 9, p. 91511, 2014.

[61] Y. Wu and R. D. Reitz, "Effects of Exhaust Gas Recirculation and Boost Pressure on Reactivity Controlled Compression Ignition Engine at High Load Operating Conditions," *Journal of Energy Resources Technology*, vol. 137, no. 3, p. 32210, 2015.

[62] D. Splitter, M. Wissink, D. DelVescovo, and R. D. Reitz, "Improving the Understanding of Intake and Charge Effects for Increasing RCCI Engine Efficiency," SAE Technical Paper 2014-01-1325, 2014.

[63] D. Splitter, R. Hanson, S. Kokjohn, and R. D. Reitz, "Reactivity Controlled Compression Ignition (RCCI) Heavy-duty Engine Operation at Mid and High Loads with Conventional and Alternative Fuels," SAE Technical Paper 2011-01-0363, 2011.

[64] U. Asad, M. Zheng, D. S.-K. Ting, and J. Tjong, “Implementation Challenges and Solutions for Homogeneous Charge Compression Ignition Combustion in Diesel Engines,” *Journal of Engineering for Gas Turbines and Power*, vol. 137, no. 10, p. 101505, 2015.

[65] J. Bengtsson, P. Strandh, R. Johansson, P. Tunestål, and B. Johansson, “Closed-loop Combustion Control of Homogeneous Charge Compression Ignition (HCCI) Engine Dynamics,” *Int. J. Adapt. Control Signal Process.*, vol. 18, no. 2, pp. 167–179, 2004.

[66] M. Zheng and R. Kumar, “Implementation of Multiple-pulse Injection Strategies to Enhance the Homogeneity for Simultaneous Low-NOx and Soot Diesel Combustion,” *International Journal of Thermal Sciences*, vol. 48, no. 9, pp. 1829–1841, 2009.

[67] L. del Re, F. Allgöwer, L. Glielmo, C. Guardiola, and I. Kolmanovsky, *Automotive Model Predictive Control*, vol. 402. London, UK: Springer, 2010.

[68] C. Atkinson and G. Mott, “Dynamic Model-based Calibration Optimization: An Introduction and Application to Diesel Engines,” SAE Technical Paper 2005-01-0026, 2005.

[69] BorgWarner, “Pressure Sensor Glow Plug (PSG) for Diesel Engines.” [Online]. Available: http://emissions.borgwarner.com/products/diesel-cold-start-technology/pressure-sensor-glow-plug-psg. [Accessed: 04-Mar-2016].

[70] S. Yu, H. Choi, S. Cho, K. Han, and K. Min, “Development of Engine Control using the In-cylinder Pressure Signal in a High Speed Direct Injection Diesel Engine,” *International Journal of Automotive Technology*, vol. 14, no. 2, pp. 175–182, 2013.

[71] H. Su, Y. Zhang, J. Wang, and L. Liu, "Researches of Common-rail Diesel Engine Emission Control Based on Cylinder Pressure Feedback," presented at the IEEE Vehicle Power and Propulsion Conference, Harbin, China, 2008.

[72] F. Zurbriggen, R. Hutter, and C. Onder, "Diesel-Minimal Combustion Control of a Natural Gas-Diesel Engine," *Energies*, vol. 9, no. 1, p. 58, 2016.

[73] J. Shutty and R. Czarnowski, "Control Strategy for a Dual Loop EGR System to Meet Euro 6 and Beyond," presented at the Directions in Engine-Efficiency and Emissions Reduction Research (DEER) Conference, 2009.

[74] G. Zamboni and M. Capobianco, "Experimental Study on the Effects of HP and LP EGR in an Automotive Turbocharged Diesel Engine," *Applied Energy*, vol. 94, pp. 117–128, 2012.

[75] N. E. Kahveci, S. T. Impram, and A. Umut Genc, "Boost Pressure Control for a Large Diesel Engine with Turbocharger," presented at the American Control Conference (ACC), Portland, USA, 2014.

[76] B. Youssef, P. Moulin, and O. Grondin, "Model Based Control of Turbochargers: Application to a Diesel HCCI Engine," presented at the IEEE International Conference on Control Applications, Singapore, 2007.

[77] V. Mueller, R. Christmann, S. Muenz, and V. Gheorghiu, "System Structure and Controller Concept for an Advanced Turbocharger/EGR System for a Turbocharged Passenger Car Diesel Engine," SAE Technical Paper 2005-01-3888, 2005.

[78] H. Nakada, P. Martin, G. Milton, A. Iemura, and A. Ohata, "An Application Study of Online Reference Governor to Boost Pressure Control for Automotive Diesel

Engines," presented at the American Control Conference (ACC), Portland, USA, 2014.

[79] N. Rajaei, X. Han, X. Chen, and M. Zheng, "Model Predictive Control of Exhaust Gas Recirculation Valve," SAE Technical Paper 2010-01-0240, 2010.

[80] N. Rainer, "Fault Tolerant Oxygen Control of a Diesel Engine Air System," presented at the IFAC Symposium on Advances in Automotive Control, Munich, Germany, 2010.

[81] R. D. Reitz, "Directions in Internal Combustion Engine Research," *Combustion and Flame*, vol. 160, no. 1, pp. 1–8, 2013.

[82] PetroCanada, "Material Safety Data Sheet - Diesel Fuel." [Online]. Available: http://www.online.petro-canada.ca/datasheets/en_CA/w104.pdf. [Accessed: 14-Jan-2015].

[83] Commercial Alcohols, "Material Safety Data Sheet - Ethyl Alcohol." [Online]. Available: http://ccc.uwindsor.ca/eRPortal/ItemImages%5CCHEM1443-COMALC09.pdf. [Accessed: 14-Jan-2015].

[84] Alternative Fuels Data Center, "Fuel Properties Comparison." [Online]. Available: http://www.afdc.energy.gov/fuels/fuel_comparison_chart.pdf. [Accessed: 06-Jan-2016].

[85] H. E. Dillon and S. G. Penoncello, "A Fundamental Equation for Calculation of the Thermodynamic Properties of Ethanol," *International Journal of Thermophysics*, vol. 25, no. 2, pp. 321–335, 2004.

[86] J. Riegel, "Exhaust Gas Sensors for Automotive Emission Control," *Solid State Ionics*, vol. 152–153, pp. 783–800, 2002.

[87] Kistler, “Data Sheet, Type 5010B - 4034 Amplifier.” [Online]. Available: http://public.hofstragroup.com/4034.amplifier.pdf. [Accessed: 26-Aug-2016].

[88] Gurley Precision Instruments, [Online]. Available: http://www.gpi-encoders.com /PDF/925.pdf. [Accessed: 26-Aug-2016].

[89] S. W. Smith, *The Scientist and Engineer’s Guide to Digital Signal Processing*. San Diego, California: California Technical Pub., 1999.

[90] National Instruments, “What is a Real-Time Operating System (RTOS).” [Online]. Available: http://www.ni.com/white-paper/3938/en/. [Accessed: 12-Feb-2016].

[91] National Instruments, “FPGA Fundamentals.” [Online]. Available: http://www.ni. com/white-paper/6983/en/. [Accessed: 12-Feb-2016].

[92] National Instruments, “Parts of a PXI System - National Instruments.” [Online]. Available: http://www.ni.com/tutorial/4811/en/#toc3. [Accessed: 29-Aug-2016].

[93] U. Asad and M. Zheng, “Exhaust Gas Recirculation for Advanced Diesel Combustion Cycles,” *Applied Energy*, vol. 123, pp. 242–252, 2014.

[94] R. S. Benson and N. D. Whitehouse, *Internal Combustion Engines*. Oxford, UK: Pergamon Press, 1983.

[95] G. T. Reader, U. Asad, and M. Zheng, “Energy Efficiency Trade-off with Phasing of HCCI Combustion,” *International Journal of Energy Research*, vol. 37, no. 3, pp. 200–210, 2013.

[96] N. Ladommatos, S. Abdelhalim, and H. Zhao, “The Effects of Exhaust Gas Recirculation on Diesel Combustion and Emissions,” *International Journal of Engine Research*, vol. 1, no. 1, pp. 107–126, 2000.

[97] H. Zhao, G. Lowry, and N. Ladommatos, "Time-Resolved Measurements and Analysis of In-cylinder Gases and Particulates in Compression-ignition Engines," SAE Technical Paper 961168, 1996.

[98] S. Dev, P. Divekar, K. Xie, X. Han, X. Chen, and M. Zheng, "A Study of Combustion Inefficiency in Diesel Low Temperature Combustion and Gasoline–Diesel RCCI Via Detailed Emission Measurement," *J. Eng. Gas Turbines Power*, vol. 137, no. 12, pp. 121501–121501, 2015.

[99] T. Jacobs, D. N. Assanis, and Z. Filipi, "The Impact of Exhaust Gas Recirculation on Performance and Emissions of a Heavy-duty Diesel Engine," SAE Technical Paper 2003-01-1068, 2003.

[100] A. E. Farrell, "Ethanol Can Contribute to Energy and Environmental Goals," *Science*, vol. 311, no. 5760, pp. 506–508, 2006.

[101] G. S. Jung, Y. H. Sung, B. C. Choi, C. W. Lee, and M. T. Lim, "Major Sources of Hydrocarbon Emissions in a Premixed Charge Compression Ignition Engine," *International Journal of Automotive Technology*, vol. 13, no. 3, pp. 347–353, 2012.

[102] W. Tutak, "Bioethanol E85 as a Fuel for Dual Fuel Diesel Engine," *Energy Conversion and Management*, vol. 86, pp. 39–48, 2014.

[103] National Instruments, "Transferring Data between Devices or Structures Using FIFOs (FPGA Module) - LabVIEW 2012 FPGA Module Help." [Online]. Available: http://zone.ni.com/reference/en-XX/help/371599H-01/lvfpgaconcepts/fpga_transfer_data/. [Accessed: 14-Feb-2016].

[104] U. Asad and M. Zheng, "Fast Heat Release Characterization of a Diesel Engine," *International Journal of Thermal Sciences*, vol. 47, no. 12, pp. 1688–1700, Dec. 2008.

[105] H. Lian, J. Martz, N. Prakash, and A. Stefanopoulou, "Fast Computation of Combustion Phasing and its Influence on Classifying Random or Deterministic Patterns," presented at the ASME Internal Combustion Engine Division Fall Technical Conference, Houston, USA, 2015.

[106] M. C. Sellnau, F. A. Matekunas, P. A. Battiston, C.-F. Chang, and D. R. Lancaster, "Cylinder-pressure-based Engine Control using Pressure-ratio-management and Low-cost Non-intrusive Cylinder Pressure Sensors," SAE Technical Paper 2000-01-0932, 2000.

[107] U. Asad and M. Zheng, "Diesel Pressure Departure Ratio Algorithm for Combustion Feedback and Control," *International Journal of Engine Research*, vol. 15, no. 1, pp. 101–111, 2014.

[108] G. Zhu, J. Wang, Z. Sun, and X. Chen, "Tutorial of Model-based Powertrain and Aftertreatment System Control Design and Implementation," presented at the American Control Conference (ACC), Chicago, USA, 2015.

[109] S. Kitazono, S. Sugihira, and H. Ohmori, "Starting Speed Control of SI Engine Based on Extremum Seeking Control," presented at the 17th IFAC World Congress, Seoul, Korea, 2008.

[110] N. J. Killingsworth, S. M. Aceves, D. L. Flowers, F. Espinosa-Loza, and M. Krstic, "HCCI Engine Combustion-Timing Control: Optimizing Gains and Fuel

Consumption via Extremum Seeking," *IEEE Transactions on Control Systems Technology*, vol. 17, no. 6, pp. 1350–1361, 2009.

[111] E. Corti, C. Forte, G. Mancini, and D. Moro, "Automatic Combustion Phase Calibration with Extremum Seeking Approach," *Journal of Engineering for Gas Turbines and Power*, vol. 136, no. 9, p. 91402, 2014.

[112] D. Popovic, M. Jankovic, S. Magner, and A. R. Teel, "Extremum Seeking Methods for Optimization of Variable Cam Timing Engine Operation," *IEEE Transactions on Control Systems Technology*, vol. 14, no. 3, pp. 398–407, 2006.

[113] J. Choi, M. Krstic, K. B. Ariyur, and J. S. Lee, "Extremum Seeking Control for Discrete-time Systems," *IEEE Transactions on Automatic Control*, vol. 47, no. 2, pp. 318–323, 2002.

APPENDICES

APPENDIX A. CO_2 Regulations and Thermal Efficiency

For vehicles that use hydrocarbon fuels, the CO_2 emissions directly translate to the engine's thermal efficiency if complete combustion is assumed, as shown in Equation (A.1).

$$\eta_{brake} = 100 \times \frac{3600 \cdot M_{CO_2}}{LHV_{fuel} \cdot M_{fuel} \cdot EXH_{CO_2}} \tag{A.1}$$

In Equation (A.1), η_{brake} is the brake thermal efficiency, LHV_{fuel} is the lower heating value of the fuel in kJ/g, and EXH_{CO_2} is the exhaust CO_2 emission regulation in g/kW-hr. M_{fuel} is the molecular weight of the fuel in g/mol. Similarly, M_{CO_2} is the molecular weight of CO_2. The brake thermal efficiency requirements, corresponding to the CO_2 regulations, for engines using a hydrocarbon fuel $C_1H_{1.87}$ are shown in Figure A.1.

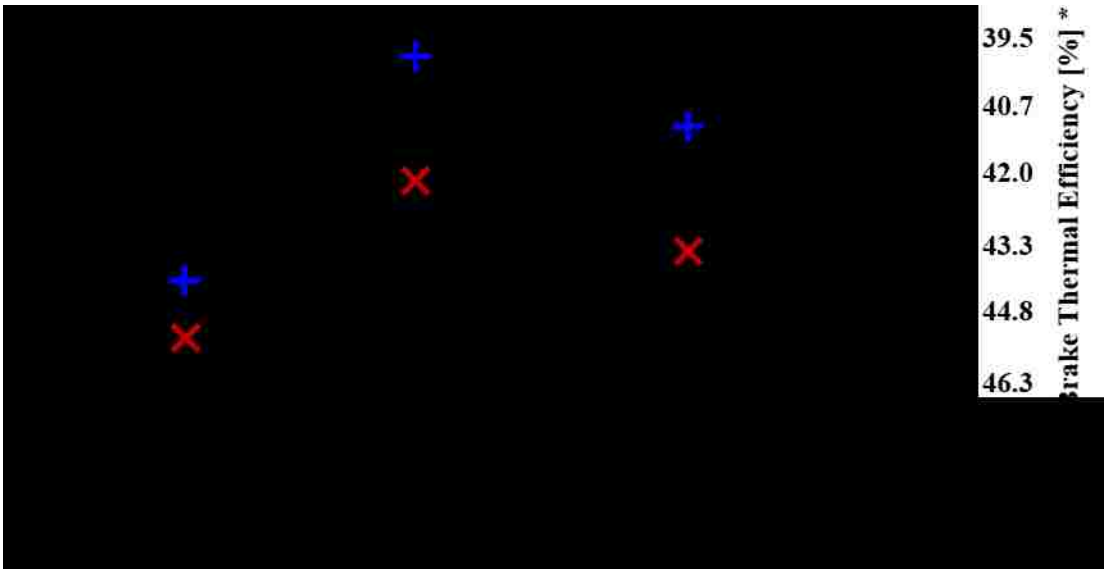

Figure A.1 Efficiency Requirements for Meeting CO_2 Emission Regulations

APPENDIX B. Properties of Commonly Used Fuels

Table A.1 Properties of Commonly Used Fuels

	Diesel	Gasoline	Biodiesel	Butanol	Ethanol	Methanol	DME	Natural Gas	Hydrogen
Formula	$C_nH_{1.8n}$	$C_nH_{1.87n}$	C_{18} to C_{21}	C_4H_9OH	C_2H_5OH	CH_3OH	CH_3-O-CH_3	CH_4 (~96%[1])	H_2
State	Liquid	Liquid	Liquid	Liquid	Liquid	Liquid	Gas	Gas	Gas
Molecular weight [kg/kmol]	~ 170	~110		74	46	32	46	~16	2
Octane	25	87	30		108-115	99,111	13	~120	130+
Cetane	43	10 to 17	52-62	17-25	08-11	3	55	0	-
LHV [MJ/kg]	42.1	42.4	36.7–40.5	33.1	26.8	20	28.4	46.3	121.5
Oxygen mass [%]	0	0	10 to 11	21.62	34.8	50	35	0	0
Stoichiometric Air-fuel Ratio[1]	14.6	14.8	12.6	11.2	9	6.45	9	17.2	34.3

	Diesel	Gasoline	Biodiesel	Butanol	Ethanol	Methanol	DME	Natural Gas	Hydrogen
Boiling temp. at 1 bar [^{O}C]	180-340	60-200	315-350	117.5	78	65	-25	-162	-252.9
Melting point [^{O}C]	–34 to –18	< -80		-89.5	-114.1	-98	-141.5	–182.6	-259.2
Q_evaporation [kJ/kg]	316.6	303	-	595	846	1100	465	510	442.7
Density [kg/m3]	840-880	720-780	860-900	810	780	790	1.97	0.72	0.09
Stoich. Mixture by Mass [%]	6.49	6.4	7.35	8.2	10	13.4	10	~5.5	2.8
Auto-ignition temp. [deg C]	180-285	220-260	~260	340	360-422	464,470	350	540	560
Kinematic viscosity [cSt]	>3	0.4-0.8	3.5-5	3.64	1.52	0.64	0.184	13.8	100
Energy for stoich. burning in 1 kg air [MJ]	2.8	2.82	2.84	2.96	2.68	2.68	2.83	2.54	3.43

APPENDIX C. Equipment List

Table A.2 List of Major Equipment for Engine Tests

Equipment	Model	Remarks
Pressure transducer	AVL GU13P	Range: 0–200 bar Sensitivity: 15 pC/bar Accuracy: ±0.6 bar
Charge amplifier	Kistler 5010B	Range: ±10–999000 pC Sensitivity: 0.01–9990 pC/bar Accuracy: ±0.5%
Air flow meter	Dresser Roots, 2M175	Max. pressure: 12 bar gauge Max. flow rate: 56.6 m^3/hr Accuracy: 0.3%
Fuel flow meter (Diesel)	Ono Sokki, FP-2140H, Reading unit: Ono Sokki, DF-210A	Range: 5-2000 ml/min Resolution: 0.1 ml Accuracy: ±0.2%
Fuel flow meter (Ethanol)	FP-213 (with alcohol provision) Reading unit: Ono Sokki, DF-210A	Range: 1-1000 ml/min Resolution: 0.01 ml Accuracy: ±0.5%
Intake and exhaust pressure regulators	SMC ITV 3051-314S5	Pressure range: 5~900 kPa Sensitivity: 0.2 % Accuracy: ±0.5%
Pressure sensor	BOSCH DS-K-TF	Range: 0-5 bar differential
Intake surge tank	Manchester Tank, CAT# 302404	Volume: 75.7 Liters Pressure rating: 13.8 bar gauge @ 100°F
Exhaust surge tank	Prentex Tanks, SN D550	Volume: 60 Liters Pressure rating : 20.7 bar gauge @ 37.8°C

Dynamometer	Schenck WS230, Eddy current dynamometer	Rated torque: 750 Nm Moment of inertia: 0.53 kgm^2
Dynamometer controller	DyneSystemsCo. DYN-LOC IV	Regulation accuracy of ±1 unit for both speed and torque
Encoder	Gurley Precision, 9125S03600H5L01E18SQ06EN	0.1°CA resolution
Coolant conditioning unit	FEV, COC11001100	Up to 10 bar Up to 130°C

APPENDIX D. Zero-D Simulations

EGR Analysis

The details of the EGR analysis approach presented in Section 4.1 are presented in the current section. The derivations of the expressions for gas concentrations and the air fuel ratios are presented. Based on the molar balance across the EGR loop (Figure 4.1) and the definition of the molar EGR ratio (R_{mol}), the moles of O_2 in the intake can be calculated as follows.

$$n_{O_2} = [O_2]_{air} \cdot n_{air} + r_{mol} \cdot n_{int} \cdot [O_2]_{exh} \tag{A.2}$$

From Equation (4.2) and Equation (4.4),

$$n_{O_2} = [O_2]_{air} \cdot n_{air} + r_{mol} \cdot n_{int} \left[\frac{n_{O_2} + \frac{\gamma}{2} n_f - n_f - \frac{\beta}{4} n_f}{n_{int} + \left(\frac{\gamma}{2} + \frac{\beta}{4} \right) n_f} \right] \tag{A.3}$$

$$n_{O_2} = \frac{[O_2]_{air} \cdot n_{air} \left[n_{int} + \left(\frac{\gamma}{2} + \frac{\beta}{4} \right) n_f \right] + r_{mol} \cdot n_{int} \left(\frac{\gamma}{2} - \frac{\beta}{4} - 1 \right) n_f}{n_{air} + \left(\frac{\gamma}{2} + \frac{\beta}{4} \right) n_f} \tag{A.4}$$

The wet concentration of O_2 in the intake is expressed as,

$$[O_2]_{int} = \frac{[O_2]_{air} \cdot n_{air} \left[1 + \left(\frac{\gamma}{2} + \frac{\beta}{4} \right) \frac{n_f}{n_{int}} \right] + r_{mol} \left(\frac{\gamma}{2} - \frac{\beta}{4} - 1 \right) n_f}{n_{air} + \left(\frac{\gamma}{2} + \frac{\beta}{4} \right) n_f} \tag{A.5}$$

Similarly, the concentration of O_2 in the exhaust can be calculated as follows.

$$[O_2]_{exh} = \frac{n_{O_2} + \left(\frac{\gamma}{2} - \frac{\beta}{4} - 1 \right) n_f}{\left[n_{int} + \left(\frac{\gamma}{2} + \frac{\beta}{4} \right) n_f \right]} \tag{A.6}$$

By substituting the expression for n_{O_2} from Equation (A.4) into Equation (A.5), the expression for the exhaust O_2 concentration can be obtained as follows.

$$[O_2]_{exh} = \frac{[O_2]_{air} \cdot n_{air} + \left(\frac{\gamma}{2} - \frac{\beta}{4} - 1\right) n_f}{n_{air} + \left(\frac{\gamma}{2} + \frac{\beta}{4}\right) n_f} \tag{A.7}$$

A similar approach is adopted for obtaining the expressions for the intake and exhaust concentrations of the other gas species. The final expressions are listed as follows.

$$[CO_2]_{int} = \frac{r_{mol} \cdot \alpha \cdot n_f}{n_{air} + \left(\frac{\gamma}{2} + \frac{\beta}{4}\right) n_f} \tag{A.8}$$

$$[H_2O]_{int} = \frac{r_{mol} \cdot \frac{\beta}{2} \cdot n_f}{n_{air} + \left(\frac{\gamma}{2} + \frac{\beta}{4}\right) n_f} \tag{A.9}$$

$$[N_2]_{int} = \frac{[N_2]_{air} \cdot n_{air} \left[1 + \left(\frac{\gamma}{2} + \frac{\beta}{4}\right) \frac{n_f}{n_{int}}\right]}{n_{air} + \left(\frac{\gamma}{2} + \frac{\beta}{4}\right) n_f} \tag{A.10}$$

$$[CO_2]_{exh} = \frac{\alpha \cdot n_f}{n_{air} + \left(\frac{\gamma}{2} + \frac{\beta}{4}\right) n_f} \tag{A.11}$$

$$[H_2O]_{exh} = \frac{\frac{\beta}{2} \cdot n_f}{n_{air} + \left(\frac{\gamma}{2} + \frac{\beta}{4}\right) n_f} \tag{A.12}$$

$$[N_2]_{exh} = \frac{[N_2]_{air} \cdot n_{air}}{n_{air} + \left(\frac{\gamma}{2} + \frac{\beta}{4}\right) n_f} \tag{A.13}$$

When EGR is quantified by measuring the concentrations of CO_2 in the intake and exhaust, the equivalence between the CO_2 EGR definition listed in Equation (3.2) and the molar EGR definition listed in Equation (4.5) can be shown. By using the expressions for

the intake and exhaust CO_2 concentrations presented in Equation (A.8) and Equation (A.11), the CO_2 EGR can be expressed as follows.

$$r_{CO_2} = \left(\frac{r_{mol} \cdot \alpha \cdot n_f}{n_{air} + \left(\frac{\gamma}{2} + \frac{\beta}{4}\right) n_f} \right) \Bigg/ \left(\frac{\alpha \cdot n_f}{n_{air} + \left(\frac{\gamma}{2} + \frac{\beta}{4}\right) n_f} \right) \tag{A.14}$$

$$r_{CO_2} = r_{mol} \tag{A.15}$$

The fresh air excess ratio (λ_{air}) is defined based on the ratio of ambient air and fuel and may be written as follows.

$$\lambda_{fr} = \frac{[O_2]_{air} n_{air}}{\left(\alpha + \frac{\beta}{4} - \frac{\gamma}{2}\right) n_f} \tag{A.16}$$

The expression developed in Equation (A.7) can be integrated into Equation (A.16) .

$$\lambda_{fr} = 1 + \frac{[O_2]_{exh} \cdot \left[(1 - r_{mol}) \cdot n_{int} + \left(\frac{\gamma}{2} + \frac{\beta}{4}\right) \cdot n_f \right]}{\left(\alpha + \frac{\beta}{4} - \frac{\gamma}{2}\right) \cdot n_f} \tag{A.17}$$

The expression can be further simplified using the definition of r_{mol}.

$$\lambda_{fr} = 1 + \frac{[O_2]_{exh} \cdot \left[n_{air} + \left(\frac{\gamma}{2} + \frac{\beta}{4}\right) \cdot n_f \right]}{\left(\alpha + \frac{\beta}{4} - \frac{\gamma}{2}\right) \cdot n_f} \tag{A.18}$$

By conducting arithmetic manipulations, the Equation (A.18) can be rearranged as follows.

$$\lambda_{fr} = \frac{1 + C_f \cdot [O_2]_{exh}}{1 - \frac{[O_2]_{exh}}{[O_2]_{air}}} \tag{A.19}$$

where,

$$C_f = \frac{\left(\frac{\gamma}{2} + \frac{\beta}{4}\right)}{\left(1 + \frac{\beta}{4} - \frac{\gamma}{2}\right)} \tag{A.20}$$

The in-cylinder air excess ratio (λ_{in-cyl}) is defined based on the ratio of in-cylinder O_2 content and fuel amount. The expression for λ_{in-cyl} may be written as follows.

$$\lambda_{in-cyl} = \frac{n_{O_2}}{\left(\alpha + \frac{\beta}{4} - \frac{\gamma}{2}\right) \cdot n_f} \tag{A.21}$$

Manipulations can be conducted on Equation (A.21) to obtain an expression for λ_{in-cyl} similar to that of λ_{fr}

$$\lambda_{in-cyl} = \frac{1 + C_f \cdot [O_2]_{exh}}{1 - \frac{[O_2]_{exh}}{[O_2]_{int}}} \tag{A.22}$$

Calculation Routine

The flow chart in Figure A.2 shows the calculation procedure throughout the closed engine cycle. The primary expression for the calculation routine is the energy balance in Equation (4.17) that is carried out at each of the calculation steps (1°CA). The step-by-step calculations begin at the crank angle of intake valve closing.

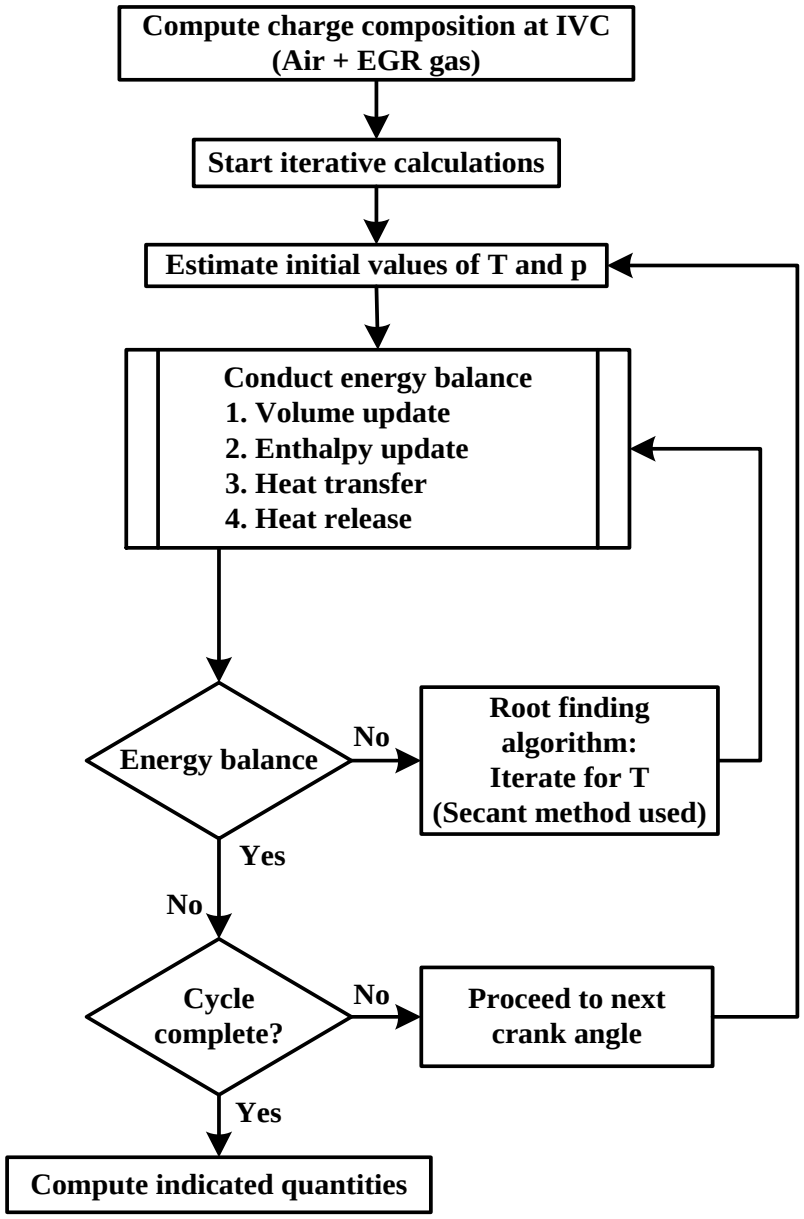

Figure A.2 Schematic of Calculation Routine for Zero-D Simulations

The details of these calculations are explained as follows:

1. The EGR calculations are carried out to compute the concentrations of the gas species based on the intake boost pressure, temperature, the EGR level and the fuel amount and fuel composition.

2. In-cylinder bulk gas temperature is the primary state variable, solved at every calculation step. The initial value of the in-cylinder trapped gas temperature is calculated using the isentropic compression/expansion process assumption.

3. Likewise, the in-cylinder pressure corresponding to the gas temperature is calculated.

4. All the components of the energy balance expression are then computed individually.

    a. Enthalpy Calculations: the significant enthalpies of the gas species are calculated for the estimated temperature value, and the total gas enthalpy is calculated using a weighted average of the constituent components. The change in enthalpy is then computed for the current calculation step.

    b. Volume Update: The piston work associated with the in-cylinder volume change is computed using the estimated cylinder pressure value.

    c. The heat release rate is calculated if the heat release model suggests the occurrence of combustion during the current crank angle event.

    d. The heat transfer amount is computed for the current crank angle duration using the estimated temperature and pressure values.

    e. The sum of all the components within the energy balance expression is computed. The error in the energy balance is then compared with the desired accuracy. If the error is larger than the desired accuracy, a new

estimate for cylinder gas temperature is made using an error minimization technique.

5. Steps 2-4 are repeated iteratively until an estimate of temperature is obtained that yields an acceptable error in the energy balance equation.

6. Steps 1-5 are repeated for each calculation interval until the closed cycle is complete, i.e. the crank angle of exhaust valve opening.

7. Once the cycle calculations are complete, the indicated quantities such as work, mean effective pressure, thermal efficiency are calculated from the calculated cylinder pressure trace.

Heat Release Shape Simulations

The calculated peak cylinder pressure for heat release shape simulations conducted in Section 4.3.2 are shown in Figure A.3. A two stage heat release profile with nearly equal energy and duration distribution among the two stages is preferable to obtain a lower peak cylinder pressure. The indicated thermal efficiency results are presented in Figure A.4. A marginal variation is observed in the indicated thermal efficiency when the heat release shape is changed while maintaining the combustion phasing and the total combustion duration at fixed levels.

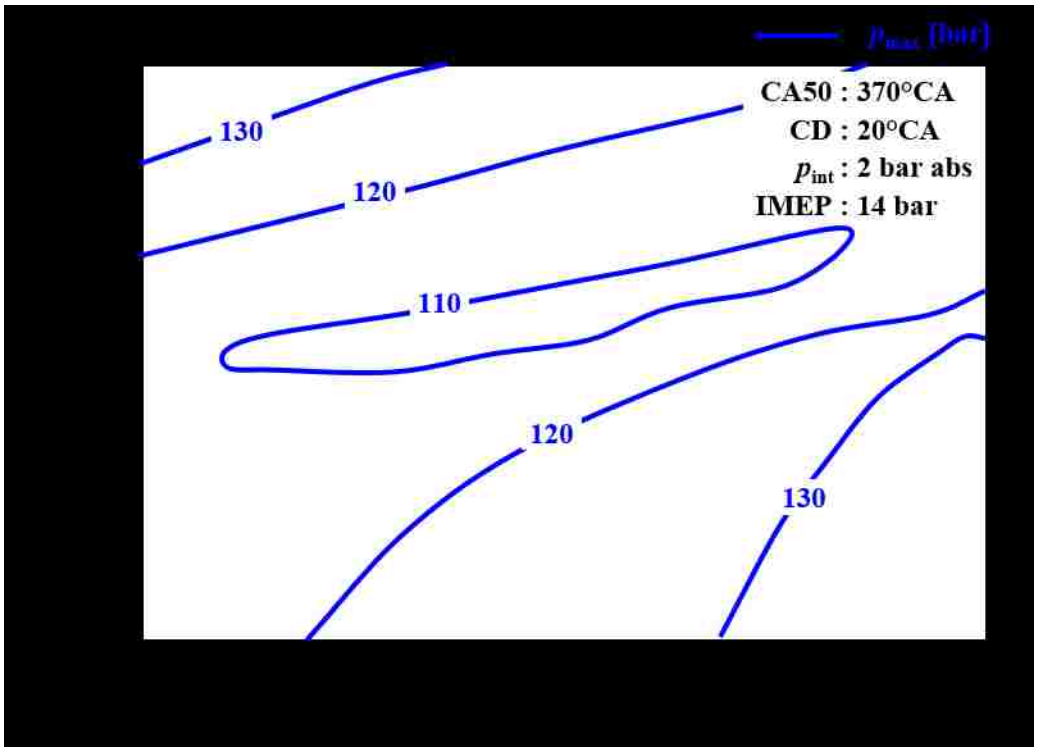

Figure A.3 Effect of Heat Release Shape on p_{max}

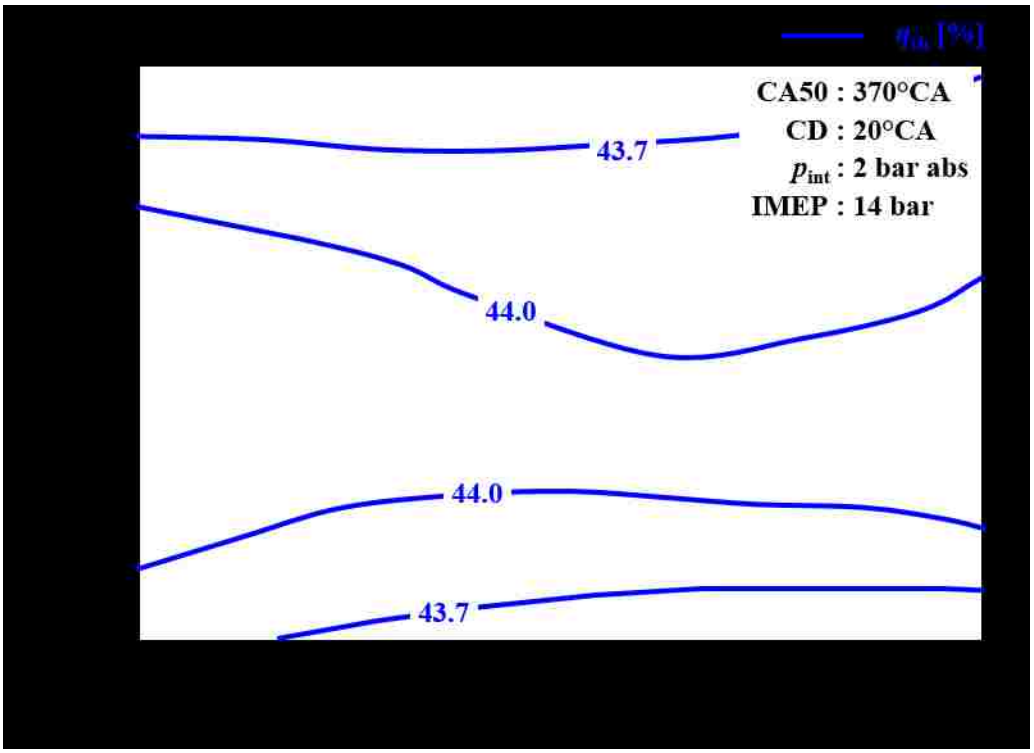

Figure A.4 Effect of Heat Release Shape on η_{th}

APPENDIX E. Additional Test Results

NO_X Measurements

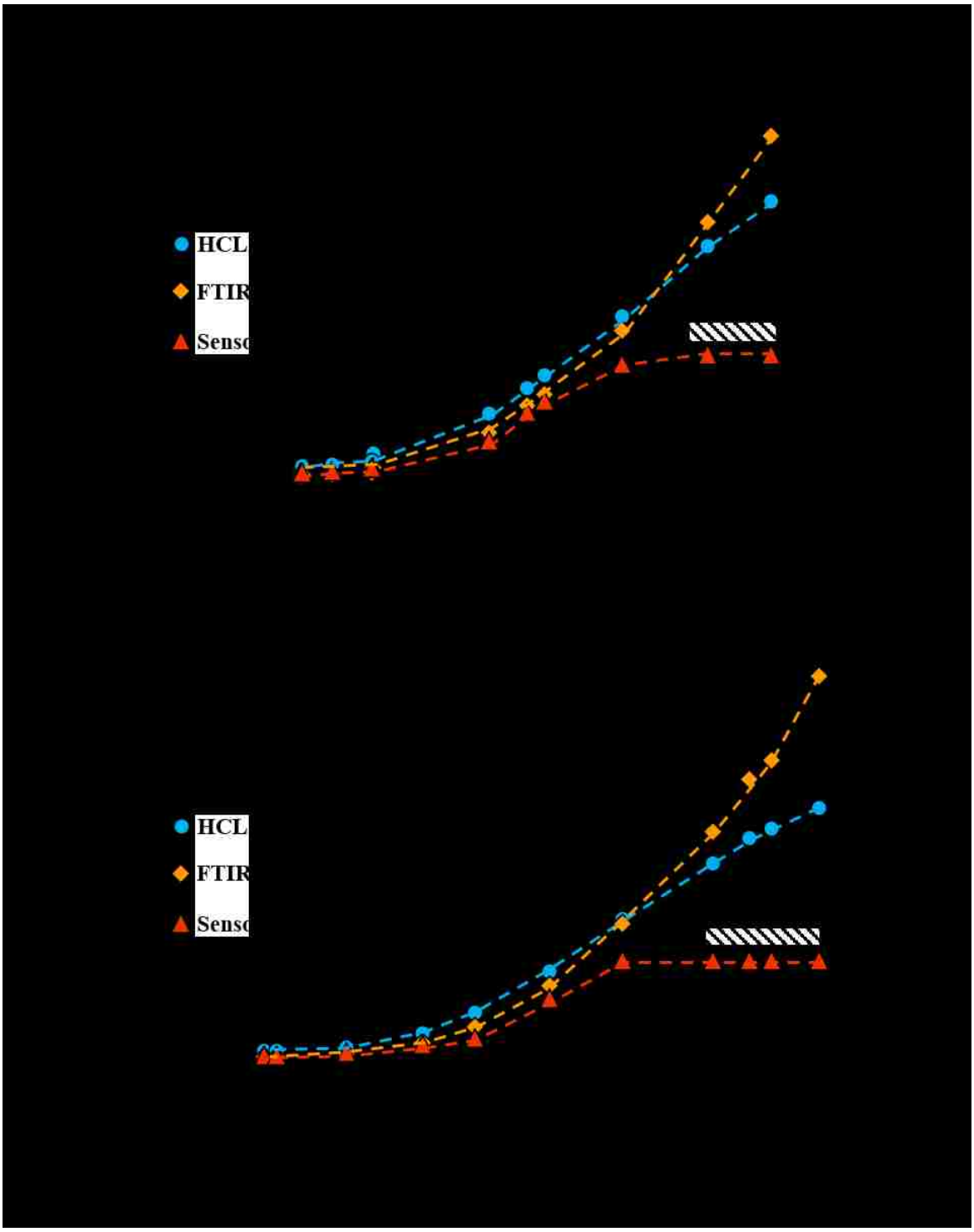

Figure A.5 NO_X Measurements with Different Devices

Effect of Cylinder Pressure Averaging on Heat Release Calculations

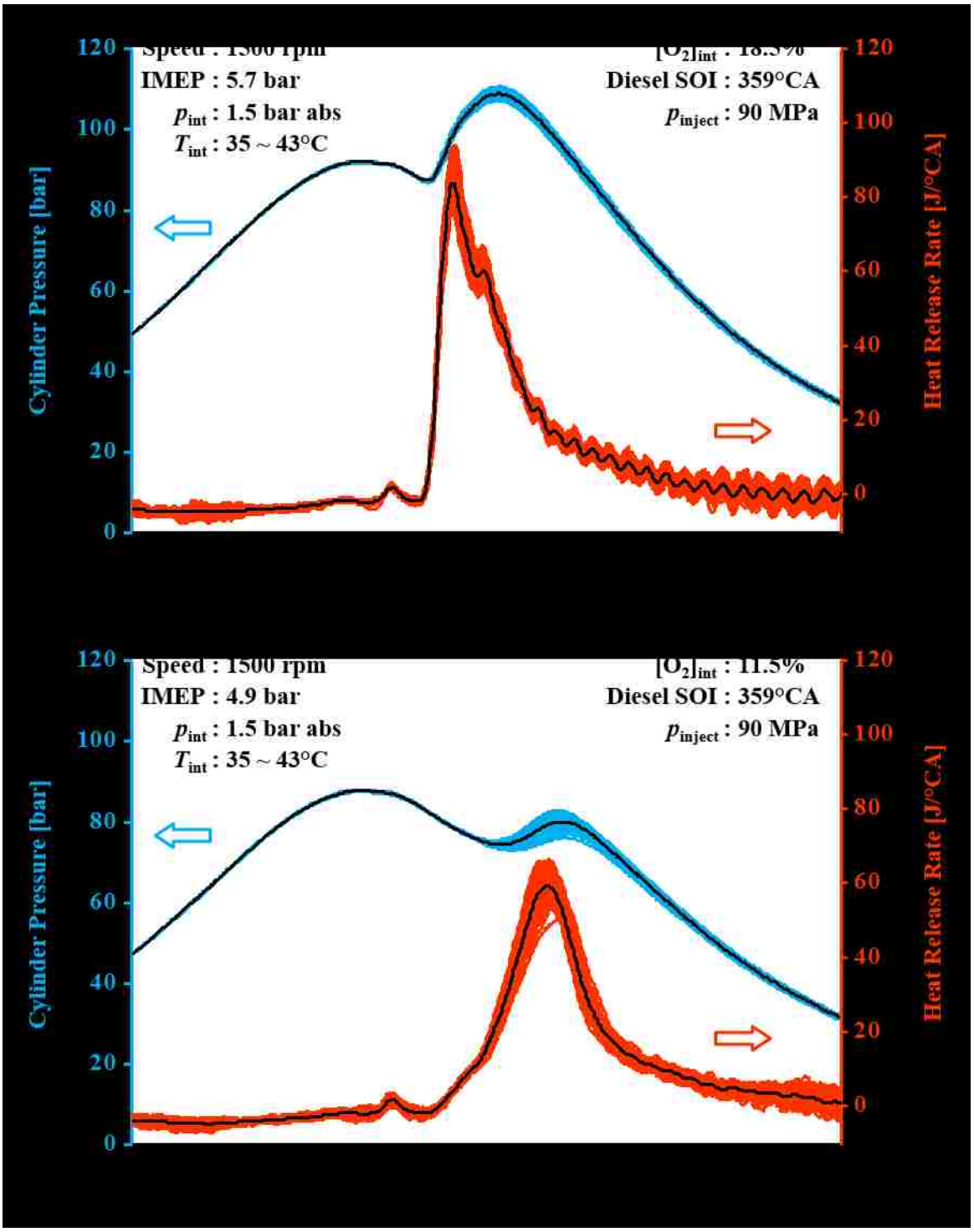

Figure A.6 SSDC: Cylinder Pressure and AHRR (200 cycles)

Effect of Engine Load Level on SSDC

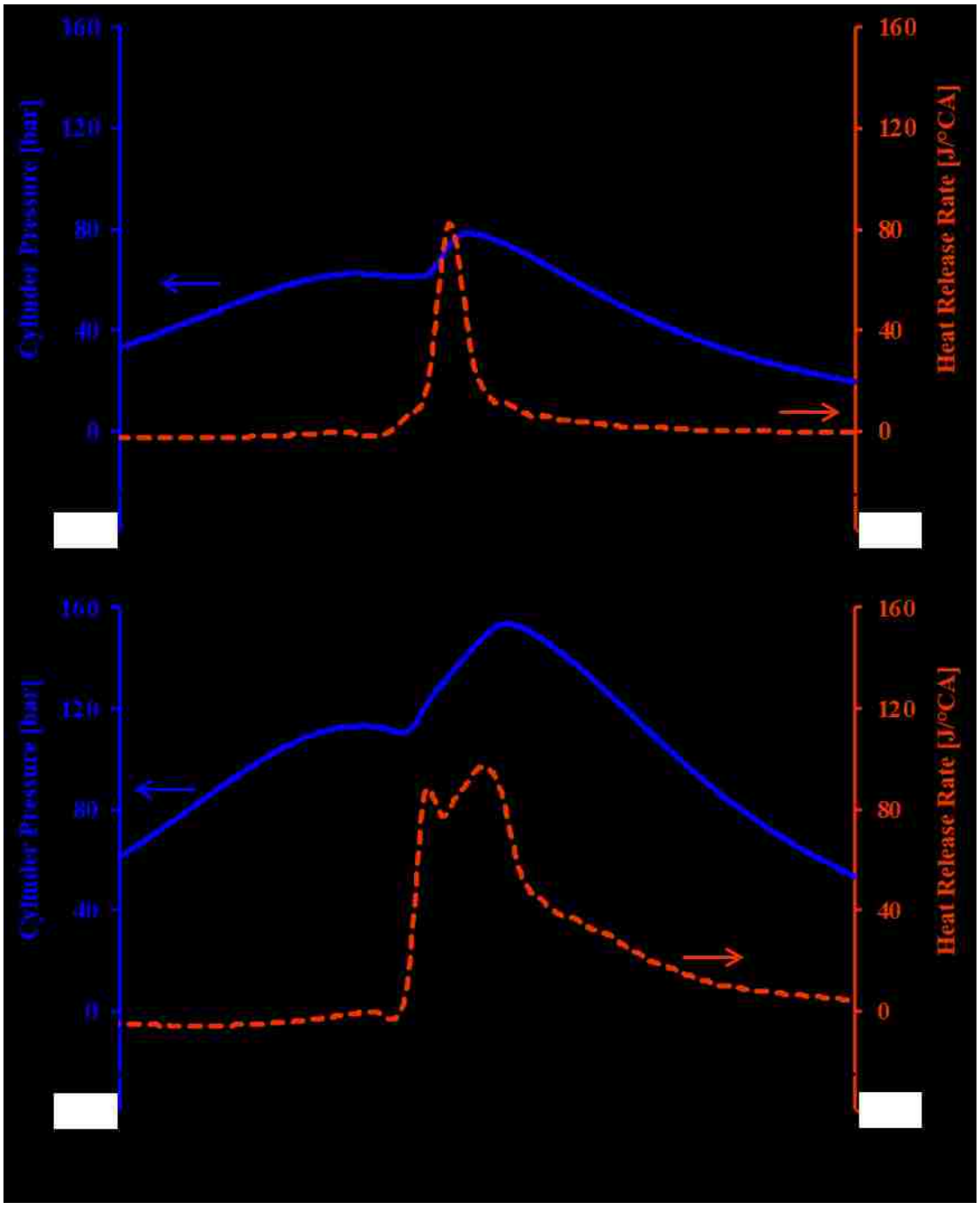

Figure A.7 SSDC: Cylinder Pressure and AHRR

Load Extension with DFC

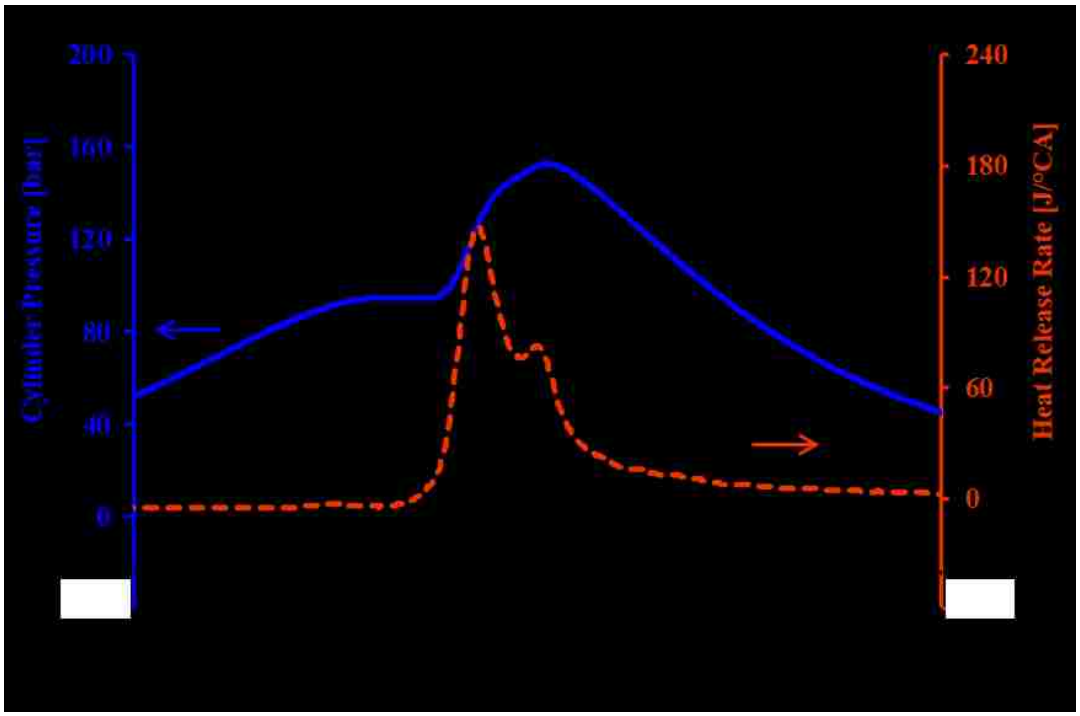

Figure A.8 DFC at 13.1 bar IMEP

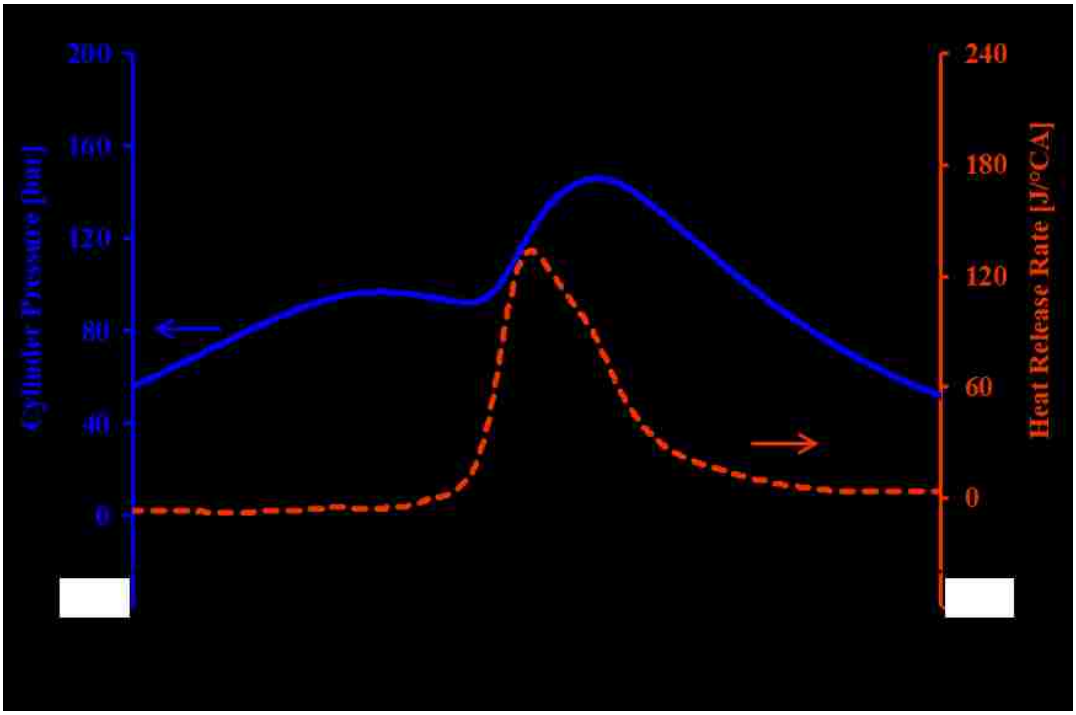

Figure A.9 DFC at 15.1 bar IMEP

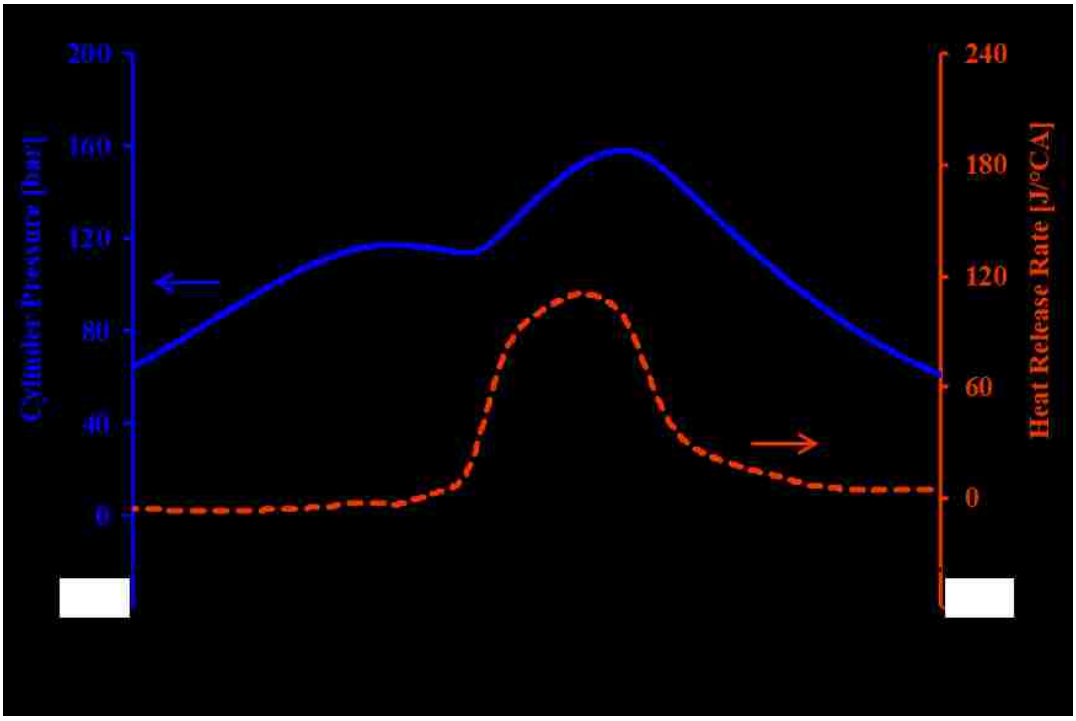

Figure A.10 DFC at 17.6 bar IMEP

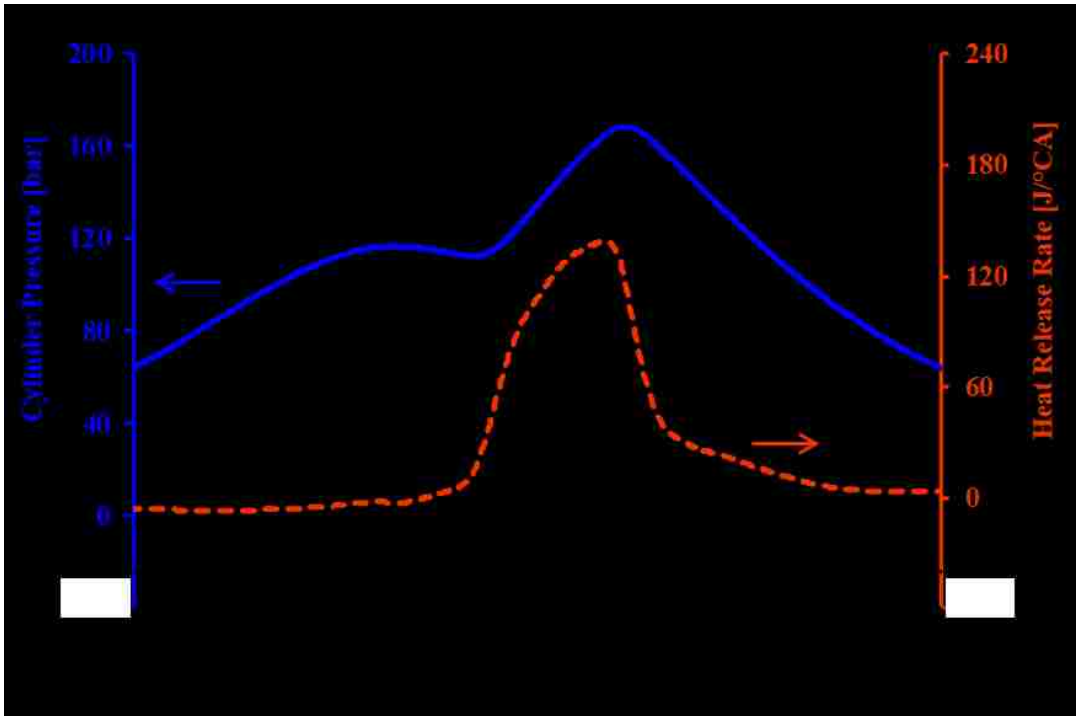

Figure A.11 DFC at 19.2 bar IMEP

APPENDIX F. Diesel Injection Characterization

An off-line injection bench (EFS 8405) is used evaluate the injector opening and closing delays as well as to characterize the injected fuel amount for the same type of injector used on the research engine. The test bench includes a common-rail injection system and a measurement chamber. During the injector characterization test, the injection duration and the common-rail pressure are varied, while the background pressure is held constant at 50 bar to simulate the pressure inside the combustion chamber during the injection event. The rate of each injection event is measured, and the injector opening and closing delays are calculated relative to the injection command, as shown in Figure A.12.

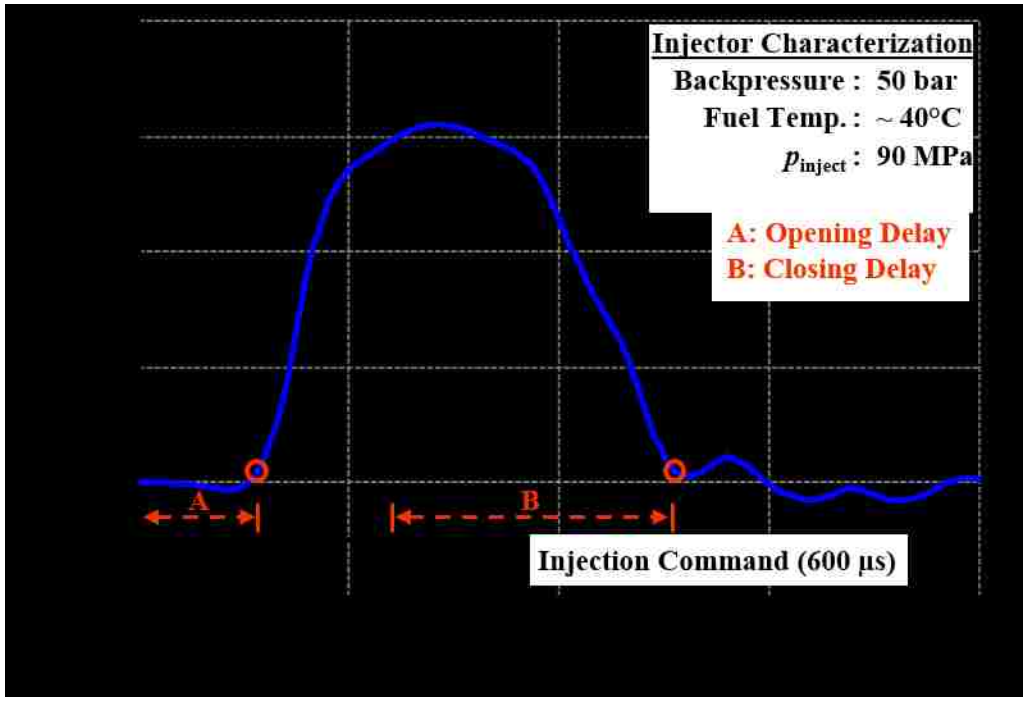

Figure A.12 Injector Characterization with EFS Bench

The opening delay, the closing delay, and the injected mass measured with the injector bench are shown in Figure A.13, Figure A.14, and, Figure A.15 respectively. The results are presented as contour plots with the measured values overlaid onto the same graph. The injector opening delay is largely insensitive to the change in the injection duration and the injection pressures. However, the injector closing delay is significantly altered by both the injection pressure and the injection duration. The injected mass increases monotonously with the increase in the injection duration and the injection pressure.

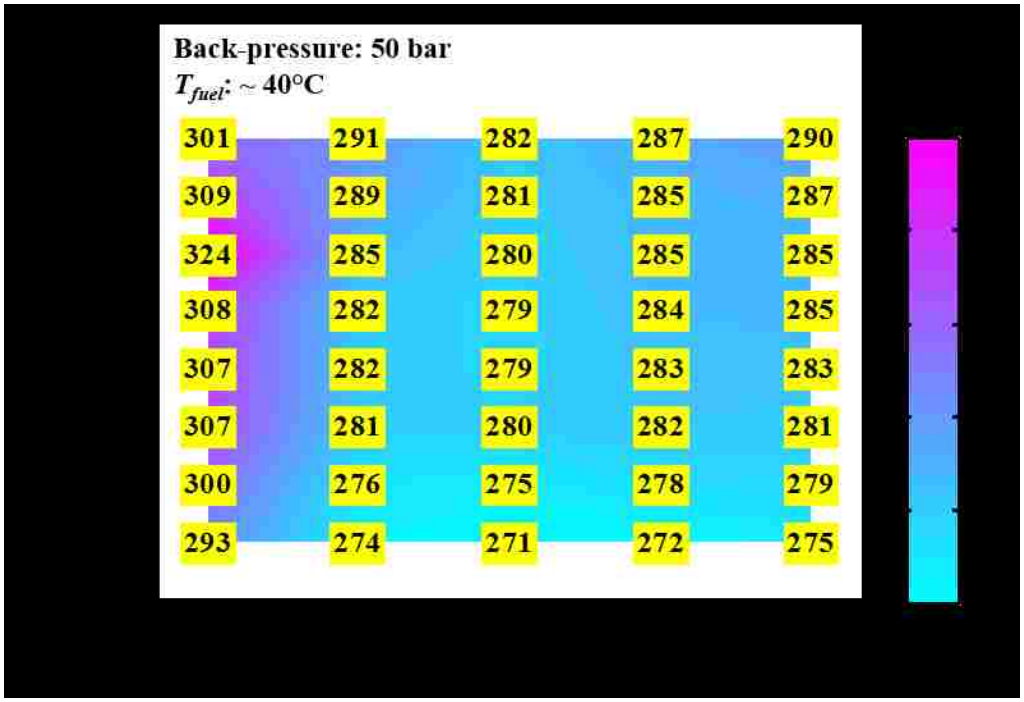

Figure A.13 Opening Delay for Delphi Solenoid Injector

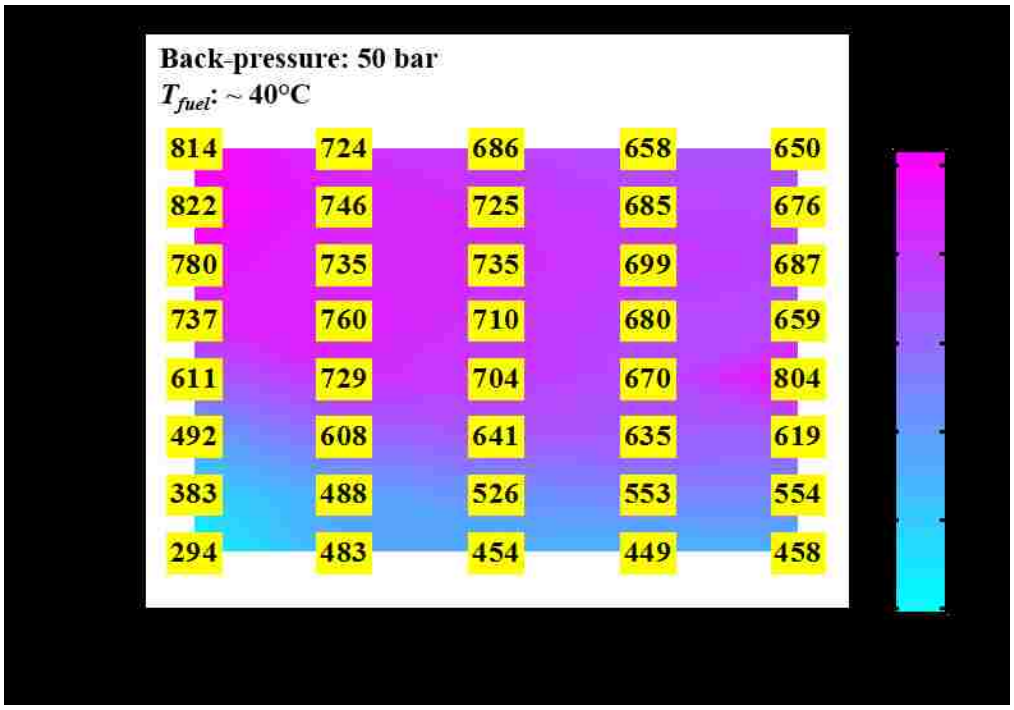

Figure A.14 Closing Delay for Delphi Solenoid Injector

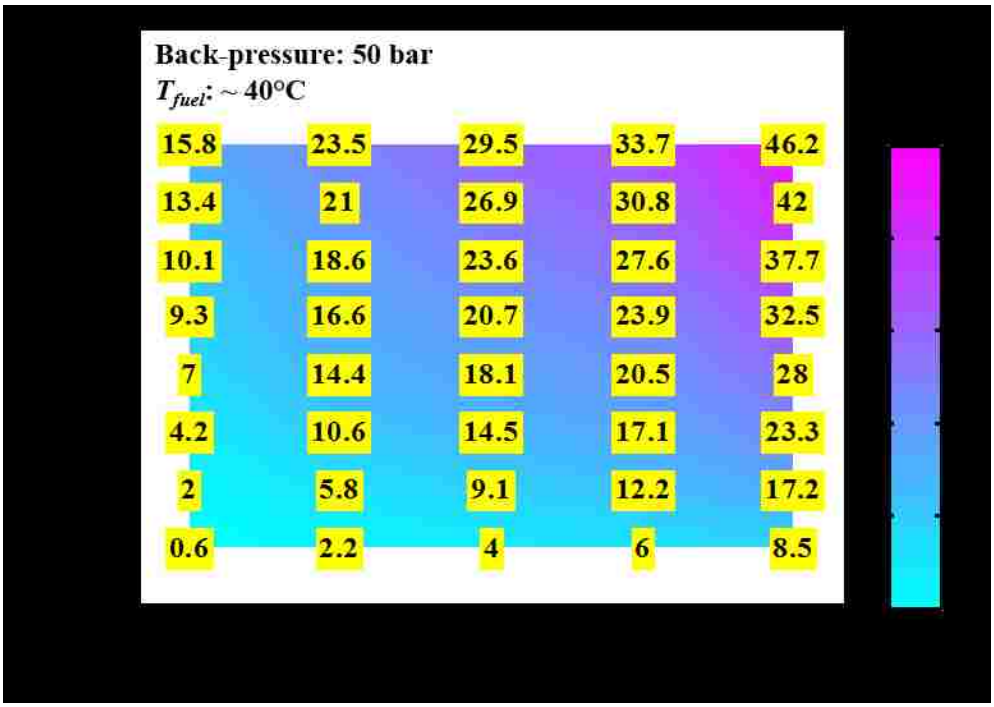

Figure A.15 Injected Mass for Delphi Solenoid Injector

APPENDIX G. Online Model Adaptation with Extremum Seeking

Simplified Engine Model

The simplified engine model is implemented in the systematic control structure, as shown in Figure 7.1. The estimated engine parameters from the engine model are used for the generation of the dynamic target. The EGR analysis and the zero-D engine cycle simulation routine are combined and simplified to minimize the computational load such that the model calculations can be completed on a cycle-by-cycle basis. An on-line parameter tuning methodology is integrated in the model calculations to perform small adjustments to the model parameters and minimize the error between the measured feedback and the model estimation. In the current section, the simplified engine model is first described, followed by the discussion of the online parameter tuning approach.

The engine model is divided into two sub-models based on the physical system structure, the air-path sub-model, and the closed-cycle sub-model. The air-path sub-model essentially comprises of the expressions for molar EGR balance and intake gas concentrations that are developed in Section 4.1. The closed-cycle sub-model represents the in-cylinder thermodynamic processes including piston work, combustion, and heat transfer. These expressions are derived from the zero-D engine cycle simulation routine described in Section 4.2.

Several measurements obtained from the sensors are used as the model inputs to improve the accuracy of the modeled variables. The measured fresh air flow, the manifold pressure, and the manifold gas temperature are used to determine the initial conditions for the model calculations. In addition, the estimated fuel mass from the off-line calibration

of fuel injectors is used to provide an estimate of the injected fuel amount. The analysis of the measured cylinder pressure provides the heat release parameters that are necessary for the estimation of combustion parameters.

Online Model Calibration

In addition to utilizing the physical measurements as model inputs, other measurements are used in the online model adaptation subroutine to improve the model performance online. The extremum seeking (ES) method is used as the optimization method to identify the model parameters that would yield a minimal error between the measured results and the model estimations. ES is a model-free online optimization scheme that minimizes a pre-defined cost function based on the input to output correlation of an unknown system.

The structure of the ES based model parameter calibration architecture is presented in Figure A.16. The modeled IMEP is compared to the IMEP calculated from the measured cylinder pressure. Correction is applied to the fuelling amount obtained from the offline calibration of the fuel injectors such that adjustments are made to the fuel amount based on the IMEP feedback. Secondly, adjustments are made to the estimated residual gas fraction so that the difference between the measured exhaust O_2 concentration and the model output is minimized.

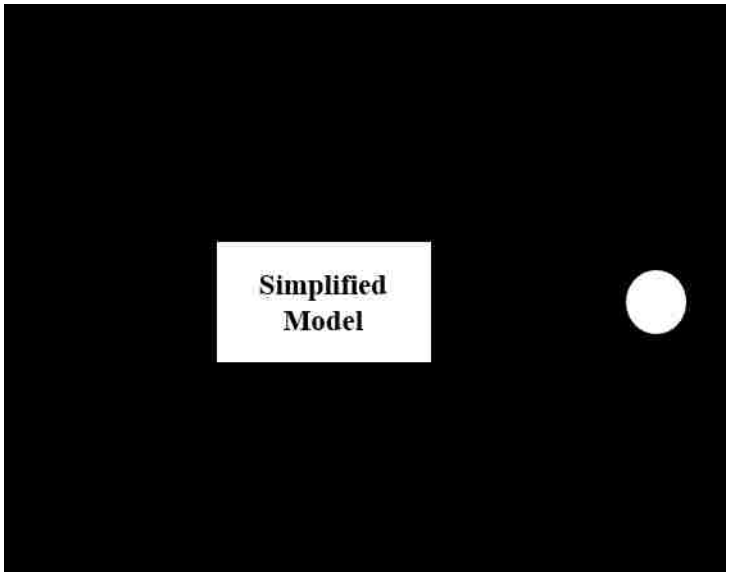

Figure A.16 Structure of Online Model Parameter Calibration

Extremum Seeking Method

Extremum seeking (ES) is a model-free gradient-based optimization method which has been applied to several automotive control problems [109]–[112]. The ES algorithm runs iteratively and guides a control input such that a pre-defined cost function is maximized or minimized. In the current research, the ES method is adopted to perform online calibration of model parameters. The cost function evaluates the difference between the measured plant output and the model estimation. ES is used to modulate the model parameters such that the cost function reaches a local minimum.

The general structure of the perturbation based ES algorithm applied to model parameter calibration is presented in Figure A.17. The basic principle behind the ES algorithm applied for the minimization of the cost function can be briefly explained as follows. When the cost function output (J) is not at its minimum, the plant input (u) could be on either side (left or right) of the optimum plant input (u*) which is yields the minimum

value for the cost function output. The ES algorithm introduces a periodic perturbation into the control signal which causes periodic oscillations in the plant output. By comparing the input perturbations with the resulting oscillations of the plant output, the gradient information of the cost function can be extracted. The ES algorithm then manipulates the control input such that the gradient of the cost function approaches zero. A more detailed description of the ES method is provided in [113].

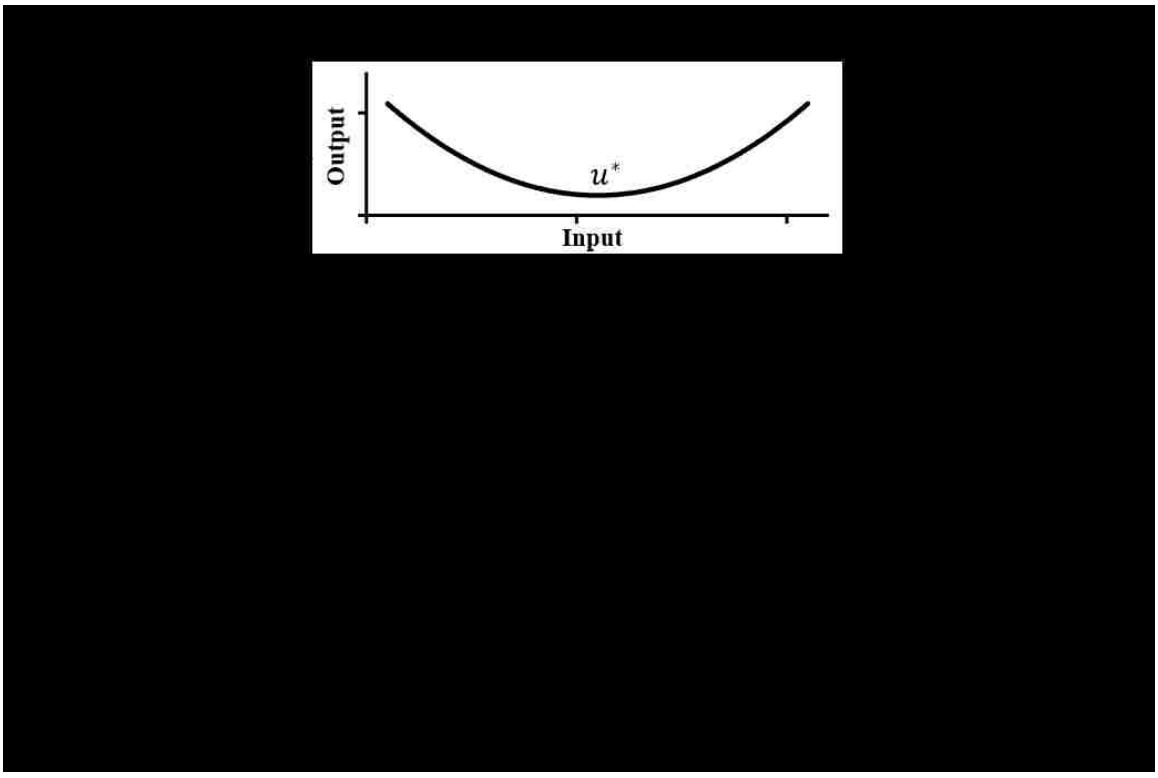

Figure A.17 Perturbation Based ES Structure Applied to Model Calibration

Model Parameter Adaptation with ES

The calibration of the model parameters is conducted by designing a cost function that evaluates the difference between the measured plant output and the model output. ES is

then used to modulate the model parameters such that the cost function reaches a local minimum. The structure of the model parameter adaptation is shown in Figure A.16

The cost function, $\mathrm{J}(y)$, designed for the model parameter adaptation is presented as follows.

$$\mathrm{J}(y) = \frac{e_{IMEP}}{C_{J1}} + \frac{e_{Ex\_O_2}}{C_{J2}} \tag{A.23}$$

where, e_{IMEP} is the error between the measured and the model estimated IMEP values. Similarly, $e_{Ex\_O_2}$ is the error between the sensor measurement of the exhaust O_2 concentration and the model estimated exhaust O_2 concentration. The constants, C_{J1} and C_{J2} are used to normalize the error values against the largest expected error.

A correction is applied to the initial guess of the fuel amount obtained from off-line injector calibration (Figure A.15) by using the ES approach to minimize the IMEP error. For the model adaptation to minimize the exhaust O_2 estimation error, the residual gas fraction is selected as the model parameter. The frequency of the perturbations applied to the fuel amount corrections is significantly larger that the frequency of the residual gas fraction perturbations. By employing different perturbation frequencies, the ES algorithm ensures that the fuel correction occurs more frequently than the EGR correction. The significantly longer response delay of the exhaust oxygen sensor, compared to the cylinder pressure sensor necessitates the separation of the two time scales. Representative test results of the model parameter adaptation are presented in the following subsection.

Results of Online Model Parameter Adaptation

Representative results of online model calibration are presented here to demonstrate the adjustments made to the fuel amount and the total EGR rate by changing the fuel amount correction and the residual gas fraction respectively. The model calculations are programmed in the LabVIEW programming language on a dedicated RT system, and the local network communication is utilized to transfer measurement data between the measurement computers and the RT system. The model calculations are forced to update every engine cycle and the tests conducted at 1500 rpm suggest that the available computing resources and the communication link are sufficient to maintain the required calculation and data transfer rates.

An engine test is conducted by rapidly changing the IMEP setpoint with the closed-loop IMEP and CA50 control active. The model calculations are carried out in parallel during the test, and the data is logged on a cycle-by-cycle basis. A comparison between the modeled IMEP and the measured feedback is shown in Figure A.18. The estimated fuel amount based on the injector characterization and the corrected fuel amount are also plotted on the same figure.

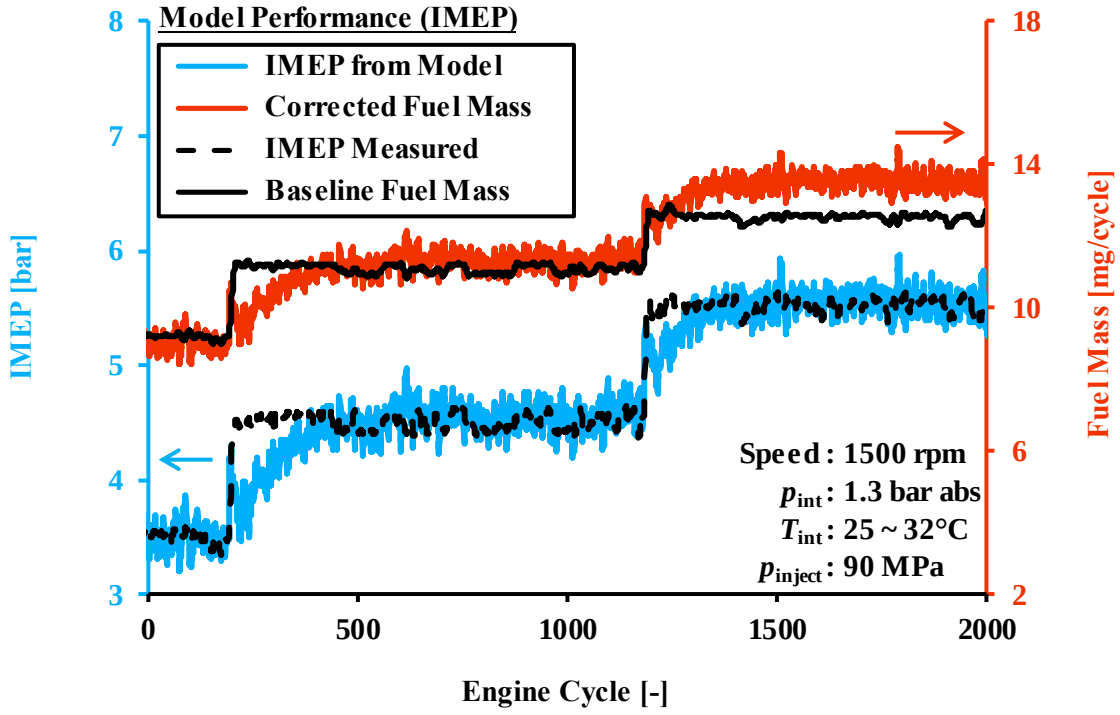

Figure A.18 Online Fuel Correction to Improve Model Estimations

The average model output matches the measured IMEP, although noticeable cyclic oscillations in the estimated IMEP persist. The primary cause of the oscillations in the estimated IMEP is the adopted ES optimization structure wherein the algorithm introduces artificial perturbations in the fuel mass correction to minimize the filtered error between the measurement and model output.

The measurement and modeled intake and exhaust O_2 concentrations are presented in Figure A.19. The ES optimization scheme performs corrections to the estimated EGR rate by adjusting the residual gas fraction such that the error between the measured exhaust O_2 concentration and the model output is minimized. Even though a consistent matching is observed between the measured and modeled exhaust O_2 concentration, a steady-state offset persists between the measured intake O_2 concentration and the model estimate.

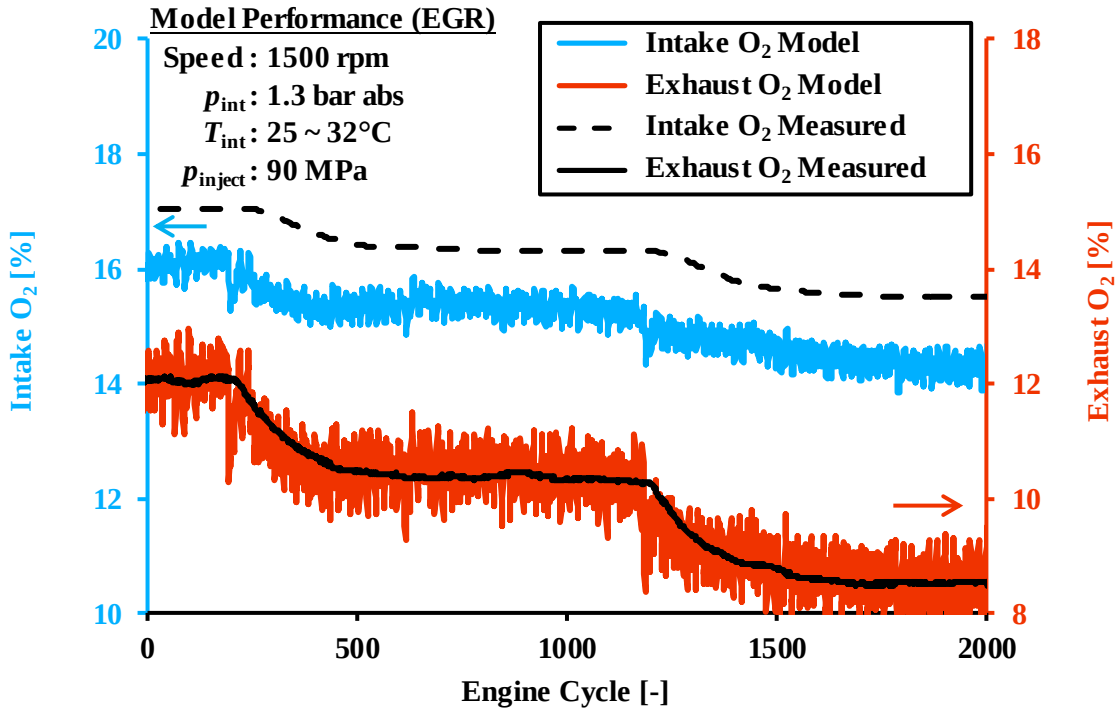

Figure A.19 Model Estimation of Intake and Exhaust O_2 Concentrations

Other modeling inaccuracies that are not considered in the simplified model may be responsible for the intake O_2 concentration offset. Nevertheless, the model can capture the overall trend in the intake O_2 concentration, which is typically not measured in production engines. For the current engine test, the intake O_2 concentration measurement is conducted using the exhaust gas analyzer system while the exhaust O_2 concentration is obtained from the exhaust O_2 sensor.

The initial estimate of EGR based on the simplified model and the corrected EGR rate are plotted in Figure A.20. The corrected EGR rate is consistently higher than that estimated from the intake manifold measurements and an assumption of a fixed volumetric efficiency. The actual EGR rate is not measured during the test. Therefore, the accuracy of either of the two EGR rate estimations is unclear. However, the offset between the

estimated and the measured intake O_2 concentration suggests that the EGR rate is over predicted by the simplified model calculations.

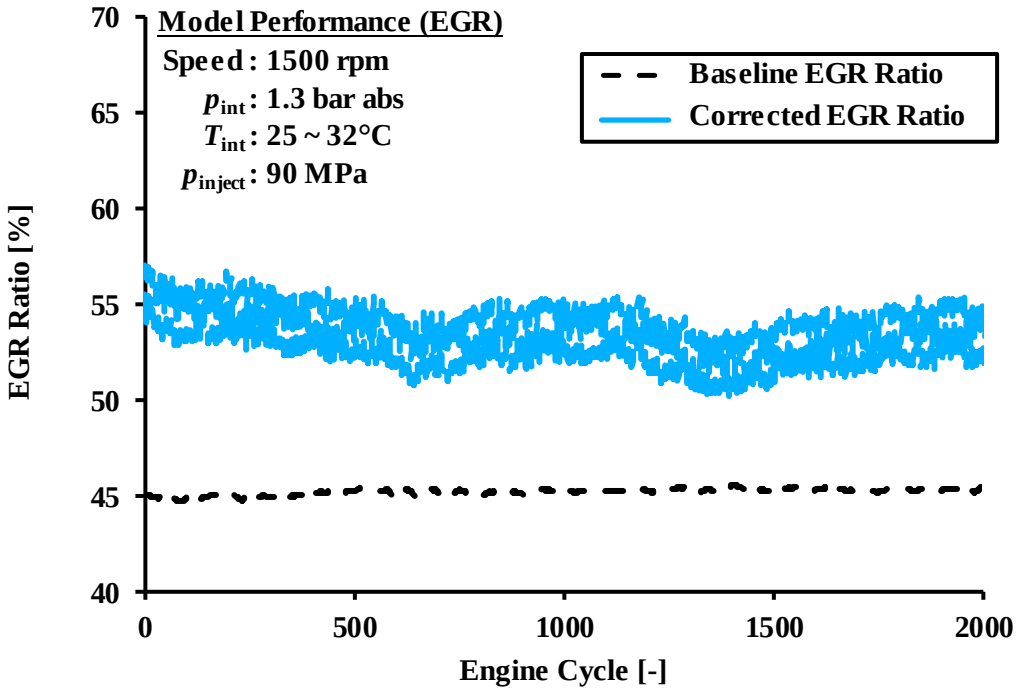

Figure A.20 Online EGR Rate Corrections to Improve Model Estimations

LIST OF PUBLICATIONS

Refereed Journal Articles

1. **P. Divekar**, X. Chen, J. Tjong, and M. Zheng, "Energy Efficiency Impact of EGR on Organizing Clean Combustion in Diesel Engines," *Energy Conversion and Management*, vol. 112, pp. 369-381, 2016. doi:10.1016/j.enconman.2016.01.042

2. **P. Divekar**, U. Asad, J. Tjong, X. Chen, and M. Zheng, "An Engine Cycle Analysis of Diesel-ignited Ethanol Low-temperature Combustion," Proceedings of the *Institution of Mechanical Engineers, Part D: Journal of Automobile Engineering*, vol. 230, no. 8, pp. 1057-1073, 2016. doi:10.1177/0954407015598244

3. X. Han, **P. Divekar**, G. Reader, M. Zheng, and J. Tjong, "Active Injection Control for Enabling Clean Combustion in Ethanol-diesel Dual-fuel Mode," *SAE International Journal of Engines*, vol. 8, no. 2, pp. 890-902, 2015. doi:10.4271/2015-01-0858

4. S. Dev, **P. Divekar**, K. Xie, X. Han, X. Chen, and M. Zheng, "A Study of Combustion Inefficiency in Diesel LTC and Gasoline-diesel RCCI via Detailed Emission Measurement," *Journal of Engineering for Gas Turbines and Power*, vol. 137, no. 12, pp. 121501-1, 2015. doi: 10.1115/1.4030521

5. **P. Divekar**, U. Asad, X. Han, X. Chen, and M. Zheng, "Study of Cylinder Charge Control for Enabling Low Temperature Combustion in Diesel Engines," *Journal of Engineering for Gas Turbines and Power*, vol. 136, no. 9, pp. 091503, 2014. doi:10.1115/1.4026929

6. T. Gao, **P. Divekar**, U. Asad, X. Han, G. Reader, M. Wang, M. Zheng, and J. Tjong, "An Enabling Study of Low Temperature Combustion with Ethanol in a Diesel Engine," *Journal of Energy Resources Technology*, vol. 135, no. 042203, pp. 1-8, 2013. doi: 10.1115/1.4024027

7. U. Asad, **P. Divekar**, X. Chen, M. Zheng, J. Tjong, "Mode Switching Control for Diesel Low Temperature Combustion with Fast Feedback Algorithms," *SAE International Journal of Engines*, vol. 5, no. 3, pp. 850-863, 2012.

Refereed Conference Publications

8. Q. Tan, **P. Divekar**, Y. Tan, X. Chen, and M. Zheng, "A Diesel Engine Combustion Phasing Optimization Using a Model Guided Extremum Seeking Approach," Proceedings of the 35th Chinese Control Conference, July 27-29, 2016, Chengdu, China.

9. Q. Tan, **P. Divekar**, Y. Tan, X. Chen, and M. Zheng, "Engine Model Calibration Using Extremum Seeking," Proceedings of the 8th IFAC International Symposium on Advances in Automotive Control, June 19-23, 2016, Norrköping, Sweden.

10. S. Dev, **P. Divekar**, T. Yanai, X. Chen, and M. Zheng, "Hydrocarbon Specification and Estimation of Combustion Efficiency of Diesel Ignited Ethanol and Butanol Engines," SAE Technical Paper 2016-01-0773, 2016.

11. **P. Divekar**, Q. Tan, X. Chen, M. Zheng, and Y. Tan, "Diesel Engine Fuel Injection Control using a Model-guided Extremum-seeking Method," Proceedings of the ASME Dynamic Systems and Control Conference DSCC, October 28-30, 2015, Columbus, USA.

12. **P. Divekar**, Q. Tan, X. Chen, and M. Zheng, "Characterization of Exhaust Gas Recirculation for Diesel Low Temperature Combustion," Proceedings of the Engine and Powertrain Control, Simulation and Modeling - 4th E-COSM Workshop, August 2015, Columbus, USA.

13. **P. Divekar**, Q. Tan, Y. Tan, X. Chen, and M. Zheng, "Nonlinear Model Reference Observer Design for Feedback Control of a Low Temperature Combustion Diesel Engine," Proceedings of the American Control Conference (ACC), 2015, pp. 13-18. IEEE, July 2015, Chicago, USA.

14. **P. Divekar**, Z. Yang, D. Ting, X. Chen, and M. Zheng, "Efficiency and Emission Trade-Off in Diesel-Ethanol Low Temperature Combustion Cycles," SAE Technical Paper 2015-01-0845, 2015.
15. **P. Divekar**, X. Han, S. Yu, X. Chen, and M. Zheng, "The Impact of Intake Dilution and Combustion Phasing on the Combustion Stability of a Diesel Engine," SAE Technical Paper 2014-01-1294, 2014.
16. Q. Tan, **P. Divekar,** X. Chen, M. Zheng, and Y. Tan, "Exhaust Gas Recirculation Control through Extremum Seeking in a Low Temperature Combustion Diesel Engine," Proceedings of the American Control Conference, 2014, Portland, USA.
17. U. Asad, **P. Divekar**, M. Zheng, and J. Tjong, "Low Temperature Combustion Strategies for Compression Ignition Engines: Operability limits and Challenges," SAE Technical Paper 2013-01-0283, 2013.

Other Conference Publications

18. X. Han, **P. Divekar**, J. Tjong, and M. Zheng, "Multiple-event Combustion of Neat n-Butanol Application on a Modern Common-rail Diesel Engine," Proceedings of the Combustion Institute – Canadian Section Spring Technical Meeting, May 2016, Waterloo, Canada.
19. Z. Yang, C. Aversa, M. Ives, **P. Divekar**, D. Ting, and M. Zheng, "Hydrogen as a By-product of Diesel Engine Low Temperature Combustion," Natural Gas and Hydrogen Storage Symposium & Industry Connection Event, June 2015, Windsor, Canada.
20. G. Bryden, Z. Yang, **P. Divekar**, and M. Zheng, "Ignition Delay, Heat Release Profile, and Emission Correlation in Diesel Low Temperature Combustion," Proceedings of the Combustion Institute – Canadian Section Spring Technical Meeting, May 2015, Saskatoon, Canada.
21. **P. Divekar,** S. Dev, X. Han, X. Chen, and M. Zheng, "Study of Exhaust Gas Recirculation – A Low Temperature Combustion Enabler," Proceedings of the

Canadian Society for Mechanical Engineering International Congress 2014, Toronto, Canada.

22. G. Bryden, C. Aversa, **P. Divekar**, and M. Zheng, "Preliminary Investigation of the Influence of Low Temperature Combustion on Diesel Engine Heat Release Profiles," Proceedings of Combustion Institute – Canadian Section Spring Technical Meeting, Université Laval, May 13-16, 2013, Quebec City, Canada.

23. **P. Divekar**, X. Han, T. Yanai, S. Yu, X. Chen, and M. Zheng, "Control Techniques of Low NO_X Combustion in a High Compression Diesel Engine," Powertrain Modeling and Control Conference, 2012, Bradford, UK.

VITA AUCTORIS

NAME:	Prasad Sajjan Divekar
PLACE OF BIRTH:	Kolhapur, MS, INDIA
YEAR OF BIRTH:	1986
EDUCATION:	Bachelor of Engineering in Automobile Engineering Rajarambapu Institute of Technology, Shivaji University, India June 2008 Masters of Science in Automotive Engineering Clemson University's International Center for Automotive Research (CU-ICAR), SC, USA August 2010 Ph.D. Mechanical, Automotive and Materials Engineering University of Windsor, ON, Canada August 2016